

**SUN-INDUCED FLUORESCENCE OF PHYTOPLANKTON  
IN THE OCEAN: LINKING PHYSIOLOGY  
AND REMOTE SENSING**

by

**Yannick Huot**

**Submitted in partial fulfillment of the requirements  
for the degree of Doctor of Philosophy**

at

**Dalhousie University  
Halifax, Nova Scotia  
December 2004**

**© Copyright by Yannick Huot, 2004**



Library and  
Archives Canada

Bibliothèque et  
Archives Canada

Published Heritage  
Branch

Direction du  
Patrimoine de l'édition

395 Wellington Street  
Ottawa ON K1A 0N4  
Canada

395, rue Wellington  
Ottawa ON K1A 0N4  
Canada

*Your file    Votre référence*

*ISBN: 0-494-00953-5*

*Our file    Notre référence*

*ISBN: 0-494-00953-5*

#### NOTICE:

The author has granted a non-exclusive license allowing Library and Archives Canada to reproduce, publish, archive, preserve, conserve, communicate to the public by telecommunication or on the Internet, loan, distribute and sell theses worldwide, for commercial or non-commercial purposes, in microform, paper, electronic and/or any other formats.

The author retains copyright ownership and moral rights in this thesis. Neither the thesis nor substantial extracts from it may be printed or otherwise reproduced without the author's permission.

#### AVIS:

L'auteur a accordé une licence non exclusive permettant à la Bibliothèque et Archives Canada de reproduire, publier, archiver, sauvegarder, conserver, transmettre au public par télécommunication ou par l'Internet, prêter, distribuer et vendre des thèses partout dans le monde, à des fins commerciales ou autres, sur support microforme, papier, électronique et/ou autres formats.

L'auteur conserve la propriété du droit d'auteur et des droits moraux qui protègent cette thèse. Ni la thèse ni des extraits substantiels de celle-ci ne doivent être imprimés ou autrement reproduits sans son autorisation.

---

In compliance with the Canadian Privacy Act some supporting forms may have been removed from this thesis.

Conformément à la loi canadienne sur la protection de la vie privée, quelques formulaires secondaires ont été enlevés de cette thèse.

While these forms may be included in the document page count, their removal does not represent any loss of content from the thesis.

Bien que ces formulaires aient inclus dans la pagination, il n'y aura aucun contenu manquant.

  
**Canada**

DALHOUSIE UNIVERSITY

To comply with the Canadian Privacy Act the National Library of Canada has requested that the following pages be removed from this copy of the thesis:

Preliminary Pages

Examiners Signature Page (pii)

Dalhousie Library Copyright Agreement (piii)

Appendices

Copyright Releases (if applicable)

To those who wanted, but could not, and to those whose life was  
shattered by short-sighted, stupid, or greedy people.

# Table of Contents

<i>List of Tables</i> .....	<i>x</i>
<i>List of Figures</i> .....	<i>xi</i>
<i>Abstract</i> .....	<i>xv</i>
<i>List of abbreviations</i> .....	<i>xvi</i>
<i>Acknowledgment</i> .....	<i>xvii</i>
 <i>Chapter 1 Introduction</i> .....	 <i>20</i>
1.1 Phytoplankton physiology and global issues .....	20
1.2 Fluorescence and oceanography .....	21
1.3 Thesis outline.....	25
 <i>Chapter 2 Background</i> .....	 <i>28</i>
2.1 A short historical perspective .....	28
2.1.1 In the beginning.....	28
2.1.2 Active fluorescence in oceanography .....	29
2.1.3 Passive fluorescence in oceanography .....	30
2.2 Key concepts in sun-induced fluorescence.....	33
2.2.1 Mathematical description and variables of interest.....	33
2.2.2 The quantum yield of fluorescence .....	38
2.3 The photosynthetic apparatus and fluorescence .....	40
2.3.1 Fluorescence: basic relationships. ....	45
2.4 Models of in vivo chlorophyll fluorescence .....	46
2.4.1 Butler's model of fluorescence.....	46
2.4.2 The model of Kiefer and Reynolds .....	51
2.4.3 Sun-induced fluorescence .....	54

<b>2.5</b>	<b>The quantum yield of fluorescence in the ocean.....</b>	<b>60</b>
<b>2.6</b>	<b>Excess irradiance and photosynthesis.....</b>	<b>61</b>
2.6.1	Non-photochemical quenching.....	62
<b>2.7</b>	<b>Observations of non-photochemical quenching in phytoplankton.....</b>	<b>66</b>
<b>2.8</b>	<b>Effect of nutrients on the quantum yield of fluorescence.....</b>	<b>66</b>
<b>2.9</b>	<b>The tools of the trade: Instrumentation and relationships. ....</b>	<b>72</b>
2.9.1	The Turner Designs fluorometer and fluorescence $\pm$ DCMU .....	72
2.9.2	The PAM fluorometer .....	73
2.9.3	The FRR fluorometer .....	76

### *Chapter 3 A mechanistic model of photosynthesis and fluorescence ..... 80*

<b>3.1</b>	<b>Introduction.....</b>	<b>80</b>
<b>3.2</b>	<b>Background .....</b>	<b>85</b>
3.2.1	Han's model of photosynthesis.....	85
<b>3.3</b>	<b>Model development .....</b>	<b>96</b>
3.3.1	Addressing some limitations of the Han model for fluorescence work.....	96
3.3.2	Model overview .....	98
3.3.3	The NADP pool: linking the light reactions to biosynthetic reductions .....	101
3.3.4	The puddle model and quantum yields in terms of rate constants .....	103
3.3.5	NPQ parameter in terms of rate constants .....	108
3.3.6	Han's model vs. the fluorescence model of photosynthesis .....	109
3.3.7	Parameterization of $k_{qE}$ .....	109
3.3.8	Effective cross-section and the dissipation factor .....	116
3.3.9	Limiting the rate of repair.....	117
3.3.10	Nitrogen limitation .....	119
3.3.11	Review of the model .....	120
3.3.12	Two types of photoacclimation .....	125
3.3.13	Setting some constants.....	131
<b>3.4</b>	<b>Results .....</b>	<b>134</b>
3.4.1	Basic photosynthesis model.....	135
3.4.2	Basic photosynthesis model with photoinhibition.....	137

3.4.3	Effect of photoprotection on the rates of photosynthesis and $\phi_f$ .....	141
3.4.4	Nitrogen limitation and the quantum yield of fluorescence .....	148
3.4.5	The influence of $k_I$ .....	152
3.4.6	Acclimation to irradiance.....	155
3.4.7	Revisiting the experiment of Cullen et al. (1988) .....	164
3.4.8	Preliminary observations on the experiment to guide the modeling .....	167
3.4.9	Comparing the model and data.....	167
<b>3.5</b>	<b>Discussion.....</b>	<b>172</b>
3.5.1	Limitations of the puddle model.....	172
3.5.2	Effect of irradiance on the repair rates .....	174
3.5.3	Effect of temperature on enzymatic rates .....	175
3.5.4	Target for the photoinactivation of photosystem II.....	176
3.5.5	Other relevant processes not modeled.....	176
3.5.6	Effects of nutrient limitation beyond a decreased repair rate .....	177
3.5.7	Photoacclimation of $\gamma_{NPQ}$ .....	178
<b>3.6</b>	<b>Conclusions.....</b>	<b>179</b>

## *Chapter 4 A fluorescence model for the inversion of ocean color using a floating radiometer ..... 181*

<b>4.1</b>	<b>Preface to chapter 4.....</b>	<b>181</b>
<b>4.2</b>	<b>Introduction.....</b>	<b>181</b>
4.2.1	Contributions to upwelling radiance and reflectance.....	183
4.2.2	Inverse models using inherent optical properties spectral shapes .....	186
4.2.3	Raman scattering .....	187
4.2.4	Methods to separate fluorescence emission from backscattered radiance.....	188
4.2.5	Objectives .....	189
<b>4.3</b>	<b>Methods.....</b>	<b>190</b>
4.3.1	Description of the fluorescence model.....	190
4.3.2	The inverse model for backscattered photons .....	198
4.3.3	Application to the Bering Sea.....	200
4.3.4	Application to Lunenburg Bay .....	202
4.3.5	Data collection and Hydrolight simulations .....	208

<b>4.4 Results .....</b>	<b>213</b>
4.4.1 Fluorescence spectral components .....	213
4.4.2 Parameterization using the Hydrolight dataset.....	213
4.4.3 Inversion in the Bering Sea.....	215
4.4.4 Inversion in Lunenburg Bay .....	225
<b>4.5 Discussion.....</b>	<b>235</b>
4.5.1 Origin of non-random residuals.....	236
4.5.2 Bering Sea timeseries .....	241
4.5.3 Lunenburg Bay inversion.....	242
4.5.4 Comparison with published work.....	244
<b>4.6 Conclusions.....</b>	<b>246</b>

*Chapter 5 New algorithms for MODIS sun-induced chlorophyll fluorescence and a comparison with present data products ..... 247*

<b>5.1 Preface to chapter 5.....</b>	<b>247</b>
<b>5.2 Introduction.....</b>	<b>247</b>
<b>5.3 Nature of the MODIS fluorescence measurement .....</b>	<b>248</b>
<b>5.4 Theoretical background .....</b>	<b>253</b>
<b>5.5 Procedures .....</b>	<b>258</b>
<b>5.6 The algorithms .....</b>	<b>260</b>
<b>5.7 Assessment.....</b>	<b>271</b>
<b>5.8 Discussion.....</b>	<b>300</b>
<b>5.9 Comments and recommendations.....</b>	<b>301</b>
<b>5.10 Conclusion .....</b>	<b>304</b>

*Chapter 6 Conclusion & Future Prospects ..... 306*

<b>6.1 Future prospects and directions.....</b>	<b>309</b>
---	------------

*Appendix I : Absorption coefficient as a measure of the attenuation of fluorescence radiance ..... 316*

Hydrolight simulations .....	316
Results	318
<i>Appendix II: Errors and correlation of the retrieved parameters.</i>	<i>319</i>
<i>Appendix III : Baseline correction of FLH.....</i>	<i>323</i>
<i>Appendix IV : Interpretation of the quantum yield of sun-induced chlorophyll fluorescence quantum yield.....</i>	<i>327</i>
<i>Appendix V: Copyrights agreement form .....</i>	<i>330</i>
<i>Bibliography .....</i>	<i>331</i>

## *List of Tables*

Table 2-1: List of symbols and units .....	34
Table 3-1: Table of symbols and units. ....	87
Table 3-2: Main equations of the model.....	121
Table 3-3: Values for the constants used in the model.....	132
Table 4-1: List of symbol and units.....	184
Table 4-2: Comparison of the two inverse models used in this study.....	207
Table 4-3: Fitted parameters, $k_i$ from the Hydrolight simulations for Lunenburg Bay Nova Scotia for $K_{0.65-2.75}$ (see equation 4.21). ....	217
Table 4-4: Fitted parameters, $e_i$ from the Hydrolight simulations for Lunenburg Bay Nova Scotia for $\mathring{E}(\lambda, 65)$ .....	218
Table 5-1: List of symbols and units. ....	249
Table 5-2: A comparison of the quantum yield parameters.....	272

## List of Figures

Figure 2.1: MODIS images of chlorophyll concentration, fluorescence line height (total radiance minus background radiance not due to fluorescence) and ratio of fluorescence to chlorophyll (index of fluorescence efficiency). ....	32
Figure 2.2: The Z-scheme provides a mechanism through which energy from sunlight is used to oxidize a water molecule on the donor side of photosystem II and ultimately reduces a CO <sub>2</sub> molecule on the acceptor side of PSI (carbon fixation). ....	43
Figure 2.3: Schematic of Butler's bipartite model. See text for definition of symbols. ....	47
Figure 2.4: Model of Kiefer and Reynolds for photosynthesis and fluorescence. ....	52
Figure 2.5: Reflectance spectra $L_u(\lambda, 0.65)/E_d(\lambda, 0^+)$ normalized to the area under the curve. ....	55
Figure 2.6: Cleveland and Perry 1987 revisited. ....	70
Figure 2.7: Fluorescence quenching analysis parameters. ....	75
Figure 2.8: Fluorescence transients measured by the FRR method. ....	77
Figure 3.1: Han's (2002) model of photosynthesis. ....	86
Figure 3.2: Schematic representation of the photosynthesis and fluorescence model with acclimation. ....	99
Figure 3.3: The three states of the reaction centers and associated rate constants. ....	104
Figure 3.4: Excess radiation. ....	112
Figure 3.5: Schematic representation of the effect of photoprotection due to increasing energy dependent non-photochemical quenching. ....	118
Figure 3.6: Model of photosynthesis used in present work. ....	122
Figure 3.7: Schematic representation of the acclimation model. ....	127
Figure 3.8: Acclimation function for the rate of change of the optical cross-section. ....	130
Figure 3.9: Basic photosynthesis model. ....	136
Figure 3.10: Basic photosynthesis model with photoinhibition. ....	139
Figure 3.11: Diel changes in the rate of charge separation with photoinhibition. ....	140
Figure 3.12: Effect of photoprotection on the photosynthetic rates. ....	142
Figure 3.13: Photosynthesis with damage and fluorescence, including the effect of photoprotection by energy dependent quenching ( $\gamma_d = 0.0005$ , [ $\mu\text{mol m}^{-2}$ ] <sup>-1</sup> ). ....	143
Figure 3.14: Effect of photoprotection on the quantum yields of photosynthesis and	

fluorescence.....	145
Figure 3.15: Comparison of the quantum yield of fluorescence and the quantum yield of photochemistry for different capacities for non-photochemical quenching ( $\gamma_d$ , $[\mu\text{mol m}^{-2}]^{-1}$ , see legend). ....	147
Figure 3.16: Effect of nitrogen stress on the photochemical rates and fluorescence quantum yield. ....	149
Figure 3.17: Effect of nitrogen stress on the diel changes in photochemistry and fluorescence. ....	151
Figure 3.18: Ratio of morning (AM) to afternoon (PM) natural fluorescence emission divided by incident irradiance (F/E) in continuous cultures of <i>Thalassiosira weissflogii</i> grown on a 14:10 hours sinusoidal light-dark cycle. ....	153
Figure 3.19: The influence of $k_t$ on the fluorescence quantum yield under damaging conditions. ....	154
Figure 3.20: Steady-state values of seven variables for different growth irradiance levels. ....	156
Figure 3.21: Kinetics of acclimation upon step change in irradiance. ....	158
Figure 3.22: Consequences of acclimation on photosynthesis. ....	159
Figure 3.23: Consequences of acclimation on fluorescence. ....	161
Figure 3.24: Results from the experiments carried out by Cullen et al. (1988). ....	165
Figure 3.25: Model run to compare with the experiment of Cullen et al. (1988). ....	169
Figure 3.26: Photosynthetic parameters to compare the model with the results of Cullen et al. (1988). ....	171
Figure 3.27: Quantum yields for the different processes modeled at PSII during model run to reproduce the Cullen et al. (1988) experiment. ....	173
Figure 4.1: Hydrolight simulation inputs. ....	212
Figure 4.2: Five emission spectra for phytoplankton fluorescence normalized to their maximum values. ....	214
Figure 4.3: Comparison of the empirical parameterization (estimated) and the Hydrolight simulated dataset for $K_{0.65-2.75}$ (top panels; using equation 4.21) and $\hat{E}(\lambda, 0.65)$ (bottom panels; using equation 4.22). ....	216
Figure 4.4: Time series of the fitted parameters with the inverse model and measured incident irradiance. ....	219
Figure 4.5: Modeled and measured reflectance spectra at two times in the timeseries (79 and 493 seconds) collected at station 35 in the Bering Sea on June 27, 2001. ....	222
Figure 4.6: Measured and modeled optical properties at station 35 in the Bering Sea in	

June 2001. ....	223
Figure 4.7: Fits and representative data of the retrieved absorption coefficient of phytoplankton if the quantum yield of fluorescence is maintained constant in the model.....	226
Figure 4.8: Time series comparison of measured and retrieved optical measurements with the inverse model.....	230
Figure 4.9: Selected reflectance spectra for the inversion. The spectra were selected to follow immediately the time of the discrete samples. Top panel: full spectrum. Bottom panel: Fluorescence region only. ....	233
Figure 4.10: Comparison of measured and retrieved absorption coefficients at LMB1 buoy during the summer of 2003.....	234
Figure 4.11: Retrieved quantum yield versus irradiance for the Bering Sea timeseries (Figure 4.4).....	243
Figure 5.1: Relationships between the optical properties of phytoplankton and water. .	263
Figure 5.2: Attenuation coefficient of fluorescence excitation irradiance. ....	266
Figure 5.3: Correction factors normalized to the value at 1 mg chl m <sup>-3</sup> applied to <i>FLH</i> to retrieve chlorophyll concentration and the quantum yield of fluorescence. ....	268
Figure 5.4: Relationship between the <i>FLH</i> and the chlorophyll concentration with our parameterization (see equation 5.20) using $\phi_{chl}=0.012$ , and $\overset{o}{E}_{PAR}=1750\text{ }\mu\text{mol m}^{-2}\text{ s}^{-1}$ .....	273
Figure 5.5: Modeled relationships between the estimates obtained using the baseline method and emitted fluorescence at 678 nm. ....	275
Figure 5.6: Simplified model (reduced spectral dependence) of fluorescence emission in water to illustrate the different approaches to calculate the depth where 63.2% of the fluorescence originates.....	278
Figure 5.7: Ratio of calculated absorbed irradiance weighted for its efficiency of emission at the surface: $(=\int_{400}^{700}\int_0^Z a_{\phi}(\lambda)\cdot\overset{o}{E}(\lambda,0)\cdot e^{-(K(\lambda)+a_f)\cdot z}\cdot dz\cdot d\lambda)$ for different depths <i>Z</i> and a range of chlorophyll concentrations.....	281
Figure 5.8: MODIS level 3 dataset for Jan 15, 2001 for the subsene off the west coast of Central America.....	284
Figure 5.9: Top panel: Comparison of our fluorescence estimate of the chlorophyll concentration, $chl_{fluor}=FLH\cdot\beta_{\phi}/(\phi_{chl}\cdot\overset{o}{E}_{PAR})$ (see equations 5.8 and 5.14) with MODIS chlorophyll product (chlor_a2, SeaWiFS analog chlorophyll algorithm). ....	286
Figure 5.10: Map of derived products. ....	289

Figure 5.11: Comparison of quantum yields.....	291
Figure 5.12: MODIS level 3 dataset for Jan 15, 2001 for the subscene of the Arabian Sea. .....	293
Figure 5.13: Comparison of algorithms.....	294
Figure 5.14: Map of derived products for the Arabian Sea. ....	297
Figure 5.15: Comparison of quantum yields for the Arabian Sea.....	298
Figure 5.16: Quantum yield and gilvin estimates. ....	299
Figure 5.17: Effect of different chlorophyll algorithms on the estimate of $\phi_{est}$ .....	303
Figure 6.1: Correlation coefficient between fluorescence and chlorophyll (see legend). .....	313
Figure I.1: Percent error when using $a(678)$ to approximate the attenuation of upwelling fluorescence radiance at 678 nm (see text for details).....	317
Figure II.1: Three idealized cost-functions for a one dimensional regression. The cost- function (in this chapter the sum of squared differences) is minimum at the best-fit parameter values $\hat{\theta}$ .....	320
Figure II.2: Error ellipses for the fitted parameters taken two at a time on last spectra of the Bering Sea timeseries. The expected correlation coefficient between the two plotted parameters is also provided in each graph.....	321

## *Abstract*

When phytoplankton are bathed in the natural radiance field of the ocean, some of the chlorophyll molecules emit red light in a phenomenon known as sun-induced chlorophyll fluorescence (SICF). In this thesis, I approach the study of SICF from several perspectives. For field studies deploying floating spectroradiometers, an inversion model of reflectance in the fluorescence band is developed and applied. The model is used in two optical regimes: in coastal waters of Nova Scotia, where chromophoric dissolved organic matter absorption was sufficiently high to prevent the retrieval of phytoplankton biomass using standard ocean color algorithms; and in the Bering Sea, where phytoplankton biomass dominated the optical signal. In the first example, the retrieval of phytoplankton biomass was possible using the fluorescence signal corrected for changes in the quantum yield of fluorescence with irradiance. In the second application, the accurate retrieval of phytoplankton absorption from ocean color allowed the quantum yield of fluorescence to be estimated. For global observations of fluorescence from space (i.e., provided by the MODIS spectroradiometer on the Aqua and Terra satellites), I created and applied two algorithms for retrieving the quantum yield of fluorescence or phytoplankton biomass. A comparison with the MODIS chlorophyll data product showed that 86% of the retrievals using the new fluorescence algorithm were within a factor of two of the standard ocean color algorithm. The new algorithm for the quantum yield will be an improvement in regions where the 412 nm band is poorly retrieved, but will perform similarly to the previous algorithm in other regions. Lastly, in a theoretical study I developed a mechanistic model of phytoplankton fluorescence at the level of the chloroplast. This approach reconciles fluorescence emission with photosynthesis and heat dissipation in phytoplankton on timescales varying from seconds to days. The model includes photochemical and non-photochemical quenching, damage and repair of photosystem II (PSII), acclimation of the antenna size of PSII, the ratio of photoprotective to photosynthetic pigments, and nutrient limitation. The results of this thesis should allow better retrieval and interpretation of the physiological and taxonomic information contained in sun-induced fluorescence.

## *List of abbreviations*

Abbreviation	Definition
$Q_A$	First quinone of the photosynthetic electron transport chain
$Q_B$	Second quinone of the photosynthetic electron transport chain
$P_{680}$	Dimer of chlorophyll molecule at the core of photosystem II
$Y_z$	Tyrosine
$q_T$	Quenching of fluorescence due to reduction of excitation energy to PSII
$q_E$	Energy dependent quenching of fluorescence
$q_I$	Quenching due to photoinhibition of photosynthesis
ATP	Adenosine triphosphate
DCMU	Herbicide Diuron; 3-(3,4-dichlorophenyl)-1, 1-dimethylurea
DNA	Deoxyribonucleic acid
FRRF	Fast repetition rate fluorometer
HPLC	High precision liquid chromatography
$I$	Phaeophytin
LHCI, LHCII	Light harvesting complex, for photosystem I and for photosystem II
MERIS	Medium resolution imaging spectrometer
MODIS	Moderate resolution imaging spectroradiometer
NADPH, NADP	Reduced and oxidized form of nicotinamide adenine dinucleotide phosphate
NPQ	Non-photochemical quenching
PAM	Pulse amplitude modulat(ed/ion)
PAR	Photosynthetically available radiation
PQ	Plastoquinone
PSI, PSII	Photosystem I, photosystem II
PSU	Photosynthetic unit
PUR	Photosynthetically utilizable radiation
TSRB	Tethered spectroradiometer buoy
$Y_z$	Tyrosine

# *Acknowledgment*

A doctorate is very much like practicing for soccer, nobody else can do it for you, but without a team accompanying you, you get really tired of it quickly and it becomes meaningless. All the while, in the back of your mind there is always that hope of “playing in the big leagues” one day. I have been lucky to have a very talented, knowledgeable, generous, and friendly group accompanying me through the trials and tribulations of my Ph.D; many of which are A-league players!

First, I have to thank Dr. John Cullen. It must have been somewhat of a shock when I showed up in his lab, with all but no background in biology, and even less knowledge about anything related to the ocean. What I have achieved here — and it goes beyond the content of this thesis — I owe to him. The support he provided throughout my masters and doctorate — as everything else he does — was beyond all expectations. He spared no efforts to ensure that I had all the time, resources, freedom, and opportunities I could have wished for. To be part of John’s lab means that every moment is a learning experience: there is no better way to learn science and “how it should be done” than working, studying, and writing with John. John, if on day I have students, I hope I can provide as much to them as you did for me.

In the first years of my Ph.D., I did not ask much from my committee members, Dr. Douglas Campbell, Dr. Keith Thompson, and Dr. Marlon Lewis. This, however, was the proverbial “calm before the storm”. In the last year the demands I put on them were enormous, to say the least, with short deadlines and thick piles of papers to read. Thank you for keeping up with it all, you made what seemed an impossible timeline back in

February possible by October. All along, it has been nice to feel that you had my success at heart; it has really kept me well on track.

I also want to thank Dr. Warwick Vincent, my external examiner. The version of the thesis he received contained one more chapter than the version you are ~~about to read~~ holding: it was a *very* hefty document and because I have cut every deadline very close he was given little time to read it. When he accepted the responsibility, he could not have known what he was in for. Despite the nearly insurmountable task of just getting through the document, he managed to thoroughly examine it and his suggestions and comments have made for a much better thesis. Thank you!

In my first year I had the opportunity to spend three months with Dr. Patrick Neale at the Smithsonian Environmental Research Center. This was a formidable time! To spend a summer with Pat and his group was an amazing learning experience. I also had the opportunity to embark on two cruises in the Bering Sea. I have to thank Ned Cokelet for this opportunity, and the crew of the Ronald Brown for helping make the cruises so enjoyable and successful.

Many people provided advice, help, or data for this thesis: Marcel Babin, Audrey Barnett, Catherine Brown, Richard Davis, Stephane Kirchhoff, Sam Laney, Ricardo Letelier, Jasmine Nahorniak, Mark Merrimen, Claire Normandeau, Wes Paul, Cathy Ryan, Natasha Rondón, and Tara Tapics. Thank you very much for your help. By listing some, I am bound to forget others, which have been just as important. Please forgive me, your help has, however, has not gone unnoticed and was much appreciated when I received it!

Although I have already thanked them as colleagues, I would also like to give more personal thank to Claire, Steph, and, of course, Guillaume. Your friendship has meant a lot over the past few years.

Finally, I need to thank Catherine (Kitty) Brown. Beyond enduring more reviews of my chapters than anyone, co-authoring papers and posters with me, and collaborating on many other projects, she also married me this summer! This thesis was in more than one way a shared effort. For all the good times past, and those to come, thank you Kitty!

I would like to thank FCAR, NSERC, and DFO for their support through scholarships, the Smithsonian Institution for a Postgraduate fellowship, and NSF for financing the Antarctic Biology Training Course. I would further like to acknowledge the financial support received from funding to Dr. John J. Cullen from: NSERC Research Partnerships with NRC and Satlantic, NSERC Discovery grants, the National Oceanographic Partnership Program, the Canadian Foundation for Climate and Atmospheric Sciences, ONR, and NOAA.

# *Chapter 1 Introduction*

## **1.1 *Phytoplankton physiology and global issues***

Phytoplankton are the ocean's primary producers: they form the basis of nearly all marine food webs. Their growth rate and biomass determine the overall productivity of marine ecosystems, including the biomass of commercially important species. The influence of phytoplankton reaches beyond the marine ecosystem. Since phytoplankton are responsible for nearly half of all carbon fixed by primary producers on earth (Field et al. 1998), they play a central role in the earth's carbon cycle and have a potentially important role in mediating present and future climate change (Chisholm et al. 2001; Geider et al. 2001). We have long known, however, that assessing the impact of phytoplankton requires going beyond measuring biomass to quantifying their physiological state, on which their growth rates depends (Geider et al. 1998). Thus, to advance our understanding of how marine ecosystems will respond to — or mediate — global problems such as climate change (Houghton et al. 2001) and declining fish stocks (Myers and Worm 2003), we need to quantify phytoplankton processes on global scales.

Tremendous progress has been made in the past 30 years in understanding global marine ecosystems (e.g. Longhurst 1996). Much of this progress has been driven by satellite remote sensing. Since the launch of the Coastal Zone Color Scanner (CZCS) satellite in 1978, we have been able to obtain global estimates of phytoplankton biomass. However, quantifying the physiology of phytoplankton remotely has

remained elusive, and we have continued to rely on ship-based measurements. Very recent developments cast new light on the problem, providing hope of further understanding phytoplankton physiology globally and remotely through a better description of the species composition (Alvain et al. 2004), their stoichiometry (Behrenfeld et al. in press). In addition, one of the most promising technological advance to understand phytoplankton physiology globally has been the recent addition on satellites of spectral bands allowing the detection of sun-induced chlorophyll fluorescence (Gordon 1979). While chlorophyll fluorescence has long been known to provide information about the physiology of plant and algae (Govindjee 1995 and references therein), we have presently little basis for interpreting the satellite measurement of sun-induced fluorescence (Abbott and Letelier 1999). This thesis focuses on this measurement and its interpretation.

## **1.2 *Fluorescence and oceanography***

When phytoplankton absorb light, a portion of the absorbed energy is used in photosynthesis, another portion is dissipated as heat, the remainder, which is a small but variable fraction, is re-emitted as fluorescence, observable as a dim red glow. Despite its dimness, the fluorescence signal is one of our most powerful probes of phytoplankton photosynthesis and physiology. This signal can be observed actively by modifying the incident irradiance with an artificial light source to measure specific aspects of the emission, or observed passively by measuring the amount of light fluoresced under natural lighting conditions. Studies of active fluorescence have led to leaps in our

understanding of photosynthesis (Butler 1978; Govindjee 1995; Falkowski and Raven 1997; Joliot and Joliot 2003). In the ocean, the observation of passive fluorescence has been proposed as a way to measure chlorophyll concentration (e.g. Neville and Gower 1977; Kiefer et al. 1989; Fisher and Kronfeld 1990; Cullen et al. 1997; Coleman et al. 2000; Fell et al. 2000) and primary productivity (e.g. Topliss and Platt 1986; Kiefer et al. 1989; Chamberlin et al. 1990; Chamberlin and Marra 1992). However, fluorescence emission is also dependent on biochemical and biophysical processes within the cell which is itself influenced by interactions with the environment, and, consequently, extracting information from the fluorescence signal is not a simple endeavor (Lazár 1999; Maxwell and Johnson 2000).

Active fluorescence can be measured at sea, using both *in situ* profiling fluorometers as well as on-board fluorometers in a flow-through mode or configured for processing discrete samples. Although caution is required when interpreting depth profiles or time series obtained from fluorometers (Strickland 1968; Maerker and Szekiolda 1976; Slovacek and Hannan 1977; Cullen 1982; Ostrowska et al. 2000a; Ostrowska et al. 2000b; Cullen and Davis 2003), fluorescence is probably the best method to estimate quasi-synoptically *in situ* chlorophyll concentration (one index of autotrophic biomass) on short temporal or spatial scales, especially in oligotrophic areas. In addition to providing estimates of chlorophyll concentration, active fluorometry allows the estimation of the photosynthetic efficiency of the phytoplanktonic assemblage (Butler 1978; Vincent 1981; Genty et al. 1989) and parameters related to the dissipation of heat (Schreiber et al. 1986). However, until recently, only benchtop fluorometers could

measure these parameters (Falkowski and Kolber 1995). The recent development of the pump and probe (Kolber and Falkowski 1993) and the Fast Repetition Rate Fluorometer (Falkowski and Kolber 1995; Kolber et al. 1998) (FRRF, see List of abbreviations at the front of the thesis) which are sufficiently sensitive to make measurements on open-ocean concentrations of chlorophyll *a* (*chl*, mg chl  $\text{m}^{-3}$ ), has allowed *in situ* estimation of some photosynthetic parameters.

Sun-induced or passive fluorescence can also be measured at sea (Morel and Prieur 1977) using profiling (e.g. Topliss and Platt 1986; Kiefer et al. 1989; Chamberlin et al. 1990; Chamberlin and Marra 1992; Garcia-Mendoza and Maske 1996; Maritorena et al. 2000) and floating radiometers (e.g. Cullen et al. 1997; Letelier et al. 1997) or from radiometers on moored buoys (Abbott et al. 2000). From these measurements, by dividing the measured fluorescence signal by an estimate of the amount of light absorbed by phytoplankton (Cullen et al. 1997; Abbott and Letelier 1999; Maritorena et al. 2000; Morrison 2003) an apparent fluorescence yield can be obtained. In surface waters, however, this signal is strongly influenced by non-photochemical processes that divert energy away from the fluorescing pigments (for example through increased dissipation of absorbed energy as heat), which complicates interpretation (Cullen and Lewis 1995; Cullen et al. 1997).

Fluorescence, photosynthesis, and heat dissipation are competitive and mutually exclusive processes, and it is possible to derive models relating the yield of one process to the others (e.g. Butler 1978; Havaux et al. 1991; Lavergne and Trissl 1995). Given these relationships, profiles of fluorescence yield have been used to estimate primary

production (Topliss and Platt 1986; Kiefer et al. 1989; Chamberlin et al. 1990; Chamberlin and Marra 1992; Garcia-Mendoza and Maske 1996); at least one commercially available instruments has a built-in algorithm to estimate photosynthesis from a single cast (for a critique of the method see Kolber and Falkowski 1993). This is a rather fantastic claim considering that the following variables all contribute to variability in the measured signal: light history (e.g. due to mixing, waves, sun angle and cloud cover variations, Ögren 1994) and light intensity (diel, seasonal, e.g. Kiefer 1973a; Kiefer and Reynolds 1992; Kolber and Falkowski 1993; Ibelings et al. 1994); physiological status (nutrients, temperature, e.g. Kiefer 1973a; Cleveland and Perry 1987); the taxonomy of the phytoplankton (Heaney 1978; Campbell et al. 1998); and processes such as Raman scattering and backscattering (Maritorena et al. 2000; Morrison 2003).

Sun-induced fluorescence can also be measured by remote sensing from aircraft (Neville and Gower 1977; Gower et al. 1999; Fell et al. 2000) and satellites (Abbott and Letelier 1999; Gower et al. 1999). Recently, the Moderate Resolution Imaging Spectroradiometer (MODIS) has been launched on the Terra (EOS AM, December 1999) and AQUA (EOS PM, May 2002) platforms (Esaias et al. 1998). One band (two other bands are used during processing) is dedicated to the observation of chlorophyll fluorescence. In addition, in January 2002 the platform Envisat was launched with the Medium Resolution Imaging Spectroradiometer (MERIS) on board with one band dedicated to measuring passive fluorescence. By measuring the fluorescence signal, these satellites may provide unprecedented information about the physiological state of phytoplankton in synoptic images with tremendous potential to enhance our

understanding of phytoplanktonic processes in the global ocean. However, the optimal utilization of these resources will depend on our ability to interpret the observations correctly, and much work remains to be done to reach this goal. In a document outlining the theoretical bases and methods to be used with the MODIS satellite data, Abbott and Letelier (1999) write: "Understanding the variability of the chlorophyll natural fluorescence due to changes in phytoplankton physiology is a critical step in the interpretation of changes observed in the fluorescence line height". Clearly, this step has yet to be taken. The lack of a proper scientific foundation is compounded by the fact that the near-surface layer of the ocean, from which all remote sensing fluorescence signals originate, is much more complex compared to deeper water due to its high variability on multiple time scales (Cullen et al. 1997; Abbott and Letelier 1999; Maritorena et al. 2000). Furthermore, there has been a limited amount of laboratory work done at high irradiances suitable to compare with in situ results.

### **1.3 Thesis outline**

The objective of the research presented in this thesis is to provide some of the necessary information to measure and interpret the fluorescence signal, particularly the sun-induced fluorescence signal, at the surface of the ocean in situ or under remote sensing conditions. I will focus mainly on two key aspects:

- 1) The measurement and extraction of valuable information from the fluorescence signal in situ, and from remote sensing conditions.*
- 2) The interpretation of this information in surface waters using a new model of fluorescence.*

In the next chapter, I will introduce the basic concepts and relationships used in fluorescence work and provide some background on fluorescence measurements. Sections 2.1 and 2.2 are written to give a general overview of the history and fundamental concepts used in sun-induced fluorescence. Sections 2.3 to 2.9 will provide further background information to a reader not familiar with chlorophyll fluorescence and will aid their understanding of the main chapters of the thesis. Concepts reviewed in these sections will be assumed known to readers of subsequent chapters.

Chapter 3 will describe a new mechanistic model of fluorescence and photosynthesis that is designed to be used in mixing models of the ocean. This model attempts to provide a framework for understanding the links between fluorescence, photosynthesis, photoacclimation and nutrient stress under any irradiance level and on timescales from seconds to days.

Chapter 4 examines the retrieval of the fluorescence signal from a tethered spectroradiometer buoy. A fluorescence model is developed to take into account the particular geometry of the instrument. Two examples of utilization of the model are given. The first is from coastal waters heavily influenced by colored dissolved organic matter where fluorescence is used to retrieve phytoplankton absorption. The second is from the Bering Sea where rapid changes due to non-photochemical quenching are observed in the fluorescence signal and changes in the quantum yield of fluorescence are retrieved.

Chapter 5 describes new models to retrieve and analyze the fluorescence signal from remote sensing measurements in open ocean waters. The model is adapted to the

characteristics of the MODIS sensors and provides a method to retrieve the quantum yield of fluorescence or the chlorophyll concentration. This chapter also takes a critical look at the baseline method used by the standard MODIS algorithm.

Chapter 6 provides the general conclusions of the thesis, and suggests future directions for work with sun-induced fluorescence.

## *Chapter 2 Background*

This chapter provides some background on fluorescence for readers not familiar with this area of research. The first two sections are a general overview of the history and basic concepts while the following sections provide a more in depth discussion of the current state of knowledge on this topic as it relates to oceanographic work.

### **2.1 *A short historical perspective***

This section is not meant to be a comprehensive or exhaustive history of fluorescence in oceanography. Instead, it is intended to be a succinct description of the origins of fluorescence measurements in the ocean and will concentrate on some of the pioneering work in various aspects of the field.

#### **2.1.1 In the beginning...**

As reviewed by Govindjee (1995), chlorophyll fluorescence was first reported in 1834 by Sir David Brewster, a Scottish priest who observed alcohol extracts of laurel leaves in sunlight. We owe the term fluorescence (coined in 1852) to G.G. Stokes, as well as the recognition that it is in fact due to light *emission*. Stokes is also credited with the discovery of chlorophyll *a* fluorescence in fresh red algae. Prior to his discovery, fluorescence from quinine sulfate solutions had been attributed to “epipolic dispersion”, “internal dispersion” or “dispersive reflexion”.

The first insight into the possibility of using the fluorescence signal to obtain information about photosynthetic processes came in a paper by Kautsky and Hirsch in

1931 (“Neue Versuche zur Kohlensäurassimilation”, or, as translated in English: “New experiments on carbon dioxide assimilation”). Using only their eyes to observe the emission, they related qualitatively the temporal variation in the fluorescence signal to the rate of CO<sub>2</sub> assimilation published elsewhere.

### **2.1.2 Active fluorescence in oceanography**

In an oceanographic context, fluorescence as a method to measure chlorophyll concentration in extracts was introduced by Yentsch and Menzel (1963). Prior to that, colorimetric methods were used (Krey 1958) that were much less sensitive. Three years later, Lorenzen (1966) described a method for continuous measurement of chlorophyll concentration *in vivo* by flow-through fluorometry. These methods are still used routinely today, with little change, to measure chlorophyll concentrations at sea (e.g. Arar and Collins 1997; Dandonneau and Neveux 1997).

Later on, manipulation of the physiological state of phytoplankton using herbicides (e.g. Samuelsson and Öquist 1977; Samuelsson et al. 1978; Cullen and Renger 1979; Roy and Legendre 1979; 1980; Vincent 1981) and the recording of fluorescence observations led to further understanding of the photosynthetic apparatus. Improvements in methods in the 1980's and 1990's brought the development of a suite of new fluorometers. By solely manipulating the light field incident on the algae, and observing the effect it has on the fluorescence originating from known states of the reaction centers (open or closed), these instruments provide a large amount of physiological information non-intrusively (Schreiber et al. 1986; Falkowski and Kolber 1993; Kolber and Falkowski 1993; Kolber et al. 1998).

### 2.1.3 *Passive fluorescence in oceanography*

Maritorena and colleagues (2000) suggest that the first measurement of passive fluorescence *in situ* was made in 1966 by Tyler and Smith (1970) in the San Vicente reservoir using the Scripps spectroradiometer. This signal, however, was not recognized as fluorescence. It was Gordon (1974) who asserted that the peak centered at around 685 nm in the irradiance reflectance spectrum multiplied by the attenuation coefficient from the data of Tyler and Smith (1970) was “anomalous dispersion” due to chlorophyll absorption:

“I present this as direct evidence that chlorophyll absorption at 670 nm in marine phytoplankton can cause sufficient variation of the real part of the refractive index of the particles to give rise to observable scattering effects.”

Five years later, prompted by papers by Morel and Prieur (1977) and Neville and Gower (1977) measuring reflectance, Gordon (1979) wrote the following in the introduction to a paper laying out the radiative transfer theory for chlorophyll fluorescence in water:

“It will be shown that it is possible to explain the observed enhancement of the diffuse reflectance near 685 nm completely in terms of the *in vivo* fluorescence of chlorophyll *a*, which suggests that the anomalous dispersion explanation is probably not correct.”

Neville and Gower (1977) used measurements from overflights of spectral reflectance to show that the height of the peak observed at 685 nm (they were not sure at

that time if it was fluorescence or anomalous dispersion) was strongly correlated with chlorophyll concentration in Saanich Inlet. Their paper was the first to demonstrate the possibility of using sun-induced fluorescence in reflectance spectra to determine chlorophyll concentration. Furthermore, they measured fluorescence remotely.

The idea of using natural chlorophyll fluorescence to measure photosynthesis has been assessed by different groups in the late 1980's and early 1990's (Topliss and Platt 1986; Kiefer et al. 1989; Chamberlin et al. 1990; Chamberlin and Marra 1992; Kiefer and Reynolds 1992; Stegmann et al. 1992). The method continues to be used with variable levels of success (e.g. Lizotte and Priscu 1994; Garcia-Mendoza and Maske 1996; Yoshikawa and Furuya 2004).

On the 18<sup>th</sup> of December 1999, MODIS TERRA was launched providing the first images from space of fluorescence. Figure 2.1 shows one of those scenes; NASA's interpretation (<http://visibleearth.nasa.gov/cgi-bin/viewrecord?848>) of the ratio of fluorescence line height to chlorophyll concentration was the following:

“A high ratio implies lower growth rates. That is, light is being captured by phytoplankton but they are re-emitting it as fluorescence rather than using it for photosynthesis. The cooler colors represent higher growth rates. Phytoplankton in the Arabian Sea are probably growing more rapidly than elsewhere, perhaps in response to dust inputs (which are rich in iron) from the Arabian Peninsula.”

The simplicity of this interpretation is somewhat misleading. While it may be

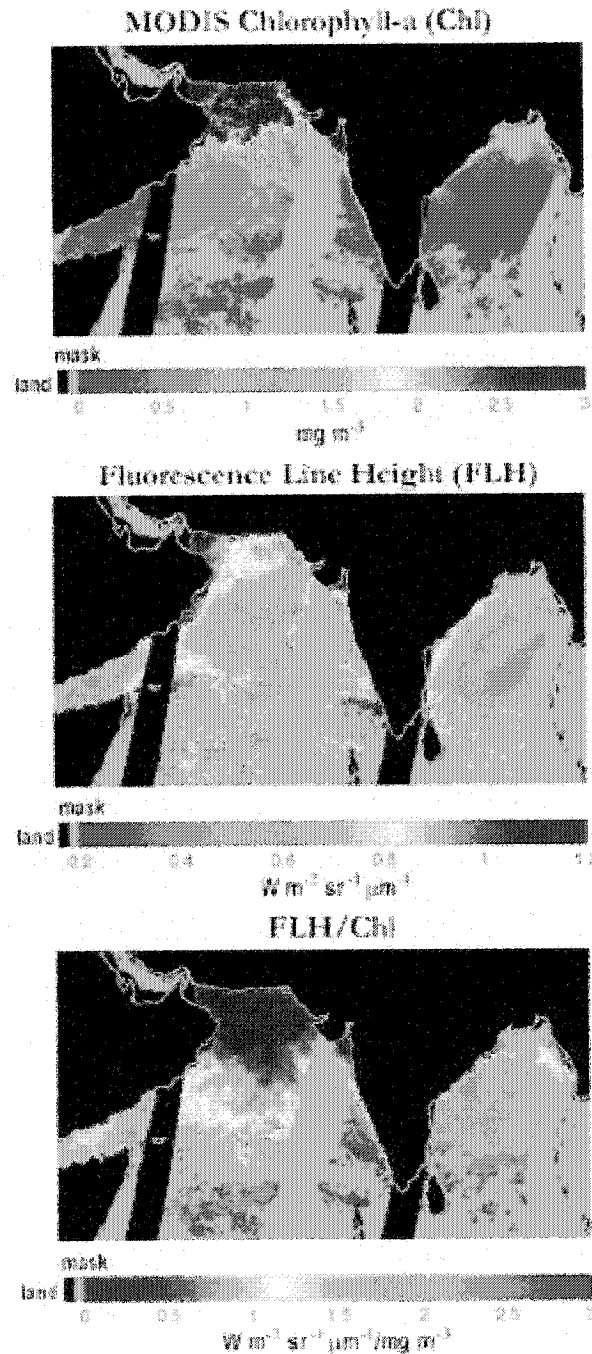


**Figure 2.1: MODIS images of chlorophyll concentration, fluorescence line height (total radiance minus background radiance not due to fluorescence) and ratio of fluorescence to chlorophyll (index of fluorescence efficiency). Figures modified from The Visible Earth webpage (<http://visibleearth.nasa.gov/cgi-bin/viewrecord?848>).**

correct, it is only one of several possible interpretations given our present understanding of sun-induced fluorescence.

## 2.2 Key concepts in sun-induced fluorescence

Section 2.2 provides a “short-cut” through the background material by providing an overview of important concepts. After reading section 2.2 a reader not interested in a more detailed discussion, should skip sections 2.3 to 2.9 and go directly to chapter 3.

### 2.2.1 Mathematical description and variables of interest

In this section, I define terms and provide some basic relationships within a simplified context to describe sun-induced fluorescence emission. Points made here are not referenced, as they will be thoroughly examined later.

The upwelling radiance at 683 nm,  $L_u$  ( $\mu\text{mol m}^{-2} \text{s}^{-1} \text{nm}^{-1} \text{sr}^{-1}$ , see Table 2-1 for a list of symbols and units), measured at a given depth ( $z_{\text{sens}}$ , m) is the sum of the backscattered radiance,  $L_{ub}(683, z_{\text{sens}})$  ( $\mu\text{mol m}^{-2} \text{s}^{-1} \text{nm}^{-1} \text{sr}^{-1}$ ) and the radiance due to chlorophyll fluorescence<sup>1</sup>  $L_{uf}(683, z_{\text{sens}})$  such that,

$$L_u(683, z_{\text{sens}}) = L_{ub}(683, z_{\text{sens}}) + L_{uf}(683, z_{\text{sens}}). \quad 2.1$$

In practice, the backscattered radiance can be removed from the radiance signal and the portion due to fluorescence isolated. Using principles of ocean optics, it can be shown that the fluorescence radiance can be described as

---

<sup>1</sup> In reality, other sources like Raman scattering and fluorescence from other fluorophores also contribute to the signal, but their contribution is in most cases small or can, for the purposes of this analysis, be included in the  $L_{ub}$  term.

Table 2-1: List of symbols and units

Symbol	Definition	Units
$a$	Absorption coefficient	$\text{m}^{-1}$
$a_{\varphi}^*, \bar{a}_{\varphi}^*$	Chlorophyll specific absorption coefficient and average weighted chlorophyll specific absorption coefficient	$\text{m}^2 (\text{mg chl})^{-1}$
$a_{sol}^*$	Chlorophyll specific absorption coefficient for a solution of chlorophyll	$\text{m}^2 (\text{mg chl})^{-1}$
$A$	Proportion of open reaction centers	Unitless
$C_f$	Fraction of fluorescence emission at the observed wavelength	$\text{nm}^{-1}$
$chl$	Concentration of chlorophyll a	$(\text{mg chl}) \text{m}^{-3}$
$E_d$	Downwelling irradiance	$\mu\text{mol m}^{-2} \text{s}^{-1} \text{nm}^{-1}$
$\overset{o}{E}$	Scalar irradiance	$\mu\text{mol m}^{-2} \text{s}^{-1}$ if spectral: $\mu\text{mol m}^{-2} \text{s}^{-1} \text{nm}^{-1}$
$E_k$	Saturation irradiance for photosynthesis. Equal to the irradiance at which the maximal gross photosynthesis and straight line passing through 0 with a slope equal to the initial slope of a PvsE curve intercept.	$\mu\text{mol m}^{-2} \text{s}^{-1}$
$\overset{o}{E}_{PAR}$	Scalar irradiance in the 400 to 700 nm region	$\mu\text{mol m}^{-2} \text{s}^{-1}$
$F_o, F_m, F_v$	Minimum, maximum and variable fluorescence in the dark acclimated state $F_v = F_m - F_o$	Unitless
$F_o', F_m', F'$	Minimum, maximum and realized fluorescence in the light acclimated state	Unitless
$F_{DCMU}$	Fluorescence measured in the presence of DCMU (roughly equal to $F_m$ )	Unitless
$f$	Babin et al. function of nutrients and irradiance	Unitless
$K_d, \bar{K}_{PAR}$	Diffuse attenuation coefficient and average diffuse attenuation coefficient for PAR	$\text{m}^{-1}$
$k_x$	Rate constant, where $x$ can be $T$ =transfer of energy from antenna to RC, $F$ =fluorescence, $D$ =non-radiative decay, $t$ =transfer from RC to antenna, $d$ =non-radiative decay within the RC, $p$ =charge stabilization, $A$ = all radiationless decay	$\text{s}^{-1}$
$L_u$	Upwelling radiance	$\mu\text{mol m}^{-2} \text{s}^{-1} \text{nm}^{-1} \text{sr}^{-1}$

$L_{uf}$	Upwelling radiance due to fluorescence emission	$\mu\text{mol m}^{-2} \text{ s}^{-1} \text{ nm}^{-1} \text{ sr}^{-1}$
$L_{ub}$	Upwelling radiance due to backscattering	$\mu\text{mol m}^{-2} \text{ s}^{-1} \text{ nm}^{-1} \text{ sr}^{-1}$
$n_{PSII}$	Ratio of PSII reaction centers to chlorophyll a molecules	$\text{mol electrons (mol chl a)}^{-1}$
$N_{S_1}$	Number of molecule in the first excited singlet state	Unitless
$N_{status}$	Nutritional status of the phytoplankton community, defined as the ratio of the nutrient limited growth rate to the maximal growth rate	Unitless
$NPQ_f$	Non-photochemical quenching parameter $0 \leq NPQ_f \leq \infty$	Unitless
$p$	Connectivity parameter ( $0 < p < 1$ )	Unitless
$P_f^B$	Fluorescence based photosynthetic rate	$\text{electrons chl}^{-1} \text{ s}^{-1}$
$Q_a^*$	Portion of fluorescence emission not reabsorbed within the cell	Unitless
$q_{CN}$	Complete non-photochemical quenching; $0 \leq q_{CN} \leq 1$	Unitless
$R_{rs}$	Remote sensing reflectance	$\text{sr}^{-1}$
$z$	Depth	m
$\phi_e$	Quantum yield of electron transport	Unitless
$\phi_{F_x}$	Fluorescence yield in the dark acclimated state, where $x$ can be $m$ =maximum, $o$ =minimum	$\frac{\text{(Photons emitted)}}{\text{(Photons absorbed)}}^{-1}$
$\phi'_{F_x}$	Fluorescence yield in the light acclimated state, where $x$ can be $m$ =maximum, $o$ =minimum	$\frac{\text{(Photons emitted)}}{\text{(Photons absorbed)}}^{-1}$
$\phi_f, \bar{\phi}_f$	Quantum yield and average quantum yield of fluorescence	$\frac{\text{(Photons emitted)}}{\text{(Photons absorbed)}}^{-1}$
$\phi_p, \phi_p^{\max}$	Quantum yield and maximum quantum yield of photochemistry	$\frac{\text{(Moles product)}}{\text{(Moles photons absorbed)}}^{-1}$
$\Phi_f$	Fluorescence photon flux emitted from an elementary volume per unit volume	$\mu\text{mol photons m}^{-3} \text{ s}^{-1} (\text{nm}^{-1} \text{ is spectral})$
$\gamma$	Geometrical factor relating the fluorescence emission to fluorescence measured by a fluorometer	Unitless
$\Psi_x$	Butler model probability, where $x$ can be $T$ =trapping excitation energy by the RC, $P$ =photochemistry once the RC is in excited state, $F$ =fluorescence from antenna	Unitless

$\psi_{xy}$	Kiefer and Reynold probability, where $x$ can be $cs$ =charge separation, $cr$ =charge recombination, $F$ =fluorescence or $d$ =non-radiative deactivation, while $y$ can be $o$ =open or $s$ =shut (closed)	Unitless
$\kappa_u$	Attenuation coefficient for upwelling radiance	$m^{-1}$
$\lambda, \lambda_{ex}, \lambda_{em}$	Wavelength, excitation irradiance wavelength, nm emission irradiance wavelength	
$\mu, \mu_{max}$	Growth rate and maximal growth rate	$d^{-1}$
$\sigma_{PSII}$	Functional absorption cross section for PSII	$m^2(\mu mol \text{ photons})^{-1}$
$\tau_{co_2}$	Turnover time for photosynthetic apparatus	s
$\tau_{S_1}$	Lifetime for the deexcitation of the first singlet state	s
$\tau_o$	Intrinsic lifetime for the deexcitation of fluorescence	s
$\tau_x$	Lifetime for the deexcitation of fluorescence	s

---

$$L_{uf}(683, z_{sens}) = \frac{1}{C_f 4\pi} \underbrace{\varphi_f}_{\text{Quantum yield}} \underbrace{\overset{\circ}{E}_{PAR}(z_{sens})}_{\text{Absorbed irradiance at depth } z_{sens}} \underbrace{chl \bar{a}_\phi^* Q_a^*(683)}_{\text{Portion not reabsorbed within the cell}} \underbrace{\frac{1}{\bar{K}_{PAR} + \kappa_u(683)}}_{\text{Attenuation of exciting and emitted radiance}}, \quad 2.2$$

Emission at 683 nm  
 Ratio of total to 683 nm emission  
 Geometrical factor  
 Absorbed irradiance at depth  $z_{sens}$   
 Attenuation of exciting and emitted radiance

where  $C_f$  is a constant relating the emission at 683 nm to the whole fluorescence band,

$\varphi_f$  is the quantum yield of fluorescence,  $\overset{\circ}{E}_{PAR}$  is the photosynthetically available scalar irradiance,  $chl$  is the chlorophyll concentration,  $\bar{a}_\phi^*$  is the mean chlorophyll specific absorption coefficient of phytoplankton weighted by the irradiance spectrum,  $Q_a^*$  is the portion of irradiance emitted by fluorescence and not reabsorbed within the cell,  $\bar{K}_{PAR}$  is the depth averaged attenuation coefficient for  $\overset{\circ}{E}_{PAR}$ , and  $\kappa_u(683)$  is the attenuation coefficient for upwelling radiance at 683 nm.

Equation 2.2 is usually solved two parameters, one at a time (all other parameters are estimated or measured): 1) chlorophyll concentration when an estimate of biomass is sought or 2) the quantum yield of fluorescence when information about the physiology of phytoplankton is sought. In the latter case, this is because most of the physiological information present in the fluorescence signal is contained in  $\varphi_f$ , but physiological changes in  $\bar{a}_\phi^*$  and  $Q_a^*$  also occur. Nevertheless, in most cases,  $\varphi_f$  is the parameter that we hope to retrieve and interpret. The estimates of the other variables in equation 2.2 can be done *in situ* and in the lab, or alternatively estimates can be obtained from remote

sensing algorithms and models. Once  $\varphi_f$  is measured the next step is to interpret it.

### 2.2.2 The quantum yield of fluorescence

The quantum yield of fluorescence,  $\varphi_f$ , is defined as the number of photons emitted (at all wavelengths) divided by the number of photons absorbed by the fluorescing system. In the ocean, the fluorescing system could be an assemblage of cells, a single cell or a portion of a cell such as photosystem II. It is worth noting that, in phytoplankton, the fluorescing molecules are only a fraction of the cellular pigments; only chlorophyll and phycobilins fluoresce significantly, though many pigments can contribute to the excitation energy of the fluorescing pigments. This is different from many other fluorescing systems. For an optically thin fluorophore, the relationship between the photon flux emitted per unit volume ( $\Phi_f$ ,  $\mu\text{mol photons m}^{-3} \text{ s}^{-1}$ ) and the quantum yield is given by  $\Phi_f = \varphi_f a \bar{E}$ , where  $a$  ( $\text{m}^{-1}$ ) is the absorption coefficient, and

#### Box 1: Nutritional status ( $N_{\text{status}}$ ) and growth rate ( $\mu$ )

Following the review by Parkhill et al. (2001) important distinctions have to be made regarding the growth conditions and nutrient status of phytoplankton.

When nutrients are available in concentrations that do not limit the growth rate and other environmental factors are constant, the physiological condition is said **nutrient replete** and phytoplankton assume **balanced growth**. That is, over a daily cycle the growth rate will be the same if measured by the concentrations of different cellular components (e.g. DNA, chlorophyll, carbon).

When a nutrient is limiting growth, the physiological condition of phytoplankton is said to be **nutrient stressed**. This refers to two nutritional states: **nutrient limitation** and **nutrient starvation**. In the former, a nutrient is in short supply, but the fluxes are steady and sufficient to allow the phytoplankton to assume a balanced, albeit reduced, growth rate. Under nutrient starvation, the availability of the nutrient decreases with time relative to the demand so that phytoplankton cannot acclimate physiologically and their **growth is unbalanced**. However, unbalanced growth is not limited to the state of starvation and will occur whenever the nutritional status changes, for example during acclimation to other environmental changes.

$\bar{E}^0$  ( $\mu\text{mol photons m}^{-2} \text{ s}^{-1}$ ) is the scalar irradiance. The symbol  $F$  (usually in relative units) is often used to represent the portion of  $\Phi_f$  measured by a fluorometer. The quantum yield of fluorescence *in vivo* is highly variable depending on the conditions of observation, the physiological status of the algae and the species observed. The focus of this thesis is the measurement of fluorescence made passively at the surface of the ocean. These measurements represent the fluorescence yield of the whole phytoplankton community as influenced by the nutrient status of the community,  $N_{\text{status}}$  (unitless) and the irradiance history (see for example Neale and Marra 1985),  $E_{\text{hist}}$ :

$$\phi_f(N_{\text{status}}, E_{\text{hist}}, \text{species}).$$

In steady state cultures,  $N_{\text{status}}$  can conveniently be described by the ratio of the nutrient limited growth rate to the maximal growth rate,  $\mu/\mu_{\text{max}}$  (see box 1). It is not as straightforward to describe the nutrient status in the natural environment as different species forming the community at a given time may have a different nutrient status. The influence of the nutrient status on the quantum yield of fluorescence will most likely occur in one of two ways: 1) through a change in the capacity of the cell to quench the fluorescence emission and/or 2) a change in the stoichiometry of pigments within the cell.

#### 2.2.2.1 Quenching

Any process reducing the quantum yield of fluorescence is referred to as quenching. *In vivo*, two types of quenching have been described: photochemical and non-photochemical quenching.

*Photochemical quenching* — Photochemical quenching is due to the

photosynthetic utilization of the absorbed energy: because energy must be conserved, absorbed photons going to photosynthetic processes cannot be fluoresced and vice versa. Under saturating irradiance, photosynthetic reaction centers are closed (electron acceptors are reduced) and photochemical quenching is minimal; in turn, the quantum yield of fluorescence is maximal ( $\phi'_{F_m}$  with associated  $F'_m$ ). Under low irradiance, reaction centers are open, photochemical quenching is maximal, and the fluorescence quantum yield is minimal ( $\phi'_{F_o}$  with associated  $F'_o$ ). These changes allow information about the photosynthetic capacity to be obtained using fluorescence.

*Non-photochemical quenching* — Non-photochemical quenching refers to the reduction of the fluorescence quantum yield due to all processes that are not photosynthetic. This includes many processes with different time scales of response to changes in irradiance. The extent of quenching under a given irradiance level will depend on species and light history. Non-photochemical quenching will alter the inverse relationship described above between photosynthesis and fluorescence: an increase in non-photochemical quenching leads to a decrease in both  $\phi_f$  and the quantum yield of photosynthesis.

### **2.3 The photosynthetic apparatus and fluorescence**

Because fluorescence and photosynthesis are intimately linked, it is almost impossible to discuss one without the other and this requires a considerable amount of terminology. The photosynthetic apparatus is composed of two reaction centers acting in series, the well recognized Z-scheme (e.g. Clayton 1980; Falkowski and Raven 1997; Hall and Rao 1999), to transform electromagnetic energy into chemically stored energy

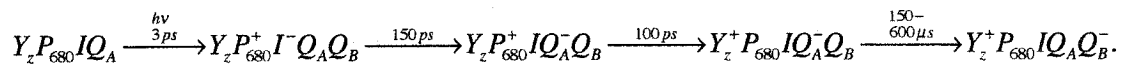
(Figure 2.2). These reaction centers are embedded in the thylakoid membrane inside the chloroplast, the center of all photosynthesis in eukaryotic cells.

Each reaction center is composed of two proteins, which act as a scaffolding for the molecules responsible for the transformation of electromagnetic energy into chemical energy. In higher plants, photosystem II, the first of the two photosystems in the chain, is responsible for a large fraction of chlorophyll fluorescence emitted at room temperature (e.g. Govindjee 1995; Pfündel 1998). It is composed of the proteins D1 and D2 as well as a series of molecules participating in the electron transport chain, including four Mn atoms, a tyrosine ( $Y_z$ ), a chlorophyll dimer ( $P_{680}$ ), a phaeophytin ( $I$ ), and two quinones,  $Q_a$  and  $Q_b$ . In addition, the reaction center is linked to a fixed core antenna of light-absorbing chlorophyll-protein complexes (including the minor chlorophyll protein, CP43 and CP47). Another group of chlorophyll-protein complexes and accessory pigments forms the peripheral antenna (often called the light harvesting complex, LHC), which is not directly embedded into the same protein matrix, and funnels its excitation energy to the reaction center. Unlike the core antenna, the peripheral antenna can sometimes separate from the reaction center (Gilmore and Govindjee 1999).

When the antenna chlorophyll or the core chlorophyll absorbs light energy, the chlorophyll molecule's electronic and vibrational state changes and an exciton is created. This exciton is thought to equilibrate rapidly among the many chlorophyll molecules surrounding the reaction center and the PSII reaction center's own chlorophylls, the special pair of chlorophyll molecules referred to as  $P_{680}$  (Trissl 1999). The lifetime of this exciton is finite and if it is not transferred to another acceptor (and eventually

“stabilized”), the relaxation of the energy will lead to fluorescence or heat. However, often during its residence on  $P_{680}$ , the excited chlorophyll dimer will transfer one of its electrons to the first electron acceptor, phaeophytin  $a$  ( $I$ ). This process is called charge separation and leads to the formation of a (reversible) radical pair:  $P_{680}^+$  and  $I^-$ .

Phaeophytin  $a$  is often called an intermediate electron acceptor due to the short lifetime of its radical state, and its role is to pass the electron to the first quinone ( $Q_A$ ). At this point, the charge is said to be stabilized or trapped as this excited state is long lived and the probability of charge recombination with  $P_{680}^+$  is much decreased. The  $P_{680}^+$ , which is in an oxidized state, will then be reduced by the transfer of an electron from a tyrosine ( $Y_z$ ) on the donor side of photosystem II (not shown on Figure 2.2). The tyrosine obtains the electron from the manganese complex, which after four photochemical cycles oxidizes two water molecules leading to the evolution of a di-oxygen molecule. Later  $Q_A$  will pass its electron to the second quinone ( $Q_B$ ). The whole reaction can be written as:



The last step of the reaction is much slower, hundreds of microseconds compared to hundreds of picoseconds for the previous ones. When excitons are created at a high rate, this step acts as a bottleneck.

When  $Q_A$  is oxidized, photochemistry can proceed from the absorption of photons

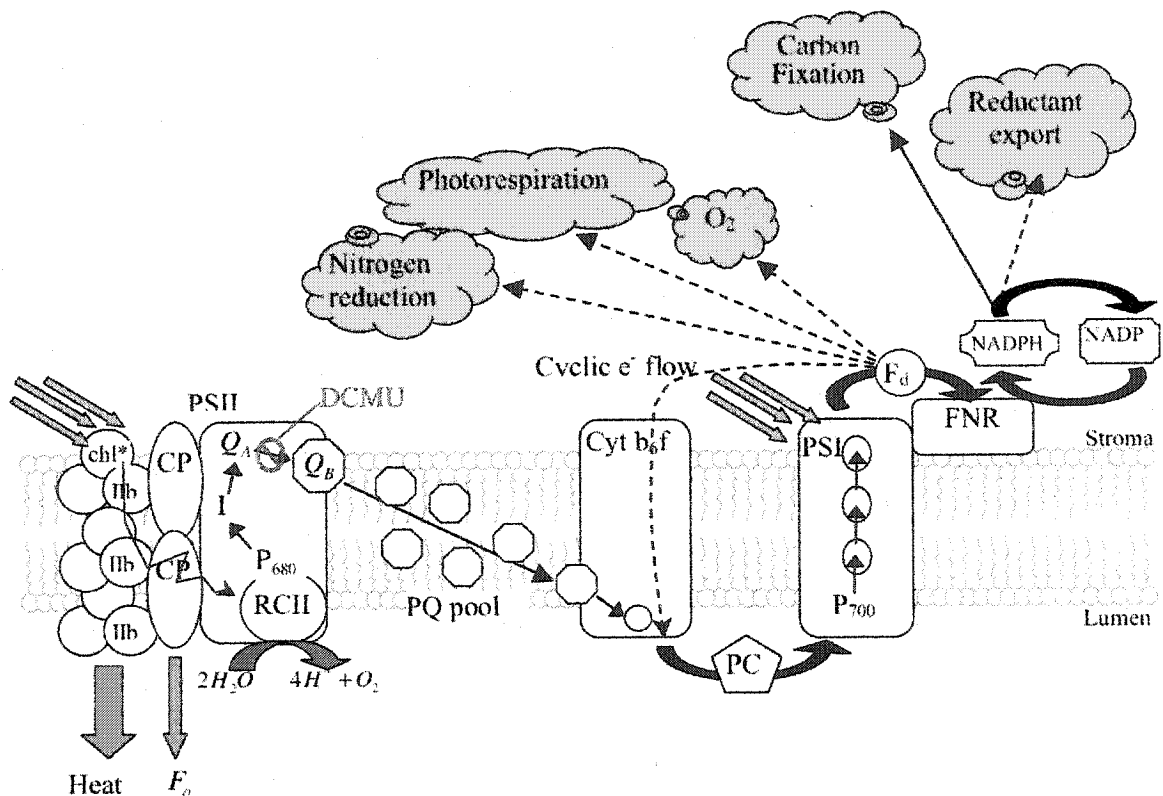


**Figure 2.2:** The Z-scheme provides a mechanism through which energy from sunlight is used to oxidize a water molecule on the donor side of photosystem II and ultimately reduces a  $CO_2$  molecule on the acceptor side of PSI (carbon fixation). On the left of the figure, photosystem II is represented with two minor chlorophyll protein complexes (CP) and trimeric LHCII (IIb) complexes attached. On the right is located the PSI complex with the attached Ferredoxin/NADP<sup>+</sup>/ oxidoreductase (FNR), but without its light harvesting complex. In between PSII and PSI the cytochrome  $b_6/f$  (Cyt  $b_6/f$ ) complex is represented. The red arrows represent the path of energy that leads to linear electron flow and carbon fixation. The dashed red arrows represent the alternate use of reducing power from the donor side of PSI. The orange arrows represents the incident irradiance while the green arrows represent alternate sinks for the absorbed energy within PSII. Adapted from (Kolber and Falkowski 1993; Gilmore and Govindjee 1999; Noctor and Foyer 2000).

and the PSII reaction center is said to be open. When  $Q_A$  is in its reduced state ( $Q_A^-$ ), the reaction center is said to be closed, and excitons cannot proceed further than  $I$ . If the rate of exciton production is greater than the rate of  $Q_A^-$  re-oxidation, then more of the absorbed energy cannot be used in photosynthesis and has to be released by other pathways with heat and fluorescence as the two main processes. This leads to an increase in the fluorescence quantum yield: the number of photons fluoresced per photons absorbed increases.

This short overview suggests that open reaction centers ( $Q_A$ ) will lead to less fluorescence and closed reaction centers ( $Q_A^-$ ) will lead to more fluorescence. Furthermore, at high photon fluence rates, more of the reaction centers will be closed leading to higher fluorescence yields while at low fluence rates the fluorescence yield will be lower (or photochemically quenched) as more of the energy will proceed to photochemistry. These relationships work well under low irradiance. However, as irradiance increases, photoprotective processes (e.g. Ruban and Horton 1995; Niyogi 1999) come into play, protecting photosystems from damage, and the reciprocal relationship between photosynthesis and fluorescence fails.

In the next section, I will provide the most basic relationships pertaining to fluorescence, in the subsequent section I will look at the quantitative relationships between fluorescence and photosynthesis under low light by providing an overview of three models of fluorescence. Following that, I will look at the processes that cause these simple relationships to fail.

### 2.3.1 Fluorescence: basic relationships.

Following the approach of Lackowitz (1983) and Gilmore and Govindjee (1999), I provide here some basic relationships for fluorescence from any fluorophore.

Upon the absorption of a photon, a molecule is excited from the ground state ( $S_0$ ) to a higher electronic and vibrational energy level ( $S_1$  or  $S_2$ ). Internal conversion will allow deexcitation of the molecule back to the lowest vibrational state of the  $S_1$  level; this process is very rapid  $\sim 10^{-13}$  s. The deexcitation from the  $S_1$  level can follow two routes: fluorescence, and radiationless decay. Radiationless decay will be described in more detail in the next section. Presently, I use it to group together all processes that are not fluorescence. Let us call  $k_F$  ( $s^{-1}$ ) the first-order rate constant for the deexcitation by fluorescence, and  $k_A$  ( $s^{-1}$ ) the first order rate constant for the deexcitation by radiationless decay. Following a flash of light at  $t_o$ , and assuming all molecules are in the  $S_1$  state (a state achieved rapidly after the flash), the number of molecules in the  $S_1$  level is given by  $N_{S_1}(t) = N_{S_1}(t_o) e^{-(k_F + k_A)t}$ . Hence, the lifetime defined as the time when 1/e of the initial excited molecules remain in the  $S_1$  state, is given by  $\tau_{S_1} = 1/(k_A + k_F)$ . The intrinsic lifetime of fluorescence, that is the lifetime of the  $S_1$  state if only fluorescence was present is given by  $\tau_o = 1/k_F$ . The ratio of the number of molecules deexcited from the  $S_1$  through fluorescence to those deexcited by fluorescence and radiationless decay is the quantum yield of fluorescence; it can be expressed as  $\phi_f = k_F/(k_F + k_A)$ . Because  $k_F$  is assumed to remain constant as an intrinsic property of the molecule, the fluorescence lifetime ( $\tau_F$ ) from the measurement of the rate of decrease of fluorescence just after an

excitation pulse describe the deexcitation of the excited state:  $\tau_F = \tau_{S_1}$  and, therefore, measurements of the lifetime of fluorescence provide direct measurements of changes in  $k_A$ .

## 2.4 Models of in vivo chlorophyll fluorescence

### 2.4.1 Butler's model of fluorescence

Butler's bipartite model (1978) is a simple yet convenient model to understand processes of fluorescence; many more detailed models have been developed since (e.g. Schatz et al. 1988; Kiefer and Reynolds 1992; Dau 1994; Laverne and Trissl 1995). In the most recent models, the number of parameters involved tends to obscure the important processes. Butler's model provides a background for the research in this thesis.

Figure 2.3 illustrates the mechanisms involved in Butler's bipartite model. I have slightly modified the original symbols to be consistent with their present usage. In my discussion, I will closely follow Butler's description of the model (Butler 1978).

When a photon is absorbed by the chlorophyll in the core or antenna, the chlorophyll reaches an excited state ( $Chl^*$ ) very rapidly ( $t \sim 10^{-15}s$ ) and decays to the first excited singlet state ( $t \sim 10^{-13}s$ ) (Whitmarsh and Govindjee 1999). The excitation can be further dissipated in three different ways, each associated with a rate constant ( $k, s^{-1}$ ): non-radiative decay (heat),  $k_D$ ; transfer to the reaction center,  $k_T$ ; or fluorescence,  $k_F$ . If the energy is transferred to the reaction center chlorophyll (i.e.  $P_{680}Q_A \rightarrow P_{680}^*Q_A$ ), it can then be dissipated following three paths: the energy can be returned to the chlorophyll antenna (i.e.  $P_{680}^*Q_A + Chl \rightarrow P_{680}Q_A + Chl^*$ ) with rate  $k_r$ , dissipated as heat within the reaction

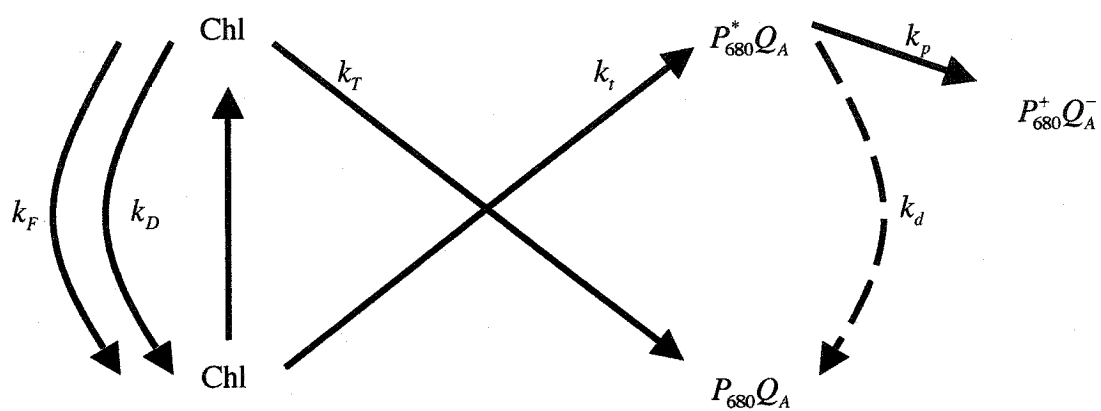


**Figure 2.3: Schematic of Butler's bipartite model. See text for definition of symbols.**

center,  $k_d$  or it can go to photochemistry,  $k_p$ .

Before describing the model further, a distinction has to be made regarding the configuration of antennae and reaction centers in the thylakoid membrane. These configurations are often described in terms of a connectivity parameter ( $0 < p < 1$ , unitless, see Joliot and Joliot 2003 and references therein). Two extreme possibilities exist. The first is that all antenna chlorophyll have access to all reaction centers ( $p = 1$ ), hence if one reaction center is closed the energy can be redirected to an open reaction center. Such a configuration is termed the matrix model or lake model. In the second configuration, each reaction center has its own antenna ( $p = 0$ ). This configuration is called the separate package, separate units or puddle model. Most organisms seem to fall in between the two extremes (Trissl and Lavergne 1995; Bernardt and Trissl 1999). In constructing the model, the configuration will affect the shape of the curve for induction of fluorescence versus time or irradiance, but it will not change the expressions in which the fully closed state is compared with the fully open state of the reaction centers. Following Butler's description, I will fully describe the puddle model and give the expression for the lake model.

Let us call  $A$  the fraction of open reaction centers such that

$$A = (\text{number of } Q_A) / (\text{number of } Q_A^- + Q_A).$$

The quantum yield of photochemistry ( $\varphi_p$ , (excitons stabilized at  $Q_A$ )(photons absorbed)<sup>-1</sup>) is the fraction of excitons that are dissipated through  $k_p$  (equal to the probability). It is given by

$$\phi_p(A) = \Psi_T \Psi_P A, \quad 2.3$$

where  $\Psi_T = k_T / (k_F + k_D + k_T)$  and  $\Psi_P = k_p / (k_p + k_i + k_d)$  are respectively the probability of trapping the excitation energy from the chlorophyll antenna by the reaction center and the probability for photochemistry once the reaction center is in its excited state ( $P_{680}^* Q_A$ ).

The quantum yield for fluorescence  $\phi_f$  is given by

$$\phi_f = \Psi_F A + \Psi_F (1 - A) \left[ 1 + \Psi_T \Psi_i + (\Psi_T \Psi_i)^2 + \dots \right], \quad 2.4$$

where  $\Psi_F = k_F / (k_F + k_D + k_T)$  is the probability of fluorescence from the antenna chlorophyll and  $\Psi_i = k_i / (k_i + k_d)$  is the probability of dissipation of energy from the excited (closed) reaction center to the antenna chlorophyll. Hence, the first term in equation 2.4 represents the fluorescence from units that have open reaction centers and the second term represents the fluorescence coming from units with closed reaction centers. In the second term, fluorescence per reaction center is increased by  $\sum_{n=0}^{\infty} \Psi_T^n \Psi_i^n$  which represent multiple visits of a closed reaction center by an exciton. Since this series converges to  $(1 - \Psi_T \Psi_i)^{-1}$ , it is possible to rewrite equation 2.4 as

$$\phi_f = \Psi_F + \Psi_F \left[ \frac{\Psi_T \Psi_i (1 - A)}{1 - \Psi_T \Psi_i} \right]. \quad 2.5$$

At low fluence rate, when all reaction centers are open ( $A=1$ ),  $\phi_{F_0} = \Psi_F$  and the quantum yield for fluorescence is minimal. When all the reaction centers are closed ( $A=0$ ), the quantum yield of fluorescence is maximal and

$$\phi_{F_m} = \Psi_F + \Psi_F \left[ \frac{\Psi_T \Psi_t}{1 - \Psi_T \Psi_t} \right]. \quad 2.6$$

For the lake model, the relationship for the yields become (Butler 1978)

$$\phi_p(A) = \Psi_T A \left[ \frac{1}{1 - \Psi_T \Psi_t (1 - A)} \right] \text{ and } \phi_f = \Psi_F \left[ \frac{1}{1 - \Psi_T \Psi_t (1 - A)} \right]. \quad 2.7$$

The results above provide a good background for the interpretation of ratio of variable fluorescence ( $F_v$ ) to maximal fluorescence  $F_m$  where  $F_v = F_m - F_o$ , and  $F_o$  is the minimum fluorescence (when all reaction centers are open). First it should be noted that because fluorescence is emitted in all directions, in a first approximation (a more detailed description is given in Ostrowska et al. (2000a)), the relationship between  $F$ , the fluorescence signal observed by a fluorometer and  $\phi_f$  is given by  $F = \gamma \phi_f \overset{\circ}{E}_{abs}$ , where  $\gamma$  is a constant related to the geometry of observation and  $\overset{\circ}{E}_{abs}$  is the absorbed irradiance.

When both  $\gamma$  and  $\overset{\circ}{E}_{abs}$  are constant during observation, we can write

$$\frac{F_v}{F_m} = \frac{\phi_{F_m} - \phi_{F_o}}{\phi_{F_m}} = \Psi_T \Psi_t = \phi_p(A=1) \Psi_t. \quad 2.8$$

This analysis shows that the parameter  $F_v/F_m$  is proportional to the maximum photochemical yield of PSII,  $\phi_p(A=1) = \phi_p^{\max}$ , where  $\phi_p^{\max}$  is the maximal quantum yield of photosynthesis (as defined here by charge stabilization) under the physiological status studied. However, since  $\phi_p(1) = \Psi_T$  and  $F_v/F_m$  is directly proportional to  $\Psi_T$ , any processes that will affect  $k_D$  (energy transfer from the antennae to the reaction center) will have proportional effects on both and, this will not be the case for processes that

affect  $k_d$ . It is interesting to note that Butler's model is now often cited when one asserts that  $F_v/F_m = \phi_p(1)$ . However, the model was created to explain how and why observations differed from the predictions of earlier models that predicted  $F_v/F_m = \phi_p(1)$ ; this is done in Butler's model by adding dissipation of energy within the reaction centers due to  $k_d$ . It seems, however, that when most of the reaction centers are active, that is they can transfer an electron to  $Q_A$ ,  $k_d \ll k_i$ . Nonetheless, under certain types of non-photochemical quenching conditions, when quenching occurs within the reaction center (Long et al. 1994; Koblížek et al. 1999), it may be necessary to consider this process.

#### **2.4.2 The model of Kiefer and Reynolds**

Here I give the relationships obtained from the model of Schatz et al. (1988) often referred to as the "reversible radical pair model" as adapted by Kiefer and Reynolds (1992) and simplified by Babin et al. (1996b). The Schatz model is homologous to the Butler (1978) model (Dau 1994) but its formulation is more consistent with our present understanding of excitation capture in PSII. In this model, probabilities,  $\psi_{xy}$ , (where  $x$  represents a photochemical event:  $cs$  for charge separation,  $cr$  for charge recombination,  $F$  for fluorescence,  $d$  for deactivation (radiationless) and  $st$  for stabilization while  $y$  represents the reaction center state whether  $o$  for open or  $s$  for shut) are given to each of the processes involved in the first steps of the photochemical process, from the absorption of a photon to charge stabilization (see Figure 2.4).

Similarly to Butler's model, expressions can be derived for the quantum yields (equivalent to the probability here, as a probability of 1 is equivalent to all absorbed photons being used to form a product) of photochemistry and fluorescence as

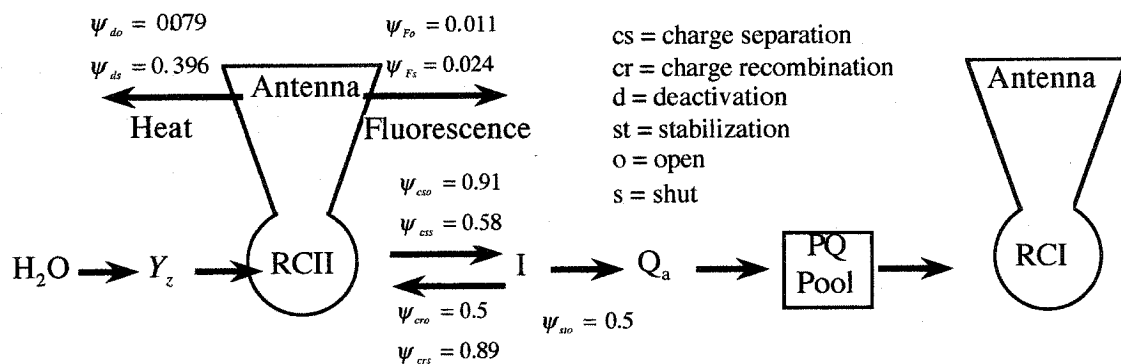


**Figure 2.4: Model of Kiefer and Reynolds for photosynthesis and fluorescence.**

$$\phi_p = \frac{A \psi_{cso} \psi_{sto}}{1 - \psi_{cso} \cdot \psi_{cro}}, \text{ and} \quad 2.9$$

$$\phi_f = \frac{A \psi_{Fo}}{1 - \psi_{cso} \psi_{cro}} + \frac{(1-A) \psi_{Fs}}{1 - \psi_{css} \psi_{cfs}}. \quad 2.10$$

which can be rewritten as,

$$\phi_f = A \phi_{Fo} + (1-A) \phi_{Fm}, \quad 2.11$$

where  $\phi_{Fo} = \psi_{Fo} / (1 - \psi_{cso} \psi_{cro})$  and  $\phi_{Fm} = \psi_{Fs} / (1 - \psi_{css} \psi_{cfs})$ . To relate this to parameters commonly measured at sea, Babin et al. (1996b) further suggest that  $A$  can be conveniently expressed in terms of the photosynthesis irradiance saturation parameter ( $E_k$ , moles photons  $m^{-2} s^{-1}$ ) and scalar incident irradiance in the PAR region ( $\bar{E}_{PAR}$ , moles photons  $m^{-2} s^{-1}$ ; for further definition see section on remote sensing of chlorophyll fluorescence) as

$$A = e^{-\bar{E}_{PAR}/E_k}. \quad 2.12$$

Note that this equation is proposed by Babin et al. (1996) on the basis of one-hit target theory (e.g. Emerson and Arnold 1932; Harm 1980) extended by Dubinsky et al. (1986) for continuous irradiance. In the Dubinsky et al. (1986) formulation,  $A$  is given as,

$$A = e^{-\sigma_{PSII} \tau_{CO_2} \bar{E}_{PAR}}, \quad 2.13$$

where  $\sigma_{PSII}$  is the functional absorption cross-section for PSII and  $\tau_{CO_2}$  is the turnover time for  $CO_2$  evolution. From a remote sensing perspective, this relationship is only useful if one can obtain an estimate of  $E_k$ . It should be noted that one-hit target theory is valid for the puddle model and single flash kinetics, but the lake model and models with

intermediate antenna connectivity (e.g. Lavergne and Trissl 1995) depart from target theory at least during the kinetics of induction (Havaux et al. 1991). Equation 2.13 will hence be valid in the case of the puddle model or at very low (when  $A \sim 1$ ) or saturating irradiance (when  $A \sim 0$ ). Departure from this relationship is expected as the proportion of reaction centers sharing antennae increase.

#### **2.4.3 *Sun-induced fluorescence***

The sun is an intense source of light and the ocean can be seen as a dilute chlorophyll solution, and consequently the ocean fluoresces in daylight; in reflectance spectra of ocean color, this signal is clearly discernable as a peak over the background of backscattered light centered near 683 nm (see Figure 2.5). After some processing (e.g. Culver and Perry 1997; Abbott and Letelier 1999; Coleman et al. 2000), the fluorescence spectrum or the fluorescence line height (FLH), equivalent to the amplitude of the fluorescence, can be obtained.

Theory for the augmentation of the upwelling spectral irradiance by solar-induced fluorescence has been developed by many researchers (e.g. Gordon 1979; Kishino et al. 1984; Topliss and Platt 1986; Preisendorfer and Mobley 1988; Kiefer et al. 1989; Stegmann et al. 1992; Babin et al. 1996b). As detailed in these papers, the theoretical aspect of ocean optics and basic photochemical principles are well understood. The biological component of the theory is dependent on the physiology of the algae, which in turn is dependent on external influences, and consequently has been harder to describe quantitatively. In this section, I will describe a basic model of solar-induced fluorescence, adapted mostly from Babin et al. (1996b), but taking into account further spectral

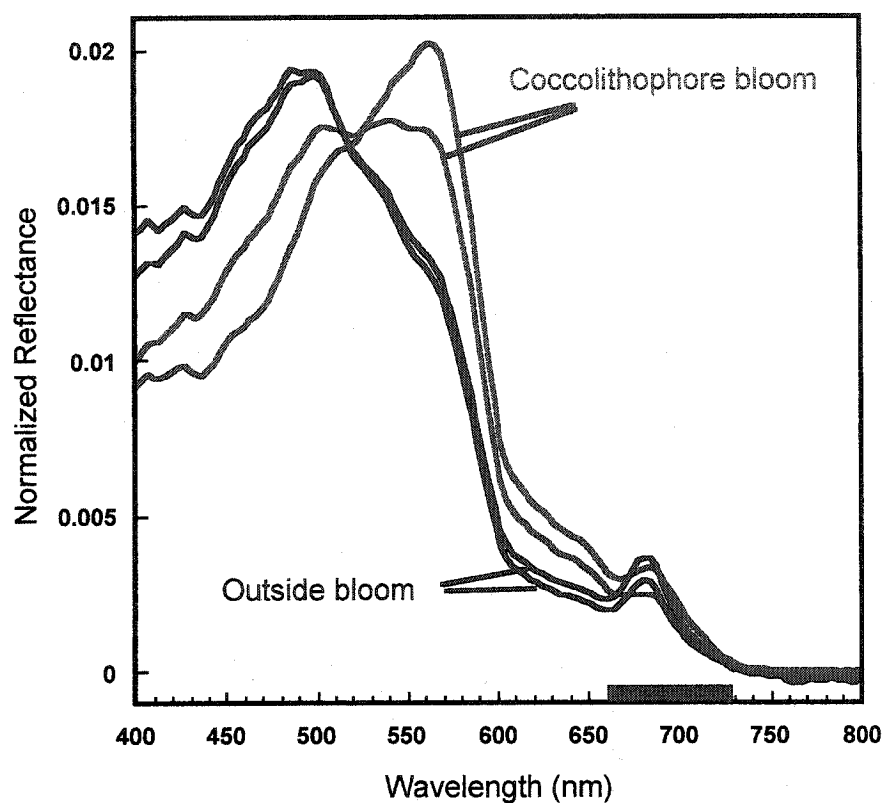


**Figure 2.5:** Reflectance spectra  $L_u(\lambda, 0.65)/E_d(\lambda, 0^+)$  normalized to the area under the curve. The spectra were measured during a cruise in the Bering Sea in September 2000. During this cruise, a coccolithophore bloom was encountered. Two spectra are shown from inside and outside the bloom. Because the reflectance is much higher in a coccolithophore bloom, normalization of the spectra was necessary. The red bar indicates the region where fluorescence emission is evident on the graph.

characteristics. The fluorescence flux emitted from a thin layer of seawater ( $\Phi_f dz$ ; mol quanta  $m^{-2} s^{-1} nm^{-1}$ ) can be expressed as,

$$\Phi_f(\lambda_{em}, z) dz = \frac{1}{C_f(\lambda_{em})} \overset{\circ}{E}_{PAR}(z) chl(z) \bar{a}_\varphi^*(z) Q_a^*(\lambda_{em}, z) \bar{\varphi}_f(z) dz, \quad 2.14$$

where,  $C_f$  is the reciprocal of the fraction of fluorescence emitted at  $\lambda_{em}$  to the total emission ( $nm^{-1}$ ),  $\overset{\circ}{E}_{PAR}$  ( $\mu mol$  quanta  $m^{-2} s^{-1}$ ) is the scalar photosynthetically available radiation,  $\bar{a}^*$  ( $m^2$  (mg chl a) $^{-1}$ ) is the mean chlorophyll-specific absorption coefficient of phytoplankton weighted by the irradiance spectrum,  $Q_a^*$  is a dimensionless factor providing the fraction of fluorescence in the emission spectral band not reabsorbed (Morel and Bricaud 1981) within the cell,  $\bar{\varphi}_f$  is the mean weighted quantum yield for fluorescence at  $\lambda_{em}$ . The mean chlorophyll *a* specific absorption coefficient is defined as

$$\bar{a}^*(z) = \frac{\int_{400}^{700} a_\varphi^*(\lambda, z) \overset{\circ}{E}(\lambda, z) d\lambda}{\int_{400}^{700} \overset{\circ}{E}(\lambda, z) d\lambda}, \quad 2.15$$

where  $a_\varphi^*(\lambda)$  ( $m^2$  (mg chl a) $^{-1}$ ) is the chlorophyll *a* specific *in vivo* absorption of phytoplankton. The spectrally averaged quantum yield is defined as,

$$\bar{\varphi}_f = \frac{\int_{\lambda_{em}} \int_{400}^{700} \varsigma(\lambda \rightarrow \lambda_{em}, z) \overset{\circ}{E}(\lambda, z) a_\varphi^*(\lambda, z) d\lambda d\lambda_{em}}{\int_{400}^{700} \overset{\circ}{E}(\lambda, z) a_\varphi^*(\lambda, z) d\lambda}, \quad 2.16$$

where  $\varsigma(\lambda \rightarrow \lambda_{em}, z)$  is the spectral redistribution function for chlorophyll fluorescence.

The spectral redistribution function provides the fraction of the irradiance absorbed by all pigments in the cell at  $\lambda$  which is reemitted at  $\lambda_{em}$ . Generally, the simplifying

assumption that the spectral redistribution function is spectrally constant with excitation irradiance is made (e.g. Kiefer et al. 1989). This is obviously an approximation since the light absorbed by non-photosynthetic pigments or by pigments associated with PSI will not fluoresce with the same quantum yield (SooHoo et al. 1982; Johnsen and Sakshaug 1996; Johnsen et al. 1997; Lutz et al. 1998). The portion of emitted light not reabsorbed (Collins et al. 1985; Mitchell and Kiefer 1988; Babin et al. 1996b; Garcia-Mendoza and Maske 1996; Ostrowska et al. 2000a; Wozniak et al. 2000) by pigments within the cell is given by

$$Q_a^*(\lambda_{em}) = \frac{a_\phi^*(\lambda_{em})}{a_{sol}^*(\lambda_{em})}, \quad 2.17$$

where  $a_{sol}^*$  is the chlorophyll specific absorption of the pigments if they were in solution.

Following the analysis of the variation in  $a_\phi^*$  with chlorophyll (Bricaud et al. 1995), Babin *et al.* (1996b) have related this parameter to *in situ* chlorophyll concentration ( $r^2=0.43$ ) and found that it varied from  $\sim 1$  to  $\sim 0.3$  as chlorophyll concentration went from 0.03 to 30 mg chl a m<sup>-3</sup>.

Equation 2.14 (see also equation 2.2) can be broken down as follows:

$\overset{o}{E}_{PAR} chl \bar{a}_\phi^*$  corresponds to the amount of photosynthetically available radiation that is absorbed and  $Q_a^* \bar{\phi}_f / C_f$  corresponds to the portion of the absorbed radiation that is re-emitted at  $\lambda_{em}$  and not absorbed within the cell (Ostrowska et al. 2000a). The term,  $Q_a^* \bar{\phi}_f$  has been referred to as the realized yield by Maritorena *et al.* (2000).

At a given depth,  $z$  (m), the amount of PAR irradiance is given by

$$\overset{\circ}{E}_{PAR}(z) = \int_{400}^{700} \overset{\circ}{E}(0^-, \lambda) e^{-K(\lambda)z} d\lambda, \quad 2.18$$

where  $\overset{\circ}{E}(0^-, \lambda)$  is the spectral scalar irradiance just below the surface, and  $K(\lambda)$  is the spectral diffuse attenuation coefficient for scalar irradiance.

Because the upwelling light field is usually observed using a radiance sensor pointing at the nadir, it is useful to convert the emitted flux over a thin layer to an upwelling radiance. This is done by assuming an isotropic emission by the phytoplankton such that the small element of upwelling radiance from the layer at depth  $z$  is given by

$$dL_{uf}(z, \lambda) = \frac{\Phi_f(\lambda, z) dz}{4\pi}. \quad 2.19$$

To obtain the radiance due to fluorescence at the depth of the sensor, one has to integrate the upwelling radiance coming from all depths below the sensor, taking into account its attenuation by the upwelling radiance attenuation coefficient  $\kappa_u$  ( $m^{-1}$ )

$$L_{uf}(z_{sens}, \lambda_{em}) = \int_{z_{sens}}^{\infty} dL_{uf}(z, \lambda_{em}) e^{-\kappa_u(\lambda)[z_{em} - z_{sens}]} = \frac{1}{4\pi} \int_{z_{sens}}^{\infty} \Phi_f(\lambda, z) e^{-\kappa_u(\lambda)[z_{em} - z_{sens}]} dz. \quad 2.20$$

Using equations 2.14, 2.19 and 2.20 we can now obtain the radiance at the sensor depth due to the emission by fluorescence in terms of the incident irradiance at the surface,

$$L_{uf}(z_{sens}, \lambda_{em}) = \frac{1}{4\pi C_f(\lambda_{em})} \int_{z_{sens}}^{\infty} chl(z) \bar{a}^*(z) \bar{\phi}_f(z) \overset{\circ}{E}_{PAR}(z) Q_a^*(\lambda, z) e^{-\kappa_u(\lambda)[z_{em} - z_{sens}]} dz. \quad 2.21$$

Until now, the derivation has been spectrally rigorous, the next step leads to considerable simplification and requires a series of assumptions about spectral and depth dependence.

Firstly, because 90% of the surface fluorescence signal originates from the upper ~5 meters even in the clearest waters (Babin et al. 1996b), and because this region is likely to be homogeneous in terms of most physiological parameters (that is the timescale of mixing is assumed shorter than the timescale of photoacclimation (Cullen and Lewis 1988)), the dependence with depth of many variables is dropped (this assumption will be revisited later in the thesis). Secondly, the attenuation of PAR (see equation 2.18) over such a short pathlength can be approximated with reasonable accuracy using a broadband, depth averaged attenuation coefficient  $\bar{K}_{PAR}$ . Thirdly, the chlorophyll concentration is assumed uniform over that depth. Equation 2.21 can then be simplified as

$$L_F(z_{sens}, 683) = \frac{1}{4\pi C_f} \bar{E}_{PAR}^o(z_{sens}) chl \bar{a}_\phi^* Q_a^*(683) \bar{\phi}_F \frac{1}{\bar{K}_{PAR} + \kappa_u(683)}. \quad 2.22$$

The use of a broadband attenuation coefficient allows such a simplification, however this equation could be recast in terms of photosynthetically usable radiation (PUR) or, even better, fluorescence exciting radiation. However, it should be noted that the only difference mathematically between a PUR-based and a PAR-based model would be the use of an attenuation coefficient for PUR instead of PAR. In practice, some of these assumptions may not stand under certain conditions and equation 2.22 may have to be modified to address, for example, changes in the quantum yield of fluorescence with depth.

Except for  $\bar{\phi}_F$ , and perhaps  $Q_a^*$ , the parameters in equation 2.22 can all be measured relatively easily. The concentration of chlorophyll can be estimated *in situ*

using ocean color or on-board using extracted samples. The absorption spectrum can be measured using a benchtop or in situ spectrophotometer or, to a certain extent, estimated from the reflectance spectrum (e.g. Roesler and Perry 1995; Carder et al. 1999b; Ciotti et al. 1999). Good relationships have been developed between  $a_{\phi}^*(\lambda)$  and *chl* (Bricaud et al. 1995; Babin et al. 1996b; Ciotti 1999). One could obtain  $a_{\phi}^*(\lambda)$  from the chlorophyll concentration when at sea to obtain rapid estimates or from a remote sensing perspective. Similarly, since  $a_{sol}^*$  remains constant (see equation 2.17), the parameter  $Q_a^*$  becomes solely a function of  $a_{\phi}^*(\lambda)$  and also shows a relationship with chlorophyll concentration (Babin et al. 1996b). These relationship originate due to the increase in cell size with chlorophyll concentration (Yentsch and Phinney 1989; Kiørboe 1993) leading to a lower  $a_{\phi}^*(\lambda)$  (e.g. Morel and Bricaud 1981; 1986). Downwelling irradiance can be measured with ease at sea, while attenuation coefficients are routinely derived from measurements using profiling radiometers or ocean color relationships (e.g. Mueller and Trees 1997).

## **2.5 The quantum yield of fluorescence in the ocean**

The quantum yield of fluorescence will vary as a function of the physiological state of phytoplankton, which is itself influenced by the environment. The most important factors affecting the quantum yield of fluorescence are the incident light and the availability of nutrients. However, the extent of their influence will be dependent upon whether the phytoplankton are acclimated to these factors (Srivastava et al. 1995). Furthermore, each species or group will have a different genetic capacity for physiological acclimation. Babin and colleagues (1996b) proposed a quantitative

framework to study these processes. They used the following relationship adapted from the work of Kiefer and Reynolds (1992) (see equation 2.11),

$$\phi_f = \left[ 1 - f \left( \overset{\circ}{E}_{PAR, NO_3} \right) (1 - A) \right] \phi_{Fo} + f \left( \overset{\circ}{E}_{PAR, NO_3} \right) (1 - A) \phi_{Fm}, \quad 2.23$$

where  $f$  is the proportion of functional reaction centers, which depends on PAR irradiance and nitrate concentration although this could be any limiting nutrient. In this formulation, the inactivated reaction centers act as thermal traps and have a fluorescence quantum yield equal to  $\phi_{Fo}$ .

In their interpretation, Babin et al. (1996a) predicted a decrease in the quantum yield of fluorescence to the  $\phi_{Fo}$  level with decreasing nitrate concentration. However, the effect of inactive reaction centers from nitrate limitation on fluorescence is not clear from the literature and other authors suggest these inactive reaction centers will increase the yield of fluorescence (e.g. Cleveland and Perry 1987; Kolber and Falkowski 1993; Graziano et al. 1996; Letelier et al. 1997; Abbott and Letelier 1999). Letelier et al. (1997) propose that nutrient limitation reduces the capacity of the photosynthetic system to utilize electrons, thus leading to the closure of reaction centers and thereby increasing the quantum yield of fluorescence. Generally, it seems that most studies suggest an increase in the yield of fluorescence with nutrient stress, however, much of this is based on extrapolation rather than measurements because  $\phi_f$  is rarely measured directly.

## **2.6 Excess irradiance and photosynthesis**

Excess irradiance is irradiance that is absorbed but not utilized for photochemistry; excess irradiance increases as the incident irradiance increases and the

quantum yield of fluorescence decreases. Because the excess irradiance is not used in photosynthesis, it must be dissipated. If the energy is not dissipated efficiently it will lead to the formation of highly reactive species that can lead to damage in the reaction centers (Anderson et al. 1998; Gilmore and Govindjee 1999; Niyogi 1999; Oxborough and Baker 2000). Damage in the reaction center leads to photoinhibition, a decrease in the rate (or quantum yield) of photosynthesis, due to high irradiance (Neale 1987; Long et al. 1994).

Plants and algae have developed many mechanisms to avoid photoinhibitory damage. These mechanisms allow an increase in the quantum yield of heat dissipation at the level of PSII. In terms of Butler's model (Butler 1978), this means increasing the rates  $k_D$  and/or  $k_d$ . It can be seen from equation 2.5 that this will lower the quantum yield of fluorescence. Photoinhibition has similar effects (Krause and Weis 1988; Krause and Weis 1991) and decreases the quantum yield of fluorescence, but it is due to damage to the photosystems (i.e. it leads to an increase in  $k_d$ ). This decrease in the quantum yield of fluorescence due to excess irradiance is called non-photochemical quenching and will be addressed in the following section.

### ***2.6.1 Non-photochemical quenching***

Non-photochemical quenching refers to the decrease of fluorescence by processes other than photosynthesis (referred to as photochemical quenching  $q_p$ ). Several parameters have been defined to measure the amount of quenching from active fluorescence measurements (Roháček and Barták 1999; Maxwell and Johnson 2000; Roháček 2002). Non-photochemical quenching includes processes such as energy dependent quenching ( $q_E$ ), quenching by the decrease of excitation energy transfer to

PSII due to state 1-state 2 transitions ( $q_T$ ), and quenching accompanying the inhibition of photosynthesis ( $q_I$ ). Below, I briefly describe these types of quenching.

#### *2.6.1.1 Energy dependent quenching, $q_E$*

This process seems to be the main mechanism of photoprotection of the photosynthetic process and provides the most important defense against supersaturating irradiance levels in higher plants and many eukaryotic algae. However, there is a large variation in the capacity for  $q_E$  in different algae (Casper-Lindley and Björkman 1998). Energy dependent quenching is related to the proton gradient across the thylakoid membrane. The high proton gradient present under high light is basically a consequence of an uncoupling of carbon fixation and utilization of ATP, and the rate of electron transport by the plastoquinone pool (Walker 1988; Kramer et al. 1999; Ort 2001). The quenching is due to an increase in the dissipation of the excitation energy as heat at the antenna level of PSII and may be due to a structural change in LHCII (Krause and Weis 1988; Demmig-Adams and Adams III 1992; Gilmore and Govindjee 1999; Horton et al. 2000; Ort 2001). This quenching is associated with the xanthophyll cycle (e.g. Demers et al. 1991; Casper-Lindley and Björkman 1998; Gilmore and Govindjee 1999): as  $\Delta pH$  increases across the thylakoid membrane, the violaxanthin de-epoxidase enzyme is activated and conversion of violaxanthin to zeaxanthin occurs in the case of higher plants and green algae. In chromophytes (e.g. diatoms, dinoflagellates and prymnesiophytes), this cycle is replaced by the de-epoxidation of diadinoxanthin to diatoxanthin. In higher plants, binding of the zeaxanthin to the LHCII and associated structural changes seems to provide the mechanism for thermal dissipation (Gilmore and Govindjee 1999; Niyogi

1999); a similar process may be occurring in chromophytes with diadinoxanthin. A working model where the protonation of reaction center proteins favors the binding to zeaxanthin and antheraxanthin leading to fluorescence quenching has been proposed (e.g. Müller et al. 2001). While Gilmore et al. (1998; Gilmore and Govindjee 1999) provide a quantitative model for this process based on the intrathylakoid pH. In higher plants, this process can be responsible for as much as 90% of the decrease in variable fluorescence (and up to 15 – 25 % of  $F_o$ ) and is induced within seconds (Krause and Weis 1991). This mechanism may not be as important in microalgae and the relationship between non-photochemical quenching,  $\Delta pH$ , and the presence of quenching xanthophylls is not as straightforward (Casper-Lindley and Björkman 1998; Masojídek et al. 1999).

#### 2.6.1.2 *Quenching by decrease of excitation energy to PS II, $q_T$*

Phosphorylation of the light harvesting complexes of photosystem II (LHCII) and subsequent detachment lowers the absorption cross-section of PSII relative to PSI and hence lowers the fluorescence yield (Allen 1995; Wollman 2001). This quenching mechanism depends on the activity of a kinase, the protein responsible for the phosphorylation. The activity of this protein is dependent on the redox state of the plastoquinone pool and the proton gradient across the membrane. In higher plants, this mechanism can quench  $F_v$  by at most 20% and has slower kinetics than  $q_E$ . The detached LHCII can be used by PSI but the occurrence of this state-transition under high light conditions in the natural environment is not certain (Krause and Weis 1988; Falkowski et al. 1994; Long et al. 1994; Allen 1995; Niyogi 1999). In cyanobacteria, which do not have LHCII, phycobilisomes diffusion changes the absorption cross-section of PSII

relative to PSI (Joshua and Mullineaux 2004) and provides an important source of non-photochemical quenching with faster kinetics than in eukaryotes (Campbell et al. 1998).

#### 2.6.1.3 *Quenching accompanying the inhibition of photosynthesis, $q_T$*

The photoinhibition of photosynthesis can be defined in many ways. Here, I will use a decrease in the rate of photosynthesis at high irradiance levels as measured by the evolution of  $O_2$  or fixation of  $CO_2$  below maximal rates due to excess light (e.g. Falkowski et al. 1994). This is equivalent to a decrease of the maximal turnover rate of the photosynthetic apparatus, or a constant maximal turnover rate and a decrease in the number of active reaction centers. In terms of fluorescence, photoinhibition of photosynthesis is seen as a decrease in maximal variable fluorescence yield on time scales of minutes to hours after exposure to excessive radiation levels. This can occur through the decrease of  $F_m$  or an increase in  $F_o$  (Valvilin et al. 1998; He and Chow 2003); an increase in  $F_o$  occurs if inhibited reaction centers are not as efficient at dissipating absorbed energy as active reaction centers. This quenching mechanism is due to an increase in the rate constant of heat dissipation, however, whereas  $q_E$  and  $q_T$  are due to photoprotective mechanisms, the distinction between photoprotection and damage is blurred in the case of photoinhibition (Greer et al. 1991; Long et al. 1994). The nature of photoinhibition of photosynthesis is not attributed consistently to the same processes by different authors. Earlier studies seemed to favor photo-oxidative damage of the D1 protein (but see Niyogi 1999) as the main source of photoinhibition whereas more recent reviews suggest the involvement of multiple stages of inactivation (without necessary damage) of the D1 protein (Aro et al. 1993; Long et al. 1994) some of which are more

rapidly reversible than others. This process is reversible upon return to lower irradiance levels; time scales for reversal are of the order of several minutes to hours (White and Critchley 1999; He and Chow 2003) and the rates depend on incident irradiance (He and Chow 2003).

## **2.7 *Observations of non-photochemical quenching in phytoplankton***

Many observations of non-photochemical quenching of fluorescence have been published for phytoplankton in the lab (e.g. Kiefer 1973a; Cullen et al. 1988 ; Koblížek et al. 1999; Bruyant et al. 2000; Koblížek et al. 2001; Lavaud et al. 2004). The occurrence of non-photochemical quenching of both  $F_o$  and  $F_m$  in the ocean have been observed as a decrease in the fluorescence levels occurring around mid-day at the surface (Kiefer 1973b; Loftus and Seliger 1975; Kiefer and Reynolds 1992; Babin et al. 1996b; Dandonneau and Neveux 1997). However, the effect of nutrient stress on non-photochemical quenching does not seem to have been addressed in the literature (but see Kiefer 1973a) and can only be inferred from measurements in studies not aimed specifically at resolving its effects.

## **2.8 *Effect of nutrients on the quantum yield of fluorescence***

A few studies exist on the effect of nutrients such as phosphorus and iron, but mostly nitrogen, with concurrent measurements of fluorescence. Here, I focus on the effect of nitrogen limitation. The effects of nitrogen stress occur at least at two levels in the cells, which affect the fluorescence emission and yield of the whole cell (Cullen et al. 1992b; Graziano et al. 1996). The first is at the level of the PSII antenna where changes

in the total pigments and their stoichiometry occur. The second is at the level of the reaction center where changes in the efficiency of charge separation or charge stabilization arise. Therefore, to interpret changes in fluorescence emission, care must be taken to separate the influence of the two (Cleveland and Perry 1987).

Observations at the cell level of nitrogen stressed phytoplankton show a lower chlorophyll concentration per cell (e.g. Sakshaug and Holm-Hansen 1977; Mingyuan et al. 1992) and this will likely lower the total amount of fluorescence emitted per cell. This decrease in chlorophyll concentration can however lead to an increase in  $a_{\phi}^*$  which can partially compensate for a decrease in chlorophyll {Cleveland, 1987 #428 see also equation 2.14}. However, the increase in  $a_{\phi}^*$  will generally be smaller than the decrease in the internal chlorophyll concentration. Moreover, the increase in  $a^*$  originates from two different processes (reviewed in Bricaud et al. 1995). The first is the decrease of the amount of pigments within the cell, which, in sufficiently large cells, leads to a decrease in the package effect (Morel and Bricaud 1986). The second is the greater decrease in chlorophyll *a* compared to other photosynthetic and photoprotective pigments (Cleveland and Perry 1987; Latasa 1995; Henriksen et al. 2002). While the first would partially compensate the decreased fluorescence emission due to the decreased chlorophyll concentration, the second, depending on changes in pigment stoichiometry, would not necessarily do so. All these changes reflect changes at the antenna level.

At the level of the photosystem, changes in the quantum yield of fluorescence with nitrogen stress are expected to occur due to a lower capacity to transfer electrons to

electron acceptors, due to either an effective decrease in the fraction of active reaction centers or a diminished efficiency of active reaction centers. Another effect of nutrient stress sometimes observed is an increase in effective absorption cross-section of PSII probably due to a larger number of LHCII per active RCII (Kolber et al. 1988).

Therefore, nitrogen stress seems to be associated with a decrease in the number of active RCII per cell but an increase in their absorption cross-section. The latter could be the cause —or the result— of the increased susceptibility to photoinhibition observed in cells under nitrogen stress (Prézelin et al. 1986; Kolber et al. 1988). Babin (1996a) referred to these changes observed with nitrogen stress as having “photoinhibition-like” effects on fluorescence, that is, leading to an increase in non-photochemical quenching.

Graziano *et al.* (1996) discussed the effect of a decline in the portion of active reaction centers on the yield of fluorescence and suggested that the effect will only be seen for non-maximum yields ( $\phi_f < \phi_{F_m}$ ). According to them, an inactive reaction center acts essentially as a closed reaction center such that only when a fraction of reaction centers are open can a decrease in the photochemical yield of the cells be observed (i.e.  $F_m$  remains the same). Furthermore, they suggest that this should lead to an increase in  $\phi_{F_o}$  while  $\phi_{F_m}$  should not be strongly affected (if at all) by nitrogen stress. This reasoning, however, assumes that inactive reaction centers cannot act as thermal traps of excitation energy (Greer et al. 1991; Long et al. 1994; Valvilin et al. 1998) and ignores the observation of the presence of non-photochemical quenching associated with photoinhibited reaction centers.

The few laboratory experiments carried out on the effect of nutrients on the

fluorescence yield seem to show that under nutrient stress the ratio of the fluorescence when all reaction centers are open ( $F_o$ ) to chlorophyll concentration (in accordance with equation 2.14 this is equal to  $\bar{a}_\phi Q_a^* \bar{\phi}_f$ ) will increase (Kiefer 1973a; Sakshaug and Holm-Hansen 1977; Cleveland and Perry 1987; Mingyuan et al. 1992) in dark-adapted samples. Cleveland and Perry (1987) suggest that this increase is not only due to a change in  $\phi_F$  but also to a concomitant change in  $a_\phi^*$  as both increase with decreasing chlorophyll concentration. A reexamination of their data shows that the changes in the quantum yield observed were in the realized quantum yield ( $\phi_f Q_a^*$ ), while changes in the actual quantum yield were only small (see Figure 2.6). However, I may have overestimated the effect of  $Q_a^*$  in Figure 2.6 as I used the change in  $a_\phi^*$  (measured from 400 to 500 nm) to represent the change in  $Q_a^*$  (at 680 nm).

Given the number of competing processes occurring concurrently under nitrogen stress, it is hard to get a clear picture of their overall effect, and only limited conclusions can be drawn. The evidence available suggests an increase in the minimum quantum yield of fluorescence in the dark of a factor of 1.5 to 2 under high nitrogen stress. At the same time, there is a strong increase in the susceptibility to photoinhibition, which should lead to a diminution of the maximal quantum yield of fluorescence when cells are placed under high irradiance. The effects of nutrient stress on energy dependent non-photochemical quenching are largely unknown though new results suggest an increase in this process under nutrient starvation (Laney et al. in prep). Under fully acclimated nitrogen limitation, however, no such changes are

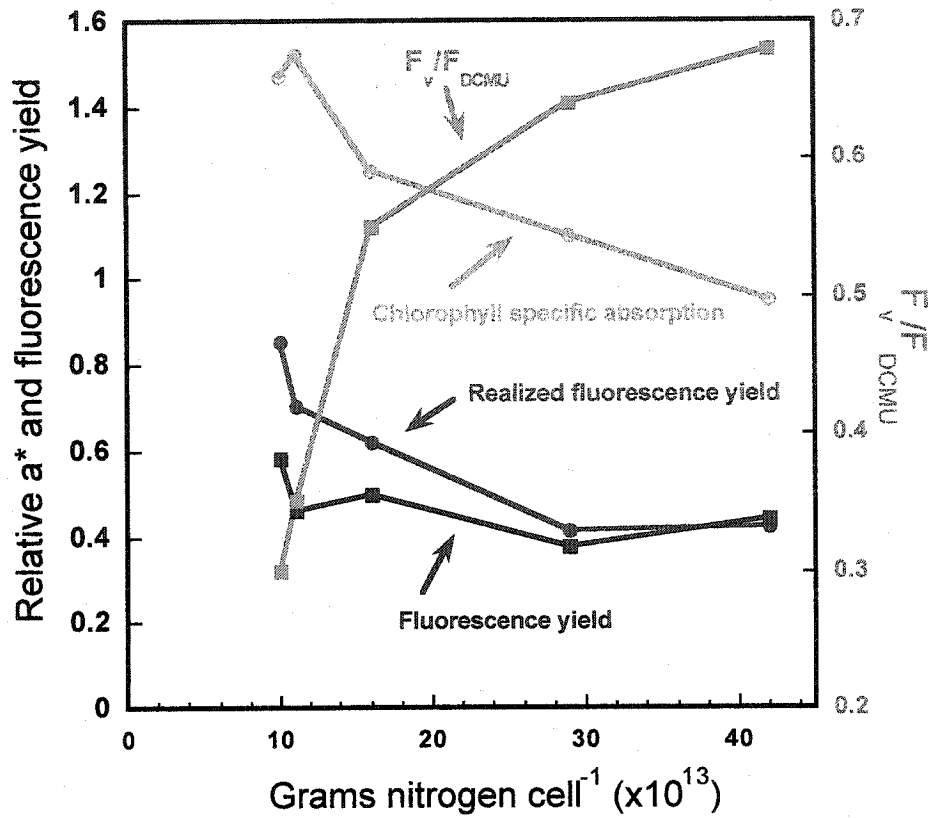


Figure 2.6: Cleveland and Perry 1987 revisited. In cultures under nitrogen starvation, Cleveland and Perry (1987) studied the changes in the realized quantum yield of fluorescence  $\phi_f Q_a^*$  (which they refer to as the fluorescence yield) and the chlorophyll specific absorption coefficient ( $a_\phi^*$ ). The main conclusion of their paper is that the quantum yield of fluorescence and the chlorophyll specific absorption both increase with increasing nutrient stress. Here I show using their data that while the realized fluorescence yield, what they actually measured, did increase, the quantum yield may have only slightly increased under high nutrient stress (when  $F_v/F_{DCMU} \approx 0.3$ ). To obtain the relative changes in the actual fluorescence yield, I divided the realized quantum yield by the chlorophyll specific absorption coefficient hence accounting for changes in the reabsorption coefficient (see equations 2.14).

found and  $F_v/F_m$  remains constant (Cullen et al. 1992b; Mingyuan et al. 1992; Parkhill et al. 2001).

Evidence of the effect of nutrient concentration in the field on the quantum yield of fluorescence is limited. This is due, in part, to the fact that phytoplankton utilize nutrients at concentrations that are lower than those that are routinely measurable. In addition, low nutrient concentrations are not equivalent to low fluxes of nutrients. In other words, a phytoplankton community's nutrient status is not measurable in terms of ambient nutrient concentrations. Hence, all variability in fluorescence characteristics due to low nutrient concentration tend to occur at nutrient levels that are undetectable (Geider et al. 1993; Olaizola et al. 1996). Furthermore, because the immediate interest of most fluorescence based studies is finding the maximum quantum yield of photosynthesis (by the proxy  $F_v/F_m$ ) or the number of active reaction centers, rarely are the quantum yields of fluorescence published or measured. A consistent decrease in  $F_v/F_m$  with decreasing chlorophyll concentration was found in a transect in the western North Atlantic (Geider et al. 1993). The portion of functional reaction centers ( $1/8 F_v/F_o$ ) showed a consistent decrease with decreasing  $\text{NO}_3 + \text{NO}_2$  concentrations (Babin et al. 1996a) in the northeast tropical Atlantic. However, Olaizola and colleagues (1996) show that even when nitrate concentrations could be measured down to a level of 1 to 2 nM, there was no significant trend in the ratio  $F_v/F_m$  with nitrate concentration. Evidence of a relationship between  $\phi'_{F_o}$ , the fluorescence quantum yield in a light adapted state but measured in the dark (that is without photochemical quenching but still non-photochemical quenching) has

been found at sea by Ostrowska and colleagues (2000a) and this parameter decreased as the nutrient concentration decreased in that study. This pattern could be due to either higher non-photochemical quenching; a lower quantum yield at lower levels of nutrient concentration, or, alternatively, it could be an artifact due to their parameterization of reabsorption and chlorophyll specific absorption as a function of chlorophyll concentration.

## **2.9 The tools of the trade: Instrumentation and relationships.**

### **2.9.1 The Turner Designs fluorometer and fluorescence $\pm$ DCMU**

The Turner Designs fluorometer is a simple fluorometer, but also probably, the best characterized. Its design is straightforward; the sample is irradiated with a weak blue light and fluorescence emission is measured at 90° from the incident light (as with most fluorometers).

The fluorometer is used primarily in two ways for the measurement of chlorophyll fluorescence. The first is to measure the concentration of chlorophyll: acetone (or another organic solvent) extracts of phytoplankton are inserted and the fluorescence level is measured. After proper calibration, this provides an estimate of chlorophyll concentration in the sample (Yentsch and Menzel 1963; Strickland and Parsons 1972). A variation on this method is to use the fluorometer to make *in vivo* chlorophyll measurements (whether in a flow-through mode or on discrete samples e.g. Lorenzen 1966). This can be done both in the lab and at sea, but should be used as a qualitative index rather than a quantitative estimate (Strickland 1968; Cullen 1982).

The second application is to measure the variable fluorescence parameter  $F_v$ .

Samples are dark adapted for ~20 to 30 minutes to allow energy dependent non-photochemical quenching to dissipate. Then, fluorescence is measured *in vivo*; this should be done with low incident photon flux to prevent a significant portion of photosystem II closure, allowing the measurement of true  $F_o$  (Parkhill et al. 2001). The sample is then poisoned with the herbicide Diuron (3-(3,4-dichlorophenyl)-1, 1-dimethylurea, DCMU), which blocks the photosynthetic electron transport chain by replacing  $Q_b$  on the reaction center protein complex, hence, closing all the reaction centers upon illumination. Therefore, under DCMU poisoning, the fluorescence level is maximal,  $F_{DCMU} \sim F_m$ . The ratio of variable fluorescence to maximal fluorescence can then be formed:  $F_v/F_{DCMU} = (F_{DCMU} - F_o)/F_{DCMU}$ . This parameter (see Butler's Model section) is related to the potential quantum yield of photosystem II (often referred to as potential yield for photochemistry):  $\phi_p^{\max} \approx F_v/F_{DCMU}$ . This parameter has a maximum equal to about 0.65 in phytoplankton. Hence, it provides a measure of their maximal photosynthetic efficiency (Butler 1978; Kolber and Falkowski 1993). Poisoning with low concentrations of DCMU can also be used to simulate different levels of closure of reaction centers in the light (e.g. Behrenfeld et al. 1998).

### 2.9.2 The PAM fluorometer

The Pulse Amplitude Modulated (PAM) fluorometer is a relatively new instrument (Schreiber et al. 1986). In addition to using a weak modulated LED light (peak emission 650 nm, intensity  $10 \text{ mW m}^{-2}$ , modulation frequency 1.6 KHz or 100 KHz) to measure the minimum fluorescence ( $F_o$ ), the instrument uses an intense (up to  $18000 \mu\text{mol}$

photon  $\text{m}^{-2} \text{s}^{-1}$ ) pulse of light ( $\sim 300$  ms) to close all the reaction centers and so  $F_m$  can be measured with weak pulses. Therefore, the PAM can provide the same information as the Turner Designs fluorometer (or any other fluorometer capable of measuring  $F_o$ ) without killing the cells. In addition, because the measuring light is modulated, it is possible to measure the fluorescence signal in the presence of actinic light (Figure 2.7). This allows for many measurements of fluorescence parameters that can be related to photosynthetic processes (Havaux et al. 1991; Flaming and Kromkamp 1998; Roháček and Barták 1999; Maxwell and Johnson 2000; Roháček 2002) such as the PSII quantum yield, photochemical quenching, non-photochemical quenching and quenching relaxation time constants. These measurements are often referred to as quenching analysis.

A few of these parameters will be used throughout the thesis:

- 1) The maximum quantum yield of charge stabilization,

$$\phi_p^{\max} = (F_m - F_o) / F_m = F_v / F_m,$$

which provides information about the quantum yield when all reaction centers are open under dark acclimated condition.

- 2) The quantum yield of *open reaction centers* for charge stabilization in the light,

$$\phi_{pA} = (F'_m - F'_o) / F'_m = F'_v / F'_m,$$

which provides information about the quantum yield of open reaction centers when they are under ambient irradiance and hence compete for excitons with enhanced heat-dissipation due to non-photochemical quenching.

- 3) The effective quantum yield of charge stabilization under light acclimated conditions for all reaction centers,

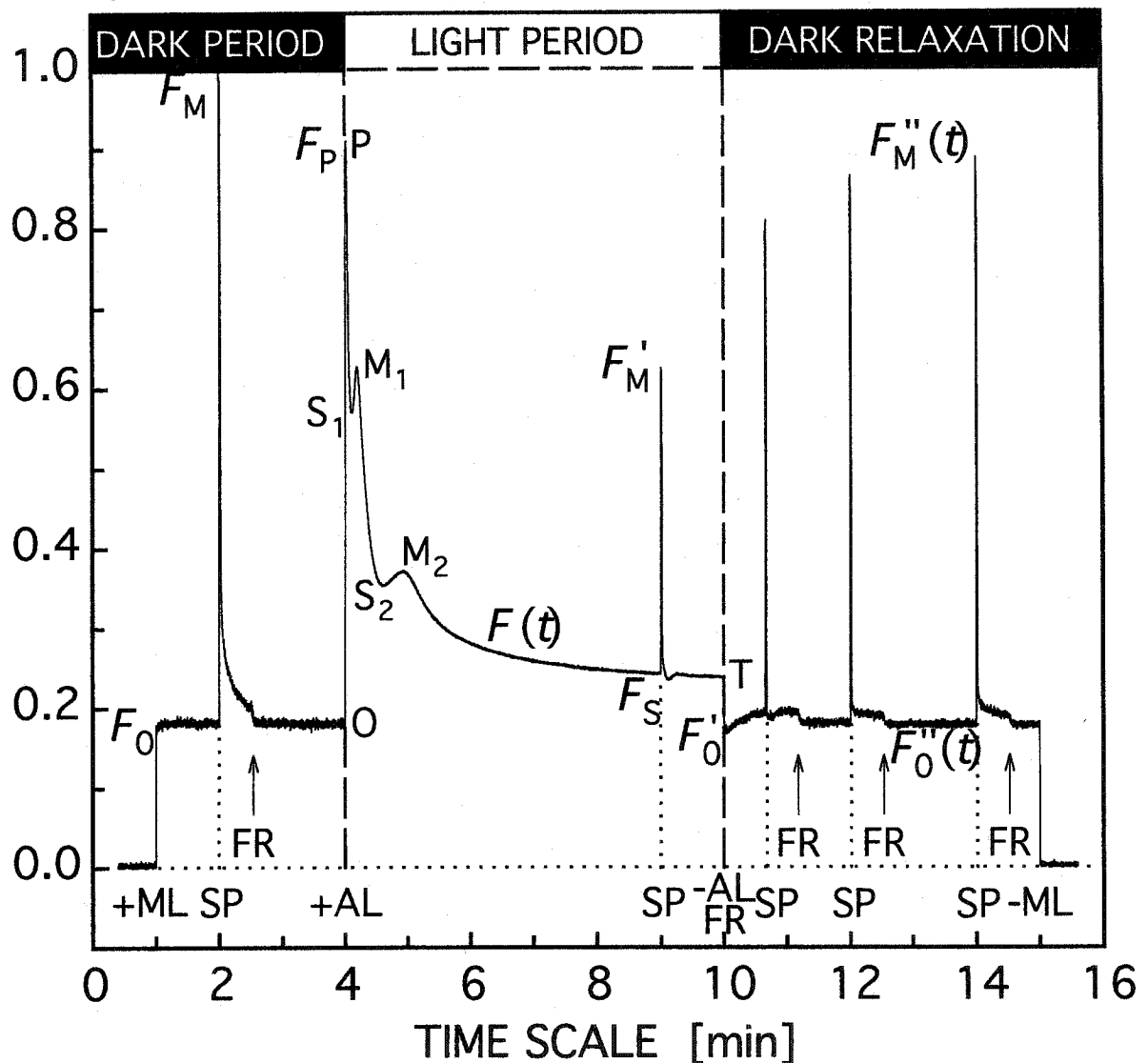


Figure 2.7: Fluorescence quenching analysis parameters. The bottom part of the graph provide the radiation regime: ML=Measuring light, performed using a weak LED light. SP=Saturation pulse (halogen lamp flash), FR=Far-red radiation ( $\lambda=735$  nm) to preferentially excite PSI. AL=Actinic light, provided by any light source. OPSMT correspond to different points on the induction curve. The prime indicates the fluorescence level in the presence of actinic light, the double prime indicates the light acclimated state but returning to dark conditions. In my notation  $F(t) = F'$ . Figure reproduced with permission from Roháček and Barták (1999).

$$\phi_p = (F'_m - F')/F'_m = \Delta F/F'_m,$$

which is the actual quantum yield of photochemistry for all PSII reaction centers.

4) The non-photochemical quenching parameter,

$$NPQ_f = (F_m - F'_m)/F'_m,$$

which provide information about the *amount or efficiency of the quencher*. This parameter follows directly from Stern-Volmer kinetics.

5) The complete non-photochemical quenching parameter,

$$q_{CN} = (F_m - F'_m)/F'_m,$$

which provides information about the *amount of quenching* of maximum fluorescence occurring.

### 2.9.3 The FRR fluorometer

The fast repetition rate fluorometer (Kolber et al. 1998) is an instrument that measures the fluorescence induction, that is, the change in the amount of fluorescence versus time or incident cumulative energy, using single turnover flashes (Figure 2.8). In the single turnover protocol, the saturation pulse occurs on the timescale for one turnover of PSII. In addition to the measurements of  $F_m$  and  $F_o$ , this method allows the determination of other physiological parameters. In particular, the extent of energy transfer between PSII reaction centers ( $p$ ) (Leverenz 1994; Trissl and Lavergne 1995; Trissl 1999) and the functional absorption cross-section ( $\sigma_{PSII}$ ) can be obtained from the induction kinetics. Time constants for the reoxidation of  $Q_a$ ,  $\tau_x$ , can be derived from the kinetics of deactivation measured with less frequent flashlets following the completion of the single turnover flash.

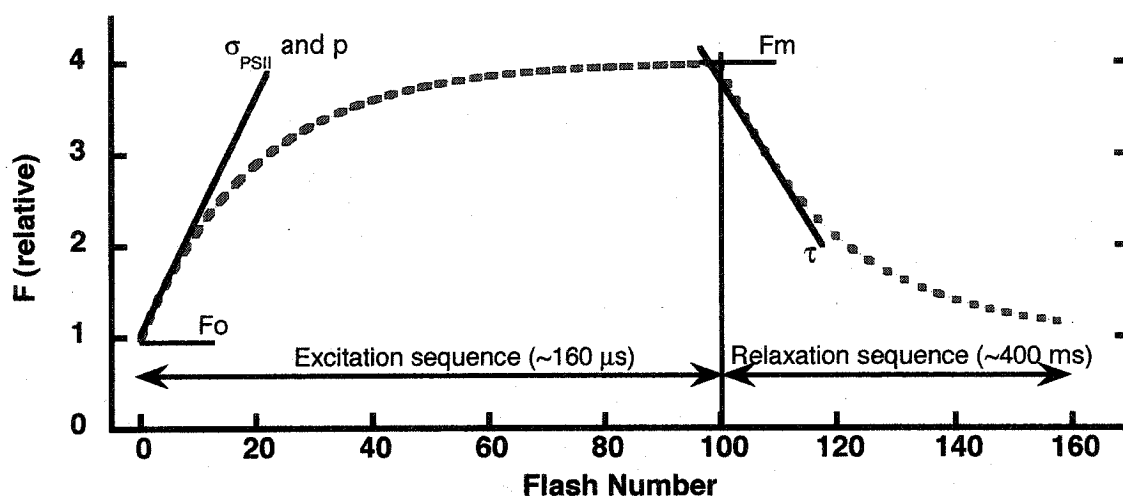


**Figure 2.8: Fluorescence transients measured by the FRR method. During the excitation sequence (single turnover flash) a series of 80 to 120 flashlets (individual smaller flashes forming the single turnover flash) of 0.125 to 1.0  $\mu$ s duration, are performed at 0.5 to 2.0  $\mu$ s intervals. The relaxation sequence consists of a series of 40 to 80 flashlets at intervals varying (ideally) exponentially from 50  $\mu$ s to 50 ms. The excitation sequence provides  $F_o$  and  $F_m$ , the functional absorption cross-section ( $\sigma_{PSII}$ ), and the extent of energy transfer between PS II reaction centers,  $p$ . Relaxation transients provide information about the kinetics of  $Q_a^-$  reoxidation. Adapted from Kolber and Falkowski (1998).**

Kolber and Falkowski (Falkowski and Kolber 1993; Kolber and Falkowski 1993) have proposed a method to measure photosynthetic rates using active fluorescence measurements. Their analysis is based on the pump and probe fluorometers, but it is equally well suited for the FRRF. In this method, they use fluorescence-based estimates to derive most of the parameters in

$$P_f^B \left( \frac{F_v}{F_m} \right) = E^o \sigma_{PSII} A \phi_e n_{PSII} \frac{F_v/F_m}{0.65}, \quad 2.24$$

where  $P_f^B$  (mol electrons (reaction center)<sup>-1</sup> time<sup>-1</sup>) is the chlorophyll specific photosynthetic rate of electron flow through the photosynthetic apparatus,  $\phi_e$  is the quantum yield of electron transport (dimensionless), and  $n_{PSII}$  is the ratio of PSII reaction centers to chl a (mol electrons [mol chl a]<sup>-1</sup>). Though I will not go into the details of the measurements, a few things should be noted. First, the measurement depends on  $n_{PSII}$  which cannot be measured by the usual FRRF fluorescence measurements. Secondly, the true value of  $F_v/F_m$  cannot be obtained in standard deployments at sea as the water remains for at most a few seconds in the dark chamber of the FRRF. Under continuous monitoring, the night-time fluorescence parameters are used to obtain these values. The relationships extend to conditions where non-photochemical quenching is present because changes in  $F_v$  and  $\sigma_{PSII}$  are measured and are expected to reflect changes in NPQ (Falkowski et al. 1994). This method has been tested by Suggett et al. (2001) in the field on a cyanobacterial bloom and they found a linear relationship between an independent measurement of primary production and the FRRF measurements; however, the slope was not equal to unity. A recent study of the parameters  $\sigma_{PSII}$  and  $n_{PSII}$  has found that

while  $\sigma_{PSII}$  is a robust measurement, the proposed use of a constant value for  $n_{PSII}$  (Kolber and Falkowski 1993) can lead to errors of a factor of 2-3 (Suggett et al. 2004).

The FASTRACKA FRR fluorometer, the only commercially available in situ FRRF, has two channels; one for measurements in the light (limited to a certain amount of red light) and one for measurements in the dark. This allows the measurement of dark-adapted samples as well as samples under growth conditions simultaneously. Though problems have been encountered in some studies due to the design of the fluorometer (e.g. Raateoja et al. 2004a; Raateoja et al. 2004b).

## *Chapter 3 A mechanistic model of photosynthesis and fluorescence*

### **3.1 Introduction**

Many models have been created to provide a mechanistic basis for the photosynthesis versus irradiance (PvsE) curve based on target theory (Emerson and Arnold 1932; Dubinsky et al. 1986; Cullen 1990) or on the steady state balance between closure and opening of reaction centers in continuous or variable light (Zonneveld 1997; Han 2001). Some of these models also reproduce the consequences of photoinhibition (Eilers and Peeters 1988; 1993; Zonneveld 1998; Han 2002; Rubio et al. 2003). The models based on the steady state balance between the opening and closure of reaction centers provide good mechanistic representations of some of the that affect photosynthesis in continuous light and provide a good description of the PvsE relationship.

The changes in the shape of the PvsE curve (in a first order approach: the initial slope and the maximum rate in saturating light) are well described by the models above as a function of physiological parameters, such as the effective absorption cross-section or the turnover rate of electron transport. The effects of environmental factors on these physiological parameters are generally studied with another type of model, the so-called acclimation models. The models proposed by Geider and colleagues (Geider et al. 1996; Geider et al. 1997; 1998; see also Geider and MacIntyre 2002) are good examples. In

these models, to drive photoacclimation, Geider and colleagues developed a regulatory ratio, which provides a measure of the balance between absorption and utilization of light. The numerator in this ratio is the photosynthetic rate under ambient irradiance and the denominator is the idealized rate (i.e. the photosynthetic rate if photosynthesis continued with a maximal quantum yield at all irradiances). Hence, this ratio provides a measure of the acclimation pressure, that is, excitation energy relative to the capacity of the cell to utilize it. To obtain the acclimated state under a given set of environmental conditions, the models regulates this ratio by changing the allocation of photosynthates to two (or three) pools of products: an enzymatic (carbon fixation) pool which utilizes electrons created by charge separation at PSII; and a pigment pool which increases the rate of light absorption and charge separation at PSII. The ultimate goal of these dynamic models is to explain changes occurring in the carbon to chlorophyll ratio, PvsE curve, and growth rate of algae as they acclimate to different levels of irradiance, nutrient status, and temperature.

As described in Chapter 2, photosynthesis and fluorescence are closely linked: high photosynthetic efficiency quenches fluorescence emission at low light whereas at higher irradiance fluorescence is quenched by increased efficiency of heat dissipation. These simple concepts have led biological oceanographers to use and misuse the active fluorescence signal in the ocean to estimate biomass or primary production. Interest in using sun-induced fluorescence to estimate primary productivity in situ (Kiefer et al. 1989) or from space (Abbott and Letelier 1999) has led to a number of models to interpret the sun-induced fluorescence signal.

The first group of models include semi-empirical relationships between the quantum yield of fluorescence and photosynthesis (Kiefer et al. 1989; Chamberlin et al. 1990; Chamberlin and Marra 1992; Stegmann et al. 1992; Yoshikawa and Furuya 2004). In their models, the authors parameterize the measured ratio of the quantum yield of carbon fixation and fluorescence as a function of irradiance and then use this parameterization to predict primary productivity. As such, the parameterized relationships do not provide a mechanistic basis for the observations, but rather a diagnostic model of the observed patterns; they describe the results without providing an explanation of the processes underlying them. In some of the early papers, contamination of the measured fluorescence signal from Raman scattering may also have distorted the results (Maritorena et al. 2000; Morrison 2003).

Babin et al. (1996b) constructed a model of fluorescence which includes non-photochemical quenching and the effect of nutrient limitation on the fluorescence emission in surface waters (see Chapter 2). This model is semi-empirical; the authors used the Schatz et al. (1988) model of fluorescence induction and adapt it to continuous light by providing a relationship between the saturation irradiance for photosynthesis and the level of closure of reaction centers. The Babin et al. (1996b) model includes a parameterization of damage, nutrient limitation, and non-photochemical quenching. Acclimation is modeled by the effect of changing the saturation irradiance for photosynthesis ( $E_k$ ,  $\mu\text{mol m}^{-2} \text{s}^{-1}$ ) on the fraction of open reaction centers. However, no functional form is proposed to explain variability in  $E_k$ . The model was developed to study the steady-state fluorescence emission at the surface and cannot be used to study

the dynamic effects of vertical mixing on fluorescence, and the link between photosynthesis and fluorescence was not made.

Morrison (2003) presented a model of sun-induced chlorophyll fluorescence which includes photochemical quenching and energy-dependent as well as photoinhibition-dependent non-photochemical quenching. While Morrison related the energy dependent quenching to the light level, the photoinhibition-dependent quenching was simply parameterized by a constant decrease of fluorescence at all irradiance levels with little mechanistic basis. This simple parameterization provided good fits to the data he collected. The model, however, does not relate these processes to photosynthesis or provide any dynamics for the patterns observed as all processes are related to an instantaneous irradiance level.

Marra (1997) proposed a simple model to reproduce diel variability observed from active fluorescence and beam attenuation. His model relates fluorescence measured with a standard fluorometer to growth, non-photochemical quenching and photoacclimation of the carbon to chlorophyll ratio. The model uses simple parameterizations with instantaneous incident irradiance to model the carbon to chlorophyll ratio and non-photochemical quenching. It provides patterns that are consistent with observations. The model's main limitations are the lack of photochemical quenching, the absence of dynamics related to photoinhibition, and the lack of light history (instantaneous changes in the carbon to chlorophyll ratio with changes in incident irradiance are unrealistic); many of these limitations were indeed recognized by the author.

While the models developed to date perform well when explaining or reproducing the processes studied, *we do not have a mechanistic model that can explain the interaction between fluorescence, photosynthesis and heat dissipation at all light levels on timescales varying from seconds to days in the ocean.* Given the importance of fluorescence measurements in the interpretation of biological oceanographic processes, I believe there is a need for such a model to guide the interpretation of fluorescence data and to allow the modeling of the photo-physiological dynamics of phytoplankton in the mixed layer of the ocean.

The objective of this chapter is, therefore, to provide a mechanistically based model of fluorescence (requiring a description of photosynthesis), which is dynamic on timescales of seconds to days. The model will not address growth of phytoplankton, but will include a simple mechanism for the process of photoacclimation. Furthermore, the model will focus on the reaction center level of organization, ignoring cell level acclimation in optical properties (Morel and Bricaud 1981; 1986; Bricaud et al. 1995; Babin et al. 1996b). The objective will be to develop a set of equations that will completely specify photosynthesis and fluorescence at any time given a scalar irradiance timeseries and some physiological parameters. The model is developed such that it can be incorporated in a model of the mixed layer of the ocean to examine the effect of mixing on fluorescence and photosynthesis at the sea surface (cf. Falkowski and Wirick 1981; Lewis et al. 1984; Franks and Marra 1994; Neale et al. 1998) and provide a tool for studying the different sources of variability in the quantum yield of fluorescence in surface waters. This will be achieved by distilling phytoplankton physiology into the

processes that are most important on timescales of seconds to days in terms of their influence on fluorescence. In this study, I do not expect to capture all the important physiological processes in all phytoplankton species, but rather to simulate an “average” eukaryotic phytoplankton assemblage in its responses. A large amount of variability is expected around the relationships developed here, but the mechanistic approach facilitates the incorporation of additional physiological mechanisms. The different processes included in the model are photochemical quenching, energy- and photoinhibition-dependent non-photochemical quenching, nitrogen limitation, and acclimation. Including photosynthesis, physiology and fluorescence in one model, will provide a tool for diagnosing the origins of the physiological variability in the observations of sun-induced fluorescence in the ocean. In this chapter, I will first review a recent model (Han 2002), address some of its limitations, and use it as the basis for the development of a new model of photosynthesis and fluorescence.

## **3.2 Background**

### **3.2.1 Han's model of photosynthesis**

In Han's (2002) model, as in many earlier models, a reaction center (RC) is assigned to one of three states: open ( $A_H$ ), closed ( $B_H$ ) or inhibited ( $C_H$ ), where  $A_H$ ,  $B_H$ , and  $C_H$  are the probabilities for each state, with  $A_H + B_H + C_H = 1$  (see Table 3-1 for a list of symbols). Figure 3.1 shows the relationships and rate constants for exchange between these pools. The equations describing the dynamics of this system are

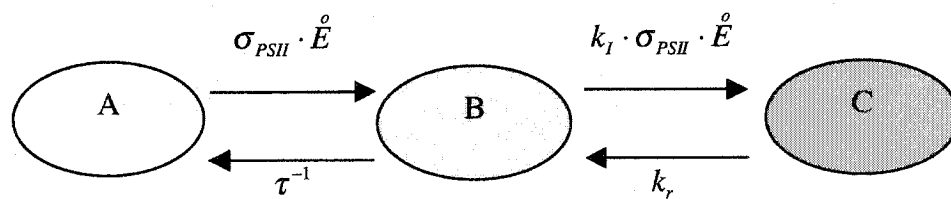


**Figure 3.1: Han's (2002) model of photosynthesis. The three pools of reaction centers are: open (A); closed (B); and inhibited (C). The rates of transfer between the three pools are shown above or below the arrows representing the transitions between the pools. See text for details. Redrawn from Han (2002).**

**Table 3-1: Table of symbols and units.**

Symbol	Description	Units
$a_{\phi}$	Phytoplankton absorption coefficient	$m^{-1}$
$a_{PSII}$	Absorption coefficient of all PSII pigments	$m^{-1}$
$A_H, B_H, C_H$	Probability that a reaction center be open ( $A_H$ ), closed ( $B_H$ ), or inhibited ( $C_H$ ) in Han's model	Unitless
$A, B, C$	Fraction of open, closed and inhibited reaction centers obtained in my model.	Unitless
$C_{1/2}$	Half saturation concentration of inhibited reaction center for repair of inhibited reaction centers	Unitless
$\overset{o}{E}, \overset{o}{E}_{ideal}$	Scalar irradiance	$\mu mol\ m^{-2}\ s^{-1}$
$k_{inh}$	Damage rate from UV radiation.	$s^{-1}$
$E_k$	Saturation irradiance for photosynthesis	$\mu mol\ m^{-2}\ s^{-1}$
$F_o, F_m$	Minimum and maximal fluorescence emission in the dark acclimated state occurring when all reaction center are open ( $F_o$ ) and closed ( $F_m$ )	Relative
$F'_o, F'_m$	Minimum and maximal and fluorescence emission in the light occurring when all reaction center are open ( $F'_o$ ) and closed ( $F'_m$ )	Relative
$F'$	Fluorescence emission in the light	Relative
$k_x$	Rate constant where the subscript $x$ can take the following value: $d$ = PSII basal thermal dissipation in functional reaction center, $f$ =PSII fluorescence, $I$ = heat dissipation associated with inhibited PSII reaction center, $ind$ =induction of energy dependent quenching, $qE$ = heat dissipation due to energy dependent quenching, $p$ = charge separation and stabilization, $r$ = repair of inhibited PSII reaction center in Han model, $rel$ =relaxation of energy dependent quenching, $sinks$ =utilization of electron for non-photosynthetic processes	$s^{-1}$

$k_{Calvin}^{RUB}$	RUBISCO-specific rate of carbon fixation	$e^- s^{-1}$ RUBISCO <sup>-1</sup>
$k_{Calvin}^{max}$	Maximal rate constant of NADPH oxidation by the Calvin cycle enzymes (per RUBISCO)	$e^- s^{-1}$
$k_{rep}^{max}$	Maximal rate constant of repair of inhibited reaction centers	$s^{-1}$
$k_{qE}^{st}$	Steady-state value of the rate constant $k_{qE}$	$s^{-1}$
$K_{Calvin}$	Rate of NADPH oxidation by the Calvin cycle	$e^- s^{-1}$
$K_{rep}$	Rate of repair of inhibited PSII reaction center without the effect of nutrient stress.	$s^{-1}$
$K_{rep}^N$	Rate of repair of inhibited PSII reaction center as affected by nutrient stress.	$s^{-1}$
$m$	Constant of proportionality between excess irradiance and $NPQ$	$[\mu mol m^{-2} s^{-1}]^{-1}$
$n_{Calvin}$	Ratio of RUBISCO to PSII	Unitless
$N$	Concentration of PSII reaction centers	$\mu mol PSII m^{-3}$
$N_{status}$	Nutrient status of the cell	Unitless
$NADPH$ $NADPH_{1/2}$	Relative concentration NADPH ( $NADPH$ ) and half saturation concentration of NADPH ( $NADPH_{1/2}$ ) for carbon fixation. ( $0 < NADPH < 1$ )	Unitless
$NPQ$ , $NPQ_f$	Non-photochemical quenching parameter, in this chapter I use $NPQ_f$ instead of $NPQ$ to express this parameter.	Unitless
$NPQ_f^{qE}$ , $NPQ_f^I$	Energy dependent ( $NPQ_f^{qE}$ ) and damage dependent ( $NPQ_f^I$ ) non-photochemical quenching parameter	Unitless
$P_C$	Rate of electron transfer to Calvin cycle	$e^- s^{-1}$
$P_C^\sigma$	Rate of electron transfer to Calvin cycle per reaction center	$e^- s^{-1} m^{-2} (\mu mol photon)^{-1}$

$P_{O_2}, P_e,$ $P_{ideal}, P_{eH}$	Photosynthetic rate of phytoplankton, for oxygen evolution ( $P_{O_2}$ ), for charge separation and stabilization ( $P_e$ ), in the idealized condition of no saturation ( $P_{ideal}$ ) and from the Han model for charge separation and stabilization ( $P_{eH}$ )	$\mu\text{mol O}_2 \text{ s}^{-1} \text{ m}^{-3}$ or $\mu\text{mol e}^{-} \text{ s}^{-1} \text{ m}^{-3}$
$P_e^{RC}$	Rate of charge separation per RCII	$(\text{e}^{-} \text{ s}^{-1} \text{ RC}^{-1})$
$P_e^{RC\sigma}$	Rate of charge separation per RCII per unit cross-sectional area	$(\text{e}^{-} \text{ s}^{-1} \text{ RC}^{-1} \text{ m}^{-2})$
$\Delta \overset{\circ}{E}_{exc}$	Excess irradiance	$\mu\text{mol m}^{-2} \text{ s}^{-1} \text{ nm}^{-1}$
$\varepsilon_{UV}$	Biological weighting function for damage to PSII	$(\mu\text{mol m}^{-2})^{-1}$
$\phi_x$	Quantum yield where the subscript $x$ can take the following value (the product is given in parenthesis, see units): $pO_2$ =oxygen evolution at the PSII reaction center (oxygen), $pA$ =photochemistry at open PSII reaction centers ( $\text{e}^{-}$ ), $f$ =PSII fluorescence (photon emitted), <b>NPQ</b> =heat dissipation in PSII due to energy dependent quenching (photon dissipated), <b>d</b> =PSII basal thermal dissipation in functional reaction center (photon dissipated), <b>I</b> =heat dissipation associated with inhibited PSII reaction center (photon dissipated), <b>p</b> =photochemistry (charge stabilization), <b>qE</b> =energy dependent non-photochemical quenching (photon dissipated), $F_o'$ =fluorescence by open PSII reaction centers in the light (photon emitted), $F_m'$ =fluorescence by closed reaction PSII centers (photon emitted), $F_i'$ =fluorescence by inhibited reaction PSII centers in the light (photon emitted), $F_i$ =fluorescence by inhibited reaction centers in the dark acclimated state (photon emitted), $F_o$ =when all reaction centers are open in the dark acclimated state (photon emitted), $F_m$ =when all reaction centers are closed in the dark acclimated state (photon emitted).	$\mu\text{mol product}$ $(\mu\text{mol photon absorbed})^{-1}$
$\phi_{F_o}', \phi_{F_m}'$	Quantum yield of fluorescence when all active reaction centers are open ( $\phi_{F_o}'$ ) and closed ( $\phi_{F_m}'$ ) in the light acclimated state.	$\mu\text{mol photon}$ $(\mu\text{mol photon absorbed})^{-1}$

---

$\phi_{F_o}'' , \phi_{F_m}''$	Quantum yield of fluorescence when all active reaction centers are open ( $\phi_{F_o}''$ ) and closed ( $\phi_{F_m}''$ ) after 20 minutes in the dark, in the absence of energy dependent non-photochemical quenching but in the presence of damage.	$\mu\text{mol photon}$  $(\mu\text{mol photon absorbed})^{-1}$
$\phi_{pO_2}^{\max}, \phi_p^{\max}$	Maximal photochemical quantum yield for oxygen evolution ( $\phi_{pO_2}^{\max}$ ), and for charge stabilization ( $\phi_p^{\max}$ )	$\mu\text{mol product}$  $\mu\text{mol photon absorbed}^{-1}$
$\gamma_{NPQ}, \gamma_{NPQ}^{opt}$	Variable capacity for non-photochemical quenching and capacity under optimal growth condition dependent on the acclimation state.	$[\mu\text{mol m}^{-2} \text{s}^{-1}]^{-1}$
$\gamma_d, \gamma_o$	Total and constant part of the capacity for non-photochemical quenching.	$[\mu\text{mol m}^{-2}]^{-1}$
$\kappa_{\sigma_{PSII}}$	Proportionality factor between the rate of electron utilization by the Calvin cycle and the rate of change of $\sigma_{PSII}^O$ .	$\text{s}^{-1}$
$\psi_d$	Probability of damage to PSII per absorbed photon by a closed reaction center	Unitless
$\sigma_{PSII}, \sigma_{PSII}', \sigma_{PSII}^{opt}$	Functional absorption cross-section of PSII in the dark ( $\sigma_{PSII}$ ), in the light ( $\sigma_{PSII}'$ ) and under optimal conditions ( $\sigma_{PSII}^{opt}$ ).	$\text{m}^2 (\mu\text{mol photon})^{-1}$
$\sigma_{PSII}^O$	Optical absorption cross-section of PSII	$\text{m}^2$
$\tau$	Turnover time for reopening closed reaction centers. In my model, this is equivalent to the turnover rate of the electron transport chain (without dark reactions).	$\text{s}$

---

$$\begin{aligned}
\frac{dA_H}{dt} &= -\overset{\circ}{E} \sigma_{PSII} A_H + \frac{B_H}{\tau} , \\
\frac{dB_H}{dt} &= \overset{\circ}{E} \sigma_{PSII} A_H - \frac{B_H}{\tau} + k_r C_H - \psi_d \sigma_{PSII} \overset{\circ}{E} B_H , \\
\frac{dC_H}{dt} &= -k_r C_H + \psi_d \sigma_{PSII} \overset{\circ}{E} B_H ,
\end{aligned} \tag{3.1}$$

where  $\overset{\circ}{E}$  is the scalar irradiance ( $\mu\text{mol quanta m}^{-2} \text{s}^{-1}$ ),  $\sigma_{PSII}$  is the effective absorption cross-section of photosystem II ( $\text{m}^2 \mu\text{mol quanta}^{-1}$ ) in the dark acclimated state,  $\tau$  is the turnover rate of the electron transport chain (s),  $k_r$  ( $\text{s}^{-1}$ ) is the rate constant for the repair of inactivated reaction centers (through de novo synthesis of reaction center protein and assembly into active photosystem II (PSII) centers e.g. Aro et al. 1993), and  $\psi_d$  (dimensionless) is the probability of damage to photosystem II per photon absorbed by closed reaction centers.

The first of equations 3.1 describes how the fraction of open reaction centers decreases with a rate equal to the rate of primary photosynthetic events in PSII ( $\overset{\circ}{E} \sigma_{PSII}$ ) times the fraction of open RCs (leading to reaction center closure); while it increases with a rate equal to the fraction of closed RCs divided by the turnover rate ( $\tau$ ) of closed RCs (reaction center reopening). The second equation shows that the rate of increase of the fraction of closed RCs is the same as the rate of closure of open RCs and the rate of decrease of closed RCs is equal to the rate of opening of RCs. In addition, the fraction of closed RCs decreases with a rate equal to the rate of damage in closed RCs ( $\psi_d \sigma_{PSII} \overset{\circ}{E}$ ) times the fraction of closed RCs and increases with the rate of repair of inhibited RCs times the fraction of inhibited RCs. The rate of damage is equal to the rate at which

primary photosynthetic events would occur if closed RCs were open ( $\overset{\circ}{E} \sigma_{PSII}$ ) times a probability that such an event leads to damage ( $\psi_d$ ). The third equation shows that the fraction of inhibited RCs increases as the rate of damage of closed RCs times the fraction of closed RCs and decreases with the rate of repair times the fraction of inhibited RCs.

To simplify the notation, spectral effects are ignored during development of the model. However, most spectral effects can be accounted for simply by replacing  $\overset{\circ}{E}$  by

$$\overset{\circ}{E}_{PAR} = \int_{400}^{700} \overset{\circ}{E}(\lambda) d\lambda$$

and  $\sigma_{PSII}$  by

$$\bar{\sigma}_{PSII} = \int_{400}^{700} \sigma_{PSII}(\lambda) \overset{\circ}{E}(\lambda) d\lambda / \int_{400}^{700} \overset{\circ}{E}(\lambda) d\lambda.$$

At steady state, the solution for the fraction of open reaction centers is

$$A_H = \frac{1}{1 + \sigma_{PSII} \overset{\circ}{E} \tau + \frac{\psi_d}{k_r} \tau \left( \sigma_{PSII} \overset{\circ}{E} \right)^2}. \quad 3.2$$

Han (2002) assumes that the observed quantum yield of photosynthesis in terms of oxygen evolution ( $\phi_{pO_2}$ ,  $O_2$  (photon absorbed)<sup>-1</sup>) decreases only because of a decrease in the fraction of open reaction centers while the quantum yield of open reaction centers remain constant at its maximal value  $\phi_{pO_2}^{\max}$  ( $O_2$  [photon absorbed]<sup>-1</sup>). Thus, he uses the following parameterization for the quantum yield of photosynthesis (in my notation)

$$\phi_{pO_2} = A_H \phi_{pO_2}^{\max}. \quad 3.3$$

The photosynthetic rate becomes

$$P_{O_2} = \phi_{pO_2} a_{\phi} \overset{o}{E} = A_H \phi_{pO_2}^{\max} a_{\phi} \overset{o}{E}, \quad 3.4$$

where  $a_{\phi}$  ( $\text{m}^{-1}$ ) is the phytoplankton absorption coefficient by all pigments. In equation 3.4 the irradiance dependence of the quantum yield is included in  $A_H$ .

While the Han model focuses on the PvsE curve for oxygen evolution, my model will concentrate the photosynthetic rate in terms of electron transport  $P_e$  ( $\mu\text{mol e}^{-} \text{s}^{-1} \text{m}^{-3}$ ). For eukaryotic microalgae under balanced growth, the maximum quantum yield for electron transport (more specifically charge separation and stabilization, see Chapter 2) obtained using fluorescence measurements,  $\phi_p^{\max}$  ( $\text{e}^{-} (\text{photon absorbed})^{-1}$ ), is close to 0.65 for many species, with lower yields observed in cyanobacteria (Campbell et al. 1998). Note that the lower maximal yield obtained by fluorescence in algae compared to higher plants ( $\phi_p^{\max} \sim 0.82$ ) or in cyanobacteria compared to algae, is not necessarily an indication of a lower photosynthetic yield as could be measured by oxygen evolution for example (Campbell et al. 1998). However, it provides a good starting point for modeling with the understanding that the real quantum yield of charge separation could be higher than that measured by fluorescence, especially if fluorescence from PSI or other fluorescing pigments is important (Campbell et al. 1998; Oxborough et al. 2000).

With the assumption of negligible fluorescence from PSI, and because the fluorescence measurement accounts almost exclusively for the light absorbed by light harvesting complexes associated with photosystem II, it is convenient to express the light absorbed only in terms of the absorption by photosystem II ( $a_{PSII}$ ,  $\text{m}^{-1}$ ), such that the

photosynthetic rate for electron transport obtained using Han's model,  $P_{eH}$  ( $\mu\text{mol e}^- \text{s}^{-1} \text{m}^{-3}$ ), would be expressed as

$$P_{eH} = A_H \phi_p^{\max} a_{PSII} \bar{E}. \quad 3.5$$

Using equation 3.5 and equation 3.2 we can obtain the photosynthetic rate in terms of charge separation at steady state as a function of light intensity,

$$P_{eH} = \frac{\phi_p^{\max} a_{PSII} \bar{E}}{1 + \sigma_{PSII} \bar{E} \tau + \frac{\psi_d}{k_r} \left( \sigma_{PSII} \bar{E} \right)^2 \tau}. \quad 3.6$$

Note that throughout this section, I have used the subscript "H" on some parameters to emphasize that I am using Han's model to obtain the relationships.

### Side note: Effects of UV radiation

The model presented by Han (2002) is well suited to study the effect of ultraviolet

(UV) radiation. The term for the rate for inactivation ( $\psi_d \sigma_{PSII} \overset{\circ}{E} B$ ) can be extended to

include UV by writing,  $B_H \left( \psi_{PAR} \sigma_{PSII} \overset{\circ}{E}_{PAR} + \int_{280}^{400} \epsilon_{UV}(\lambda) \overset{\circ}{E}(\lambda) d\lambda \right)$ , where  $\psi_{PAR}$  is the

efficiency of damage due to the absorption of PAR radiation, and  $\epsilon_{UV}(\lambda)$  ( $\mu\text{mol m}^{-2}$ )<sup>-1</sup> is a biological weighting function (cf. Cullen et al. 1992a; Cullen and Neale 1997) for the creation of an inhibited reaction center. In this case, the biological weighting function can be represented as an absorption cross-section for damage,  $\sigma_{dam}$  (m<sup>2</sup>), times a quantum yield for damage,  $\phi_{dam}$  ( $\mu\text{mol RC}$  ( $\mu\text{mol photon}$ )<sup>-1</sup>), divided by the total number of reaction centers ( $N_{RC}$ ,  $\mu\text{mol RC}$ ):  $\epsilon_{UV}(\lambda) = \phi_{dam} \sigma_{dam}(\lambda) / N_{RC}$  (e.g. Harm 1980). The rate of damage (s<sup>-1</sup>) can then be defined as

$$k_{inh} = \int_{280}^{400} \epsilon_{UV} \overset{\circ}{E}(\lambda) d\lambda.$$

Han's (2002) model assumes that the target of damage is closed reaction centers. This may be a good assumption for PAR radiation (Oxborough and Baker 2000), but may not be appropriate for UV. Assuming is that the rate of repair, is the same for PAR and UV inactivation and that open and closed reaction centers have an equal probability of being damaged by a UV photon then the set of equations becomes

$$\begin{aligned} \frac{dA_H}{dt} &= -\overset{\circ}{E} \sigma_{PSII} A_H + \frac{B_H}{\tau} - A_H k_{inh} \\ \frac{dB_H}{dt} &= \overset{\circ}{E} \sigma_{PSII} A_H - \frac{B_H}{\tau} + k_r C_H - B_H \left( \psi_{PAR} \sigma_{PSII} \overset{\circ}{E} + k_{inh} \right) \\ \frac{dC_H}{dt} &= -k_r C_H + \psi_{PAR} \sigma_{PSII} \overset{\circ}{E} B_H + (A_H + B_H) k_{inh} \end{aligned}$$

Because the repair rate is described explicitly (e.g. Neale 2000), this model is general and accounts for dose or dose rate dependence (see also Huot et al. 2000).

### **3.3 Model development**

#### **3.3.1 Addressing some limitations of the Han model for fluorescence work.**

The models developed by Han (2001; 2002) were strictly to study the processes influencing the PvsE curve. To use this model as the basis for a fluorescence and photosynthesis model, some of the assumptions that were made during its development have to be addressed.

##### **3.3.1.1 Constant effective absorption cross-section**

The first assumption made is that the effective absorption cross-section (e.g. Dubinsky et al. 1986) of an acclimated phytoplankter remains constant at all irradiances. This is not the case since non-photochemical quenching in the antenna (e.g. due to energy dependent non-photochemical quenching, see chapter 2) decreases the effective absorption cross-section when irradiance increases (Falkowski and Raven 1997). Therefore, it is appropriate to use an effective absorption cross-section that is light dependent (which I denote  $\sigma'_{PSII}$ ,  $\text{m}^2 \mu\text{mol quanta}^{-1}$ ).

To provide a fully mechanistic description of  $\sigma'_{PSII}$  with illumination, one would need a complete model of energy dependent non-photochemical quenching (Ruban and Horton 1995; Gilmore et al. 1998; Gilmore and Govindjee 1999), reallocations of antenna capacity through processes such as state transitions (Haldrup et al. 2001; Wollman 2001) and connectivity of reaction centers (e.g. Havaux et al. 1991; Trissl and Lavergne 1995). Such a model would be difficult to construct, requiring, amongst other things, accounting for the change in the proton motive force across the thylakoid membrane, an area of

active research in higher plants (Kramer et al. 1999). Instead, to model  $\sigma'_{PSII}$ , I will use a simple parameterization based on the observation that the fluorescence parameter  $NPQ$  is linearly related to the “excess irradiance” absorbed by the plant (Björkman and Demmig-Adams 1994; Demmig-Adams and Adams III 1996).

The second assumption is that the turnover time ( $\tau$ ) remains constant for all concentrations of closed reaction centers. This implies that for any level of reaction system closure, the fraction of reaction centers reopening per unit time remains constant. This can only occur if the capacity to process electrons by the reactions downstream of photosystem II is never saturated. This however, is unlikely at high irradiance levels (or at low temperature) due to the rate limitation of enzymatic reactions of the Calvin-Benson cycle (e.g. Sukenic et al. 1987; Falkowski and Raven 1997).

To address the limitation by processes downstream of photosystem I, I will model the fate of the pool of a product of linear electron transport. The simulated pool will be the pool of NADP that is reduced to NADPH by electrons from the donor side of photosystem I (see Chapter 2 for more details). The depletion rate of NADP (as it is reduced to NADPH) will be proportional to the electron transport rate and its regeneration rate is due to the dark reactions (carbon fixation and other sinks).

Finally, the third assumption addressed is that the rate of repair of inhibited reaction centers is a constant fraction of the inhibited reaction centers per unit time. This can only occur if the repair capacity of the cell is very large, and never limited. It is, however, more realistic to assume that at high damage levels the repair rate will saturate once enzymatic reactions reach maximal capacity. This limitation will simply be

addressed by allowing the rate of repair to saturate at a maximum level.

Before I start building the model, I would like to provide a short descriptive overview to provide a basis for the following sections.

### 3.3.2 *Model overview*

Seven differential equations form the basis of the model. As in the model developed by Han (2002), I use three differential equations to represent the three states of the reaction center: open, closed and inhibited (Figure 3.2 top). The absorption of a photon leads to the closure of the reaction center, while the utilization of the electron in the dark reactions (through the NADP pool) allows the closed reaction centers to reopen. The damage to reaction centers will occur through the probability that a closed reaction center becomes damaged, while the repair rate will allow recovery to the closed state. The repair rate will be a function of the nitrogen status of the cell ( $N_{status}$ ).

One differential equation is used to follow the state of the NADP pool. Electrons can only be transferred if NADP is oxidized; therefore, when carbon fixation is slower than the rate of reaction center closure, most of the NADP will be reduced to NADPH and most reaction centers will be closed.

Two equations are used to describe photoacclimation, which will occur through a change in the composition and size of the optical absorption cross-section; high growth irradiance leads to a smaller absorption cross-section and a greater fraction of photoprotective to photosynthetic pigments. Because the pigment pools are not followed, the change in the ratio of photoprotective to photosynthetic pigment will be modeled as a change in the capacity for energy-dependent non-photochemical quenching, without

**Figure 3.2: Schematic representation of the photosynthesis and fluorescence model with acclimation. The top portion shows the model in a low-light acclimated state and the bottom part shows the model in a high-light acclimated state; the only difference is the size of the optical cross-section (area of trapezoid) of the reaction center and the ratio of photoprotective to photosynthetic pigments. The model has three states for the reaction center: it can be open (pale blue circle), closed (red cross), or inhibited (white circle). The transitions between the three pools are represented by arrows. The absorption of photons by open reaction centers leads to the closure of reaction centers, the absorption by closed reaction centers has a probability of leading to the inhibition of the reaction center. An inhibited reaction center is repaired to a closed reaction center with a repair rate that depends on the nitrogen status of the cell ( $N_{status}$ ). Closed reaction centers are reopened by the transfer of an electron to NADP, which is reduced at the same time to NADPH. The NADPH pool is oxidized to the NADP pool by the utilization of the reducing energy during carbon fixation (and other sinks). The box on the lower left shows another dynamic portion of the model where the energy-dependent non-photochemical quenching changes with incident irradiance (represented by wider yellow bars at high incident irradiance) allowing a greater fraction of the absorbed irradiance to be dissipated at high irradiance.**

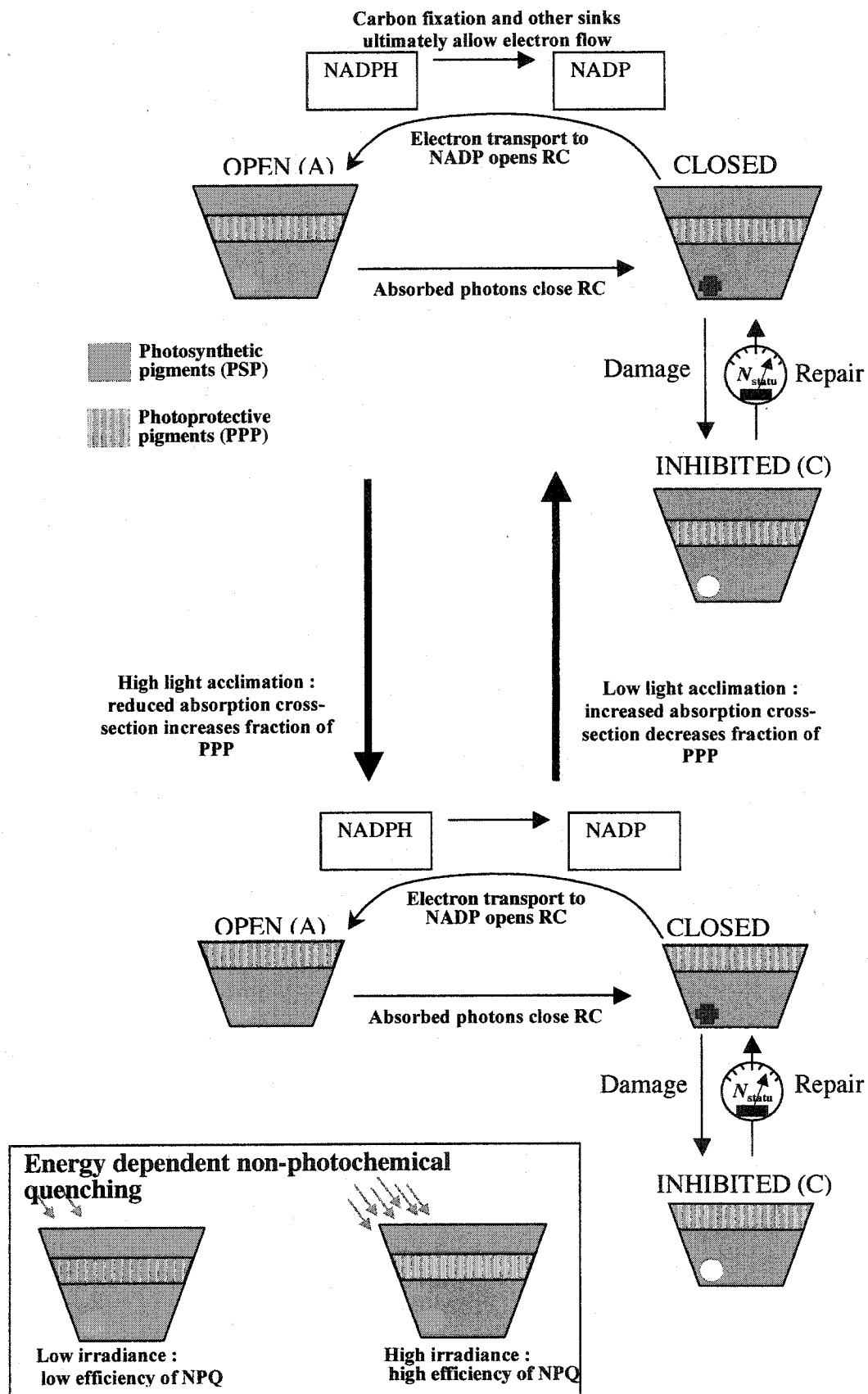


Figure 3.2: See previous page for caption.

modifying the absorption cross-section.

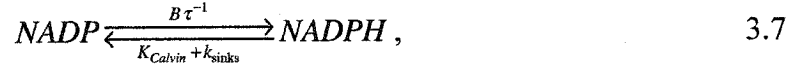
The last differential equation is used to represent the changes in the xanthophyll cycle pigments with incident irradiance. The box in the lower left of Figure 3.2 represent schematically the model for non-photochemical quenching. To simulate the xanthophyll cycle, at high incident irradiance, the photoprotective pigments will be in a state that will allow more of the energy to be dissipated as heat (represented by a more yellow color) than under low incident irradiance. This increase in the capacity for heat dissipation will be simulated by changing the rate constant for energy dependent quenching in the PSII model.

This completes the overview of the model; in the next section, I describe the dynamics of the NADP pool.

### **3.3.3 *The NADP pool: linking the light reactions to biosynthetic reductions***

The product of linear photosynthetic electron transport is the reductant NADPH (reduced form of nicotinamide adenine dinucleotide phosphate, NADP). A simple reaction scheme for the reaction can be constructed by assuming two competing sinks for NADPH (or more generally electron acceptors on the donor side of PSI): the first is the Calvin cycle (carbon fixation) while the second includes all electron utilization by processes other than carbon fixation (e.g. Falkowski and Raven 1997). These include pseudocyclic electron flow around PSI (the Mehler reaction e.g. Ort and Baker 2002) and nitrate reduction (for a review of these processes and others see Noctor and Foyer 2000). The dependence of these other sinks for electrons on light intensity or physiological state is not easily determined and much remains to be learned about their regulation in

microalgae (e.g. Flameling and Kromkamp 1998; Lomas and Glibert 2000; Lomas et al. 2000; Ort and Baker 2002). Therefore, at this point, only the simplest model is warranted and I will assume that a constant fraction of the NADPH formed is used up by these processes per unit time (first order reaction) with a rate constant,  $k_{\text{sinks}}$  ( $\text{s}^{-1}$ ). The oxidation-reduction reaction for NADP can then be written as



where  $B\tau^{-1}$  is the rate of electron transfer to NADP, and  $K_{\text{Calvin}}$  ( $\text{e}^{-} \text{s}^{-1}$ ) is the rate with which the NADPH is oxidized and used by the Calvin-Benson cycle. The differential equation representing this reaction is

$$\frac{dNADP}{dt} = -\frac{B}{\tau} NADP + K_{\text{Calvin}} + k_{\text{sinks}}. \quad 3.8$$

In the model I will use a relative pool size of 1 for NADP plus NADPH such that  $NADP + NADPH = 1$ . If we assume for simplicity that the Calvin cycle can be represented by a saturating function in which the substrate is NADPH, we can then model  $K_{\text{Calvin}}$  as

$$K_{\text{Calvin}} = n_{\text{Calvin}} \frac{k_{\text{Calvin}}^{\text{max}} NADPH}{NADPH_{1/2} + NADPH} = n_{\text{Calvin}} K_{\text{Calvin}}^{\text{RUB}}, \quad 3.9$$

where  $NADPH_{1/2}$  is the half saturation concentration of NADPH,  $n_{\text{Calvin}}$  is the ratio of the number of RUBISCO enzymes to PSII reaction centers,  $k_{\text{Calvin}}^{\text{max}}$  is the maximum rate of electron transfer to  $\text{CO}_2$  by the Calvin cycle ( $\text{e}^{-} \text{s}^{-1} \text{RUBISCO}^{-1}$ ), and  $K_{\text{Calvin}}^{\text{RUB}}$  is the RUBISCO specific rate of carbon fixation. Because the enzymatic reaction catalyzed by RUBISCO is the limiting step in the Calvin cycle, it is useful to have its concentration as

the numerator of  $n_{\text{Calvin}}$  to represent the capacity of the dark reactions to utilize electrons. Equation 3.9 assumes that the ATP (adenosine triphosphate) or  $\text{CO}_2$  is not limiting the rate of carbon-fixation and that the complex enzymatic reaction scheme of the Calvin cycle is well represented by the Michaelis-Menten functional form, which holds for one enzymatic reaction. This approach follows the same underlying idea as the work of Rubio et al. (2003), that the dark reactions are limiting the rate of photosynthesis through a saturating function, except that the implementation through the pool of an end product of the photosynthetic chain is different.

In the next section, I will provide some context for the description of the model by defining the quantum yields in terms of rate constants within the context of a puddle model of PSII organization.

#### ***3.3.4 The puddle model and quantum yields in terms of rate constants***

Han's model assumes no connectivity between reaction centers. That is, the light absorbed by pigments associated with one reaction center cannot be used by another reaction center. This is referred to as the puddle model (see Chapter 2). To simplify the development and to be consistent with Han's model, I will use a puddle model that assumes no connectivity between the antennas of different reaction centers; the limitations of this model are discussed later. In a pure puddle model, the state of one reaction center does not influence directly the state of another reaction center (but is affected indirectly through non-photochemical quenching).

We can write the following equation for the quantum yield of photosynthesis in PSII (see Figure 3.3 for a schematic representation)

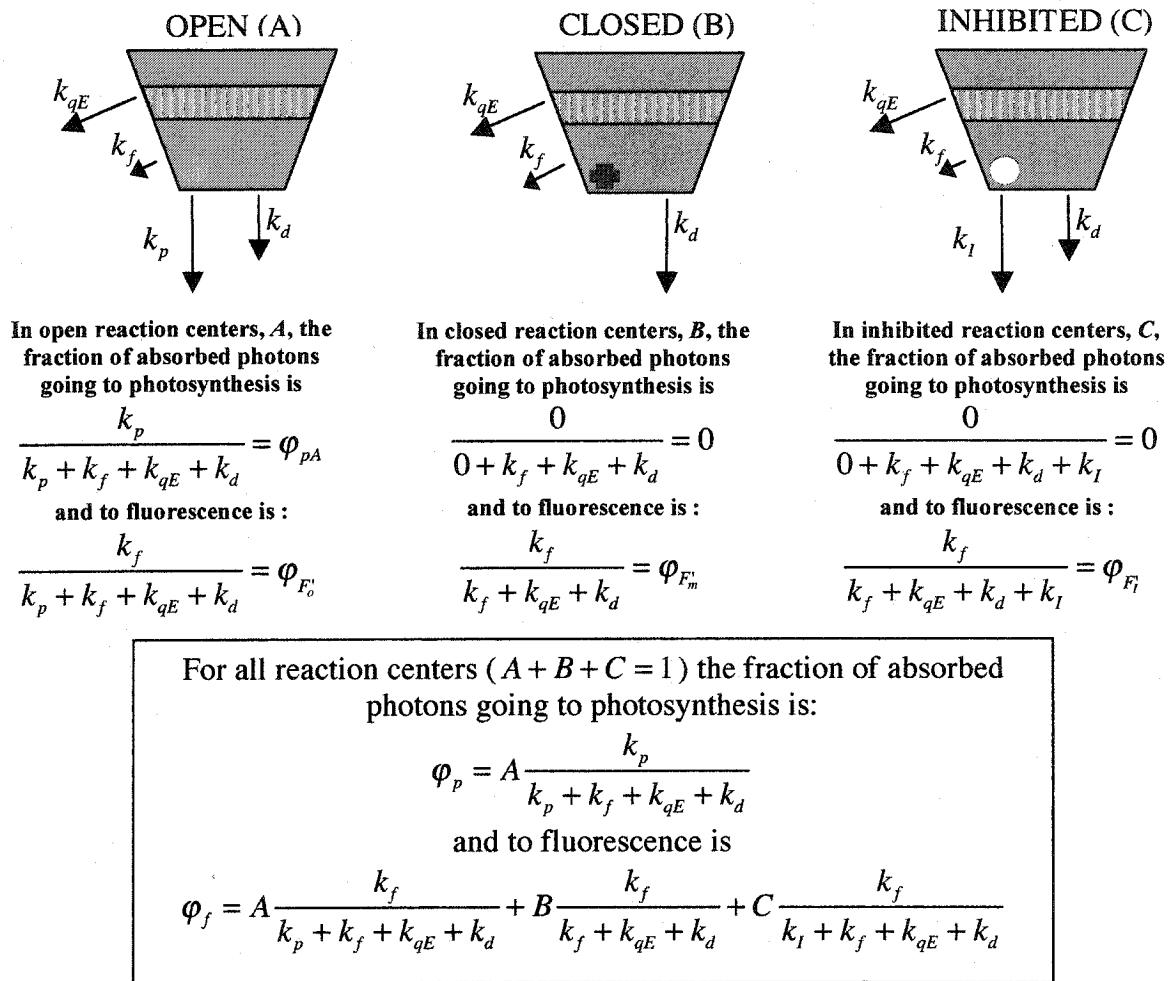


**Figure 3.3: The three states of the reaction centers and associated rate constants.** Each state can be represented in terms of its first order rate constant for deexcitation of absorbed energy and their intrinsic quantum yields. All reaction centers share three common rate constants for deexcitation:  $k_{qE}$  for energy dependent quenching,  $k_f$  for fluorescence, and  $k_d$  for heat dissipation. In addition, in open reaction centers energy can be used for charge separation (photosynthesis) with rate constant  $k_p$  while in inhibited reaction centers heat can be dissipated with a rate constant  $k_I$ . The intrinsic quantum yield for photosynthesis (charge separation) and fluorescence are given below each state as well as the quantum yield when all reaction centers are taken together (box). In a puddle model,  $k_I$  has no influence on the quantum yield of photosynthesis.

$$\varphi_p = A \frac{k_p}{k_d + k_f + k_p + k_{qE}} = A \varphi_{pA}, \quad 3.10$$

where  $A$  is the fraction of open PSII reaction centers,  $k_d$  ( $s^{-1}$ ) is the basal rate constant for heat dissipation,  $k_f$  ( $s^{-1}$ ) is the rate constant for fluorescence,  $k_p$  ( $s^{-1}$ ) is the rate constant for photosynthesis,  $k_{qE}$  ( $s^{-1}$ ) is the rate constant for heat dissipation by energy dependent non-photochemical quenching, and  $\varphi_{pA}$  is the effective quantum yield of open reaction centers.

The maximal quantum yield of photochemistry in PSII, that is the quantum yield in the dark acclimated state when all reaction centers are open ( $A_f = 1$ ) and non-photochemical quenching is completely dissipated ( $k_{qE} = 0$ ) is expressed as (Butler 1978; Roháček 2002):

$$\varphi_p^{\max} = \frac{k_p}{k_p + k_d + k_f} = \frac{F_m - F_o}{F_m}. \quad 3.11$$

We can describe the quantum yield of fluorescence for PSII in terms of rate constants and the fraction of reaction centers in the three states,

$$\begin{aligned} \varphi_f &= A \frac{k_f}{k_d + k_f + k_p + k_{qE}} + B \frac{k_f}{k_d + k_f + k_{qE}} + C \frac{k_f}{k_d + k_f + k_i + k_{qE}}, \\ &= A \varphi_{F_o'} + B \varphi_{F_m'} + C \varphi_{F_i'} \end{aligned} \quad 3.12$$

where  $B$  and  $C$  are respectively the fractions of closed and inhibited reaction centers,  $k_i$  is the rate constant for heat dissipation of an inhibited reaction center,  $\varphi_{F_o'}$ ,  $\varphi_{F_m'}$ , and  $\varphi_{F_i'}$  are respectively the intrinsic quantum yield of reaction centers in the open, closed and inhibited state in the light acclimated state. Therefore, the cell fluorescence quantum

yield is given by the quantum yield of open reaction centers times the fraction of open reaction centers plus the quantum yield of closed centers times the fraction of closed centers plus the quantum yield of inhibited center times the fraction of inhibited centers. When RCII is photoinactivated, the absorption cross-section of the reaction center is not affected but its capacity to utilize the energy for photochemistry is. Observational evidence, however, suggests that inhibited reaction centers can still sink more energy than closed reaction centers (e.g. Valvilin et al. 1998), this capacity is modeled here with the addition of the rate constant  $k_I$  (see Figure 3.3). Therefore, with increasing damage, the quantum yield of fluorescence will be quenched relative to its maximal level, due to inhibition.

I can also express the quantum yield of dissipation of excitation away from RCII due to non-photochemical quenching in terms of rate constants as

$$\varphi_{qE} = A \frac{k_{qE}}{k_d + k_f + k_p + k_{qE}} + B \frac{k_{qE}}{k_d + k_f + k_{qE}} + C \frac{k_{qE}}{k_d + k_f + k_I + k_{qE}}, \quad 3.13$$

and, similarly, for the quantum yield for basal heat dissipation,

$$\varphi_d = A \frac{k_d}{k_d + k_f + k_p + k_{qE}} + B \frac{k_d}{k_d + k_f + k_{qE}} + C \frac{k_d}{k_d + k_f + k_I + k_{qE}}. \quad 3.14$$

The quantum yield for heat dissipated in inhibited reaction centers due to the inhibited state is given by

$$\varphi_I = C \frac{k_I}{k_d + k_f + k_I + k_{qE}}. \quad 3.15$$

By definition, the quantum yield for photosynthesis, fluorescence, basal heat dissipation,

energy-dependent and inhibition-dependent non-photochemical quenching (equations 3.10, 3.12, 3.13, 3.14, and 3.15) sum to unity.

I will now define more yields that are often used in fluorescence work,

$\phi'_{F_m}, \phi'_{F_o}, \phi_{F_m}, \phi_{F_o}$ , these correspond to the fluorescence level  $F'_m, F'_o, F_m$ , and  $F_o$  used in the pulse amplitude fluorescence protocols (see Chapter 2) and are defined within the puddle model as

$$\begin{aligned}\phi'_{F_m} &= (A+B) \frac{k_f}{k_d + k_f + k_{qE}} + C \frac{k_f}{k_d + k_f + k_I + k_{qE}} \\ &= (1-C) \frac{k_f}{k_d + k_f + k_{qE}} + C \frac{k_f}{k_d + k_f + k_I + k_{qE}}, \\ \phi'_{F_o} &= (A+B) \frac{k_f}{k_d + k_f + k_p + k_{qE}} + C \frac{k_f}{k_d + k_f + k_I + k_{qE}} \\ &= (1-C) \frac{k_f}{k_d + k_f + k_p + k_{qE}} + C \frac{k_f}{k_d + k_f + k_I + k_{qE}}, \\ \phi_{F_m} &= \frac{k_f}{k_d + k_f},\end{aligned}$$

and

$$\phi_{F_o} = \frac{k_f}{k_d + k_f + k_p}.$$

Note that the  $\phi_{F_m}$  and  $\phi_{F_o}$  levels defined above correspond to those when no damage is present. In some protocols, the  $F_m$  and  $F_o$  are measured after ~20 minutes in the dark corresponding to a state where all the energy dependent non-photochemical quenching has dissipated but damage is still present at essentially the same level as in the light, I will refer to these levels as the  $F''_m$  and  $F''_o$ . Under those conditions the corresponding

quantum yields become,

$$\begin{aligned}\phi_{F_m}'' &= (A+B) \frac{k_f}{k_d+k_f} + C \frac{k_f}{k_d+k_f+k_I} \\ &= (1-C) \frac{k_f}{k_d+k_f} + C \frac{k_f}{k_d+k_f+k_I},\end{aligned}\tag{3.16}$$

and

$$\begin{aligned}\phi_{F_o}'' &= (A+B) \frac{k_f}{k_d+k_f+k_p} + C \frac{k_f}{k_d+k_f+k_I} \\ &= (1-C) \frac{k_f}{k_d+k_f+k_p} + C \frac{k_f}{k_d+k_f+k_I}.\end{aligned}\tag{3.17}$$

All quantum yields derived in this section are defined with respect to the light absorbed by all pigments associated with photosystems II.

### 3.3.5 NPQ parameter in terms of rate constants

The parameter *NPQ* is defined in the fluorescence literature as

$$NPQ = NPQ_f = (F_M - F_M')/F_M' .\tag{3.18}$$

The choice of the *NPQ* symbol is unfortunate because it is also the abbreviation commonly used for non-photochemical quenching. To avoid confusion, I use the symbol *NPQ<sub>f</sub>* to refer to  $(F_M - F_M')/F_M'$ . The measurement of *NPQ<sub>f</sub>* under normal conditions will include all processes that lead to non-photochemical quenching of the  $F_M'$  measurement, including state-transition, energy-dependent, and photoinhibition-dependent quenching.

Without damage, however, the diminution of  $F_M'$  will arise mostly from energy dependent quenching. Under these conditions, we can define the parameter

$NPQ_f^{qE} = (F_M - F_M')/F_M'$  when there is no damage. This parameter can be expressed in

terms of rate constants as follows (see also Roháček 2002):

$$NPQ_f^{qE} = \frac{k_{qE}}{k_d + k_f}. \quad 3.19$$

The parameter  $NPQ_f^{qE}$  therefore represents the amount of absorbed energy dissipated as heat due to energy dependent non-photochemical quenching relative to that dissipated by basal non-photochemical processes (fluorescence and heat).

### 3.3.6 *Han's model vs. the fluorescence model of photosynthesis*

It is useful at this point to compare Han's model for the quantum yield of photochemistry (equation 3.3) with the model used in the fluorescence literature (equation 3.10). Both describe the realized quantum yield of photosynthesis as the fraction of open reaction centers multiplied by the quantum yield of open reaction centers. There are, however, two subtle differences in these models, stemming from the exclusion of energy dependent non-photochemical quenching from Han's model. In the fluorescence model (equation 3.10) the level  $A$  (e.g. Kramer et al. 2004) and  $\phi_{pA}$  depend on the increased heat dissipation due to non-photochemical quenching ( $k_{qE}$  parameter). The maximum quantum yield used by Han in his model is one for dark conditions (i.e. equivalent to  $\phi_p^{\max}$  not  $\phi_{pA}$ ), which does not account for changes in the quantum yield of photosynthesis with increasing irradiance; all changes in the quantum yield of photosynthesis with irradiance are assumed to originate in the closure of reaction centers.

### 3.3.7 *Parameterization of $k_{qE}$*

I model energy-dependent non-photochemical quenching by changing the value

of the rate constant  $k_{qE}$ . Therefore, to constrain the model I need to define the rules that govern these changes as a function of irradiance. In the next two sections I describe the rules I will use.

In practice, in the light, through state transitions, a fraction of the light-harvesting complex of photosystem II can be transferred to photosystem I (Wollman 2001). The implication of this from the standpoint of the quantum yield of charge separation at PSII (assuming that detached LHCII, are still considered PSII pigments) is the same as an increase in the dissipation of energy in the antenna. Since both occur when irradiance is in excess at PSII they will be modeled as one process here, at the cost of not accounting for their different kinetics (e.g. Krause and Weis 1988).

### 3.3.7.1 *Excess radiation*

If photosynthesis proceeded with constant efficiency at all irradiances, the relationship between photosynthesis and irradiance would be linear with a slope equal to the initial slope of the PvsE curve (and for gross photosynthesis an intercept of zero):

$$P_{ideal} = a_{PSII} \varphi_p^{\max} \overset{o}{E}. \quad 3.20$$

I will refer to the rate of photosynthesis under this hypothetical situation as the idealized rate of photosynthesis ( $P_{ideal}$ ). The decrease in the rate of electron transport and thus gross photosynthesis with irradiance, results from the closure of reaction centers and the increased dissipation of heat. In addition, several other processes not considered in my model will affect net oxygen evolution (Flameling and Kromkamp 1998). As irradiance increases, the difference between the achieved rate of photosynthesis,  $P_{eH}$ , and the idealized rate increases. The difference in irradiance for the same rates of

photosynthesis in the idealized and achieved case (see Figure 3.4) is referred to as the “excess irradiance” or “excess radiation”(Björkman and Demmig-Adams 1994).

We can calculate the excess irradiance  $\Delta \overset{\circ}{E}_{exc} = \overset{\circ}{E} - \overset{\circ}{E}_{ideal}$  where  $\overset{\circ}{E}_{ideal}$  is the irradiance at which the idealized rate is the same as the achieved rate at  $\overset{\circ}{E}$ . Returning to the Han model and using equation 3.6 and 3.20 under the condition of no photoinhibition ( $\psi_d=0$ ) we can write

$$P_{ideal}\left(\overset{\circ}{E}_{ideal}\right) = P_{eH}\left(\overset{\circ}{E}\right),$$

which, by using equation 3.5 (setting  $\psi_d$  to 0) and equation 3.20, can be expanded to

$$a_{PSII} \varphi_p^{\max} \overset{\circ}{E}_{ideal} = A_{H\psi_d=0} \varphi_p^{\max} a_{PSII} \overset{\circ}{E}, \quad 3.21$$

where  $A_{H\psi_d=0}$  is the fraction of open reaction centers when  $\psi_d = 0$  in equation 3.2.

Solving for  $\overset{\circ}{E}_{ideal}$  we have,

$$\overset{\circ}{E}_{ideal} = \overset{\circ}{E} A_{\psi_d=0}, \quad 3.22$$

such that

$$\Delta \overset{\circ}{E}_{exc} = \overset{\circ}{E} - \overset{\circ}{E}_{ideal} = \overset{\circ}{E} (1 - A_{H\psi_d=0}). \quad 3.23$$

This result is proportional to the excess photochemical capacity calculated by

$$P_{ideal}\left(\overset{\circ}{E}\right) - P_{eH}\left(\overset{\circ}{E}\right) = a_{PSII} \varphi_p^{\max} \overset{\circ}{E} (1 - A_{H\psi_d=0}) \text{ but differs from the Geider et al. (Geider et$$

al. 1996; Geider and MacIntyre 2002) regulatory ratio as the latter is given by

$$P_{eH}\left(\overset{\circ}{E}\right) / P_{ideal}\left(\overset{\circ}{E}\right), \text{ which is equal to } A_{H\psi_d=0}, \text{ within the simplified context of this}$$

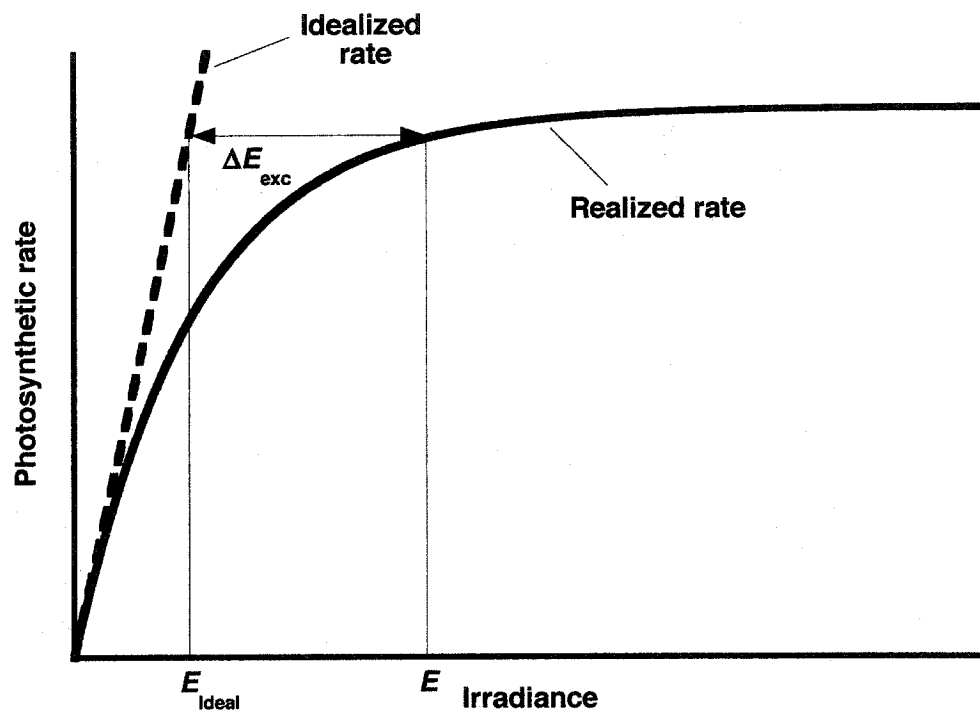


**Figure 3.4: Excess radiation.** The excess radiation is the difference in irradiance for the same rate of gross photosynthesis in the idealized and realized cases. The idealized rate is the line defined by the initial slope of the realized rate (i.e. when the quantum yield is maximal).

analysis.

### 3.3.7.2 NPQ, excess irradiance, and the dissipation factor

I assume (generally observed in higher plants e.g. Björkman and Demmig-Adams 1994; Demmig-Adams and Adams III 1996) that the relation between excess irradiance and  $NPQ_f$  is linear and that they are both equal to zero in the dark, which implies that

$$NPQ_f^{qE} = m \Delta \overset{o}{E}_{exc}, \quad 3.24$$

where  $m$  is a proportionality constant. Using equation 3.19 we have

$$k_{qE}^{st} \frac{1}{k_d + k_f} = m \Delta \overset{o}{E}_{exc}, \quad 3.25$$

where  $k_{qE}^{st}$  represents the steady state value of the parameter  $k_{qE}$  for a given  $\overset{o}{E}$ . Finally,

using equation 3.23, rearranging and equating  $\gamma_d = m(k_d + k_f)$  we have

$$k_{qE}^{st} = \gamma_d \Delta \overset{o}{E}_{exc} = \gamma_d \overset{o}{E} (1 - A_{H\psi_d=0}). \quad 3.26$$

The dissipation factor at the steady state becomes a linear function of the excess irradiance, where  $\gamma_d$  can be interpreted as the capacity for non-photochemical quenching in a given acclimation state. That is, for a given irradiance and closure of reaction centers, a greater capacity (high  $\gamma_d$ ) for non-photochemical quenching leads to a greater value of  $k_{qE}^{st}$  which, in turn, leads to higher heat dissipation.

I will further separate the parameter  $\gamma_d$  into a constant part  $\gamma_o$  and a variable part  $\gamma_{NPQ}$ , the latter of which can be modified through acclimation:  $\gamma_d = \gamma_o + \gamma_{NPQ}$ . The

parameter  $\gamma_o$  is the capacity for energy dependent non-photochemical quenching at the lowest irradiance, which allows survival (e.g. compensation irradiance without grazing losses). Because  $\phi'_{F_m}$  (corresponding to  $F'_m$ ) is dependent on  $C$ , when running my model, a fraction of  $NPQ_f$  obtained from fluorescence parameters (see equation 3.19 and accompanying text) will originate from photoinhibition due to damage to the reaction centers ( $NPQ_f^I$ ),  $NPQ_f = NPQ_f^{qE} + NPQ_f^I$ .

### 3.3.7.3 Energy dependent quenching and damage

Here, I want to modify the relationship derived in equation 3.26 to take into account damage. One of the limitations of equation 3.26 is that I have not included a decline of the capacity for energy dependent quenching when a large fraction of the reaction centers are damaged and, thus, a smaller fraction of the photons absorbed will lead to energy dependent non-photochemical quenching. This decline in the efficiency for energy dependent quenching is expected on the basis that, at high damage, the build-up of a pH gradient across the thylakoid membrane at a given irradiance should be lower, leading to the diminution of  $NPQ_{fqE}$ . However, this decrease will only occur if a sufficient number of reaction centers are damaged to decrease the rate of electron transport below the capacity to utilize electrons (approximated here by  $n_{Calvin} k_{Calvin}^{max}$ ). To account for this effect I rewrite equation 3.26 as

$$k_{qE}^{st} = \gamma_d \bar{E} \left( 1 - \left[ A + C \frac{(n_{Calvin} k_{Calvin}^{max} - P_e^{RC})}{n_{Calvin} k_{Calvin}^{max}} \right] \right), \quad 3.27$$

where  $P_e^{RC}$  is the rate of charge separation per RCII ( $e^- s^{-1} RC^{-1}$ ). This equation leads to a

decrease in non-photochemical quenching with an increasing fraction of damaged reaction centers only when the concentration of damage is sufficient to decrease  $P_e^{RC}$  below  $n_{Calvin} k_{Calvin}^{max}$  (as will become clear later, I will build into the model an “overcapacity” of PSII relative to  $n_{Calvin} k_{Calvin}^{max}$ ). The parameter  $P_e^{RC}$  is also described in more detail later.

#### 3.3.7.4 Kinetics of energy dependent quenching

Equation 3.27 represents the steady state solution. Upon a shift to higher light levels the rate of change can be modeled as

$$\frac{dk_{qE}}{dt} = k_{ind} (k_{qE}^{st} - k_{qE}), \quad 3.28$$

where  $k_{ind}$  is the induction rate constant for non-photochemical quenching. While upon a decrease in irradiance, the change can be modeled as

$$\frac{dk_{qE}}{dt} = k_{rel} (k_{qE}^{st} - k_{qE}), \quad 3.29$$

where  $k_{rel}$  is the relaxation rate constant for energy-dependent non-photochemical quenching. Such a parameterization is possible because the rate constants driving the equilibrium in the fraction of open reaction centers ( $A$ ) are much shorter than those regulating  $k_{qE}$  such that  $A$  reaches a pseudo-steady-state much faster (order of milliseconds e.g. Lavergne and Trissl 1995) than  $k_{qE}$  (order of minutes e.g. Lavaud et al. 2004) upon a light shift (though the slower changes in  $k_{qE}$  will lead the pseudo-steady-state of  $A$  to change). This parameterization of energy dependent non-photochemical

quenching (i.e.  $NPQ_f^{qE}$  proportional to excess irradiance and affected by damage) is one of many that could be used. The simplified model is, however, useful to link non-photochemical quenching, fluorescence, and electron transport. For this work, excess irradiance will be considered the excess irradiance when observed with fluorescence measurements; that is irradiance is in excess using charge separation as a measure of electron flow.

### 3.3.8 *Effective cross-section and the dissipation factor*

Having reviewed the expressions for yields in terms of rate constants and the parameterization of  $k_{qE}$ , I can now return to the parameterization of the effective absorption cross-section. For the dark acclimated state, the effective absorption cross-section of PSII is the subsection of the optical cross-section required to promote charge separation if all absorbed radiation in that subsection leads to charge separation. For example, if 65% of the photons lead to charge separation with a given optical cross-section, the effective cross-section will be 65% of the size of the optical cross-section. In the puddle model, the effective absorption cross-section is only affected by changes occurring within open reaction centers; inhibited or closed reaction centers do not lead to photochemistry and cannot exchange absorbed energy with open reaction centers and thence do not influence the effective absorption cross-section in open reaction centers. Therefore, in the dark, the ratio of the effective absorption cross-section to the optical cross-section is equal to the maximum quantum yield of photosynthesis (e.g. Kolber et al. 1998),

$$\frac{\sigma_{PSII}}{\sigma_{PSII}^O} = \phi_p^{\max} = \frac{k_p}{k_p + k_d + k_f}, \quad 3.30$$

where  $\sigma_{PSII}^O$  is the optical cross-section of PSII ( $\text{m}^2 \mu\text{mol PSII}$ ). In the light, the effective absorption cross-section ( $\sigma_{PSII}' \text{ m}^2 \mu\text{mol photon}^{-1}$ ), with the assumption that all the energy dependent non-photochemical quenching originates in the antenna, can be written as

$$\frac{\sigma_{PSII}'}{\sigma_{PSII}^O} = \phi_{pA} = \frac{k_p}{k_d + k_f + k_p + k_{qE}}. \quad 3.31$$

Rearranging we find

$$\sigma_{PSII}' = \sigma_{PSII}^O \phi_{pA} = \sigma_{PSII}^O \frac{k_p}{k_d + k_f + k_p + k_{qE}}. \quad 3.32$$

Therefore, non-photochemical quenching has two effects (not independent of each other) in my model. Firstly, by increasing the probability of a photon going to heat, NPQ allows a greater fraction of the reaction centers to remain open; this decreases the probability of damage to the RC. Secondly, the quantum yield of photochemistry of an open reaction center decreases and, consequently, the effective absorption cross-section for charge separation is decreased. The drop in the effective absorption cross-section is a measure of the decreased quantum yield of open reaction centers. Figure 3.5 provides a schematic representation of the processes modeled in this section.

### 3.3.9 Limiting the rate of repair

Marshall et al. (2000) propose to use a Michaelis-Menten relationship to model the rate of repair of inhibited reaction centers. This functional relationship is adopted here

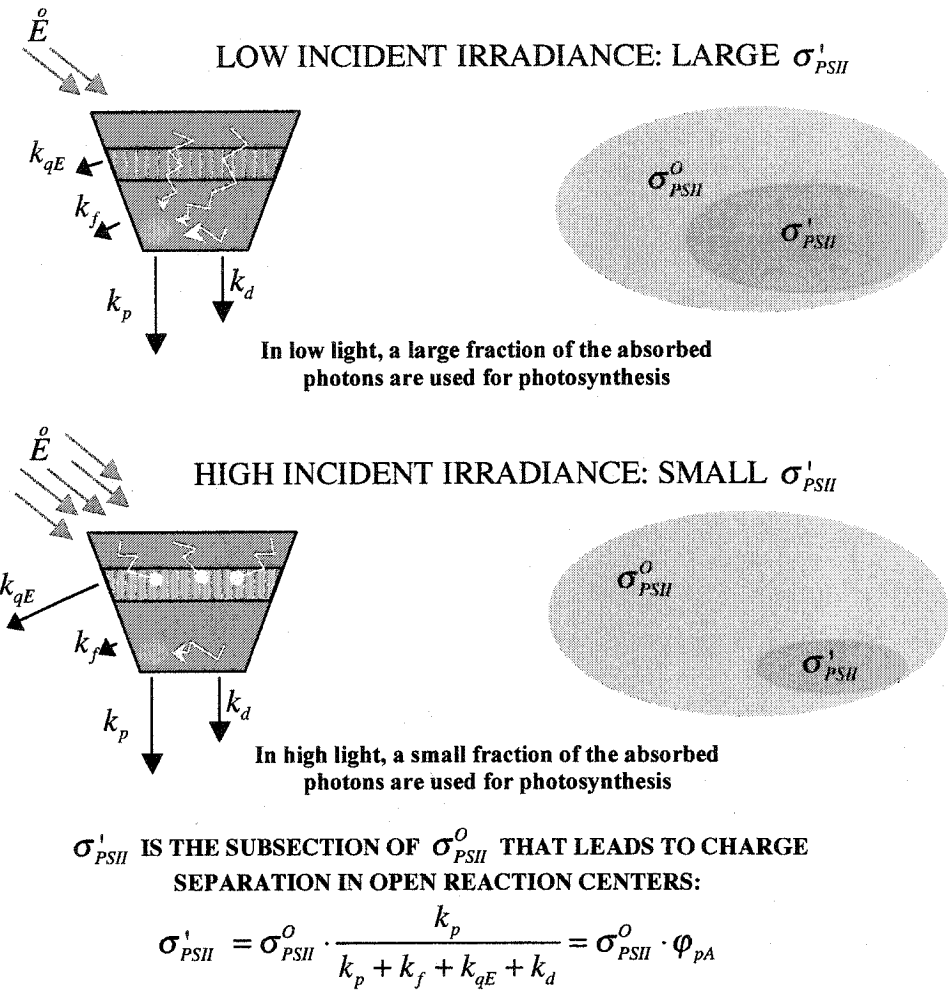


**Figure 3.5: Schematic representation of the effect of photoprotection due to increasing energy dependent non-photochemical quenching. Top portion: At low incident irradiance, a large fraction of the incident photons is used up in photosynthesis with little energy dissipation through  $k_{qE}$  leading to a large effective absorption cross-section. Lower portion: At high incident irradiance, the configuration of the reaction centers antenna changes leading to an increase in the dissipation of the absorbed energy, and to a smaller effective absorption cross-section. The relationship between the optical absorption cross-section  $\sigma^O_{PSII}$ , the effective absorption cross-section and the quantum yield of photosynthesis in open reaction centers is given below the diagram. Note that the representation is for one photoacclimation state and only regulation of energy dependent non-photochemical quenching is represented.**

$$K_{rep} = \frac{k_{rep}^{max} \cdot C}{C_{1/2} + C}, \quad 3.33$$

where  $C_{1/2}$  is the half-saturation concentration of inhibited reaction centers that saturate the repair rates. I will use for this study the same rate constants used by Marshall et al. (2000); with these constants, the departure from a simple first order rate constant is small. Variability in this relationship with taxa, temperature, nitrogen stress (see below), and incident irradiance is expected.

### 3.3.10 Nitrogen limitation

Unbalanced growth due to nitrogen limitation decreases the maximum quantum yield of photochemistry measured by fluorescence (e.g. Cleveland and Perry 1987; Parkhill et al. 2001). The decreased photochemical efficiency of the bulk fluorescence measurement implies that the efficiency of charge separation at active PSII reaction centers is decreased (equivalent to decreasing  $k_p$ ) or there is a decreased fraction of active reaction centers (lower  $A$  due to increased  $C$ ). Unbalanced growth due to nitrogen stress also increases the susceptibility to photoinhibition (Steeman Nielsen 1962; Prézelin et al. 1986). Furthermore Lesser et al. (1994) found that nitrate limited cultures had slower repair rates than nitrate replete cultures under conditions of UV damage. Consistent with these observations, I will follow the approach of Marshall et al. (2000), who opted to model the effect of nitrogen limitation as a decrease in the rate of repair of damaged reaction centers based on the premise that nitrogen is needed during the repair of the damaged D1 protein. Therefore, the rate of repair will be modified to take into account the nutrient status ( $N_{Status}$ , dimensionless) of the cell as

$$K_{rep}^N = K_{rep} N_{Status} = \frac{k_{rep}^{max} C}{C_{1/2} + C} N_{Status}, \quad 3.34$$

where  $N_{Status}$  ( $0 < N_{Status} < 1$ ) is expressed by Marshall et al. (2000) (see Flynn et al. (1999) for full the expression) as

$$N_{Status} = \frac{1}{U} \frac{(Q - Q_o)}{(Q - Q_o + Kq)},$$

where  $Q$  (g N g<sup>-1</sup> C) is the cellular nitrogen to carbon quota,  $Q_o$  (g N g<sup>-1</sup> C) is the minimum nitrogen to carbon quota of the cell,  $Kq$  (g N g<sup>-1</sup> C) is the value of  $Q$  that allows growth to be half of its maximum and  $U$  (dimensionless) is a normalization factor that allows  $N_{Status}$  to vary between 0 and 1. This expression is provided for completeness but will not be used in this chapter, as the nutrient quota of the cells is not modeled. Instead, the modeling of  $K_{rep}$  as a linear function of nutritional status provides a simple mechanism to study the effect of nutrient starvation on fluorescence. In this formulation, decreasing the nutrient status is equivalent to decreasing the maximum rate of repair.

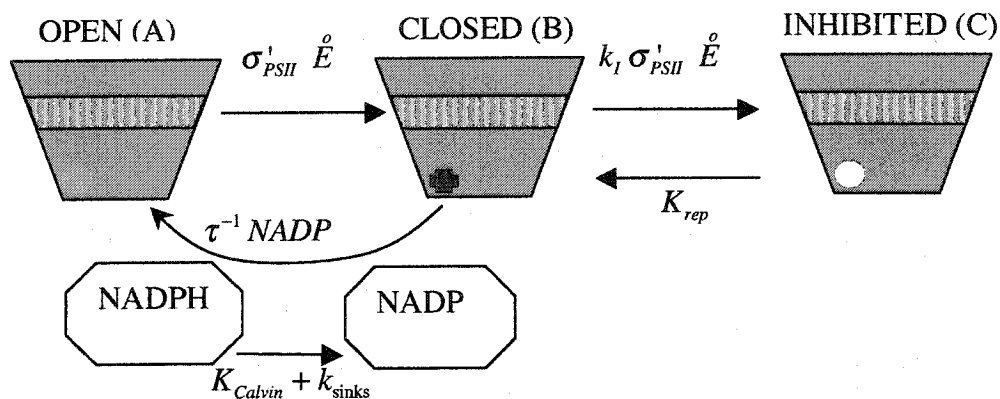
### 3.3.11 Review of the model

Table 3-2 presents the final equations used in the model of fluorescence and photosynthesis. Equations 3.35, 3.36, 3.37 represent the three states of the reaction centers accounting for the change in  $\sigma_{PSII}'$  with irradiance and the effect of the dynamics of the NADP pool (equation 3.8), a schematic of this new system of equations is given in Figure 3.6.

In addition, at any time, the bulk rate of photosynthesis ( $P_e$ ,  $\mu\text{mol e}^- \text{m}^{-3} \text{s}^{-1}$ ) is

**Table 3-2: Main equations of the model**

Equation	Equation number
$\frac{dA}{dt} = -\overset{\circ}{E} \sigma'_{PSII} A + \frac{B NADP}{\tau}$	3.35
$\frac{dB}{dt} = \overset{\circ}{E} \sigma'_{PSII} A - \frac{B NADP}{\tau} + K_{rep} C - \Psi_d \sigma'_{PSII} \overset{\circ}{E} B$	3.36
$\frac{dC}{dt} = -K_{rep} C + \Psi_d \sigma'_{PSII} \overset{\circ}{E} B$	3.37
$\frac{dk_{qE}}{dt} = \begin{cases} k_{ind} (k_{qE}^{st} - k_{qE}) & k_{qE}^{st} \geq k_{qE} \\ k_{rel} (k_{qE}^{st} - k_{qE}) & k_{qE}^{st} < k_{qE} \end{cases}$	3.28 and 3.29
$\frac{dNADP}{dt} = -\frac{B}{\tau} NADP + K_{Calvin} + k_{sinks}$	3.8
$k_{qE}^{st} = \gamma_d \overset{\circ}{E} \left( 1 - \left[ A + C \frac{(n_{Calvin} k_{Calvin}^{max} - P_e^{RC})}{n_{Calvin} k_{Calvin}^{max}} \right] \right)$ and $\gamma_d = \gamma_o + \gamma_{NPQ}$	3.27
$\sigma'_{PSII} = \sigma_{PSII}^O \phi_{pA} = \sigma_{PSII}^O \frac{k_p}{k_d + k_f + k_p + k_{qE}}$	3.32
$K_{Calvin} = n_{Calvin} \frac{k_{Calvin}^{max} NADPH}{NADPH_{1/2} + NADPH}$	3.9
$K_{rep}^N = \frac{k_{rep}^{max} C}{C_{1/2} + C} N_{status}$	3.33 and 3.34
$P_e^{RC} = A \phi_{pA} \sigma_{PSII}^O \overset{\circ}{E} = A \sigma'_{PSII} \overset{\circ}{E}$	3.39
$\phi_f = A \frac{k_f}{k_d + k_f + k_p + k_{qE}} + B \frac{k_f}{k_d + k_f + k_{qE}} + C \frac{k_f}{k_d + k_f + k_l + k_{qE}}$	3.12
<b>Acclimation</b>	
$\frac{d\sigma_{PSII}^O}{dt} = \begin{cases} \kappa_{\sigma PSII} \sigma_{PSII}^O \left( \frac{A}{A+B} \left( \sigma_{PSII}^O / \sigma_{PSII}^{opt} \right)^x - 0.3 \right) & \overset{\circ}{E} > 0 \\ 0 & \overset{\circ}{E} = 0 \end{cases}$	3.44
$\frac{d\gamma_{NPQ}}{dt} = \begin{cases} \kappa_{\gamma} \gamma_{NPQ} \left( C \left( \gamma_{NPQ} / \gamma_{NPQ}^{opt} \right)^y - 0.05 \right) & C < 0.1 \text{ \& } \overset{\circ}{E} > 0 \\ \frac{0.1}{C} \kappa_{\gamma} \gamma_{NPQ} \left( C \left( \gamma_{NPQ} / \gamma_{NPQ}^{opt} \right)^y - 0.05 \right) & C > 0.1 \text{ \& } \overset{\circ}{E} > 0 \\ 0 & \overset{\circ}{E} = 0 \end{cases}$	3.45



**Figure 3.6: Model of photosynthesis used in present work. Three pools of reaction centers are represented by the open (A), closed (B) and inhibited (C) pools as well as the two pools of NADP and NADPH. The rates of transfer between the three pools are shown above or below the arrows representing the exchange between the pools. All rates are first order rate constants except for the reopening of reaction centers, which is a bi-molecular reaction depending on the product of the concentration of two pools.**

given by

$$P_e = A \phi_{pA} a_{PSII} \overset{\circ}{E}. \quad 3.38$$

The relationship between the total absorption by PSII and the number of PSII and their individual optical absorption cross-sections ( $\sigma_{PSII}^O$ ) is given by  $a_{PSII} = N \sigma_{PSII}^O$ , where  $N$  is the concentration of PSII ( $\mu\text{mol PSII m}^{-3}$ ). The rate of charge separation per reaction center is then given by

$$P_e^{RC} = A \phi_{pA} \sigma_{PSII}^O \overset{\circ}{E} = A \sigma_{PSII}' \overset{\circ}{E}. \quad 3.39$$

My model does not account for growth or changes in the ratio of carbon to chlorophyll within the cell. As such, direct comparisons with the usual measurements made in oceanography, such as the biomass normalized PvsE curve cannot be made. However, after some simplifying assumptions the model can be compared with those measurements. Below, I derive a series of parameters with this objective in mind.

PvsE curves are generally normalized to biomass (Jassby and Platt 1976; MacIntyre et al. 2002), one commonly used proxy for biomass is the chlorophyll concentration. When normalized to chlorophyll concentration, nutrient replete PvsE curves generally have a constant initial slope independent of growth irradiance (MacIntyre et al. 2002). This will be the case unless changes in the chlorophyll specific absorption coefficient arise. This is because chlorophyll is a good proxy for cellular absorption (or PSII,  $a_{PSII}$ ) and the quantum yield of photosynthesis at low light tends to be independent of growth irradiance (Kolber et al. 1988). When the number of PSII per cell does not change (as in my model), the normalization by the optical absorption cross-

section provides a direct proxy for changes in PSII absorption (in the absence of packaging effects). Therefore, for comparison with chlorophyll specific PvsE curves I define the cross-section normalized rates of charge separation as

$$P_e^{RC\sigma} = A \phi_{pA} \overset{o}{E}. \quad 3.40$$

Equation 3.40 is useful for comparison with processes occurring near PSII, such as oxygen evolution, however, a better comparison with PvsE curves obtained from  $^{14}\text{C}$  incubation can be found by focusing on carbon fixation by using the Calvin cycle kinetics as the measure of photosynthesis. I can obtain the rate of carbon fixation (in units of electrons transferred to Calvin cycle intermediates) by defining

$$P_C = K_{Calvin}. \quad 3.41$$

To compare with chlorophyll specific PvsE curves I can normalize to the optical cross-section and obtain

$$P_C^\sigma = \frac{K_{Calvin}}{\sigma_{PSII}^o}. \quad 3.42$$

Finally, the fluorescence flux emitted by an elementary volume containing photosystem II ( $F$ ,  $\mu\text{mol m}^{-3} \text{s}^{-1}$ ) is given by

$$F = \phi_f a_{PSII} \overset{o}{E}. \quad 3.43$$

Apart from the constant terms, the set of equations in Table 3-2 specifies completely the photosynthesis and fluorescence model at any time, given an incident scalar irradiance timeseries. Below, I add acclimation to this model.

### 3.3.12 *Two types of photoacclimation*

Photoacclimation consists of modifying the photosynthetic machinery, within its genotypic capacity, to balance the rate of electron production and transfer at PSII and PSI with the rate of electron utilization by all electron sinks. The result of photoacclimation is proposed to be maximizing growth and avoiding damage on timescales of hours to days (Geider et al. 1998). Perhaps, more generally, the result should be regarded as “improving ecological fitness”; in some cases, surviving at a lower growth rate with more damage might be better than an increased growth or lower damage in the short term if accompanied by death. Regulation has the same outcome as acclimation on timescales of seconds to minutes and is dependent on the acclimation state, in addition to the limitation of the genotype. Photoadaptation, through changes in the genotype, provides variable capacities for photoacclimation and regulation on much longer timescales (Falkowski and LaRoche 1991; Cullen and MacIntyre 1998).

In constant light, there are two simple ways to achieve acclimation (e.g. Prézelin 1981; Falkowski and LaRoche 1991; Zonneveld 1997). The first is to change the size of the photosynthetic light-harvesting antenna and, if necessary, the capacity of the electron transport chain to provide a sustainable flow of electrons to a constant number of reaction centers. The second is to change the ratio of the number of photosystems (more generally photosynthetic units) to the number of dark reaction units (e.g. could be RUBISCO), keeping the absorption cross-section constant. Both of these strategies are used in phytoplankton (Falkowski and Owens 1980; Prézelin 1981; Richardson et al. 1983).

However, light in the environment is never constant, with day-to-day fluctuations

due to clouds, diel changes in solar zenith angle, and hour to seconds changes due to mixing processes and the focusing and defocusing effects of waves (the mixing and focusing processes are the aquatic equivalent of the “sun flecks” phenomenon in terrestrial systems). With this amount of variability in the light field, another factor that provides ecological fitness is the capacity to rapidly modify thermal dissipation of absorbed energy to allow efficient harvesting of light at low light and dissipation of excess irradiance at high light (Ibelings et al. 1994; Lohr and Wilhelm 1999; Külheim et al. 2002). The most important mechanism for this thermal switching is the xanthophyll cycle (e.g. Gilmore and Govindjee 1999; Latowski et al. 2004). A clear example of acclimation with irradiance in this capacity in phytoplankton is presented by MacIntyre et al. (2002) who describe the changes in pigment content as a function of growth irradiance for many phytoplankton species, showing a clear accumulation (relative to chlorophyll) of the xanthophyll pigments with increasing irradiance. A similar trend has been presented in higher plants where *Mahonia repens* growing under higher irradiance had much greater pool of xanthophyll cycle pigments relative to chlorophylls and a larger pool of compounds to scavenge reactive radicals (Logan et al. 1998). This suggests an increasing capacity for photoprotection relative to light absorption (see also Chapter 2) in algae acclimated to high light (e.g. Demers et al. 1991). This increased capacity has been observed in higher plants (Björkman and Bilger 1990) and in *Ulva rotundata* (Osmond et al. 1993). To address these two types of photoacclimation, the model will be constructed to change the size of the antennae of PSII and the capacity for non-photochemical quenching (see schematic on Figure 3.7).

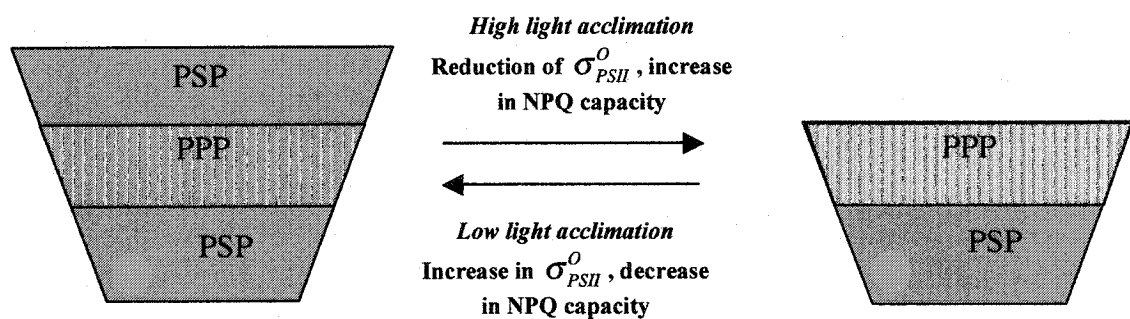


**Figure 3.7:** Schematic representation of the acclimation model. Two processes are modeled for photoacclimation. The first consists of a change in the optical cross-section of PSII, represented here by changing the size of the green portion (photosynthetic pigments, PSP). The second is a change in the capacity for non-photochemical quenching; this is shown by a change in the yellow color representing the location of the photoprotective pigment (PPP) pool (representing a greater ratio of PPP to PSP)

There is strong evidence that the acclimation of the light harvesting complexes is regulated at the level of the plastoquinone (PQ) pool (Escoubas et al. 1995) or by the redox state of electron carriers near the plastoquinone pool (Franklin et al. 2003). Hence, it is a balance between the charge separation at PSII reaction centers and the utilization of the electrons by the electron transport chain downstream of the PQ pool. When the PQ pool is oxidized in low light, the reaction centers are more open and when the PQ pool is reduced due to excess charge separation at PSII relative to electron utilization a greater fraction of the reaction centers become closed. However, because I am not modeling the PQ pool here, I will set the regulation mechanism at the reaction centers (i.e. the parameter  $A$  will be used as the regulatory parameter simulating the redox state of the first quinone,  $Q_a$ ). This directly follows from the idea that “excitation pressure” can be measured using the photochemical quenching parameter (Maxwell et al. 1994; Maxwell et al. 1995; Demmig-Adams and Adams III 1996). I will assume that the balance will occur when 30% of the active reaction centers are in the open state. This is consistent with the concept that microalgae tend to acclimate such that their photosynthetic capacity is around 70% of maximum (acclimation brings the saturation parameter of the PvsE near the growth irradiance Sakshaug et al. 1997) or somewhat higher (Laws et al. 2002). Therefore, the regulation of the optical cross-section of the PSII antennae will be controlled by the fraction of active reaction centers by,

$$\frac{d\sigma_{PSII}^O}{dt} = \begin{cases} \kappa_{\sigma_{PSII}} \sigma_{PSII}^O \left( \frac{A}{A+B} \left( \sigma_{PSII}^O / \sigma_{PSII}^{opt} \right)^x - 0.3 \right) & \dot{E} > 0 \\ 0 & \dot{E} = 0 \end{cases}, \quad 3.44$$

where  $\kappa_{\sigma_{PSII}}$  is rate for change in the optical absorption cross-section,  $\sigma_{PSII}^{opt}$  is the optimal cross-section for photochemistry, and  $x$  ( $x \leq 0$ ) is an exponent factor modifying the ratio  $(\sigma_{PSII}^O / \sigma_{PSII}^{opt})$ . Ignoring the  $(\sigma_{PSII}^O / \sigma_{PSII}^{opt})^x$  part of the equation, the change in the optical cross-section is 0 when  $A/(A+B)=0.3$ ; when  $A/(A+B)>0.3$ ,  $\sigma_{PSII}^O$  increases; and when  $A/(A+B)<0.3$ ,  $\sigma_{PSII}^O$  decreases. The parameter  $(\sigma_{PSII}^O / \sigma_{PSII}^{opt})^x$  decreases the extent of acclimation such that as  $\sigma_{PSII}^O$  departs from  $\sigma_{PSII}^{opt}$  the rate of change of  $\sigma_{PSII}^O$  is 0 at different values of  $A/(A+B)$ . The parameterization using  $(\sigma_{PSII}^O / \sigma_{PSII}^{opt})^x$  is a substitute for a complete mechanistic description of the biophysical limitation of photoacclimation. For example, the photon capture and transfer efficiency to the reaction centers is expected decrease as the size of the optical cross-section increases. A comparison of the function for two values of the parameter  $x$  is given in Figure 3.8. In the case where  $x=0$  the rate of change is equal to 0 when  $A/(A+B)=0.3$ , this is unrealistic as it means that the phytoplankton can acclimation to any light levels “perfectly” by changing  $\sigma_{PSII}^O$  leading to  $A/(A+B)=0.3$ . This would mean that to acclimate from 20 to 2000  $\mu\text{mol m}^{-2} \text{s}^{-1}$ ,  $\sigma_{PSII}^O$  would have to change by a factor of  $\sim 100$ , which is not observed (e.g. Sukenic et al. 1987). In reality, it is expected that in extreme light conditions, phytoplankton will not be able to fully acclimate and the ratio will deviate from  $A/(A+B)=0.3$  at the growth irradiance. This is what happen when  $x$  is set to -0.4; at that acclimated level, when  $d\sigma_{PSII}^O/dt = 0$ ,  $A/(A+B)$  varies from 0.1 in high light to 0.6 in low light (Figure 3.8).

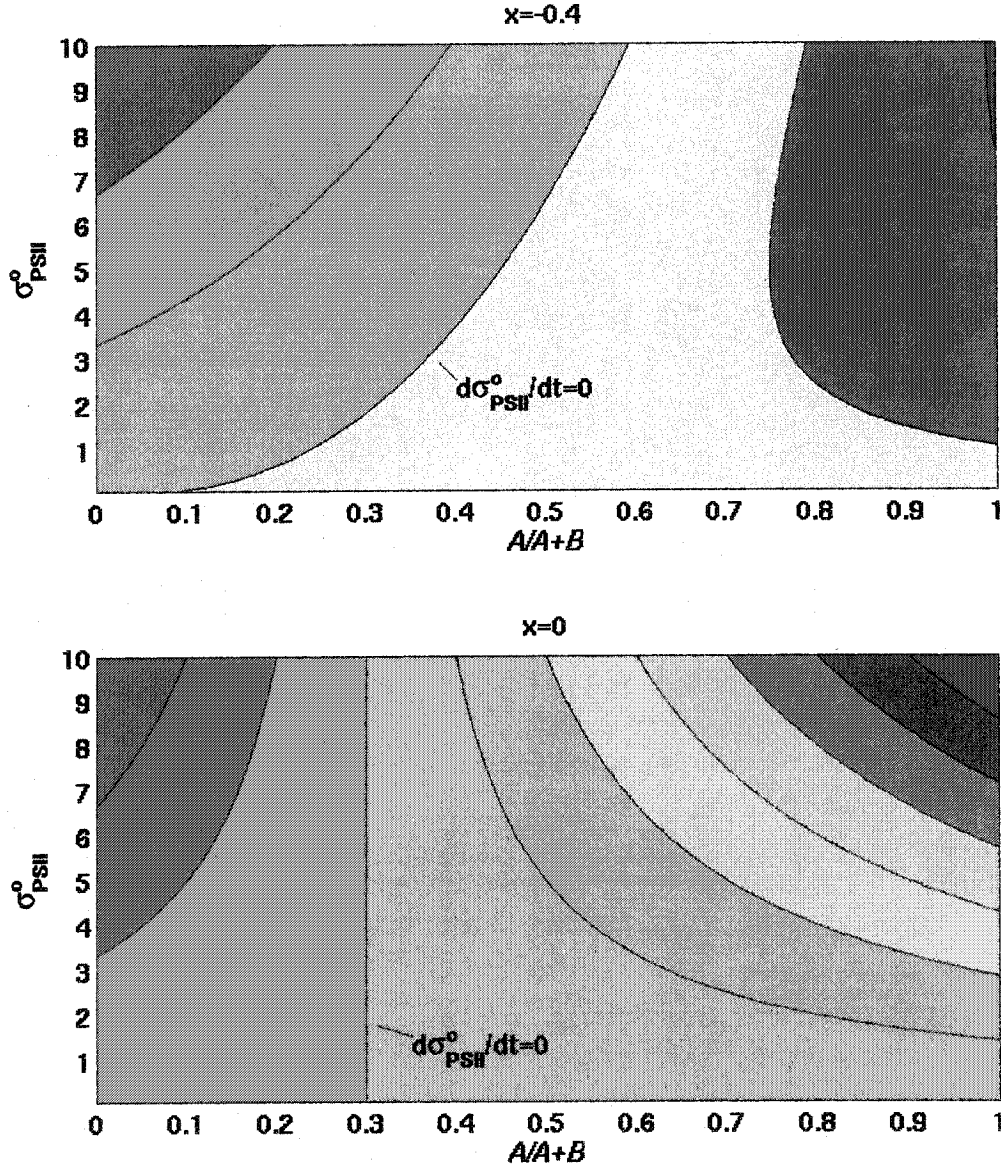


Figure 3.8: Acclimation function for the rate of change of the optical cross-section. When the rate is 0, identified on each panel, the reaction center is acclimated to the growth irradiance. Warmer colors represent an increase in  $\sigma_{PSII}^0$  while cooler colors represent a decrease. Top panel: when  $x = -0.4$ , the standard value in the model, the steady state of the ratio  $A/(A+B)$  varies. Bottom panel: when  $x = 0$ ,  $A/(A+B) = 0.3$  for any irradiance level and  $\sigma_{PSII}^0$ . Decreasing values of  $x$  imply greater biophysical limitations in the acclimation capacity of a cell. Note that the line representing  $d\sigma_{PSII}^0/dt = 0$  is not at the same color boundary on both graphs.

I did not find any guide in the literature for modeling the mechanism regulating the capacity for non-photochemical quenching; I decided to model it using the fraction of damaged reaction centers as the regulatory parameter. This choice was made because it is the process ultimately affected by photoprotection. The formulation used is

$$\frac{d\gamma_{NPQ}}{dt} = \begin{cases} \kappa_{\gamma} \gamma_{NPQ} \left( C \left( \gamma_{NPQ} / \gamma_{NPQ}^{opt} \right)^y - 0.05 \right) & C \leq 0.1 \text{ \& } \overset{\circ}{E} > 0 \\ \frac{0.1}{C} \kappa_{\gamma} \gamma_{NPQ} \left( C \left( \gamma_{NPQ} / \gamma_{NPQ}^{opt} \right)^y - 0.05 \right) & C > 0.1 \text{ \& } \overset{\circ}{E} > 0, \\ 0 & \overset{\circ}{E} = 0 \end{cases} \quad 3.45$$

where  $\kappa_{\gamma}$  is a rate constant for change in  $\gamma_{NPQ}$ ,  $\gamma_{NPQ}^{opt}$  is the capacity for photoprotection under optimal growth conditions, and  $y$  is an exponent relating the ratio  $\gamma_{NPQ} / \gamma_{NPQ}^{opt}$  to the rate of change of  $\gamma_{NPQ}$ . The dynamics of this equation are very similar to those of equation 3.44. The separation of equation 3.45 into two parts depending on the light is necessary to avoid a very high rate of acclimation at high damage levels (though see Kana et al. 1997 for a mechanism of acclimation that depend on damage rate).

### 3.3.13 Setting some constants

In this section, I attempt to provide a set of values for basic parameters; other parameters will be selected in the Results section (see Table 3-3). The values used here are consistent with literature values for these parameters, but specific circumstances may require revising them.

Measurements in microalgae have shown that under balanced growth, the maximum quantum yield of charge separation ( $\phi_p^{\max}$ ) is equal to 0.65. This is measured

Table 3-3: Values for the constants used in the model.

Constant	Value
$k_d$	$1.106 \times 10^9 \text{ s}^{-1}$
$k_f$	$6.7 \times 10^7 \text{ s}^{-1}$
$k_l$	$1.06 \times 10^9 \text{ s}^{-1}$
$k_{ind}$	$0.0167 \text{ s}^{-1}$
$k_p$	$2.178 \times 10^9 \text{ s}^{-1}$
$k_{rel}$	$0.0056 \text{ s}^{-1}$
$k_{max}^{Calvin}$	$160 \text{ s}^{-1}$
$k_{max}^{rep}$	$3.23 \times 10^{-4} \text{ s}^{-1}$
$k_{sinks}$	$20 \text{ s}^{-1}$
$NADPH_{1/2}$	0.05
$x$	-0.4
$y$	-1
$\gamma_o$	$0.0005 [\mu\text{mol photon m}^{-2}]^{-1}$
$\gamma_{NPQ}^{opt}$	$0.001 [\mu\text{mol photon m}^{-2}]^{-1}$
$\kappa_{\sigma PSII}$	$1.39 \times 10^{-4} \text{ s}^{-1}$
$\psi_d$	$3 \times 10^{-7}$
$\sigma_{PSII}^{opt}$	$1.81 \text{ m}^2 \mu\text{mol photon}^{-1}$
$\sigma_{PSII}^O$	$1.81 \text{ m}^2 \mu\text{mol photon}^{-1}$
$\tau$	$2 \times 10^{-3} \text{ s}$

by variable fluorescence using the ratio

$$\phi_p^{\max} = \frac{k_p}{k_p + k_d + k_f} = \frac{F_m - F_o}{F_m} = 0.65.$$

As noted previously, if fluorescence emission by PSI or other pigments is important this could be an underestimate of the photochemical quantum yield. For this modeling exercise, I will also set the quantum yield of fluorescence when all reaction centers are open in the dark-acclimated state to 2% (see for example Oxborough and Baker 2000). Such that we have

$$\phi_{F_o} = \frac{k_f}{k_p + k_d + k_f} = 0.02.$$

I will use the assumption generally made in fluorescence work (Gilmore and Govindjee 1999) that the rate constant for fluorescence is an intrinsic property of the chlorophyll molecule embedded in the protein matrix of PSII and assign a rate constant of  $k_f = 6.7 \times 10^7 \text{ s}^{-1}$  (Lazar et al. 2003). Using these numbers and the two equations above, we can obtain  $k_d = 1.106 \times 10^9 \text{ s}^{-1}$  and  $k_p = 2.178 \times 10^9 \text{ s}^{-1}$ . The rate constant for photochemistry obtained this way is consistent with the value measured of  $2.325 \times 10^9 \text{ s}^{-1}$  by Roelofs et al. (1992) and used by Oxborough and Baker (2000) for charge stabilization in open reaction centers.

Inhibited reaction centers tend to have quantum yields of fluorescence that are slightly higher or equal to those of open reaction centers (see Chapter 2 for a discussion of the variability observed in the lab). Therefore, I will use  $k_i = k_p$ . This is different from

the situation generally observed in higher plants where  $F_o$  increases by a factor of  $\sim 2$  when a large fraction of the reaction centers are damaged (Osmond 1994; Park et al. 1995; but see also Valvilin et al. 1998).

The turnover rate of the electron transport chain ( $\tau$ ) is taken to be 0.002 s, which is consistent with values obtained for the rate of electron transfer through the PQ pool (Falkowski and Raven 1997). RUBISCO is a relatively slow enzyme with a maximum rate of the order of 40 to 80 mol CO<sub>2</sub> mol enzyme s<sup>-1</sup>, with 80 mol CO<sub>2</sub> mol enzyme s<sup>-1</sup> being the highest values observed (Geider and MacIntyre 2002). Given an idealized value of 4 electrons used per CO<sub>2</sub> fixed, we calculate that  $k_{Calvin}^{max}$  values in terms of electron transport of up to about 360 e<sup>-</sup> RUBISCO<sup>-1</sup> s<sup>-1</sup> are realistic. I will use 160 e<sup>-</sup> RUBISCO<sup>-1</sup> s<sup>-1</sup>. The variable  $n_{Calvin}$  has been measured by Sukenic et al. (1987) and was found to increase from 1.2 to 4.6 as growth irradiance increased from 80 to 1900  $\mu\text{mol m}^{-2} \text{s}^{-1}$ . For simplicity I will use a value of 1, which is independent of growth irradiance as the acclimation process is not modeled for  $n_{Calvin}$  but rather  $\sigma_{PSII}^O$ . The induction and relaxation constants for the energy dependent quenching are taken as  $k_{ind} = 0.0167 \text{ s}^{-1}$  (consistent with rates found by Lavaud et al. 2004) and  $k_{rel} = 0.0056 \text{ s}^{-1}$ .

### 3.4 Results

The model was written in the MATLAB® language using one of the built-in ordinary differential equation solvers (ODE23), which is an automatic step-size Runge-Kutta-Fehlberg integration method. Through a sensitivity analysis, the model was found to have benign non-linearity and to be insensitive to initial conditions (results not shown).

In this section, I provide a series of figures to show the main features of the model. Constants used in the model runs are given in Table 3-3; when these constants are modified, the new values are given in the graph captions, legend, or in the accompanying text. I will progress with the examples by adding more and more dynamics into the model, starting with the basic photosynthesis model and culminating with the complete model with non-photochemical quenching and photoacclimation. Therefore, not all constants given in Table 3-3 are used for the data presented in each figure. I will also provide much of the discussion and interpretation within this Results section.

### 3.4.1 *Basic photosynthesis model*

In the first example, only the photosynthesis model is included: I did not include non-photochemical quenching ( $\gamma_d=0$ ), photoinhibition ( $\psi_d = 0$ ), or acclimation ( $\kappa_{\sigma_{PSII}} = 0$  and  $\kappa_{\gamma} = 0$ ). Therefore, the model is restricted to equations 3.8, 3.9, 3.35, 3.36. With this model, the typical shape of the PvsE curve is well reproduced (Figure 3.9 top), while the effect of changing the maximum rate of  $k_{Calvin}^{max}$  (equivalent to changing  $n_{Calvin}$ , see equation 3.9) produces a change in the maximum photosynthetic rate. The model converges to the models of Han (2001; 2002) as  $k_{Calvin}^{max}$  approaches infinity:  $\tau$  limits the rate of photosynthesis at high irradiance under these conditions. Note, however, that within the context of the Han model,  $\tau$  corresponds to the “slow” turnover time of photosynthetic units and is used to represent the slowest turnover of the photosynthetic system (here assumed to be the dark reactions). The non-zero charge separation rates at  $k_{Calvin}^{max}=0$  are due to the “other” electron sinks ( $k_{sinks}$ ), which allow a fraction of the

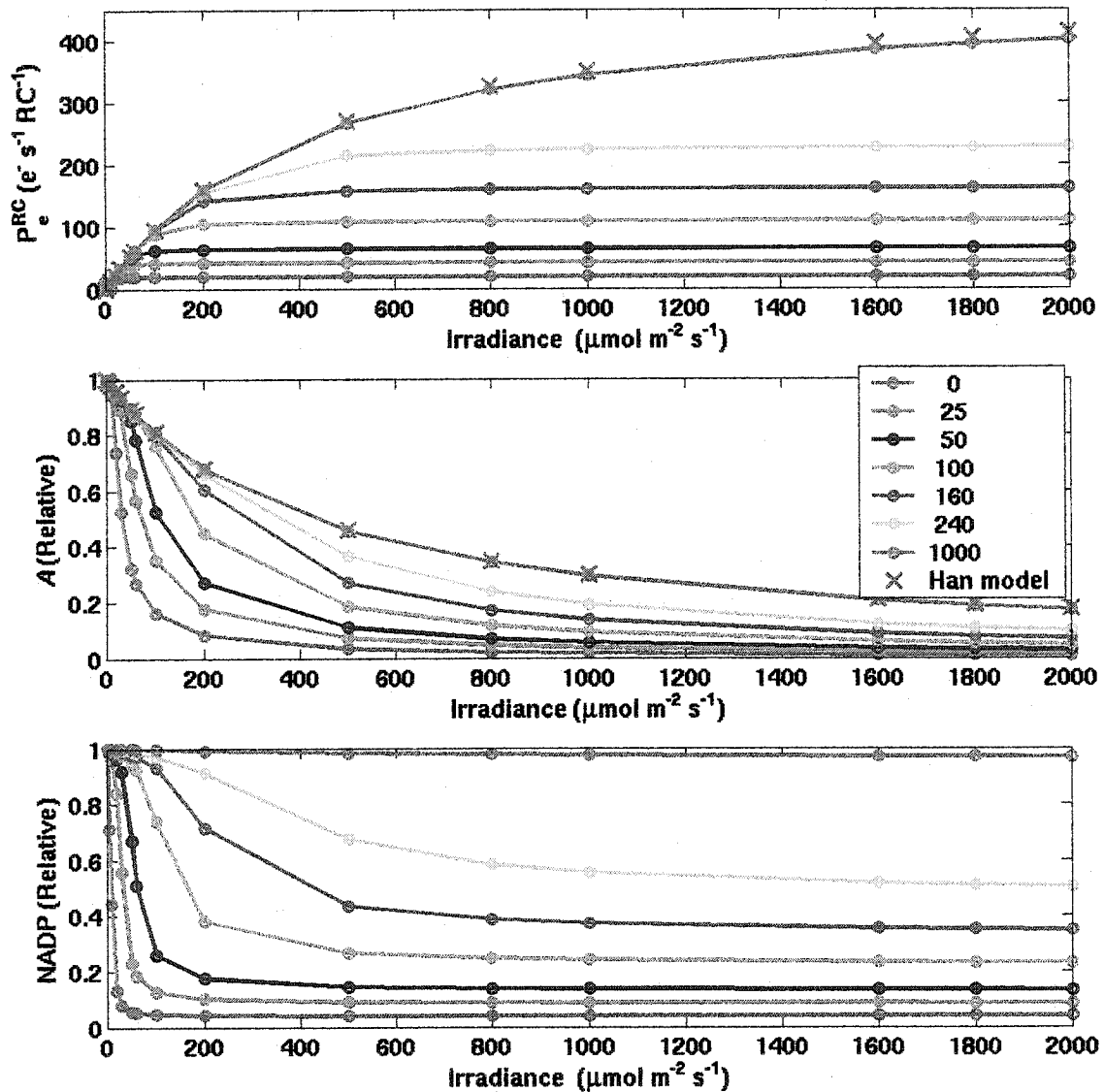


Figure 3.9: Basic photosynthesis model. The model was allowed to reach steady state and all parameters were saved. The different lines represent different values of  $k_{\text{Calvin}}^{\text{max}}$  ( $\text{s}^{-1}$ ) corresponding to different maximal rates of the Calvin cycle enzymes (see legend). Top panel: The rate of charge separation per reaction center. Middle panel: Fraction of open reaction centers. Bottom panel: Relative concentration of NADP ( $\text{NADP} + \text{NADPH} = 1$ ). Note that changing the values of  $k_{\text{Calvin}}^{\text{max}}$  has the same effect as changing the value of  $n_{\text{Calvin}}$ , the ratio of RUBISCO enzymes to PSII reaction centers (this is one possible mechanism of photoacclimation that is not simulated in my model). The Han model uses the equation described by Han (2002) with the values for the different parameters given in Table 3-3.

reaction centers to remain open at high-irradiance. Increasing  $k_{Calvin}^{max}$  leads to an increase in the fraction of open reaction centers (Figure 3.9 middle). The pool of oxidized NADP is also directly linked to  $k_{Calvin}^{max}$  (Figure 3.9, bottom); a depletion of this pool occurs when the production of electrons by PSII reaction centers exceeds the rate of electron utilization by all sinks.

All subsequent model runs will use a value of  $k_{Calvin}^{max} = 160 \text{ e}^- \text{ s}^{-1} \text{ RUBISCO}^{-1}$ . This implies that a significant decrease in the efficiency of charge separation at PSII can arise before a decline in the maximum electron transport rate occurs in the region where irradiance is saturating. Therefore, at high incident irradiance there is a significant excess capacity of PSII relative to carbon fixation (e.g. Behrenfeld et al. 1998). The decrease in efficiency can occur through a smaller number of active reaction centers or an increase in non-photochemical quenching. This allows significant damage or photoprotection to occur without a decrease in the photosynthetic rates at light saturation.

#### **3.4.2 Basic photosynthesis model with photoinhibition**

Now, the damage section of the model is added to the basic photosynthesis model presented above, such that equations 3.37 and 3.33 are also included while keeping  $\gamma_d = 0$ ,  $\kappa_{\sigma PSII} = 0$  and  $\kappa_\gamma = 0$ . That is, there is no photoprotection through non-photochemical quenching and no acclimation. Photoinhibition is modeled by the probability ( $\psi_d$ ) that a photon absorbed by a closed reaction center leads to damage. The yield of photoinactivation is estimated to be on the order of  $10^{-7}$  to  $10^{-5}$  (Anderson et al. 1998). These yields, with the repair function used (equation 3.34) provide realistic

decline in photochemical capacity (Figure 3.10 top panel). The shapes of these curves are very similar to those measured on cultures (e.g. MacIntyre et al. 2002) or at sea (e.g. Cullen et al. 1992b their figure 6). At low probabilities of damage, the fraction of damaged reaction centers increases linearly with irradiance whereas, at higher probabilities, the damage increases more rapidly at low irradiances and saturates at high irradiance levels (Figure 3.10 bottom panel), reflecting the balance between damage and repair and the decreased target pool size ( $B$ ). The excess capacity of PSII over carbon fixation is well demonstrated by the line for  $\psi_d = 1 \times 10^{-7}$  where ~40% of reaction centers are damaged at  $2000 \mu\text{mol m}^{-2} \text{s}^{-1}$  yet only a slight decrease in  $P_e^{RC}$  is observed.

The dynamics of the photosynthesis model are illustrated with a simulated timeseries (Figure 3.11). The photosynthesis model with photoinhibition included shows an increasing depression in the rate of photosynthesis at noon time with an asymmetric photosynthetic rate (Figure 3.11, top panel). The photosynthetic rate is higher in the morning than in the afternoon at the same irradiance level (hysteresis) because of the slow (relative to changes in irradiance) induction and repair of damaged reaction centers. These time courses are almost identical to those obtained by Marshall et al. (2000) in their model of photoinhibition and consistent with many published studies on the diel cycles of photosynthesis (e.g. Sournia 1973; 1974; Marra 1978; Bruyant et al. accepted). However, this does not imply that photoinhibition is the sole process responsible for the decrease of photosynthesis observed in the natural environment in the afternoon (Harris 1978). Repair continues in the dark as seen by the decreasing concentration of damaged reaction centers in the dark (Figure 3.11 bottom panel).

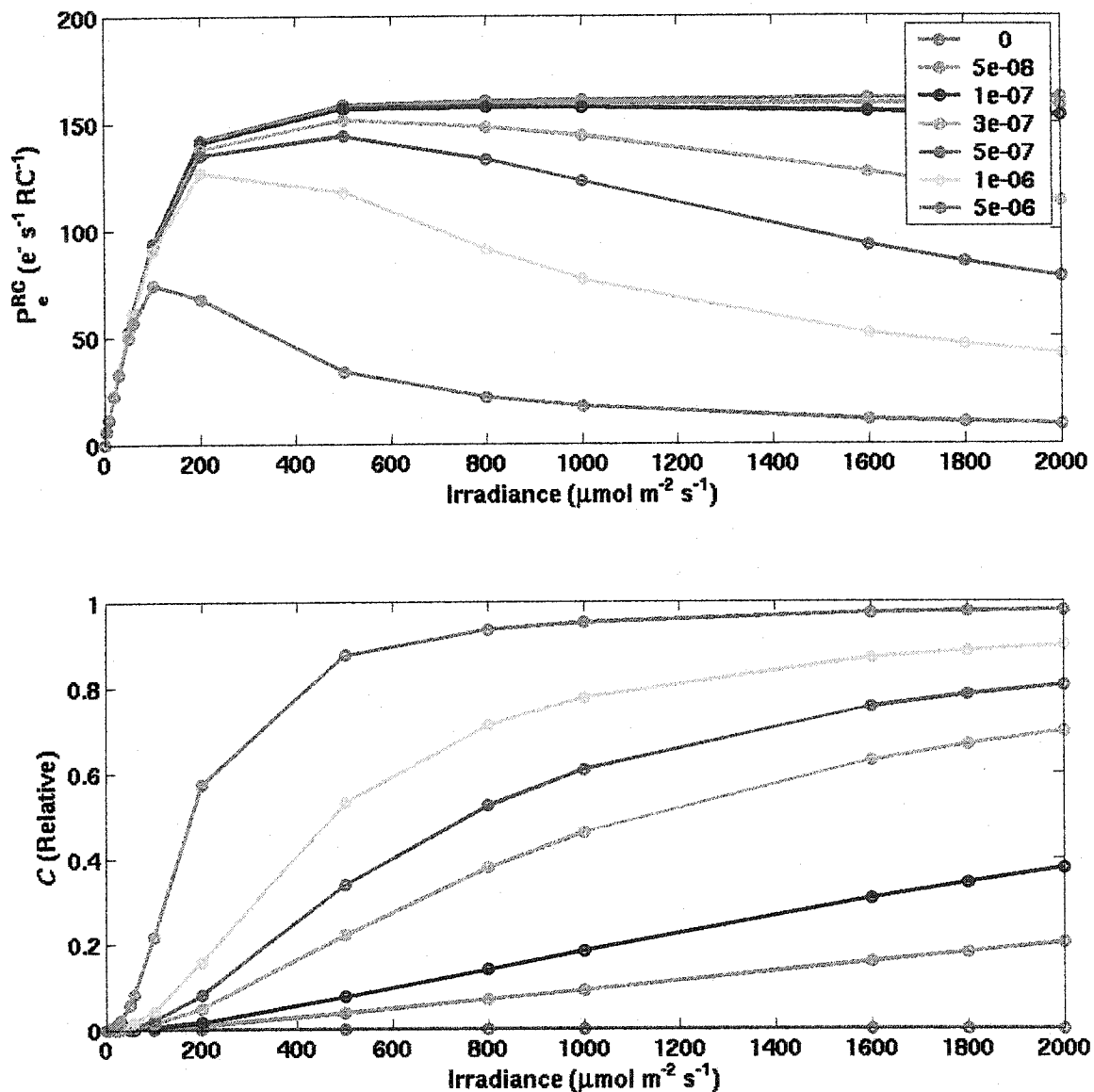
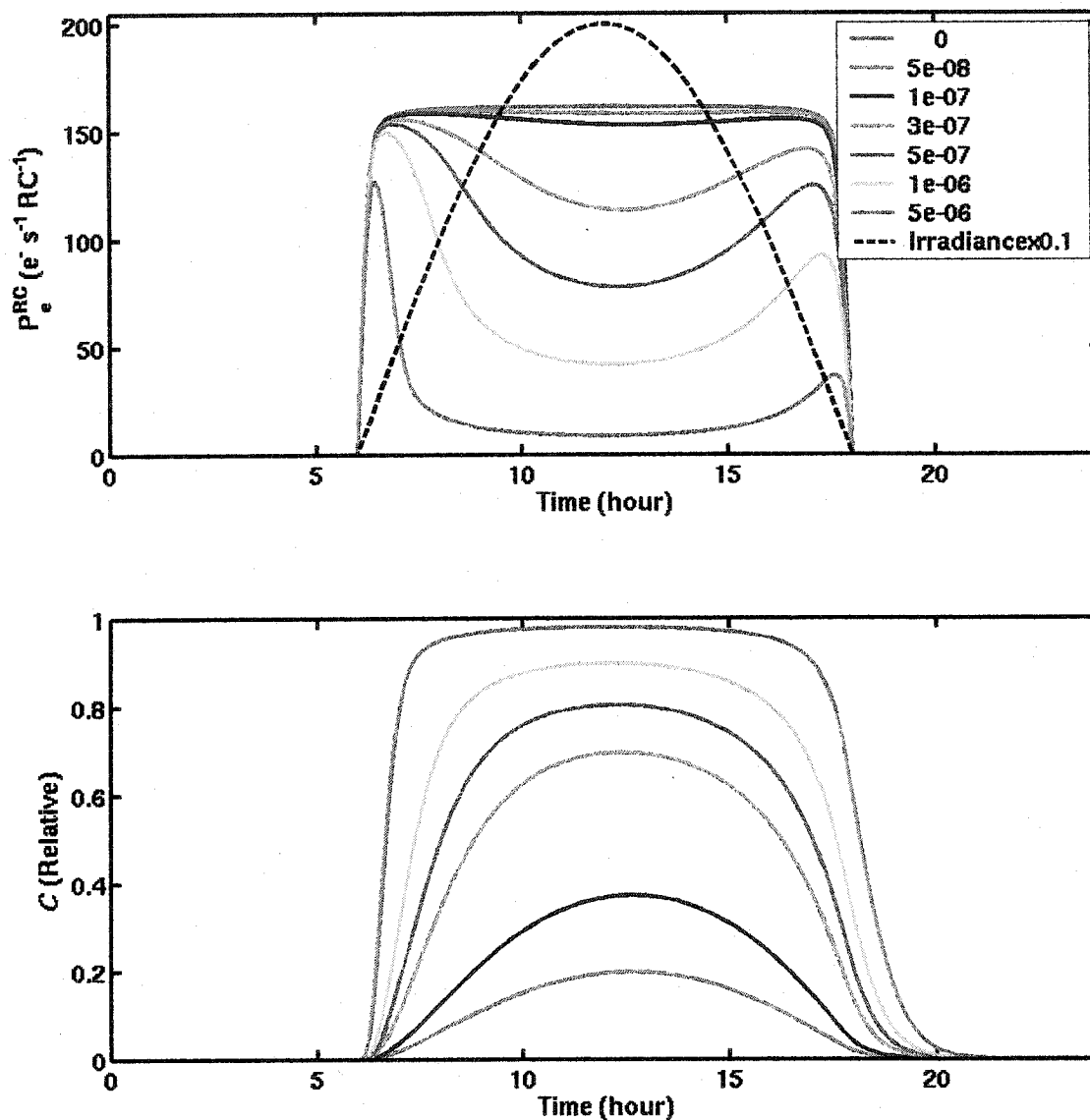


Figure 3.10: Basic photosynthesis model with photoinhibition. The different lines on both panels represent different probabilities for damage ( $\psi_d$ , see legend). Top panel: The charge separation rate per reaction center. Bottom panel: Fraction of damaged reaction centers. The model was allowed to reach steady state and all parameters were saved.



**Figure 3.11: Diel changes in the rate of charge separation with photoinhibition. Top panel: Variation in the rate of charge separation for a sinusoidal irradiance regime (dashed black line) for different probabilities of damage ( $\psi_d$ , see legend). Bottom panel: Fraction of damaged reaction centers. The dashed line represent the irradiance ( $\mu\text{mol m}^{-2} \text{s}^{-1}$ ) multiplied by 0.1, the maximum irradiance was set to  $2000 \mu\text{mol m}^{-2} \text{s}^{-1}$ .**

### 3.4.3 Effect of photoprotection on the rates of photosynthesis and $\phi_f$

In this section, I have added to the basic photosynthesis model with photoinhibition, the capacity for photoprotection by energy dependent non-photochemical quenching, by varying the parameter  $\gamma_d$  (equations 3.27, 3.28, 3.29). However, I do not allow acclimation through equations 3.44 and 3.45; instead, I set the value of  $\gamma_d$  to different constant values.

Adding photoprotection due to energy dependent non-photochemical quenching leads to a decreased amplitude of the depression in the charge separation rates at noon (Figure 3.12 top) due to a decrease in the number of damaged reaction centers (Figure 3.12 middle). This aspect of the model has, to my knowledge, not been parameterized in models of photosynthesis before.

In the absence of damage, however, a large amount of photoprotection could lower the photosynthetic rate due to an increase in the fraction of energy dissipated as heat (Long et al. 1994). The values of the  $NPQ_f$  parameter obtained for the values of  $\gamma_d$  tested in Figure 3.12 are consistent with those observed in diatoms (e.g. Lavaud et al. 2004) under high irradiance levels (see Figure 3.12 bottom). In Figure 3.12, to better illustrate the effect of photoprotection, I used a probability of damage ( $\psi_d$ ) of  $5 \times 10^{-7}$  instead of the standard  $3 \times 10^{-7}$  used elsewhere.

In Figure 3.13, apart from the dashed blue line for which  $\gamma_d = 0$ , all curves were created with the same amount of photoprotection ( $\gamma_d = \gamma_o = 0.0005$ ) but varying probability of damage ( $\psi_d$ , see legend). Without any photoprotection or damage, the

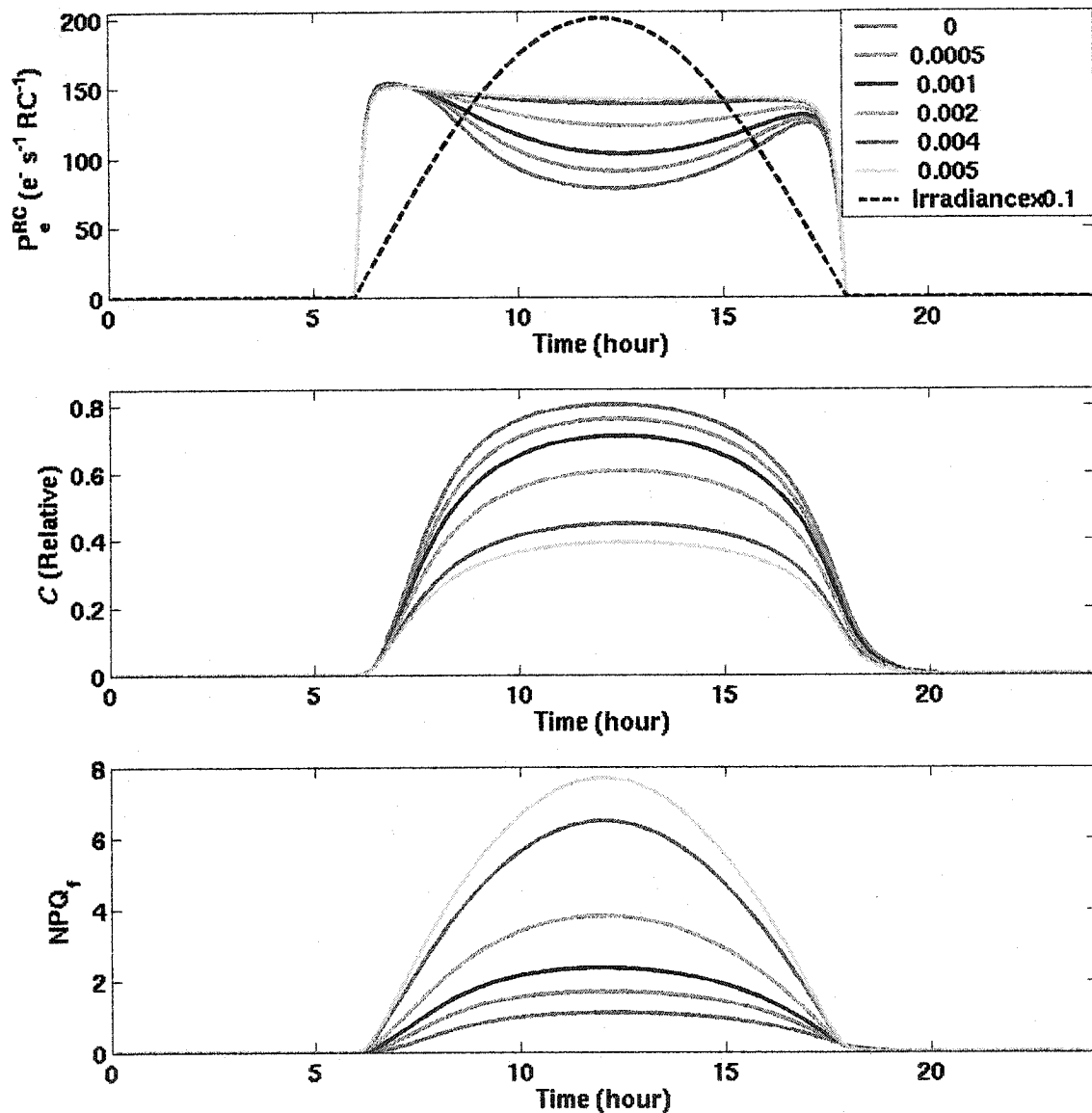


Figure 3.12: Effect of photoprotection on the photosynthetic rates. Top panel: timeseries of the rate of charge separation for different levels of photoprotection ( $\gamma_d$ ,  $[\mu\text{mol m}^{-2}]^{-1}$ , see legend). The blue line ( $\gamma_d=0$   $[\mu\text{mol m}^{-2}]^{-1}$ ) is the same simulation as the  $\psi_d = 5 \times 10^{-7}$  in Figure 3.11. Middle panel: Fraction of damaged reaction centers. Bottom panel: The parameter  $NPQ_f$ .  $NPQ_f$  is a common measure of the energy dependent non-photochemical quenching but is also affected by photoinhibition.

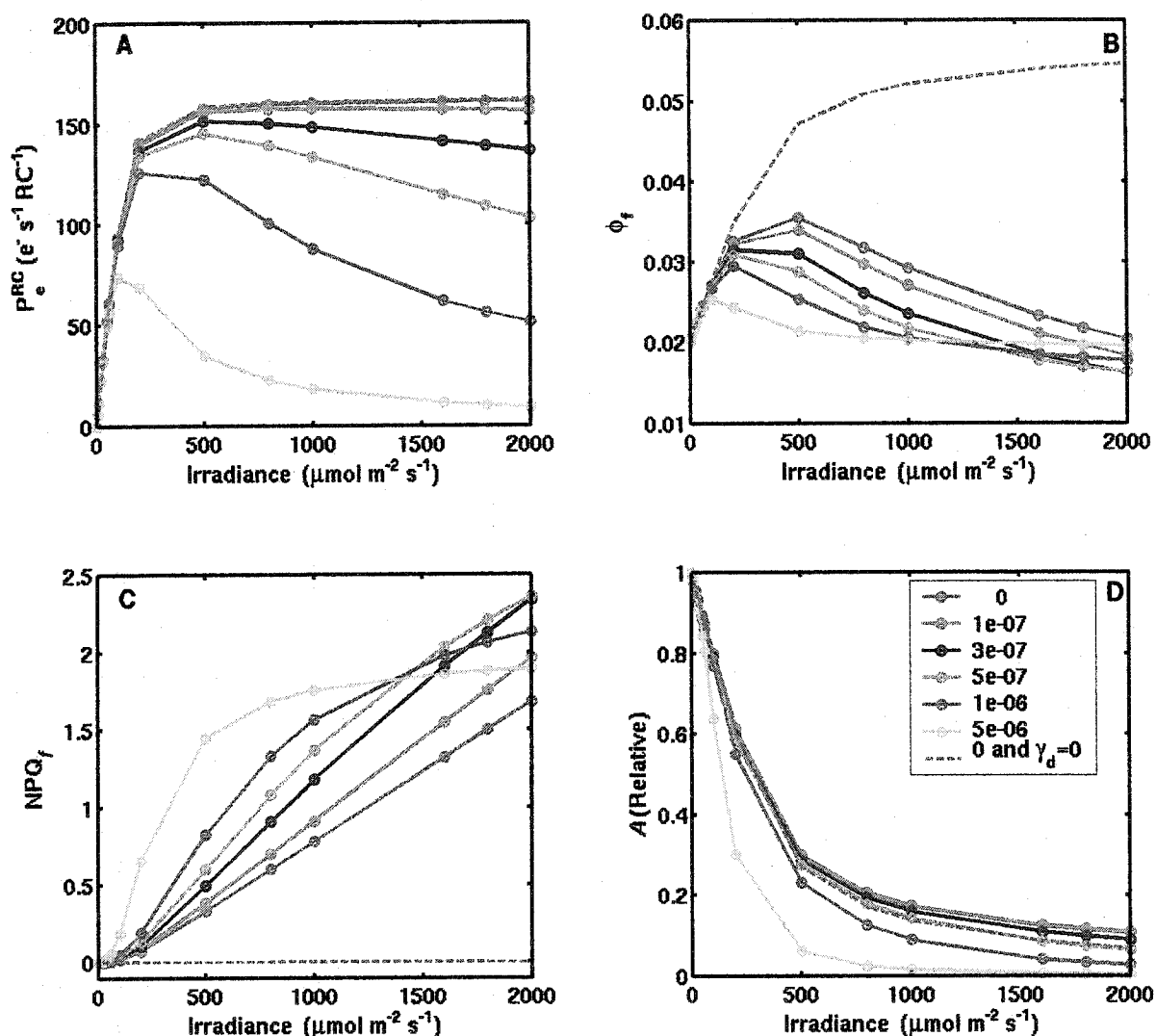
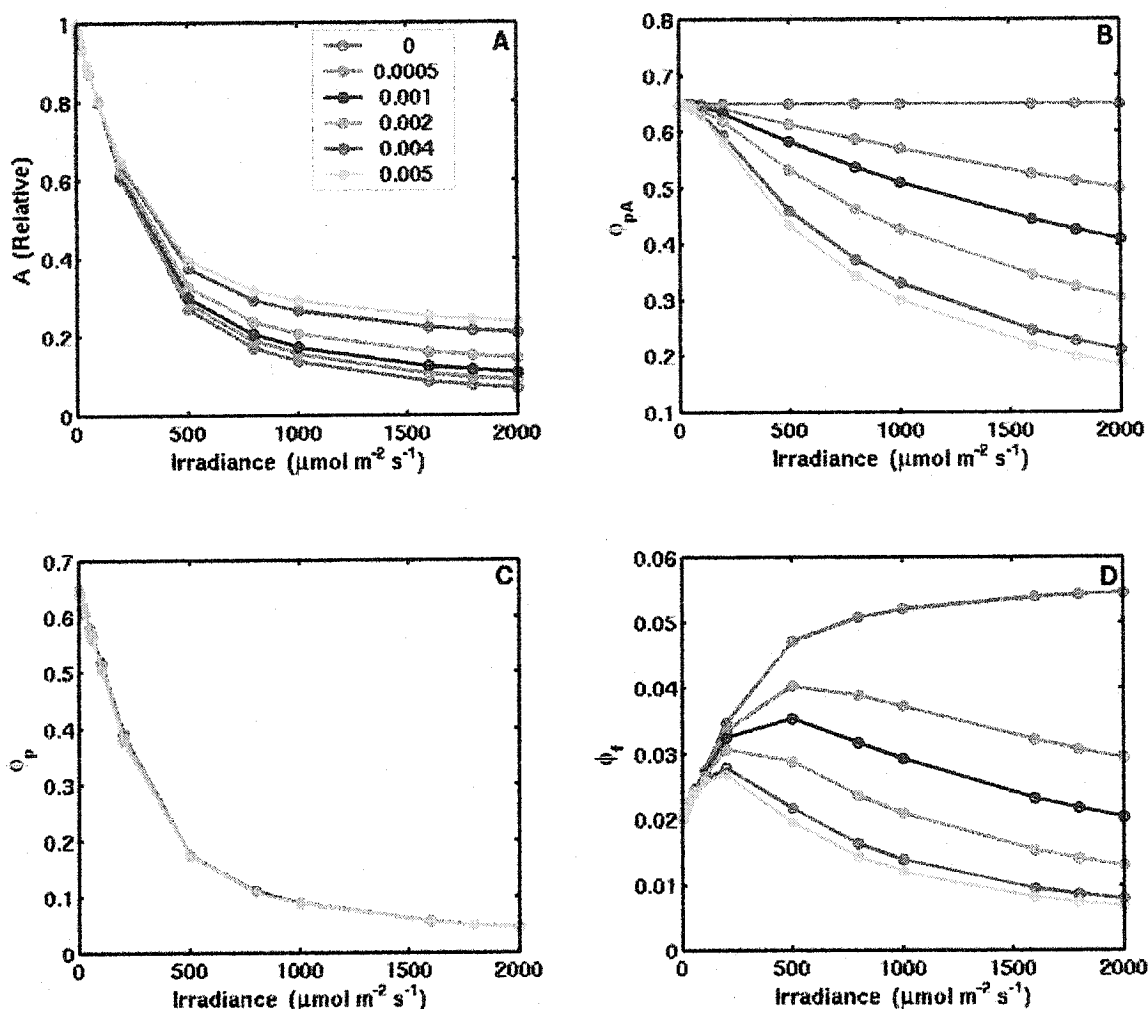


Figure 3.13: Photosynthesis with damage and fluorescence, including the effect of photoprotection by energy dependent quenching ( $\gamma_d=0.0005$ ,  $[\mu\text{mol m}^{-2}]^{-1}$ ). The different lines on each panel represent different probabilities of damage ( $\psi_d$ , see legend), while the dashed blue line has no photoprotection ( $\gamma_d=0$   $[\mu\text{mol m}^{-2}]^{-1}$ ) or damage. A) Rate of charge separation. B) Quantum yield of fluorescence. C) The fluorescence parameter  $NPQ_f$ . D) Fraction of open reaction centers.

quantum yield of fluorescence is a saturating function of irradiance, similar to the rate of charge separation (compare dashed blue lines on Figure 3.13 A&B). With photoprotection but without damage, the fluorescence yield is lowered at higher irradiances due to non-photochemical quenching (Figure 3.13 B, blue line); this decrease is accentuated by the increase in damage (Figure 3.13 B). The effect of the decline in the capacity for non-photochemical quenching due to damage is clearly observed for  $\psi_d = 1 \times 10^{-6}$  and  $5 \times 10^{-6}$  (Figure 3.13 B and C); compare yellow ( $\psi_d = 1 \times 10^{-6}$ ) and black ( $\psi_d = 5 \times 10^{-6}$ ) lines with the deep pink line ( $\psi_d = 5 \times 10^{-7}$ ). This is reflected in the  $NPQ_f$  parameter, which increases with damage (Figure 3.13 C) up to a point where damage hinders the capacity for energy dependent non-photochemical quenching (see equation 3.27). The increasing amount of damage leads to a decrease in the fraction of open reaction centers (Figure 3.13 D) since the pools of open, closed and inhibited must sum to one.

One effect of photoprotection is to keep a greater fraction of the reaction centers open (Figure 3.14A). This is due to the decrease of the quantum yield of an open reaction center as energy dissipation in the antenna is increased (Figure 3.14B). Without non-photochemical quenching, the quantum yield of an open reaction center remains constant at all irradiances (Figure 3.14B with  $\gamma_d = 0$ ). However, the increase in the fraction of open reaction centers is due to the decreased quantum yield, thus photoprotection has no effect on the realized quantum yield of all reaction centers when there is no damage (Figure 3.14C). The effect of increasing the capacity for non-photochemical quenching is



**Figure 3.14: Effect of photoprotection on the quantum yields of photosynthesis and fluorescence.** The different lines correspond to different levels of photoprotection ( $\gamma_d$ , see legend). A) Fraction of open reaction centers. B) Quantum yield of charge separation in open reaction centers. C) Quantum yield of charge separation by all reaction centers. D) Quantum yield of fluorescence. The probability of damage was equal to 0 for this comparison ( $\psi_d=0$ ), so all non-photochemical quenching is due to energy dependent quenching. All curves represent the instantaneous results at steady state.

a greater decrease in the quantum yield of fluorescence at high irradiance (Figure 3.14D).

Because increasing the capacity for non-photochemical quenching leads to a decreasing quantum yield of fluorescence at high light, this leads to a family of curves for the relationship between fluorescence and photosynthetic yields depending on the value of  $\gamma_d$  (Figure 3.15 top). These curves are very different from the published relationships that apply only to lower irradiances (e.g. Kiefer and Reynolds 1992). They greatly complicate the interpretation of sun-induced fluorescence measurements in surface waters where non-photochemical quenching is important (Cullen and Lewis 1995; Maritorena et al. 2000; Morrison 2003) even in the absence of damage. This is particularly important if one attempts to obtain information about photosynthetic rates from sun-induced fluorescence (Kiefer et al. 1989; Chamberlin et al. 1990; Chamberlin and Marra 1992; Kiefer and Reynolds 1992; Abbott and Letelier 1999). Morrison (2003) has acknowledged this limitation in terms of non-photochemical quenching due to photoinhibition at intermediate to low irradiance levels in the ocean, and proposed that much of the variability observed in the quantum yield of fluorescence at a given irradiance depended on this phenomenon. The model shows that the extension of this concept to energy dependent quenching is warranted.

The use of variable fluorescence, because it allows the determination of the maximal quantum yield of fluorescence at the same time as the quantum yield of fluorescence under ambient conditions is, however, well suited to examine photosynthesis under high irradiance. The Genty yield (Genty et al. 1989), defined as

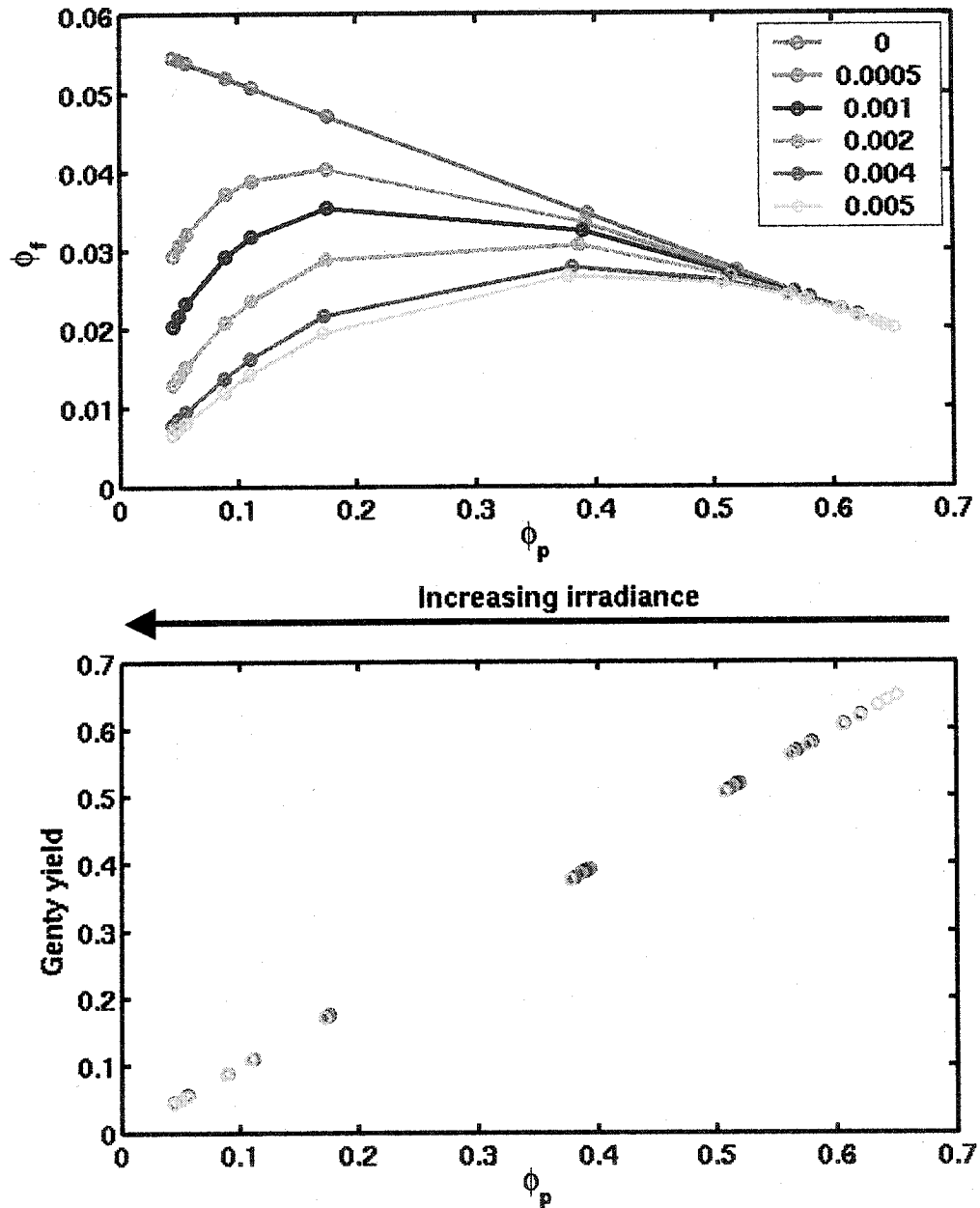
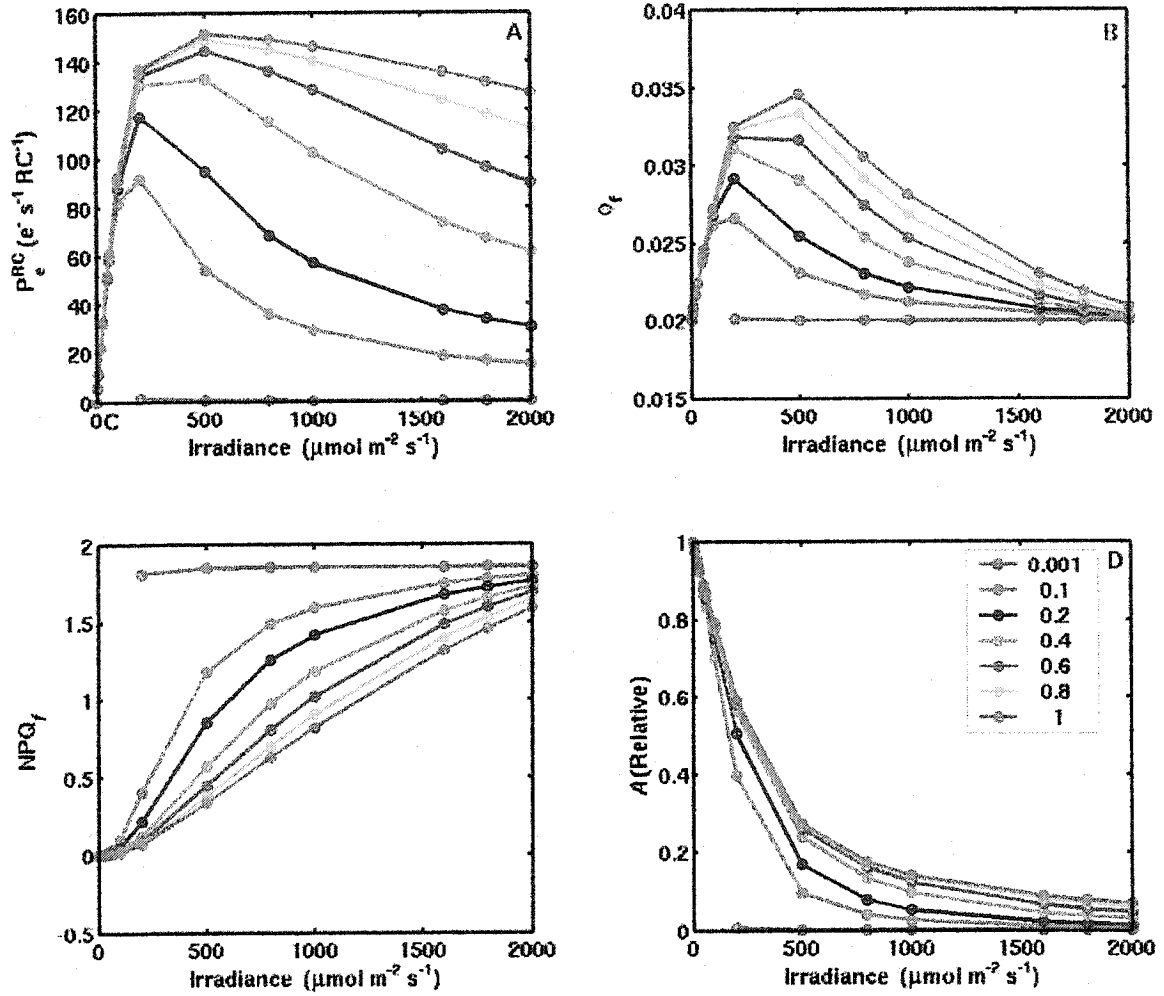


Figure 3.15: Comparison of the quantum yield of fluorescence and the quantum yield of photochemistry for different capacities for non-photochemical quenching ( $\gamma_d$ , [ $\mu\text{mol m}^{-2}$ ] $^{-1}$ , see legend). Top panel: Comparison between the quantum yield of fluorescence and the quantum yield of photochemistry ( $\phi_p = \phi_{pA} A$ ). Bottom panel: Comparison between the Genty yield ( $(F'_m - F')/F'_m$ ) and the quantum yield of photochemistry ( $\phi_p = \phi_{pA} A$ ). The probability of damage was set to 0 for this comparison ( $\psi_d = 0$ ).

$(F'_m - F') / F'_m$ , provides a measure of the quantum yield of charge separation under ambient irradiance, and showed a perfect relationship with my model (Figure 3.15 bottom) estimate of  $\phi_p$ . This is not, however, a validation of the Genty yield or of my model, but rather shows the internal consistency between the assumptions used in the derivation of the Genty yield and this model. Note, however, that the Genty yield is not limited to the puddle model (e.g. Kramer et al. 2004).

#### 3.4.4 Nitrogen limitation and the quantum yield of fluorescence

In this section, I examine the effect of nitrogen limitation on charge separation and fluorescence by varying the parameter  $N_{status}$  (equation 3.34). This is equivalent to changing the maximal rate of repair ( $k_{rep}^{max}$  in equation 3.34). Under extreme nitrogen stress, the repair rate becomes zero and the photochemical yield eventually decreases to zero (Figure 3.16A, blue line). Because the time to achieve steady state values becomes longer with decreasing irradiance (as the damage rates are low), the results at the lowest irradiances are not provided when the nutritional status is equal to 0.001 (Figure 3.16A). With decreasing values of nitrogen status ( $N_{status}$ ), the photochemical rate is increasingly lowered at the higher irradiance levels (Figure 3.16A) due to damage. This is consistent with the observations in the literature (e.g. Prézélin et al. 1986; Kolber et al. 1988). With decreasing repair capacity and increasing damage level, the quantum yield of fluorescence decreases continuously (Figure 3.16B), and reaches  $F_o$  when most of the reaction centers are damaged. The increasing damage at low repair rates leads to an increase in  $NPQ_f$  (Figure 3.16C). The decreased repair rate leads to a lower number of



**Figure 3.16: Effect of nitrogen stress on the photochemical rates and fluorescence quantum yield. The nitrogen stress was varied from extreme ( $N_{status}=0.001$ ) to none ( $N_{status}=1.0$ ), decreasing the maximal capacity for repair proportionally (see legend). A) Rates of charge separation. B) Quantum yield of fluorescence. C)  $NPQ_f$  parameter. D) Fraction of open reaction centers. The first eight points are not shown for  $N_{status}=0$  because the steady state has not been reached. All curves represent the instantaneous results at steady state. No acclimation and photoprotection ( $\gamma_d=0$ ) is present in these simulations.**

open reaction centers at high irradiance (Figure 3.16D).

The diel patterns provide further insights into the effects of nitrogen limitation as parameterized in this model on fluorescence and photochemistry. The increasing nitrogen limitation has an effect similar to an increased probability of damage (Figure 3.11) as it decreases the photochemical yield at midday (Figure 3.17A). However, the effect of nitrogen stress is associated with a more pronounced asymmetry between the morning and evening values (Figure 3.17A). The asymmetry is due to the greater time required to repair damage when the irradiance decreases after the noontime maximum in damage rates (Figure 3.17B).

The effect on fluorescence is a much lowered quantum yield of fluorescence in the afternoon compared to the morning values (Figure 3.17C). The dynamics in panel C, can be explained as follows: in the morning, at low light, the fluorescence quantum yield increases to a maximum as photochemical quenching decreases. Beyond this maximum, the decrease is due to energy dependent non-photochemical quenching. When the nutrient status is low enough ( $\sim < 0.2$ ), the yield starts increasing before noon toward the  $F_o$  level as damage accumulates. The accumulation of damage after midday leads to a lower maximum yield in the afternoon.

The effect on the parameter  $F_v''/F_m''$  (as would be measured after 20 minutes in the dark) is to decrease its value with nutrient stress, this lower value remains for longer at night, as nutrient stress increases (Figure 3.17D) and is associated solely with a decrease in  $F_m''$ .

The increase in the asymmetry between morning and afternoon in the quantum

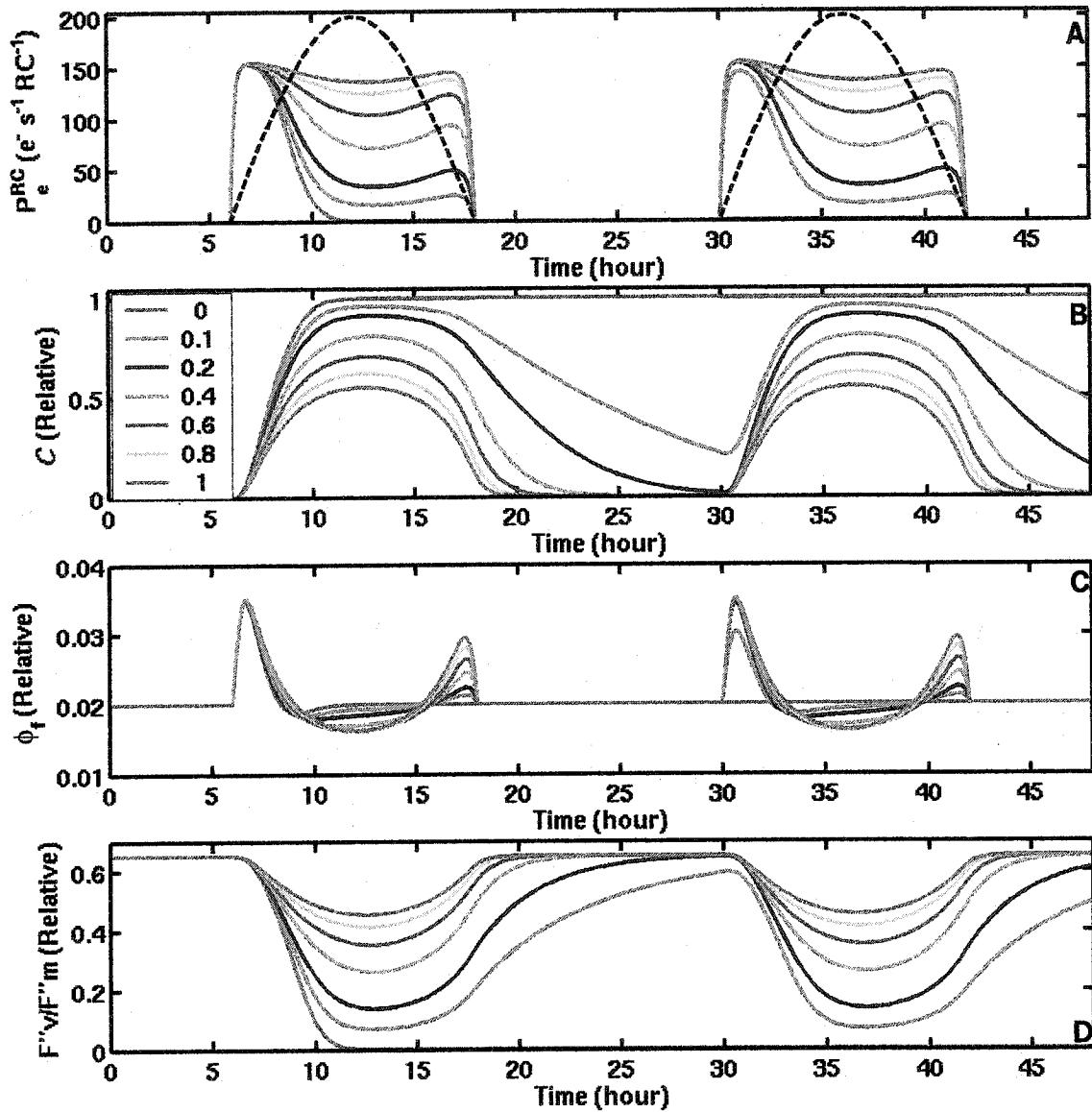


Figure 3.17: Effect of nitrogen stress on the diel changes in photochemistry and fluorescence. In this simulation, damage, repair and photoprotection due to energy dependent quenching are all included. A) Rates of charge separation. B) Fraction of damaged reaction centers. C) Quantum yield of fluorescence. D)  $F''_v / F''_m$  parameter. Different lines represent different nitrogen status of the cell ( $N_{status}$ , see legend). Dashed black lines correspond to the irradiance ( $\mu\text{mol m}^{-2} \text{s}^{-1}$ ) level divided by 10.

yield of fluorescence is consistent with the results obtained by Laney et al. (2001; Laney et al. in prep) during nutrient starvation experiments (See Figure 3.18, data courtesy of Sam Laney).

Because the model for nitrogen stress is cast in terms of nitrogen quota, it is more appropriate to simulate conditions of unbalanced growth. Under nitrogen limitation during balanced growth (see Chapter 2 for more details), the nitrogen quota of the cell can be low while the maximum photosynthetic rate can remain high (Parkhill et al. 2001); this is not the condition modeled here.

### 3.4.5 *The influence of $k_I$*

The dynamics described in Figure 3.17C for fluorescence are highly influenced by the parameter  $k_I$ , which changes the fluorescence quantum yield of an inhibited reaction center. There is, however, very little guidance in the literature to set this number. Observations in algae suggest, as noted before, that the fluorescence yield of inhibited reaction centers could be equal or higher than that of an open reaction center, but lower than that of a closed reaction center. The effect of changing  $k_I$  on the fluorescence yield is mostly observed at high levels of damage; in my model, this is particularly the case for low nutrient status and high light (Figure 3.19 top panel). The turquoise line ( $\phi_{F_I} = 0.02$ ) is the value selected for the standard model (used in Figure 3.17). Under these conditions, the quantum yield of an inhibited reaction center in the dark acclimated condition ( $\phi_{F_I}$ ) is equal to that of an open reaction center under the same conditions ( $\phi_{F_o}$ ). Using a different level for  $\phi_{F_I}$  would have important consequences for the patterns observed in

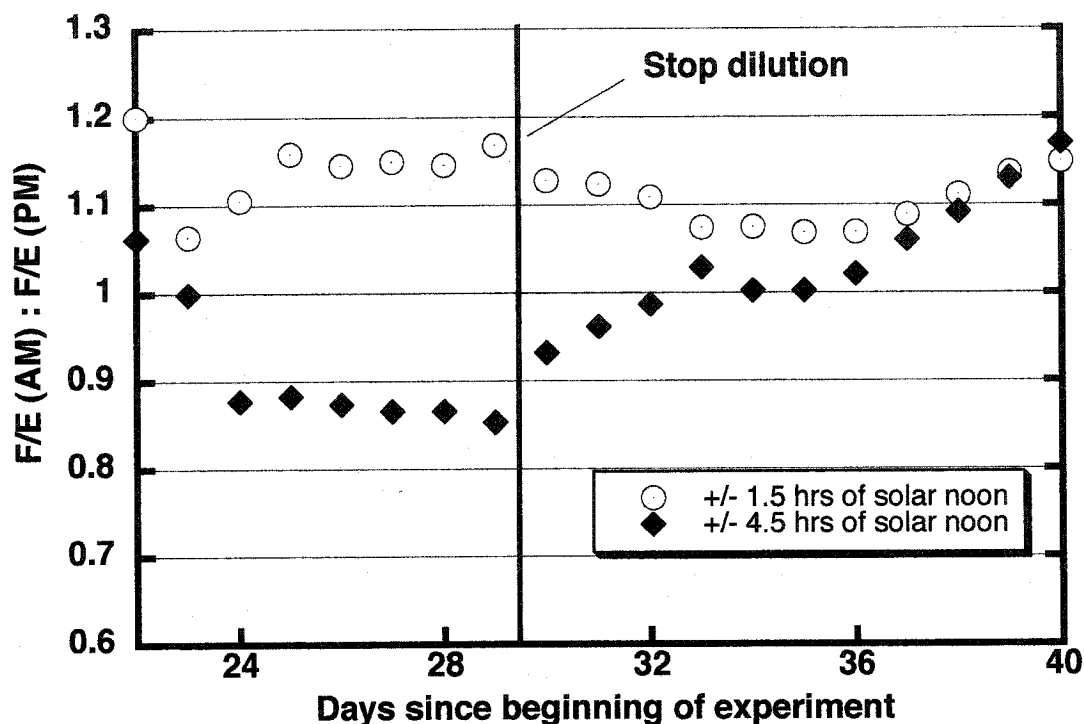
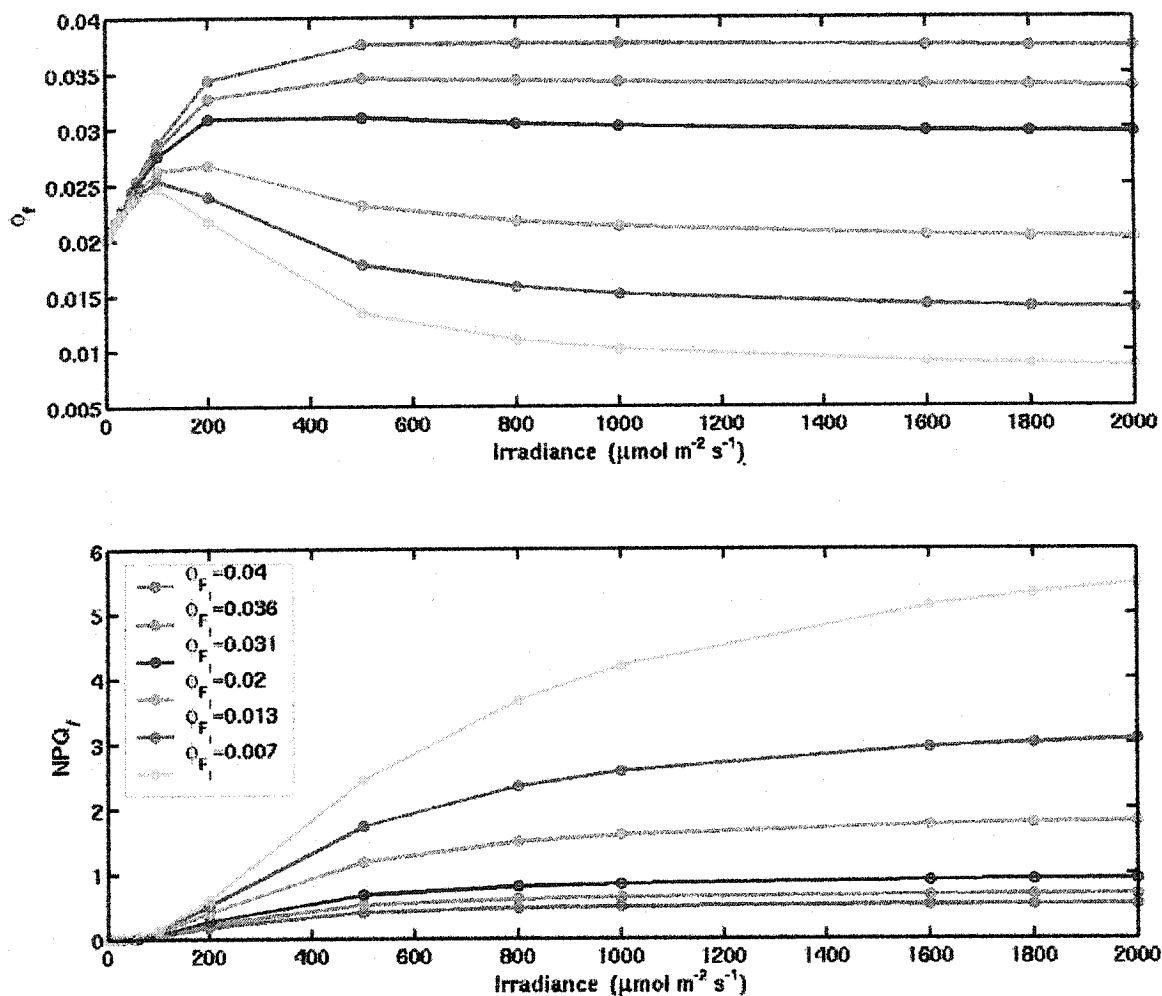


Figure 3.18: Ratio of morning (AM) to afternoon (PM) natural fluorescence emission divided by incident irradiance (F/E) in continuous cultures of *Thalassiosira weissflogii* grown on a 14:10 hours sinusoidal light-dark cycle. On day 20, the midday maximum irradiance was switched from  $80 \mu\text{mol m}^{-2} \text{s}^{-1}$  to  $400 \mu\text{mol m}^{-2} \text{s}^{-1}$  and the natural fluorescence emission was recorded continuously during the daytime. The ratio F/E before noon to F/E after noon was plotted for each day. On day 30 the dilution (nutrient addition) was stopped and the culture entered nutrient starvation conditions. The ratio  $F/E(\text{AM}) / F/E(\text{PM})$  is affected by both growth and changes in the fluorescence quantum yield. A high ratio of  $F/E(\text{AM}) / F/E(\text{PM})$  can be due to slow growth or persistent quenching in the afternoon, the latter is usually associated with photoinhibition. The different symbols correspond to different periods from solar noon. In the data showing the difference for  $\pm 4.5$  hrs of solar noon, the initial increase in the ratio after the dilution was stopped is probably due to the slower growth rate. The second slower increase starting on day 35 could be the result of the decreased capacity for repair. Sam Laney generously provided the data for this figure.



**Figure 3.19: The influence of  $k_I$  on the fluorescence quantum yield under damaging conditions. Top panel: Quantum yield of fluorescence. Bottom panel: Non-photochemical quenching parameter. Conditions were identical to the curve for  $N_{status}=0.1$  on Figure 3.16 except that  $k_I$  was varied to change the value of  $\phi_{F_I}$  (see legend). The main effect of changing  $k_I$  is to change the quantum yield of fluorescence of inhibited reaction centers. Changing  $k_I$  does not affect the PvsE curve such that for all curves presented here, the corresponding PvsE curve is given by  $N_{status}=0.1$  on Figure 3.16A.**

Figure 3.17. For example, if  $k_f$  was chosen such that  $\phi_{F_i} = 0.04$  (blue line, in Figure 3.19), this would mean that the blue line ( $N_{status} = 0.001$ ) in Figure 3.17C would go to  $\sim 0.037$  and remain there. As  $\phi_{F_i}$  decreases,  $NPQ_f$  increases (Figure 3.19 bottom panel) at high damage levels as  $F_m'$  is decreased. This increase is only related to the inhibition part of  $NPQ_f$  ( $NPQ_f^I$ ), and the energy dependent portion ( $NPQ_f^{qE}$ ) remains constant.

#### 3.4.6 Acclimation to irradiance

In this section, I add the acclimation of both the optical cross-section ( $\sigma_{PSII}^O$ , equation 3.44) and the capacity for non-photochemical quenching ( $\gamma_{NPQ}$ , equation 3.45) to the model of photosynthesis with photoinhibition and non-photochemical quenching.

Consistent with acclimation, the rate of photosynthesis at the acclimated irradiance is a saturating function of the growth irradiance (Figure 3.20A). The function used for acclimation forces the optical absorption cross-section for PSII to be optimized (Figure 3.20C) such that the fraction of active open reaction centers is as close to 0.3 (Figure 3.20B) as allowed by the parameter  $x$ . When the parameter  $x$  is set to 0, the fraction of open reaction centers at the steady state is equal to 0.3 at all irradiances, however, this leads to unrealistically large changes in the absorption cross-section (not shown). Through acclimation of  $\gamma_{NPQ}$ , the value for damaged reaction centers is kept as close to 0.05 (or below 0.05 at low irradiances, Figure 3.20B) as allowed by the parameter  $y$  by changing the capacity for non-photochemical quenching (Figure 3.20D). The increased capacity for non-photochemical quenching along with the increasing amount of damage (Figure 3.20B) leads to an increasing value of  $NPQ_f$  with increasing

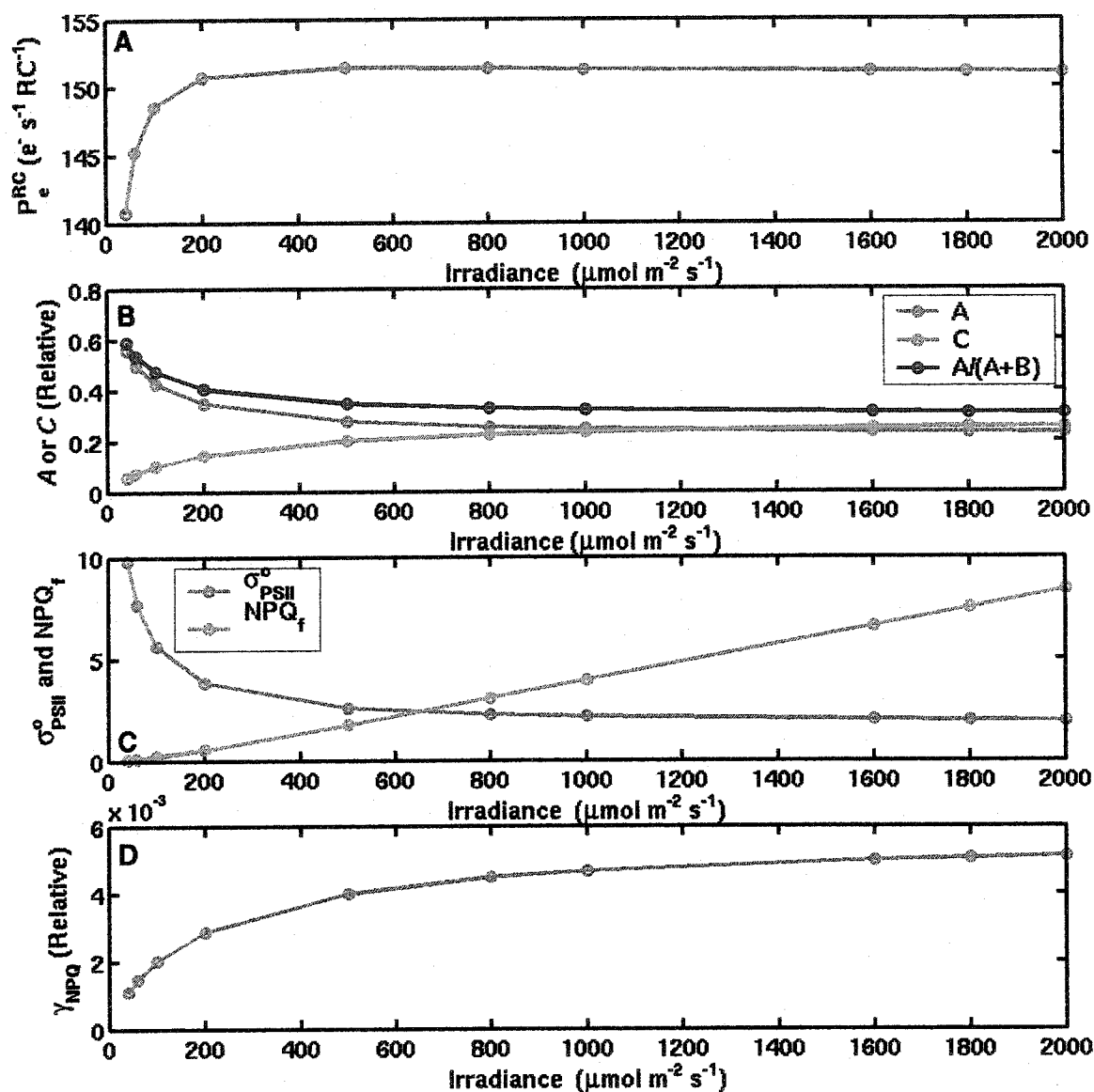
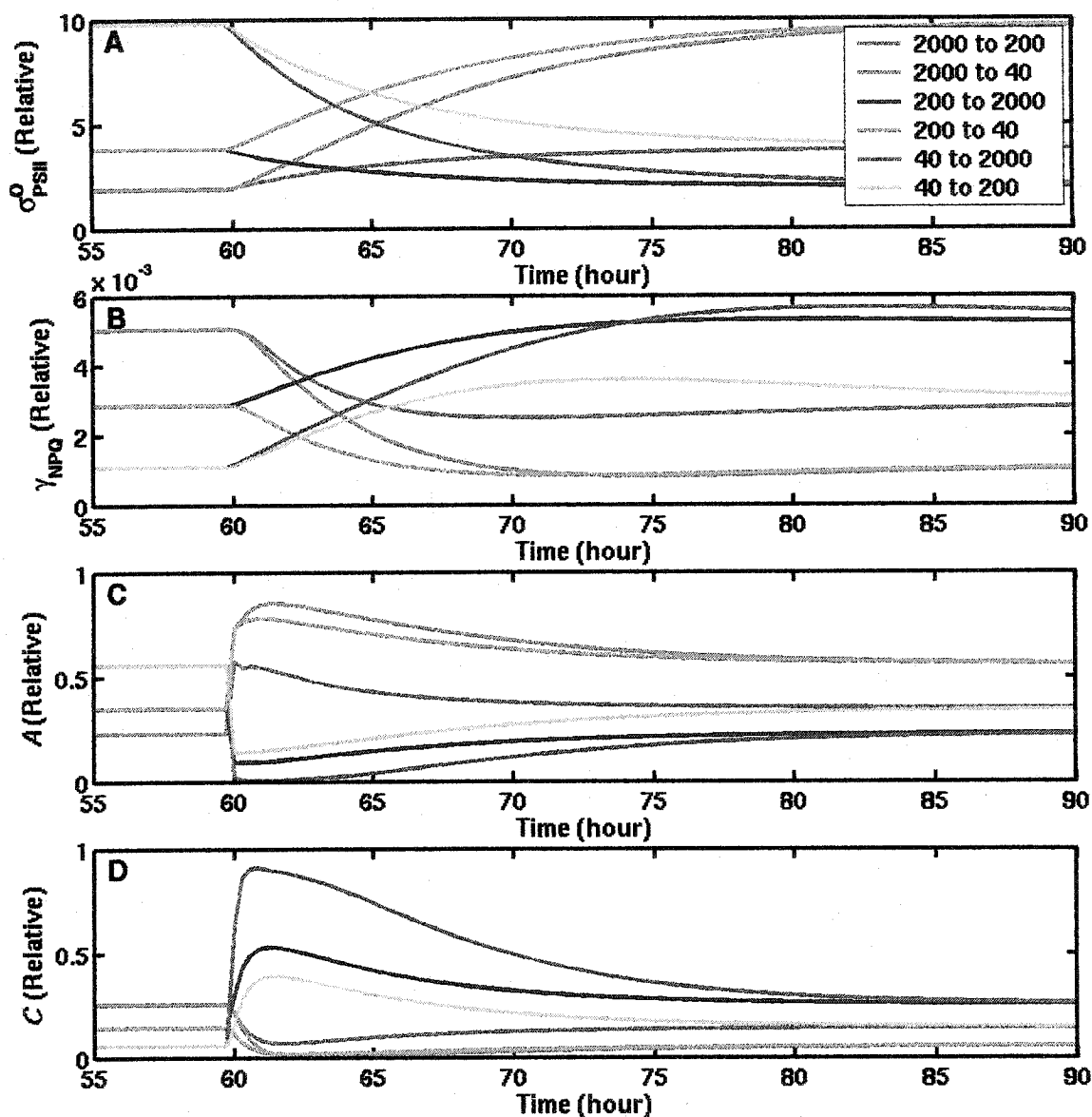


Figure 3.20: Steady-state values of seven variables for different growth irradiance levels. The model was allowed to reach the steady state at a constant irradiance and the outputs were recorded. A) Rate of charge separation. B) Fraction of open, closed, and open over active ( $A/(A+B)$ ) reaction centers. C) Optical absorption cross-section and non-photochemical quenching parameter. D) Capacity for non-photochemical quenching.

growth irradiances (Figure 3.20C).

The kinetics of the model upon a step change in irradiance is presented in Figure 3.21A for  $\sigma_{PSII}^o$  and Figure 3.21B for  $\gamma_{NPQ}$ . The acclimation rates are such that the time it takes to reach half of the difference between the initial and final state are between 5 to 10 hours. This is consistent with the rates measured by Cullen and Lewis (1988), but I have not included a different rate for the shift up and the shift down in irradiance. Just following a step in irradiance, the number of open reaction centers is higher than the steady-state solution for a light shift down and lower than the steady state solution for a light shift up (Figure 3.21C). This is because the rate constants for the closure and opening of reaction centers are much faster than the rate constant for acclimation. The same type of overshoot occurs for the concentration of damaged reaction centers, but in the opposite direction (Figure 3.21D).

The acclimation model reproduces many of the features that have been recognized as a consequence of acclimation (Steeman Nielsen and Jørgensen 1968; Prézelin 1981; Richardson et al. 1983; MacIntyre et al. 2002). Firstly, the maximal photosynthetic rates per reaction center remain constant over a wide range of acclimation irradiances (Figure 3.22A). Because the size of the enzymatic component remains constant, this is approximately equivalent to the carbon specific maximum photosynthetic rate measured in traditional PvsE curves using  $^{14}\text{C}$  (assuming the size of the accumulated carbohydrates remains low or constant relative to the carbon reducing enzymatic component for all irradiances). The constancy of the carbon specific maximum photosynthetic rate with growth irradiance is one of the main features observed by MacIntyre et al. (2002) in their



**Figure 3.21: Kinetics of acclimation upon step change in irradiance.** The model was allowed to reach steady state for 60 hours at a constant irradiance level then the irradiance was changed with a step function to another irradiance for 30 hours. A) Optical absorption cross-section. B) Capacity for non-photochemical quenching. C) Fraction of open reaction centers. D) Fraction of closed reaction centers. Irradiance levels for the light shifts are given in the legend.

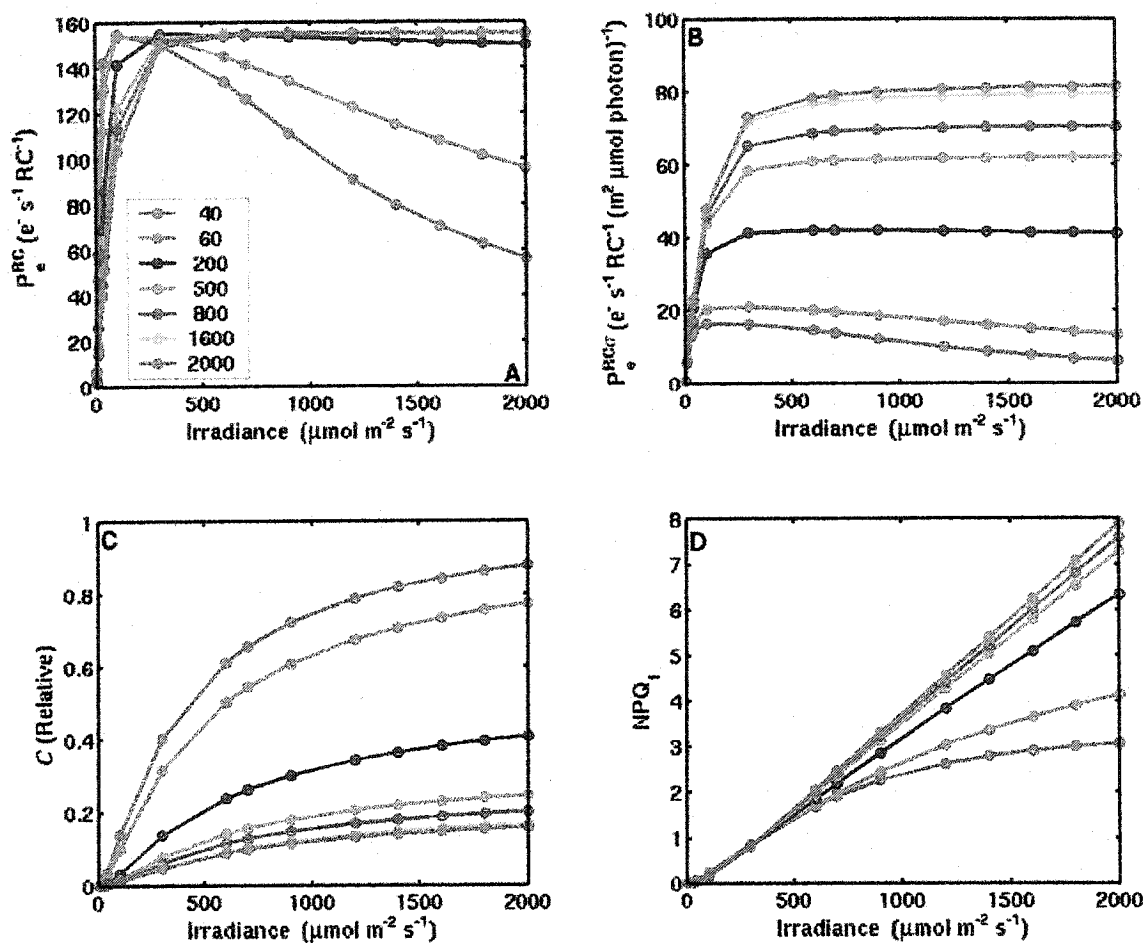


**Figure 3.22: Consequences of acclimation on photosynthesis.** The results shown are the mean of 15 minutes in the light for photosynthetic systems acclimated to different irradiances (see legend and Figure 3.20). A) Rate of charge separation. B) Rate of charge separation divided by the optical cross section. C) Fraction of damaged reaction centers. D) The  $NPQ_f$  parameter.

review. Secondly, cells acclimated to lower irradiances are more prone to photoinhibition (Figure 3.22A & C), which is a feature generally observed (e.g. Cullen et al. 1992b; MacIntyre et al. 2002). Thirdly, by normalizing the photosynthetic rate to the optical absorption cross-section, the initial slope of the curves remains constant across acclimation irradiances (Figure 3.22B). This parameter can be compared to the chlorophyll specific initial slope of the PvsE curves determined by  $^{14}\text{C}$  incorporation, assuming that chlorophyll represents a good measure of the absorption cross-section (not valid in red algae and cyanobacteria, or in large cells where the chlorophyll specific absorption coefficient varies) and that the “other sinks” modeled with  $k_{\text{sinks}}$  remain constant with irradiance at non-saturating irradiances. MacIntyre et al. (2002) found the initial slope of chlorophyll normalized PvsE curves for almost all species studied to be constant as a function of growth irradiance. Fourthly, despite lower damage levels, the acclimation of the capacity for non-photochemical quenching allows a greater amount of non-photochemical quenching in the high light acclimated cells (Figure 3.22D). There are only a few studies showing this acclimation in algae (e.g. Demers et al. 1991). It is, however, consistent with the increase in xanthophyll cycle pigments per unit chlorophyll found in all species reviewed by MacIntyre et al. (2002).

The consequences of acclimation on fluorescence indices are shown in Figure 3.23 for several levels of acclimation irradiance. In my model, there are two main consequences of photoacclimation to high irradiance (see legend). The first is to allow a greater fraction of reaction centers to remain open at a given irradiance, mainly due to the smaller optical absorption cross-section. The second is the decrease in the amount of

**Figure 3.23: Consequences of acclimation on fluorescence. A) Quantum yield of fluorescence under ambient irradiance. B) Maximum ( $F_m''$ ) and minimum ( $F_o''$ , dashed blue line) quantum yields of fluorescence in the dark acclimated state but with damage remaining (similar to a 20 minute acclimation time). C) Maximum quantum yield of fluorescence in the light. D)  $F_v'' / F_m''$  parameter. E) Ratio of the quantum yield of energy dissipation through inhibited reaction centers and energy dependent non-photochemical quenching. The results shown are after 15 minutes in the light for photosynthetic systems acclimated to different irradiances (see legend and Figure 3.20).**

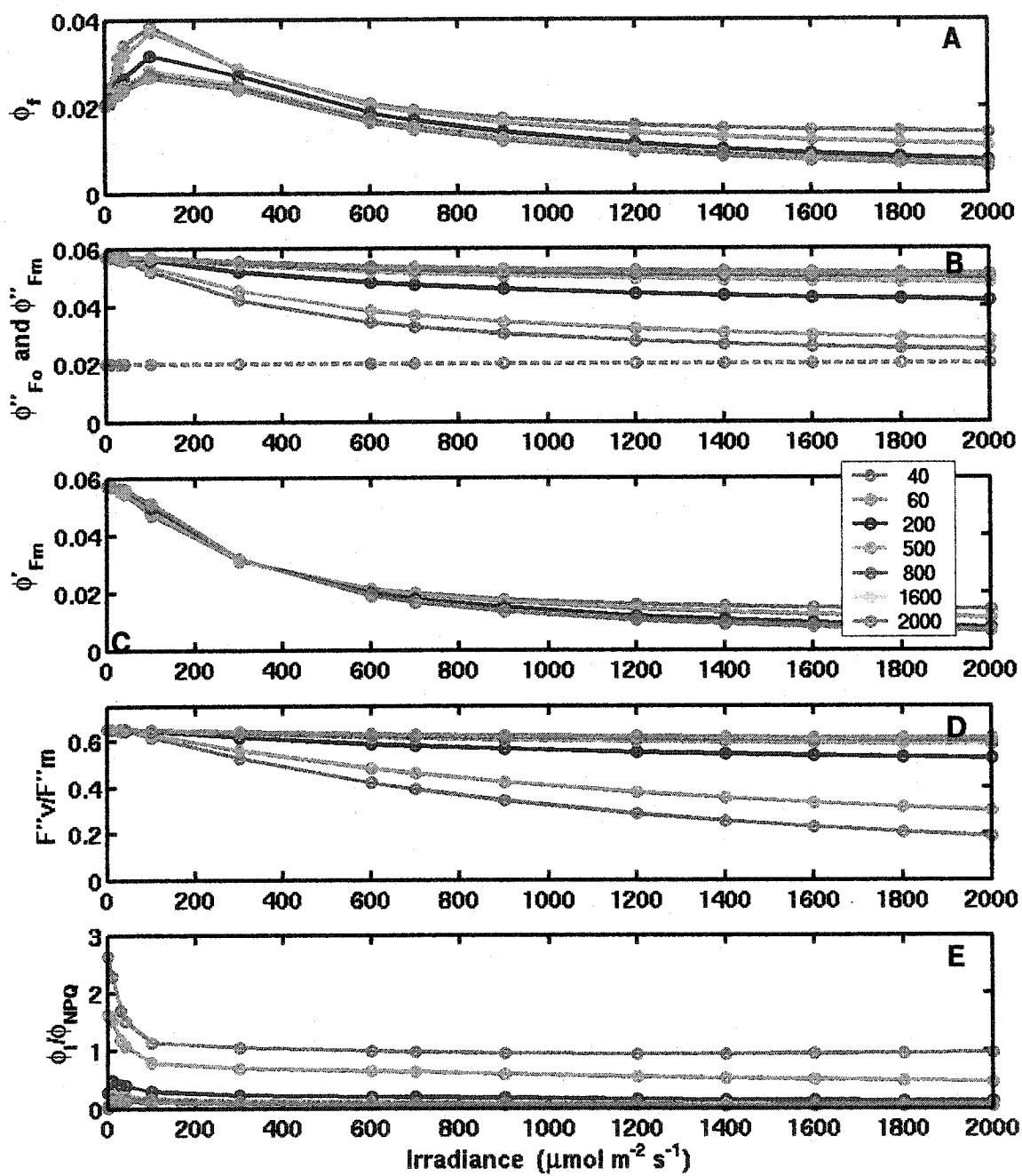


Figure 3.23: See caption on previous page.

damage. This decrease is due to two processes: the decrease of the absorption cross-section (leaving more reaction centers open), and the increase in non-photochemical quenching. All these processes interact to produce the curves observed in Figure 3.23A for fluorescence versus irradiance. At low irradiance (below  $\sim 100 \mu\text{mol m}^{-2} \text{s}^{-1}$ ), the rapid closure of reaction centers in the low light acclimated algae lead to a more rapid and greater increase of fluorescence compared to high-light acclimated reaction centers. As irradiance increases, the fluorescence yield of low-light acclimated cells decreases more rapidly than the high light acclimated algae as damage accumulates. Beyond about  $400 \mu\text{mol m}^{-2} \text{s}^{-1}$  the absolute decrease in the fluorescence yield with irradiance is similar for all acclimation light levels, while the low-light algae keep an overall higher level.

The higher fluorescence level in the low-light acclimated algae ( $\leq 200 \mu\text{mol m}^{-2} \text{s}^{-1}$ ) is due to the greater number of active reaction centers that are closed and the lower non-photochemical quenching. The similar decrease with incident irradiance above  $\sim 400 \mu\text{mol m}^{-2} \text{s}^{-1}$  is due to the dynamics of damage to reaction centers plus energy dependent quenching. Although their ratios are very different in the different acclimation states (Figure 3.23E), the sum of both processes has similar impact on the fluorescence yield. The parameter  $\phi''_{Fm}$  is inversely and exclusively affected by damage (see Equation 3.16), and shows essentially the same features as observed in Figure 3.22C. The observed values of maximum quantum yield in the light ( $\phi'_{Fm}$ , Figure 3.23C) reflect the dynamics observed in panel A and D. This is because the maximum quantum yield in the light is influenced only by non-photochemical quenching (due to damage and energy dependent

non-photochemical quenching). Figure 3.23C shows that this parameter is very similar at all irradiance levels requiring the effect of the sum of the two processes to be almost identical on the quantum yield of fluorescence in the model. Because the  $\phi_{Fo}''$  (Figure 3.23B dashed blue line) does not change with acclimation irradiance,

$F_v''/F_m'' = (F_m'' - F_o'')/F_m''$  is a direct measure of the fraction of damaged reaction centers (compare Figure 3.23D with Figure 3.22C). This is a well-known measure of photoinhibition and has been used many times in the past to describe damage (e.g. Kolber and Falkowski 1993; Osmond 1994; Park et al. 1995). It is important to reiterate here that the model described in this chapter does not address the simultaneous changes occurring in the optical properties of the cells (particularly the chlorophyll specific absorption coefficient and the reabsorption parameter) with acclimation. These processes are discussed in more detail in Chapter 2 and will depend, in addition to the acclimation state, on the size of the cells and their nutritional status.

#### 3.4.7 Revisiting the experiment of Cullen et al. (1988)

Cullen et al. (1988) presented results of an experiment in which a culture of *Thalassiosira pseudonana* was grown at  $40 \mu\text{mol m}^{-2} \text{s}^{-1}$  (12h:12h light dark cycle), transferred to an experimental container under  $\sim 20 \mu\text{mol m}^{-2} \text{s}^{-1}$  for 70 minutes, then submitted to an intense light ( $\sim 3000 \mu\text{mol m}^{-2} \text{s}^{-1}$ ) for 70 minutes, and returned to  $\sim 20 \mu\text{mol m}^{-2} \text{s}^{-1}$  for another 70 minutes (see Figure 3.24A). During the experiment, fluorescence was measured continuously using a SeaTech fluorometer and recorded every  $\sim 1$  minute (Figure 3.24A) while samples were taken about every  $\sim 20$ -30 minutes

**Figure 3.24: Results from the experiments carried out by Cullen et al. (1988). A) The fluorescence transient observed during the experiment and the irradiance (reconstructed using description in the text). B) Fluorescence measured on discrete samples dark-acclimated for 15 minutes. C) Photosynthetic parameters measured by  $^{14}\text{C}$  incorporation. All parameters are normalized to the chlorophyll concentration (which did not change during the experiment). Data provided by John Cullen.**

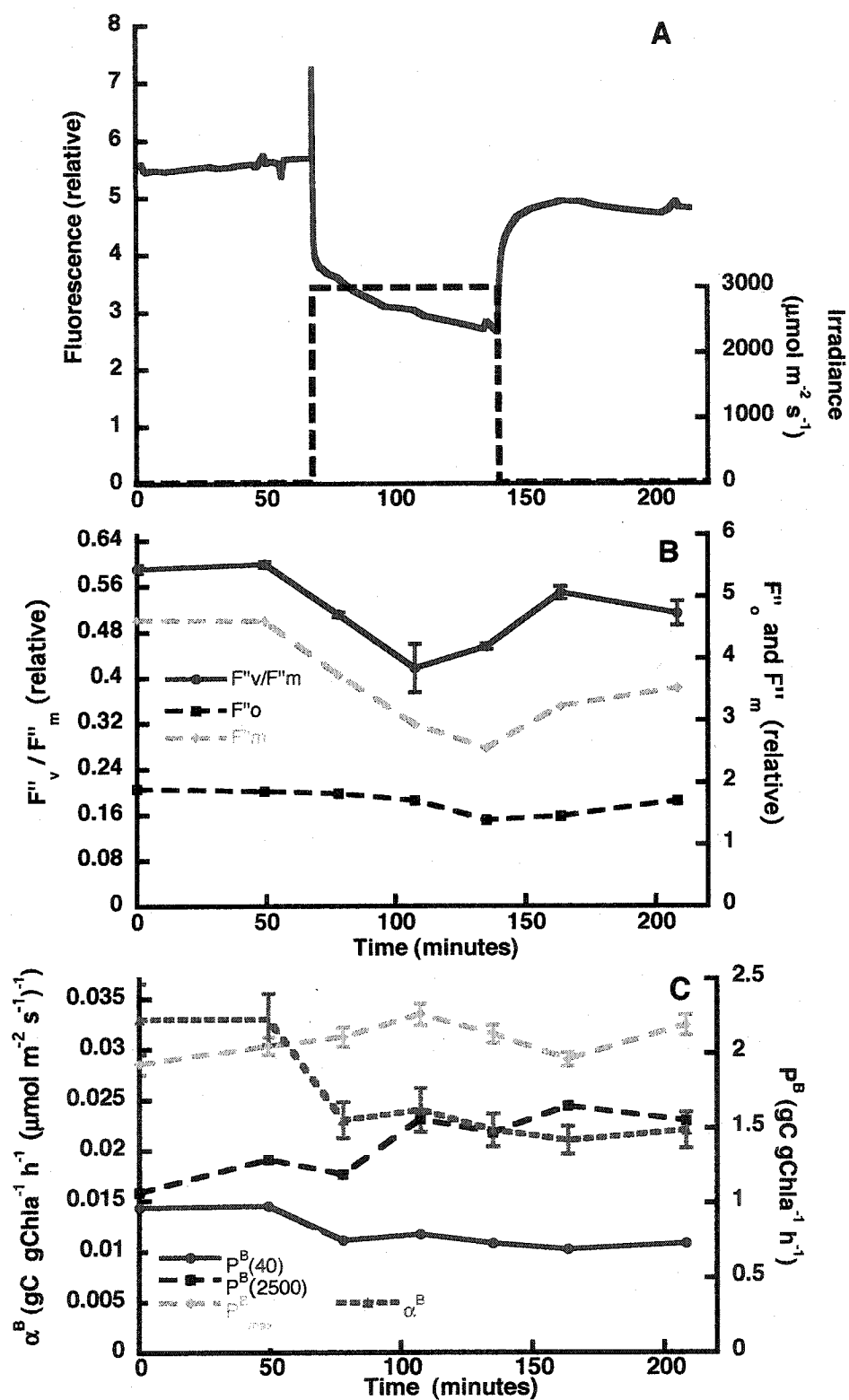


Figure 3.24: See caption on previous page.

for variable fluorescence measurements using DCMU (dark acclimated for 15 minutes) (Figure 3.24B). PvsE curves were measured using 20-minute  $^{14}\text{C}$  incubations for which they reported the chlorophyll specific initial slope, the chlorophyll specific maximum photosynthetic rates, as well as chlorophyll specific photosynthetic rates at 40 and 2500  $\mu\text{mol m}^{-2} \text{s}^{-1}$  (Figure 3.24C). In the following sections, I will compare their results with the results obtained with my model.

#### **3.4.8 Preliminary observations on the experiment to guide the modeling**

It is possible to calculate the quantum yield of charge separation (Genty et al. 1989) under ambient irradiance using  $\Delta F/F'_m = (F'_m - F')/F'_m$  obtained from the SeaTech fluorometer (using the fluorescence value before the high light to measure  $F'$  and assuming the maximum value  $F'_m$  was resolved upon turning the high light on, Figure 3.24A). I find that it is around 0.22 and lower than the value of 0.59 obtained with the DCMU method before the high light was turned on. This implies a considerable closure of reaction centers (or non-photochemical quenching) under 20  $\mu\text{mol m}^{-2} \text{s}^{-1}$ , which is about half of the growth irradiance. While it is possible that it is originating from the ambient irradiance, this high fraction of closed reaction centers could in part originate from the high intensity flash measurement with the SeaTech fluorometer (as suggested by Babin, in press).

#### **3.4.9 Comparing the model and data**

The model was run in continuous light at 40  $\mu\text{mol m}^{-2} \text{s}^{-1}$  to obtain the acclimated state. Afterwards, the irradiance was modified following the patterns used in the Cullen et al. experiment. Only the second portion is shown. To obtain patterns that are more

consistent with the measured values, two parameters were changed from the standard model (see Table 3-3) the maximum repair rate was set to 40% of its normal value and the probability for damage was set to  $0.5 \times 10^{-7}$ , six times lower than in the standard model. The quantum yield of fluorescence reproduces well the patterns observed in the fluorescence emission during the experiment (compare Figure 3.25 Top panel with Figure 3.24A). In addition, the top panel of Figure 3.25 is the fluorescence in ambient light if the fluorometer is actinic and closing different fractions of reaction centers during the measurement, leaving 0.2 or 0.5 of the reaction centers open. The closure of 50% of the reaction centers by the measuring light provides the closest match to the patterns observed. The actinic of the fluorometer was approximated by using the model run without actinic and assuming that the modeled fraction of open reaction centers would be decreased by 0.8 and 0.5 at each time point. This approximation neglects the effect of energy dependent quenching on the fraction of closed reaction centers by a short pulse of light. However, because energy dependent quenching is only present in significant amounts at high light here, and most reaction centers are closed or damaged under high light (Figure 3.25 middle panel), this approximation does not affect the patterns presented. The fractions of open, closed, and damaged reaction centers are presented in the middle panel of Figure 3.25 for the case without actinic. The parameters  $F_o''$  and  $F_m''$  are presented in the bottom panel of Figure 3.25 (to be compared with  $F_o''$  and  $F_m''$  obtained from DCMU, Figure 3.24B). In addition, the parameters  $F_m'$ , and  $F_m'$  with two different levels of energy dependent non-photochemical ( $k_{qE}=0.1$  and  $k_{qE}=0.3$ ) are also

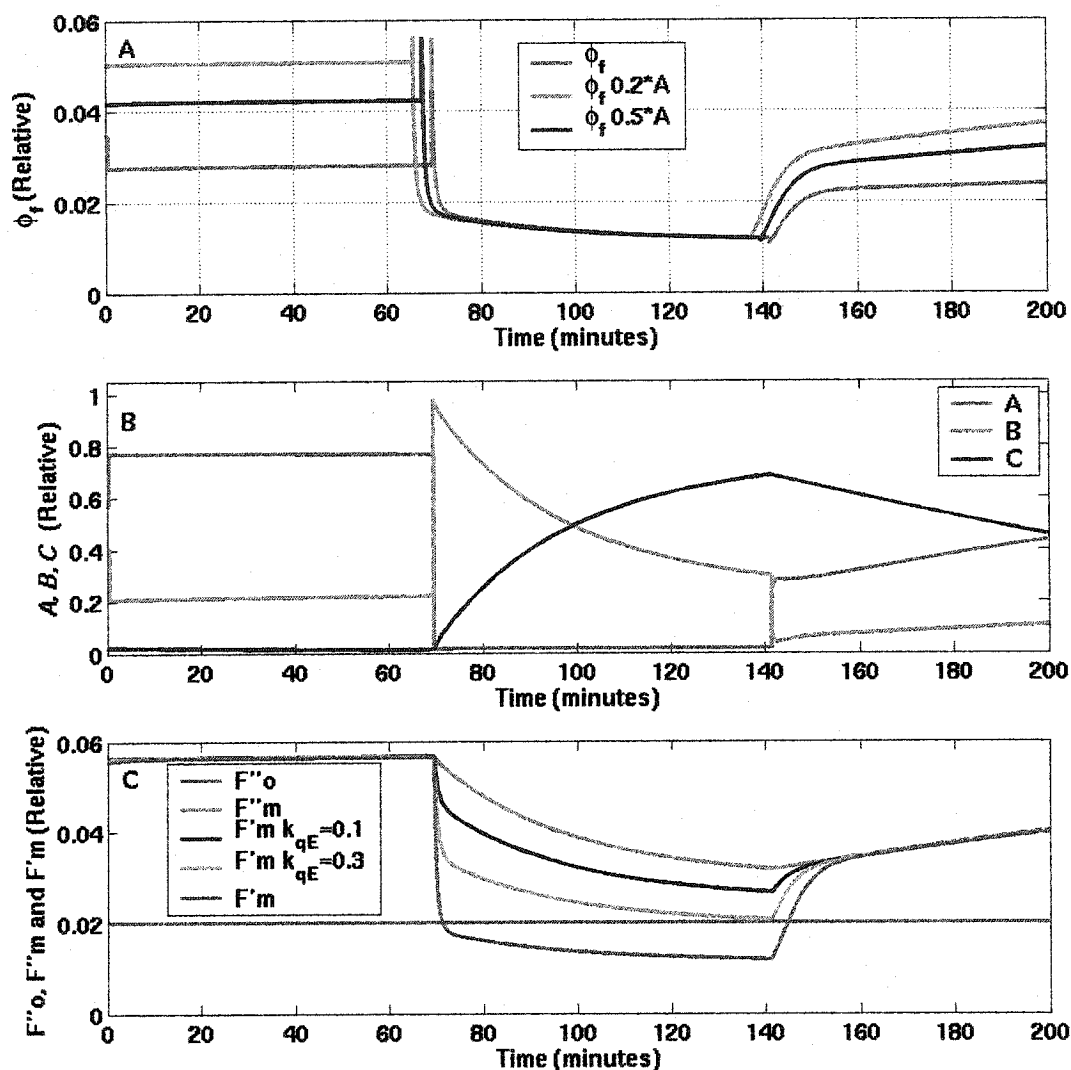


Figure 3.25: Model run to compare with the experiment of Cullen et al. (1988). A) Quantum yield of fluorescence under ambient light, which simulates the fluorescence transients, observed using the SeaTech fluorometer (Cullen et al. 1988). The three lines correspond to the conditions under which the Seatech fluorometer does not close any reaction centers during measurement, closes 50% of the reaction centers during measurement ( $\phi_f 0.5^*A$ ) and closes 80% of the reaction centers ( $\phi_f 0.2^*A$ ) during measurement. To aid visualization, the line  $0.2^*A$  and  $0.5^*A$  have been shifted 4 and 2 minutes earlier in time respectively. B) Fraction of open, closed and damaged reaction centers. C)  $F''_o$  and  $F''_m$  ( $F_o$  and  $F_d$  in Cullen et al. notation) and  $F'_m$  as well as  $F'_m$  with different levels of energy dependent non-photochemical quenching after some time in the dark ( $k_{qE}=0.1$  and  $0.3$  of the value in the light).

presented. The latter two are presented because they explain better the patterns observed in  $F_m''$  during the experiment and would be consistent with an insufficient acclimation period (stated as 15 minutes), which would not allow all energy dependent (or state transition dependent) non-photochemical quenching to dissipate.

The initial slope and the absolute values of the rates of electron transfer into carbon compounds normalized to the absorption cross-section ( $P_C^\sigma = K_{Calvin} / \sigma_{PSII}^O$  expressed in  $e^- s^{-1} (m^{-2} \mu mol \text{ photon}^{-1})$ ) obtained by the model are presented in Figure 3.26 (top and bottom). Consistent with the observation of Cullen et al. (1988), the initial slope of carbon fixation as well as the carbon fixation rate at  $40 \mu mol m^{-2} s^{-1}$  are decreased upon the light shift and remain low for the remainder of the experiment (due to inhibition). However, in the model simulation, the shift down upon the increase in irradiance is slower than in the experimental results. In their experiment, Cullen et al. noted an increase in the chlorophyll specific rate of carbon fixation at  $2500 \mu mol m^{-2} s^{-1}$ . This is not observed in the model runs, but the diminution in the rates of carbon fixation are much lower at high irradiances compared to the low irradiance levels (Figure 3.26 bottom panel). This discrepancy is probably attributable in part to growth during the experiment, which is not modeled in my model but is consistent with the observed increase in beam attenuation during the experiment (Cullen and Lewis 1988); the relatively constant chlorophyll concentration can be explained by a decrease in chlorophyll synthesis at high irradiance.

In addition to reproducing the parameters measured during the experiment of

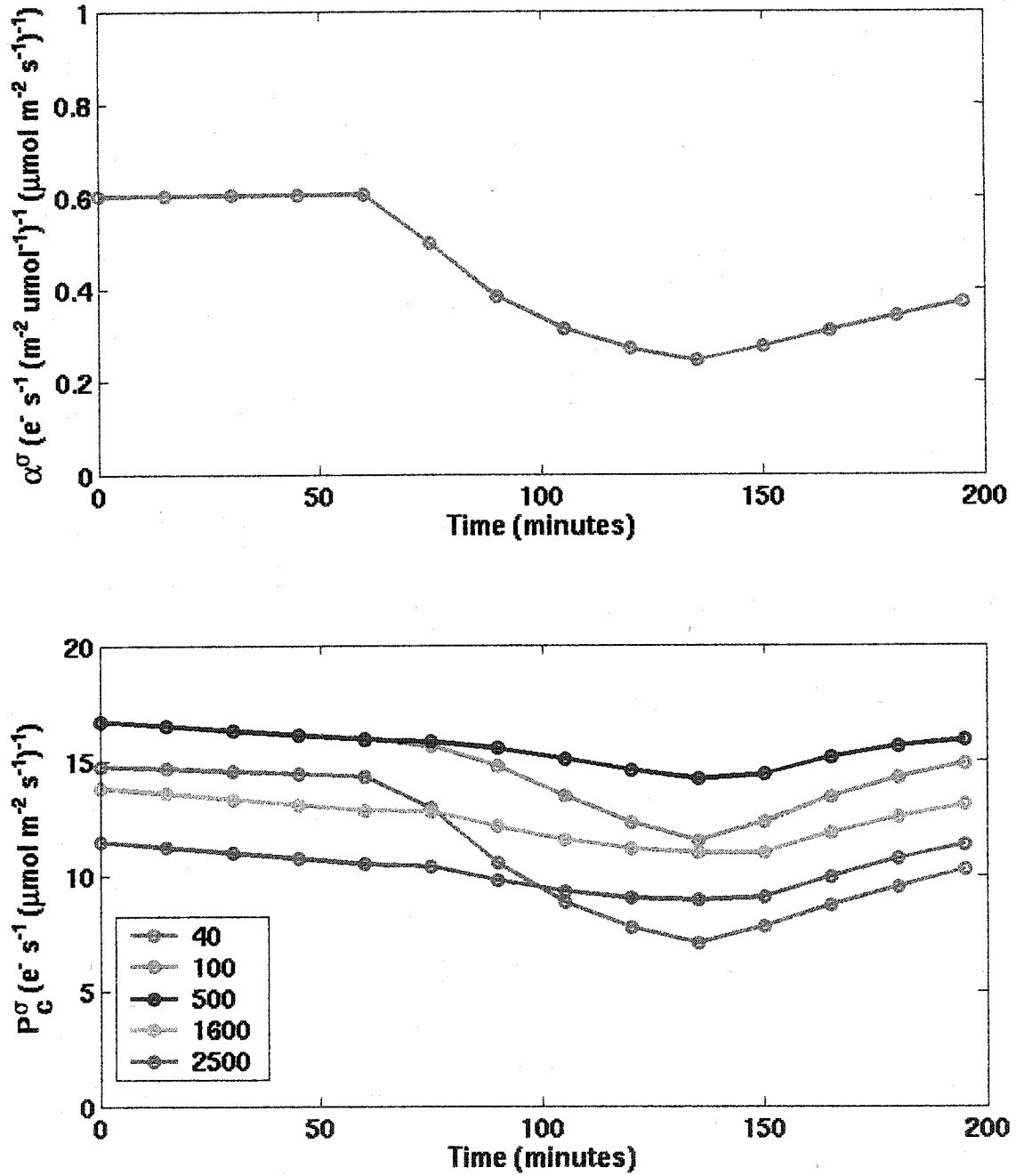


Figure 3.26: Photosynthetic parameters to compare the model with the results of Cullen et al. (1988). Top panel: Initial slope of the cross-section normalized carbon fixation vs. irradiance relationship calculated as  $P_C^\sigma(\overset{\circ}{E}=2) - P_C^\sigma(\overset{\circ}{E}=1)$ . Bottom panel: Photosynthetic rate of electron transfer to carbon fixation intermediates at different irradiances during short incubations.

Cullen et al., the model allows me to study the distribution of absorbed energy into the different processes during the experiment (Figure 3.27). The results show that before the shift to  $3000 \mu\text{mol m}^{-2} \text{s}^{-1}$ , roughly equal fractions of absorbed photons are used in photochemical charge separation ( $\phi_p$ ) and basal heat dissipation ( $\phi_d$ ) with minor fractions going to non-photochemically dissipated energy ( $\phi_{NPQ}$ ), heat dissipation in inhibited reaction centers ( $\phi_I$ ), and fluorescence ( $\phi_f$ ). Upon the light shift, a large fraction of the absorbed energy goes to non-photochemical quenching and an increasing fraction (up to ~20%) is dissipated in inhibited reaction centers. When the light is returned to the original level, the increased number of damaged reaction centers during the high light period and remaining in the dark lead to about one third of the absorbed photons being dissipated in inhibited reaction centers, one third going to photochemistry, and one third being dissipated by basal energy dissipation in the reaction centers, with minor contributions from other sinks.

### **3.5 Discussion**

#### **3.5.1 Limitations of the puddle model**

The puddle model, also referred to as the “separate unit model”, is a convenient tool to describe the kinetics of photosynthesis and fluorescence. In this model each reaction center has its own antenna and is not connected to other reaction centers (e.g. Bernardt and Trissl 1999). The convenience for modeling becomes immediately clear because a reaction center can be modeled independently of its interaction with neighboring reaction centers. It is, however, an oversimplification, and it is now accepted

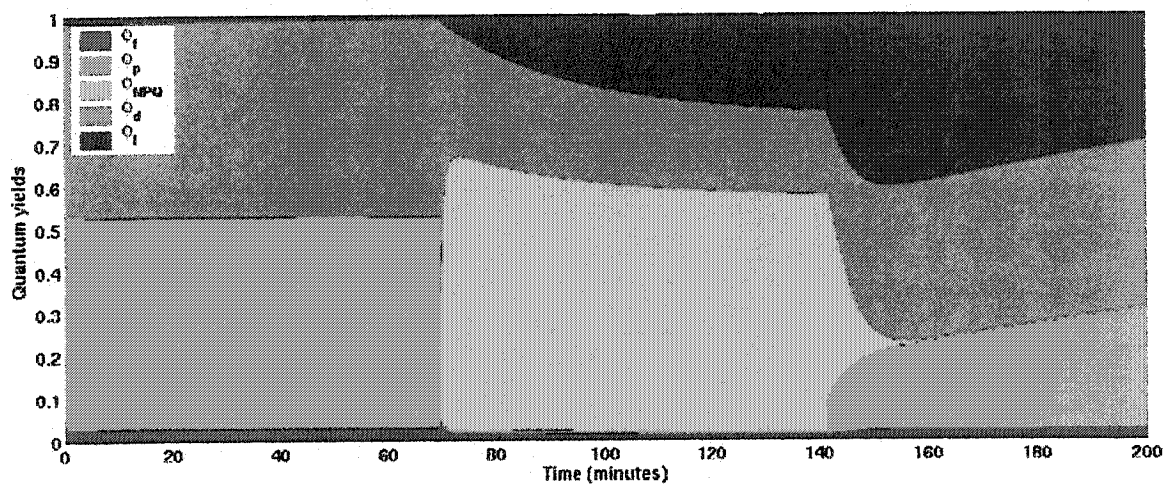


**Figure 3.27:** Quantum yields for the different processes modeled at PSII during model run to reproduce the Cullen et al. (1988) experiment. The vertical extent on the graph of each yield represents the fraction of the absorbed energy used by that process as a function of time.

that PSII reaction centers form dimers, such that two reaction centers share a common antenna (Barber and Kühlbrandt 1999 and references therein), furthermore, these dimers are likely to share excitation energy with other dimers. The implications of such an organization are that the induction kinetics for fluorescence and the steady state value of reaction center closure are different. For these conditions, most of our simple models to interpret fluorescence results at steady state lose their accuracy: they are usually designed to be perfect whether for the fully connected model or the completely separate model but imperfect for intermediate models (Havaux et al. 1991; Kramer et al. 2004). Furthermore, the capacity of an inhibited reaction center to provide photoprotection (e.g. Greer et al. 1991; Long et al. 1994; Lee et al. 2001) does not occur in the separate unit model. This is because the inhibited reaction center needs to share an antenna with at least one functional reaction center to act as a sink for excess, and potentially damaging, absorbed radiation. Though these are real limitations, the errors made by assuming a separate unit model for the purpose of my model (that is providing a consistent and simple model that allows the main factors affecting the kinetics of fluorescence to be studied) are probably small compared to the uncertainties associated with other cellular processes not modeled here. The implementation of the dimeric case is not conceptually very difficult, given the elegant formulation provided by Bernardt and Trissl (1999), and could easily be achieved when the description of other processes are incorporated in the model.

### ***3.5.2 Effect of irradiance on the repair rates***

In plants, the repair rates depend on the incident irradiance. They are very low, but not zero, in the dark (Greer et al. 1986; Wünschmann and Brand 1992; Chow 2001;

He and Chow 2003) and increase rapidly with irradiance to a maximum value at intermediate irradiance. In their study, He et al. (2003) found that the maximal repair rate coincided with the growth irradiance. In my model, for simplicity I used a repair rate that is independent of irradiance (equation 3.33). Implementing an irradiance dependent repair rate is very simple but at this time, there is no solid basis for doing so in algae and the functional description or mechanistic dependence would be largely arbitrary.

### **3.5.3 *Effect of temperature on enzymatic rates***

Enzymatic reactions are temperature dependent, this is particularly important in colder environments where the maximal enzymatic rates are decreased considerably. In my model, two enzymatic rates are important: the rate of carbon fixation and the rate of repair of damaged PSII. I did not include explicitly any temperature dependence in the model. This is because, from an ecological perspective, acclimation and adaptation to cold temperatures can offset, at least partially, the temperature dependence observed in the lab for species living in colder environments. Though the rate per enzyme is usually lower, the number of enzymes could be increased or other adaptations can balance the effect of cold temperatures on the organism's observed enzymatic rate (Steeman Nielsen and Jørgensen 1968). The temperature dependence of the repair rate, for example, could easily be derived in laboratory conditions for one or many species, but may be quite different from the measured temperature dependence rates if it was taken along a transect with various water temperatures due to the different assemblages present in these waters. However, there is no doubt that incubating natural samples under different temperatures will lead to a strong temperature dependence of the PvsE curve (Steeman Nielsen and

Jørgensen 1968; Rae and Vincent 1998). This dependence is mostly on the maximum rate of photosynthesis and on the rate of repair (Greer et al. 1986; Wünschmann and Brand 1992; Neale et al. 1998).

#### ***3.5.4 Target for the photoinactivation of photosystem II***

The choice of modeling the target for damage as closed reaction centers was made by Han (2002) and also by many of the other researchers studying the effect of photoinhibition on the PvsE curve. However, this is not necessary; open reaction centers could also be damaged (with or without the same quantum yield). It is beyond the scope of this chapter to review the considerable literature on the photoinactivation of photosystem II; it is still an area of active research (Park et al. 1995; Anderson et al. 1998; Chow 2001) and at least two mechanisms (PSII donor side and PSII acceptor side) and a multitude of triggers (Oxborough and Baker 2000) have been suggested. Oxborough and Baker (2000) critically examined the evidence and arrived at the conclusion that the two most likely triggers were doubly reduced  $Q_a$  and the formation of the triplet excited state  $^3P_{680}^*$  originating from intersystem crossing. The first occurs only in closed reaction centers while the second can happen in either the closed or the open state.

#### ***3.5.5 Other relevant processes not modeled***

Many processes have not been included in the model. They could be important under certain circumstances and warrant further examination. I will briefly mention two.

Firstly, the limitation of the first order rate approach for the modeling of the non-Calvin cycle sinks ( $k_{\text{sinks}}$ ) should be acknowledged. It has been well appreciated that large

variability in these sinks exists (Noctor and Foyer 2000; Behrenfeld et al. 2004) and, furthermore, their role as photoprotective processes is becoming increasingly accepted (Niyogi 1999; Geider and MacIntyre 2002; Ort and Baker 2002). For example, diatoms can reduce nitrate in transient periods of high light to prevent excessive closure of reaction centers (Lomas and Glibert 1999), but this is not observed in all phytoplankton (Lomas and Glibert 2000). The Mehler reaction is similarly not expected to be constant but more important under high oxygen and saturating irradiance conditions (Flameling and Kromkamp 1998; Ort and Baker 2002). Not having an accurate model for these sinks is probably the biggest limitation of the present model.

Secondly, the time for the induction of the carbon fixation mechanisms (MacIntyre et al. 1997) has not been included and can have an impact on the rates of electron utilization in microalgae and can be important in certain environments (Macintyre and Geider 1996). A simple formulation for this mechanism could easily be implemented in the future to study its effect under certain conditions.

### ***3.5.6 Effects of nutrient limitation beyond a decreased repair rate***

One effect of unbalanced growth due to nitrogen limitation is the drastic changes occurring in the stoichiometry of pigments in phytoplankton. The most obvious change is a large increase in the accessory pigments to chlorophyll *a* ratio under nitrogen starvation conditions (Henriksen et al. 2002) and particularly the ratio of xanthophyll cycle pigments to chlorophyll *a* (Latasa 1995). Therefore, if the capacity for the induction of energy dependent non-photochemical quenching is not impaired by nitrogen stress this could lead to a larger quenching potential under nitrogen stress. This is consistent with

the increased midday depression in fluorescence observed in the work of Laney and colleagues (Laney et al. 2001; Laney et al. in prep) upon the onset of starvation conditions. However, before this effect can be included in the model, it will have to be studied more comprehensively in the lab and a more mechanistic basis will have to be found.

### 3.5.7 Photoacclimation of $\gamma_{NPQ}$

Little is known about the acclimation of the capacity for non-photochemical quenching in algae (modeled using  $\gamma_{NPQ}$ ). An increase in the amount of xanthophyll cycle pigments relative to photosynthetic pigments with increased irradiance is, however, well documented (MacIntyre et al. 2002). This should lead to an increased capacity for non-photochemical quenching. However, most of this increase in the ratio of xanthophyll cycle pigments to chlorophyll *a* is due to a decrease in the chlorophyll per cell rather than an increase in the xanthophyll cycle pigments under high light.

In my model where acclimation occurs through a change in the size of the optical cross-section, a simple decrease in the photosynthetic pigments per reaction center would lead to this observed increase in the ratio of xanthophyll pigments to chlorophyll *a* (see for example Figure 3.7). Therefore, the model would only need one dynamic equation for acclimation of the optical cross-section; the capacity for non-photochemical quenching could result solely from the decrease in the optical absorption cross-section (assuming for example constant xanthophylls).

In the idealized case, not modeled here, where acclimation occurs through a constant absorption cross-section and a change in the ratio of the number of PSII to

carbon fixation capacity, changes in the xanthophyll pigments per photosystem is required to reconcile the patterns observed by MacIntyre et al. (2002). However, because the xanthophyll pigments are an integral part of the photosystems (Gilmore and Govindjee 1999 and references therein), two acclimation functions would be required, one that specifies the changes in  $n_{Calvin}$  and one that specifies the changes in  $\gamma_{NPQ}$ , as they would not have to be the result of the same process.

Therefore, the model developed here is more general in its construction than the available data require. For acclimation through changes in the absorption cross-section, only one equation is needed to account for changes in  $\gamma_{NPQ}$  and  $\sigma_{PSII}^o$ . The present configuration, however, allows for the possible implementation of acclimation at the level of  $n_{Calvin}$  in the future.

### **3.6 Conclusions**

I presented the first dynamic and mechanistic model that includes photosynthesis, heat dissipation and fluorescence in phytoplankton with photoacclimation of the absorption cross-section of photosystem II and the capacity for energy dependent non-photochemical quenching. The model is based on seven time-dependent differential equations and allows the time dependence of all the processes to be examined on timescales from seconds to days. The processes taken into account in the model are ideal for the study of the effect of mixing on photosynthesis and fluorescence in the mixed layer of the ocean (e.g. Franks and Marra 1994; Neale et al. 1998) through Lagrangian tracking of particles in a 1-D model (e.g. Ross and Sharples 2004).

Several assumptions were made during the development of the model and many aspects rely on inferences from measurements that were not directly aimed at answering the questions encountered while constructing the model. Therefore, the next step in the development of this model should be to turn to the lab to verify and ascertain some of the model's relationships. Particular attention must be given to the effects of nitrate limitation and photoinhibition on the quantum yield of fluorescence, and photoacclimation on the capacity for non-photochemical quenching rates and magnitudes. A better parameterization of the "other" sinks should also be sought.

## *Chapter 4 A fluorescence model for the inversion of ocean color using a floating radiometer*

### **4.1 Preface to chapter 4**

In this chapter, I describe the fluorescence portion of an inverse model of reflectance that I have developed with Catherine Brown, another graduate student. Here, I focus mostly on the theoretical aspects of the fluorescence model whereas Ms. Brown is responsible for the implementation of the elastic scattering aspect of inverse model and has processed much of the data required for testing the model. A description of the theoretical aspects of the incorporation of fluorescence into an inverse model, however, would be incomplete without brief summary of Brown's inverse model and a presentation of some data. I have avoided the presentation of results from Brown's inverse model and will only do so where necessary to test the fluorescence aspects of the work. Possible publication of this work will focus on using the inverse model with the fluorescence component in two regions (Bering Sea and Lunenburg Bay) to study oceanographic processes.

### **4.2 Introduction**

Since the realization that variations in colored dissolved and particulate matter concentration were causing the differences in the perceived color of the ocean (see Yentsch 1960 and references therein), one of the most important objectives driving the

development of ocean optics, has been solving the inverse problem of obtaining the constituents of the water from the spectral upwelling radiance field (Gordon 2002a). Specifically, the impetus has been to obtain parameters that will provide insights into biogeochemical oceanic processes. Parameters of interest include the concentration of different dissolved (Fichot and Miller 2002; Siegel et al. 2002; Johannessen et al. 2003) and particulate materials (O'Reilly et al. 1998; Siegel et al. 2002), the scattering or backscattering coefficients (Roesler and Perry 1995; Garver and Siegel 1997; Loisel and Stramski 2000; Maritorena et al. 2002), the absorption coefficients (Roesler and Perry 1995; Loisel and Morel 1998; Carder et al. 1999b), and optical properties of the water such as the diffuse attenuation coefficient (Austin and Petzold 1980; Clark 1999; Mueller 2000; Clark 2001). These properties can be obtained because colored dissolved and particulate matter influence the spectral upwelling light field through their mass specific absorption coefficients, volume scattering coefficients and concentrations. Inelastic processes, which change the wavelength of a photon, also affect the spectral upwelling light field (Mobley 1994; Pozdnyakov and Grassl 2003; Bukata et al. 2004). These processes include Raman scattering by water (Marshall and Smith 1990; Sathyendranath and Platt 1998) as well as fluorescence by chromophoric dissolved organic matter (CDOM e.g. Hawes 1992; Vodacek et al. 1997), some algal pigments (e.g. chlorophylls and phycobiliproteins) (Gordon 1979; Babin et al. 1996b; Hoge et al. 2003) and their decomposition products (phaeopigments e.g. Yentsch and Menzel 1963; SooHoo and Kiefer 1982b; a; Fuchs et al. 2002).

#### 4.2.1 Contributions to upwelling radiance and reflectance

Ignoring fluorescence by phycobiliproteins and phaeopigments as well as internal sources such as bioluminescence, the upwelling radiance ( $L_u(\lambda, z)$ ,  $\mu\text{mol m}^{-2} \text{s}^{-1} \text{nm}^{-1} \text{sr}^{-1}$ , see Table 4-1 for a list of symbol and units) at depth  $z$  (m) and wavelength  $\lambda$  (nm) in surface waters of the ocean can be separated into contributions from four sources such that

$$L_u(\lambda, z) = L_{ub}(\lambda, z) + L_{uR}(\lambda, z) + L_{uf}(\lambda, z) + L_{uCDOM}(\lambda, z), \quad 4.1$$

where the terms on the right of the equation sequentially represent upwelling radiance originating from photons elastically scattered in the upward direction,  $L_{ub}(\lambda, z)$ , Raman scattered photons,  $L_{uR}(\lambda, z)$ , chlorophyll *a* fluorescence,  $L_{uf}(\lambda, z)$ , and CDOM fluorescence,  $L_{uCDOM}(\lambda, z)$ . Note that in this equation the source of a photon is considered to be the last scattering/fluorescence event occurring before a photon travels upward through the horizontal plane at depth  $z$  (e.g. a photon that is successively scattered by particles then absorbed and fluoresced by CDOM before crossing the plane at depth  $z$ , is attributed to CDOM fluorescence). The radiance reflectance, ( $R_L(\lambda, z)$ ,  $\text{sr}^{-1}$ ) can then be expressed as

$$\begin{aligned} R_L(\lambda, z) &= \frac{L_u(\lambda, z)}{E_d(\lambda, z)} \\ &= \frac{L_{ub}(\lambda, z)}{E_d(\lambda, z)} + \frac{L_{uR}(\lambda, z)}{E_d(\lambda, z)} + \frac{L_{uf}(\lambda, z)}{E_d(\lambda, z)} + \frac{L_{uCDOM}(\lambda, z)}{E_d(\lambda, z)}, \\ &= R_{Lb}(\lambda, z) + R_{LR}(\lambda, z) + R_{Lf}(\lambda, z) + R_{LCDOM}(\lambda, z) \end{aligned} \quad 4.2$$

where  $E_d(\lambda, z)$  ( $\mu\text{mol m}^{-2} \text{s}^{-1} \text{nm}^{-1}$ ) is the planar downwelling irradiance, and  $R_{Lb}(\lambda, z)$ ,

**Table 4-1: List of symbol and units**

Symbol	Description	Units
$a$ $a_{CM}$ $a_{\phi}$ $a_w$	Total, colored matter, phytoplankton, and water absorption coefficient	$m^{-1}$
$\bar{a}_{\phi}^{490}(\lambda)$ $\bar{a}_{CDOM}^{400}(\lambda)$	Mean phytoplankton and CDOM absorption spectrum for the summer 2002 in Lunenburg Bay normalized to 490 and 400 nm respectively	Unitless
$a_{\phi Phaeo}^{512}$ $a_{\phi diatom}^{512}$	Phaeocystis and large diatoms absorption spectrum normalized to 512 nm	Unitless
$a_{\phi}^{yield}$	Phytoplankton absorption coefficient obtained from the inverse model when the quantum yield of fluorescence is maintained constant	$m^{-1}$
$a_f$	Attenuation coefficient of upwelling fluorescence radiance	$m^{-1}$
$b_b(\lambda)$ $b_{bpart}(\lambda)$	Total and particulate backscattering coefficient	$m^{-1}$
$G$	Proportionality factor between the radiance reflectance at 0.65 m and the ratio $b_b/a$	$sr^{-1}$
$\phi_{ai}$ $\phi_{bi}$	$i^h$ spectral components for absorption and backscattering	Units vary
$f(\lambda)$ $f_{fQ}(\lambda)$	Spectral shape of fluorescence emission inside and outside the cell	$nm^{-1}$
$e_i$	Fitted parameter for the parameterization of the Hydrolight simulations of $\bar{E}(\lambda, 0.65)$	Units vary (see Table 4-4)
$E_d$	Downwelling planar irradiance	$\mu mol\ m^{-2}\ s^{-1}$ $nm^{-1}$
$\bar{E}$	Scalar irradiance	$\mu mol\ m^{-2}\ s^{-1}$ $nm^{-1}$
$\bar{E}_{PUR}^{490}$ $\bar{E}_{PUR}^{mean}$ $\bar{E}_{PUR}^{max}$	Scalar irradiance weighted by the phytoplankton absorption coefficient normalized by its value at 490, its mean value and its maximum value	$\mu mol\ m^{-2}\ s^{-1}$
$k_i$	Fitted parameter for the parameterization of the Hydrolight simulations of $K_{0.65-2.75}$	Units vary (see Table 4-3)
$K_d$	Attenuation coefficient of downwelling planar irradiance	$m^{-1}$
$K$	Attenuation coefficient of scalar irradiance	$m^{-1}$
$K_{0.65-2.75}$	Attenuation coefficient of scalar irradiance from 0.65 to 2.75 m	$m^{-1}$

$L_u$ $L_{ub}$ $L_{uR}$ $L_{uf}$ $L_{uCDOM}$ $L_{uf}^{TSRB}$	Upwelling radiance and upwelling radiance due to backscattered photons, Raman scattered photons, chlorophyll fluorescence and CDOM fluorescence Upwelling radiance due to fluorescence measured by the TSRB	$\mu\text{mol m}^{-2} \text{s}^{-1} \text{nm}^{-1} \text{sr}^{-1}$ $\mu\text{mol m}^{-2} \text{s}^{-1} \text{nm}^{-1} \text{sr}^{-1}$
$m_f$	Slope of the fluorescence quantum yield	photon emitted (photon absorbed by all cellular pigments) $^{-1} \text{m}^{-1}$
$Q_a^*$	Fraction of the fluoresced radiance not reabsorbed inside the cell	Unitless
$R_L$ $R_{Lb}$ $R_{LR}$ $R_{Lf}$ $R_{LCDOM}$ $\mathbf{R}_L^{\text{obs}}$ $\mathbf{R}_{Lb}^{\text{mod}}$ $\mathbf{R}_{Lf}^{\text{mod}}$	Radiance reflectance Vector of observed, modeled backscattered and modeled fluoresced radiance reflectance	$\text{sr}^{-1}$ $\text{sr}^{-1}$
$S_{CM}$	Slope of the colored matter absorption spectral shape	$\text{nm}^{-1}$
$S_{bpart}$	Slope of the particle backscattering spectral shape	$\text{nm}^{-1}$
$S_{\langle f \rangle}$	Size factor for phytoplankton	Unitless
$T_{0.65}$	Transmission from 0 <sup>+</sup> to 0.65 m	unitless
$z$	Depth	m
$\phi_f$ $\phi_{f0}$	Quantum yield of fluorescence and quantum yield of fluorescence just below the sensor	photon emitted (photon absorbed by all cellular pigments) $^{-1}$
$\lambda$	Wavelength	nm
$\theta$ , $\theta_i$	Vector of parameters and element of that vector	Units vary
$\hat{\theta}$	Best fit vector of parameters	Units vary
$\theta_{sun}$ $\theta'_{sun}$	Solar zenith angle in air and in water	degrees
$\zeta$	Wavelength redistribution function	photon emitted (photon absorbed by all cellular pigments) $^{-1} \text{nm}^{-1}$

$R_{LR}(\lambda, z)$ ,  $R_{Lf}(\lambda, z)$ ,  $R_{LCDOM}(\lambda, z)$  are the reflectances ( $\text{sr}^{-1}$ ) due to elastic scattering, Raman scattering, chlorophyll fluorescence, and CDOM fluorescence.

#### 4.2.2 *Inverse models using inherent optical properties spectral shapes*

The goal of inverse modeling of reflectance is to retrieve the inherent optical properties (IOPs, see Preisendorfer 1976 in this chapter the absorption and backscattering coefficient) from the apparent optical properties (AOPs, see Preisendorfer 1976, in this chapter the radiance reflectance and the attenuation coefficient). The approach used in this chapter requires a function that expresses the AOPs in terms of IOPs. Many models exist (e.g. Gordon et al. 1988; Morel 1988; Morel et al. 2002; Albert and Mobley 2003) to express the term due to elastic scattering as a function of inherent optical properties and they are usually of the form,

$$R_{Lb}(\lambda) = h(b_b(\lambda), a(\lambda)), \quad 4.3$$

where  $h()$  represents some function of  $b_b(\lambda)$  ( $\text{m}^{-1}$ ), the total backscattering coefficient, which can be expressed as the sum of particulate backscattering ( $b_{bpart}(\lambda)$ ,  $\text{m}^{-1}$ ) and water backscattering ( $b_{bw}(\lambda)$ ,  $\text{m}^{-1}$ ), and  $a(\lambda)$  ( $\text{m}^{-1}$ ), the total absorption coefficient, which can be represented as the sum of the contributions by colored dissolved organic matter ( $a_{CDOM}(\lambda)$ ,  $\text{m}^{-1}$ ), non-algal particulate matter ( $a_{det}(\lambda)$ ,  $\text{m}^{-1}$ ), phytoplankton ( $a_\phi(\lambda)$ ,  $\text{m}^{-1}$ ), and water ( $a_w(\lambda)$ ,  $\text{m}^{-1}$ ). Once a model is adopted, the different spectral shapes of the absorption and scattering components, parameterized as simple functions of fitted parameters (in vector  $\theta$ ), are used in a non-linear regression procedure to find the best vector,  $\hat{\theta}$ , to represent the measured reflectance spectra. For the rest of this chapter, the

term “inverse model” will be restricted to this subset of modeling approaches using the optimization of contributions of the spectral IOPs within a model of the AOPs to best represent the AOP spectra; though many types of inverse model exist (Gordon 2002a). More specifically, the method uses a non-linear regression where the estimated parameters are defining the spectral shapes and amplitudes of the IOPs and the independent variables are the AOPs spectra.

In the inversion models developed to date, the Raman scattering term (Marshall and Smith 1990) and the terms for chlorophyll fluorescence (Roesler and Perry 1995; Culver and Perry 1997; Morrison 2003) and CDOM fluorescence are usually treated independently (Vodacek et al. 1994) or ignored.

#### **4.2.3 *Raman scattering***

Recently, Gordon (1999) showed that Raman scattering can amount to an important fraction (~10%) of the upwelling radiance in the blue and green wavebands in surface waters, especially at low chlorophyll concentrations (see also Morel and Gentili 2004). My simulations with Hydrolight<sup>2</sup> for the cases examined in this chapter, suggest that the fraction of upwelling radiance due to Raman is at most 2 to 3% for all wavelengths (generally increasing with longer wavelengths; results not shown) due to the high attenuation coefficient of the water. This is consistent with the results of Morel and Gentili (2004) in high chlorophyll Case 1 waters. In clear waters, a simple model of Raman scattering could be implemented (e.g. Marshall and Smith 1990; Sathyendranath and Platt 1998; Morrison 2003; Pozdnyakov and Grassl 2003). However, for the remainder of this chapter I will ignore this source of radiance with little consequence on

---

<sup>2</sup> A commercially available radiative transfer software that is specifically developed for the ocean environment.

the development or the results.

#### **4.2.4 *Methods to separate fluorescence emission from backscattered radiance***

Fluorescence emission is usually obtained by using the baseline method. In this method, the fluorescence peak observed in a reflectance or upwelling radiance spectrum of the ocean is separated from the radiance or reflectance originating from other sources by subtracting a baseline obtained by defining a straight line between two wavebands outside the fluorescence emission band (see Chapter 5). This provides a good method for comparing fluorescence emission from regions with similar optical properties. However, because the baseline is not always a good or consistent representation of the background upwelling radiance or reflectance, this can lead to a bias when comparing areas with very different optical properties (see Chapter 5 and Appendix III). Another method to separate the fluorescence signal from the background using inversion models has been proposed (Roesler and Perry 1995; Culver and Perry 1997). In these models, the background radiance is not assumed spectrally flat and is modeled with the IOPs obtained from the inversion model. Firstly, the inversion is done only in wavebands shorter than those influenced by fluorescence (up to about 650 nm) and the reflectance/radiance in the fluorescence band is extrapolated based on the reflectance model and the retrieved IOPs magnitudes (e.g. Roesler and Perry 1995). The differences between the modeled reflectance/radiance using the IOPs retrieved by the inverse model and the measured radiance in the fluorescence part of the spectrum is attributed to fluorescence.

Fluorescence wavebands have not been used in inverse models developed to date since fluorescence emission has not been included into the model used to relate the IOPs to the

AOP (usually reflectance).

#### **4.2.5 Objectives**

The objective of this chapter is to provide a formulation for the addition of the chlorophyll fluorescence term directly into inverse models of ocean color (e.g. Roesler and Perry 1995; Garver and Siegel 1997; Carder et al. 1999b; Maritorena et al. 2002; Roesler 2003; Sosik in press). By adding the fluorescence term, a new model for reflectance that includes the influence of the IOPs and fluorescence is described, and thus the spectral inversion can be extended above 650 nm. Because sun-induced fluorescence is the only passively observable signal that can be unambiguously attributed to phytoplankton in ocean water, its inclusion in inverse models opens the door to refinement of ocean color algorithms for the measurement of the phytoplankton absorption coefficient if the quantum yield of fluorescence is known. If biomass (and thus absorption) can be obtained independently, the quantum yield of fluorescence can be estimated. In such cases, information about physiology (e.g. Kiefer and Reynolds 1992) and species composition of phytoplankton (Loftus and Seliger 1975; Heaney 1978) could be obtained.

Two applications of the model are presented. The first is from the Bering Sea, where the quantum yield of fluorescence is followed over a ten-minute deployment while the incident irradiance is changing rapidly due to changes in cloud cover. Of particular interest in this timeseries is the rapid change in irradiance, which leads to large changes in quantum yield while the biomass can safely be assumed to remain constant. The second example is from eight days of a four-month timeseries in Lunenburg Bay, Nova

Scotia where measurements of  $R_L(\lambda)$  were made every 30 minutes. In the first application, I estimate variations in the quantum yield, while in the second case temporal changes in the phytoplankton absorption coefficient are estimated based on the fluorescence emission. The model is developed specifically for use with a hyperspectral Tethered Spectral Radiometer Buoy (TSRB, Satlantic Inc.), or an instrument with similar geometry. The TSRB has an irradiance sensor above the surface and a radiance sensor at  $\sim 0.65$  m below the surface. Modification of the approach to other geometries is straightforward; in the specific case of remote sensing reflectance, many of the appropriate models already exist. For other cases, radiative transfer simulations may be required to develop relationships between the IOPs and observed AOPs.

## **4.3 Methods**

### **4.3.1 Description of the fluorescence model**

#### **4.3.1.1 General aspects**

In this section, I develop a model of fluorescence that can be used directly in an inverse model of ocean color. The reflectance model is the sum of two parts, one due to the backscattered radiance and one due to chlorophyll fluorescence:

$R_L(\lambda, z) = R_{Lb}(\lambda, z) + R_{Lf}(\lambda, z)$ . I will use the backscattered reflectance model developed by Catherine Brown and colleagues (Brown et al. 2003) for the first part ( $R_{Lb}(\lambda, z)$ ). The Brown et al. model (2003) has been specifically adapted for the geometry of a hyperspectral TSRB (measuring  $L_u$  at 65 cm below the surface and  $E_d$  above the surface) as is also the case for the fluorescence portion developed here. To apply the model for

fluorescence, one must extend the spectral components of the absorption and backscattering parameters to 700 nm, which is usually straightforward. Most inverse models work by minimizing the sum of the squared differences (or another cost function) between the observed radiance reflectance vector ( $\mathbf{R}_L^{\text{obs}}(\lambda)$ , sr<sup>-1</sup>) and the reflectance model, a vector valued function ( $\mathbf{R}_{Lb}^{\text{mod}}(\lambda|\boldsymbol{\theta})$ , sr<sup>-1</sup>) by varying the  $N$  parameters in the vector of parameters  $\boldsymbol{\theta} = [\theta_1, \dots, \theta_N]$  which define the amplitude and spectral shapes of  $J$  spectral components  $\phi(\lambda|\boldsymbol{\theta})$ . The dependency notation should be read “of lambda given the vector of parameters theta”. These  $J$  spectral components are separated into two types, those that correspond to the backscattering  $\phi_{bj}(\lambda|\boldsymbol{\theta})$  and those that correspond to absorption  $\phi_{aj}(\lambda|\boldsymbol{\theta})$  of the  $j$ th component. With this notation,  $\phi_{a1}(\lambda|\boldsymbol{\theta})$  could be used, for example, to represent the spectral absorption of phytoplankton, which would be the results of a chlorophyll specific absorption vector  $a_{\phi}^*(\lambda)$  and an amplitude  $\theta_1$  corresponding to the chlorophyll concentration,  $\phi_{a\phi}(\lambda|\boldsymbol{\theta}) = a_{\phi}(\lambda) = \theta_1 a_{\phi}^*(\lambda)$ . The reconstructed total absorption and backscattering coefficients then become:

$$a(\lambda) = \sum_j \phi_{aj}(\lambda|\boldsymbol{\theta})$$

$$b_b(\lambda) = \sum_j \phi_{bj}(\lambda|\boldsymbol{\theta})$$
4.4

The general formulation with fluorescence is simply obtained by adding the modeled fluorescence vector valued function ( $\mathbf{R}_{Lf}^{\text{mod}}(\lambda|\boldsymbol{\theta})$ , sr<sup>-1</sup>) developed below (see equation 9) which leads to the general model for the regression of the  $i$ th measured

reflectance spectrum ( $\mathbf{R}_{Li}^{\text{obs}}(\lambda)$ ),

$$\mathbf{R}_{Li}^{\text{obs}}(\lambda) = \mathbf{R}_{Lb}^{\text{mod}}(\lambda|\boldsymbol{\theta}_i) + \mathbf{R}_{Lf}^{\text{mod}}(\lambda|\boldsymbol{\theta}_i) + \boldsymbol{\epsilon}_i(\lambda) \quad 4.5$$

where  $\boldsymbol{\epsilon}(\lambda)$  is a vector of errors. The least squares cost function becomes

$$\sum_{k=1}^K \left[ \mathbf{R}_{Li}^{\text{obs}}(\lambda_k) - \left\{ \mathbf{R}_{Lb}^{\text{mod}}(\lambda_k|\boldsymbol{\theta}_i) + \mathbf{R}_{Lf}^{\text{mod}}(\lambda_k|\boldsymbol{\theta}_i) \right\} \right]^2. \quad 4.6$$

where  $\lambda_k$  is the  $k^{\text{th}}$  wavelength where the reflectance is measured with a total of  $K$  wavelength measured. An optimization procedure is used to minimize the square of the differences between the measured reflectance spectrum and the modeled reflectance to obtain the estimated parameters  $\hat{\boldsymbol{\theta}}_i$ .

#### 4.3.1.2 Equation for the upwelling fluorescence radiance to use in the inverse model

Assuming a homogeneous water column with respect to IOPs, the upwelling radiance due to fluorescence emission at wavelength  $\lambda$  and depth  $z$  in the ocean can be modeled as follows (Babin et al. 1996a; Maritorena et al. 2000 see also Chapter 5),

$$L_{uf}(\lambda, z) = \frac{1}{4\pi} Q_a^*(\lambda) \int_{400}^{700} \int_z^{\infty} a_{\varphi}(\lambda_{ex}) \zeta(Z, \lambda_{ex} \rightarrow \lambda) \overset{\circ}{E}(\lambda_{ex}, z) e^{-[K(\lambda_{ex}) + a_f(\lambda)](Z-z)} dZ d\lambda_{ex}, \quad 4.7$$

where  $Q_a^*$  is the fraction of light emitted inside the cell and not reabsorbed,  $\zeta$  is the fluorescence redistribution function for irradiance absorbed in waveband  $\lambda_{ex}$  by all cellular pigments and reemitted at the emission wavelength  $\lambda$  ( $\text{nm}^{-1}$ ),  $\overset{\circ}{E}$  is the scalar irradiance,  $K$  is the diffuse attenuation coefficient for scalar irradiance and  $a_f$  is the absorption of fluorescence upwelling radiance and  $Z$  (m) is the integration variable.

To simplify the problem, the spectral redistribution function is often assumed

independent (discussed in more detail later) of depth:  $\varsigma(z, \lambda_{ex} \rightarrow \lambda) = \varsigma(\lambda_{ex} \rightarrow \lambda)$  this allows us to take it outside the depth integral and the depth integration can then be carried out easily to obtain,

$$L_{uf}(z, \lambda) = \frac{1}{4\pi} Q_a^*(\lambda) \int_{400}^{700} \varsigma(\lambda_{ex} \rightarrow \lambda) \frac{a_\phi(\lambda_{ex}) \dot{E}(\lambda_{ex}, z)}{K(\lambda_{ex}) + a_f(\lambda)} d\lambda_{ex}. \quad 4.8$$

The problem can be simplified by noting that in reality the spectral shape of the emission (but not the magnitude) is independent of the excitation wavelength, such that we can conveniently express the spectral redistribution function as

$\varsigma(\lambda_{ex} \rightarrow \lambda) = f_f(\lambda) \phi_f(\lambda_{ex})$ , where  $f_f(\lambda)$  is a constant emission spectral shape ( $\text{nm}^{-1}$ ) and  $\phi_f(\lambda_{ex})$  is the quantum yield of fluorescence defined as the number of photons emitted at all wavelengths divided by the absorbed irradiance at wavelength  $\lambda_{ex}$  by all cellular pigments.

Although it is well documented that the quantum yield of fluorescence for algal cells is strongly dependent on the excitation wavelength at least in some species (Loftus and Seliger 1975; SooHoo et al. 1982; Johnsen et al. 1997; Lutz et al. 1998; Raateoja et al. 2004b), for convenience, I will follow the assumption generally made in ocean optics research that the quantum yield is independent of excitation wavelength:

$\varsigma(\lambda_{ex} \rightarrow \lambda) = f_f(\lambda) \phi_f(\lambda_{ex}) = f_f(\lambda) \phi_f$ . This assumption allows the simplification of equation 4.8 to

$$L_{uf}(\lambda, z) = \frac{1}{4\pi} Q_a^*(\lambda) f_f(\lambda) \phi_f \int_{400}^{700} \frac{a_\phi(\lambda_{ex}) \overset{\circ}{E}(\lambda_{ex}, z)}{K(\lambda_{ex}) + a_f(\lambda)} d\lambda_{ex} \quad 4.9$$

$$L_{uf}^{TSRB}(\lambda, 0.65) = \frac{1}{4\pi} Q_a^*(\lambda) f_f(\lambda) \phi_f \int_{400}^{700} \frac{a_\phi(\lambda_{ex}) \overset{\circ}{E}(\lambda_{ex}, 0.65)}{K(\lambda_{ex}) + a_f(\lambda)} d\lambda_{ex}$$

In equations 4.9, the bottom equation refers specifically to the upwelling radiance due to fluorescence measured by the TSRB ( $L_{uf}^{TSRB}(\lambda, 0.65)$ ),  $\mu\text{mol m}^{-2} \text{s}^{-1} \text{nm}^{-1} \text{sr}^{-1}$ ).

Because equation 4.9 specifies that both the irradiance ( $\overset{\circ}{E}(\lambda_{ex}, z)$ ) and the fluorescence radiance ( $L_{uf}(\lambda, z)$ ) must be measured at the same depth, if they are not measured at the same depth one measurement has to be propagated vertically. In the case of the TSRB the two natural choices are above the surface, where  $E_d$  is measured, or below the surface at 0.65 m, where upwelling radiance is measured. In the first case, the measured upwelling radiance must be propagated to the surface, and in the second, the downwelling irradiance must be propagated to 0.65 m. When inelastic sources are absent, both possibilities are straightforward and can be approximated fairly well by an exponential decay or increase with depth. However, when inelastic sources are present, especially in the case of an inelastic source with variable quantum yield with depth such as fluorescence, propagating the radiance from 0.65 m to the surface can lead to significant errors as it assumes that the quantum yield remains constant. This is why I decided to propagate the irradiance down to 0.65 m rather propagate the upwelling radiance to above the surface.

With the assumptions about the wavelength dependence of the excitation and the depth dependence of the quantum yield (the assumption of the constancy of the spectral

emission dependence is believed to be very good for chlorophyll) the quantum yield retrieved is expressed as:

$$\varphi_f = \frac{\int_{400}^{700} \int_z^{\infty} \zeta(Z, \lambda_{ex} \rightarrow \lambda) a_{\varphi}(\lambda_{ex}) \overset{\circ}{E}(\lambda_{ex}, z) e^{-(K(\lambda_{ex}) + a_f(\lambda))(Z-z)} dZ d\lambda_{ex}}{\int_{400}^{700} \int_z^{\infty} a_{\varphi}(\lambda_{ex}) \overset{\circ}{E}(\lambda_{ex}, z) e^{-(K(\lambda_{ex}) + a_f(\lambda))(Z-z)} dZ d\lambda_{ex}}. \quad 4.10$$

In words,  $\varphi_f$  is the mean quantum yield weighted by the absorbed flux at depth

$(a_{\varphi}(\lambda) \overset{\circ}{E}(\lambda_{ex}, 0^-) e^{-K(\lambda)z})$  and the attenuation of the upwelling fluorescence radiance

$(e^{-a_f(\lambda)z})$ . The value of  $\varphi_f$  in equation 4.10 is in fact the quantity retrieved by the model

developed here.

#### 4.3.1.3 Criteria for inserting fluorescence in an inverse model

To be useful in an inverse model, the fluorescence portion has to be expressed only in terms of parameters that influence the upwelling light field of the ocean (such that they can be retrieved using an inverse model) or in terms of readily calculable parameters such as the solar zenith angle. Typically an inverse model will retrieve the amplitude of the following IOPs:  $a_{\varphi}(\lambda)$ ,  $a_{CM}(\lambda) \equiv a_{CDOM}(\lambda) + a_{det}(\lambda)$ , and  $b_{bpart}(\lambda)$  whereas the spectral dependence is prescribed a priori. Some models also allow the spectral shapes to be varied, requiring more fitted parameters (see Bering Sea model below). Therefore, the fluorescence model can be expressed in terms of  $a(\lambda)$ ,  $b_b(\lambda)$ , their constituents, and other known parameters.

#### 4.3.1.4 Approach to constrain equation 4.9 during the inversion

Starting from equation 4.9 we need to express  $Q_a^*(\lambda)$ ,  $f_f(\lambda)$ ,  $\overset{\circ}{E}(\lambda, z)$ ,  $K(\lambda, z)$

and  $a_f(\lambda)$  in terms of  $a(\lambda)$ ,  $b_b(\lambda)$ ,  $a_\phi(\lambda)$ ,  $a_{CM}(\lambda)$ ,  $b_b(\lambda)$  and other known quantities. Furthermore,  $a(\lambda)$ ,  $b_b(\lambda)$ ,  $a_\phi(\lambda)$ ,  $a_{CM}(\lambda)$ ,  $b_b(\lambda)$ , have to be described in terms of the model parameters  $[\theta_1, \dots, \theta_N]$ . I will now provide an overview of these terms, before giving a more detailed description in the results.

For Case 1 waters, a parameterization of  $Q_a^*(\lambda)$  based on a central trend of cellular optical properties as a function of chlorophyll can be used, similar to the one that I derive in Chapter 5 (see also Babin et al. 1996b). This parameterization would not, however, work in Case 2 waters where cells are typically large and highly packaged and the optical properties of the water are not strongly dependent on the chlorophyll concentration. It will also fail when the cells present in Case 1 waters do not follow the central statistical trends (Ciotti et al. 1999; Bricaud et al. in press). For the present model,  $Q_a^*(\lambda)$  is combined with the  $f(\lambda)$  spectral shape and assumed constant  $f_{fQ}(\lambda) = Q_a^*(\lambda) f_f(\lambda)$  ( $\text{nm}^{-1}$ ). This can be achieved by using the chlorophyll *a* fluorescence emission spectrum for an algal culture (see results) for  $f_{fQ}(\lambda)$ . Maritorena et al. (2000) used the term “realized quantum yield” for the quantum yield retrieved when the parameter  $Q_a^*(\lambda)$  is not accounted for.

In the case of the TSRB, one must convert the measured planar downwelling irradiance ( $E_d(\lambda, 0^+)$ ,  $\mu\text{mol m}^{-2} \text{s}^{-1} \text{nm}^{-1}$ ) to an estimate of  $\overset{\circ}{E}(\lambda, 0.65)$  ( $\mu\text{mol m}^{-2} \text{s}^{-1} \text{nm}^{-1}$ ), the scalar irradiance at the depth of the upwelling radiance sensor (0.65 m). In other words, what is needed is a function of the form

$\bar{E}(\lambda, 0.65) = h_E(E_d(\lambda, 0^+), a(\lambda), b_b(\lambda), \theta'_{sun})$ , where  $a(\lambda)$  and  $b_b(\lambda)$  are the total absorption and backscattering coefficients respectively and  $\theta'_{sun}$  is the zenith angle of the sun in water. The zenith angle of the sun can easily be calculated for any location and time. The approach used here to obtain the function for the scalar irradiance at 0.65 m is to run a series of radiative transfer simulations for a range of  $E_d(\lambda, 0^+)$ ,  $a(\lambda)$ ,  $b_b(\lambda)$ , and  $\theta_{sun}$  and derive a simple empirical function that best represents the simulations (see below).

A similar approach is used for  $K(\lambda)$ , the attenuation for the downwelling excitation irradiance, using the same Hydrolight simulations as above to provide a function for  $K_{0.65-2.75}(\lambda) = h_K(\lambda, E_d(\lambda, 0^+), a(\lambda), b_b(\lambda), \theta_{sun})$ . In this case,  $K(\lambda)$  is represented by  $K_{0.65-2.75}(\lambda)$  which is the attenuation coefficient for scalar irradiance from 0.65 to 2.75 meters. This is used in place of  $K(\lambda_{ex})$  in equation 7. The depth of 2.75 m was chosen because the simulations were done for an irradiance sensor at 2.75 m on the instrumented buoy in Lunenburg Bay (see below). Because the attenuation coefficient is spectrally resolved (and not broad band such as for PAR), the changes with depth are small, furthermore because most of the upwelling fluorescence radiance originates from ~5 meters below the sensor in the clearest waters and less in more absorptive waters (Babin et al. 1996b), it is more realistic to limit the simulation to a layer near the sensor rather than extending the calculation to depth greater than ~5 meters (see Chapter 5 for another approach).

Unless the measurement is made in a highly scattering environment, the attenuation coefficient for the attenuation of upwelling fluorescence radiance  $a_f(\lambda)$ , can be approximated with high accuracy by  $a_f(\lambda) = a(\lambda) = a_w(\lambda) + a_\phi(\lambda) + a_{CM}(\lambda)$ . This approximation was verified using another set of Hydrolight simulations (See Appendix I).

#### 4.3.1.5 Fluorescence reflectance model

Equation 4.9 was for the upwelling radiance by dividing equation 4.9 by the irradiance measured above the surface to obtain reflectance and replacing  $Q_a^*(\lambda)f(\lambda)$  by  $f_{fQ}(\lambda)$ , provides an appropriate model for the TSRB fluorescence reflectance as

$$\mathbf{R}_{I_f}^{\text{mod}}(\lambda) = \frac{f_{fQ}(\lambda)\phi_f}{4\pi E_d(\lambda, 0^+)} \int_{400}^{700} \frac{a_\phi(\lambda_{ex})\mathring{E}(\lambda_{ex}, 0.65)}{K_{0.65-2.75}(\lambda_{ex}) + a_f(\lambda)} d\lambda_{ex}, \quad 4.11$$

where  $f_{fQ}(\lambda)$  is normalized such that  $\int_0^\infty f_{fQ}(\lambda) d\lambda = 1$ , hence, the quantum yield obtained

by the inversion is defined in terms of the fluorescence emitted over all emission wavelengths. Both sides of equation 4.11 are implicitly dependent on  $\theta$ . Equation 4.11 will allow inversion of the fluorescence band once appropriate models are described for  $K_{0.65-2.75}(\lambda_{ex})$  and  $\mathring{E}(\lambda_{ex}, 0.65)$  in terms of IOPs or other known variables.

#### 4.3.2 The inverse model for backscattered photons

An inverse model for the retrieval of the IOPs from three moorings deployed during the summers of 2002 and 2003 in Lunenburg Bay, Nova Scotia, Canada has been developed (Brown et al. 2003). These moorings consist of a surface Hyperspectral TSRB and a chain of four irradiance sensors at depth. For the MB1 mooring analyzed below

(MB1, near Blue Rocks, NS), the shallowest irradiance sensor was at 2.75 meters during the summer of 2002. For completeness, I summarize the model development which will be detailed elsewhere (C. Brown, in prep).

The radiance reflectance at 0.65 m is given by

$$R_{Lb}(\lambda, 0.65) = \frac{L_{ub}(\lambda, 0.65)}{E_d(\lambda, 0.65)} = \frac{L_{ub}(\lambda, 0.65)}{E_d(\lambda, 0^+) T_{0.65}(\theta_{sun}, \tau_a, W, IOP)}, \quad 4.12$$

where  $T_{0.65}$  is the transmission from just above the surface to 0.65 m for downwelling irradiance  $T_{0.65} = E_d(\lambda, 0.65)/E_d(\lambda, 0^+)$  and is dependent on the atmospheric conditions, here represented by the optical thickness of the atmosphere ( $\tau_a$ ), the wind speed ( $W$ , m s<sup>-1</sup>) and the inherent optical properties of the surface layer ( $IOP$ , m<sup>-1</sup>). The following relationship is found to parameterize reflectance well (Morel et al. 2002 and references therein) in waters where absorption dominates,

$$R_{Lb}(\lambda, 0.65) = G(\theta_{sun}, \tau_a, W, IOP) \frac{b_b(\lambda)}{a(\lambda)}, \quad 4.13$$

where  $G(\theta_{sun}, \tau_a, W, IOP)$  is a proportionality factor. Using equations 4.12 and 4.13 we can write the ratio of upwelling radiance at 0.65 m to the downwelling irradiance above the surface as,

$$\mathbf{R}_{Lb}^{\text{mod}}(\lambda|\boldsymbol{\theta}) = \frac{L_{ub}(\lambda, 0.65)}{E_d(\lambda, 0^+)} = T_{0.65}(\theta_{sun}, \tau_a, W, IOP) G(\theta_{sun}, \tau_a, W, IOP) \frac{b_b(\lambda)}{a(\lambda)}, \quad 4.14$$

where both sides of equation 4.11 are implicitly dependent on  $\boldsymbol{\theta}$ . Relationships for  $T_{0.65}(\theta_{sun}, \bar{W}, \bar{\tau}_a, IOP)$  and  $G(\theta_{sun}, \bar{W}, \bar{\tau}_a, IOP)$  in terms of IOPs consistent with those found in Lunenburg Bay have been obtained (Brown et al. 2003) using the Hydrolight

simulations described below assuming constant wind speed ( $\overline{W}$ ) and atmospheric conditions ( $\overline{\tau_a}$ ). Equation 4.14 is the equation for the backscattered reflectance term, hence, using equations 4.11 and 4.14, we have a complete model of reflectance to use in equation 4.6 and can proceed with the inversion.

#### 4.3.3 Application to the Bering Sea

Despite their derivation for Lunenburg Bay, I will use here the same values of the relationships for  $T_{0.65}(\theta_s, \overline{W}, \overline{\tau_a}, IOP)$  and  $G(\theta_s, \overline{W}, \overline{\tau_a}, IOP)$  for the Bering Sea. This is valid because, for the station analyzed, the total absorption and scattering coefficients are within the range modeled for Lunenburg Bay. However, in contrast with the Lunenburg Bay parameterizations, which were derived for clear sky conditions, the station analyzed from the Bering Sea shows a varied radiance distribution: the sky was almost completely overcast with a small area of clear sky. This small patch of clear sky moved during about 5 minutes in front of the sun, leading to a sunny patch on the surface of the ocean. It would be futile to try to model this kind of radiance distribution with the tools available to me at this time. Hence, lacking a better description, I use the clear sky model; this description will provide a radiance distribution that is too diffuse for the case when the patch of sky was in front of the sun and too peaked in the solar direction when the patch was not in front of the sun. The solar zenith angle in air was calculated with the Matlab script written by Vincent Roy (*sun\_position.m* obtained from <http://www.mathworks.com/matlabcentral/fileexchange/loadCategory.do>, in June 2004) which implements the algorithm presented by Reda and Andreas (2003). For the station

analyzed, the solar zenith angle was equal to 72°. This value is slightly outside the range of the Hydrolight simulations but, due to the smooth and slowly changing nature of the function at high zenith angles, it is not expected to lead to a significant error. The Fresnel equation was used to obtain the in-water solar zenith angle.

The model has seven fitted parameters ( $N=7$ ) and three spectral components. Two are for colored matter absorption:

$$a_{CM}(\lambda) = \phi_{aCM}(\lambda) = \theta_1 \exp(-\theta_2(\lambda - 400)), \quad 4.15$$

where  $\theta_1 = a_{CM}(400)$  and  $\theta_2$  is the exponential rate of decrease with wavelength of the CM absorption ( $s_{CM}$ ,  $\text{nm}^{-1}$ , often referred to as the “slope coefficient of CM absorption”).

Two other parameters are used for phytoplankton absorption,

$$a_{\phi}(\lambda) = \phi_{a\phi} = \theta_4 [\theta_3 a_{\phi Phaeo}^{512}(\lambda) + (1 - \theta_3) a_{\phi diatom}^{512}(\lambda)]. \quad 4.16$$

where  $a_{\phi Phaeo}^{512}(\lambda)$  and  $a_{\phi diatom}^{512}$  are respectively the *Phaeocystis* and microphytoplankton absorption spectra normalized to 512 nm such that  $\theta_3$  is the fraction of the total phytoplankton absorption at 512 nm due to *Phaeocystis* and  $1 - \theta_3$  is the fraction due to diatoms, and  $\theta_4$  is the total absorption by phytoplankton at 512 nm ( $a_{\phi}(512)$ ). This linear mixing approach is modified from the work of Ciotti et al. (2002) where they used two extreme shapes normalized to the mean phytoplankton absorption to represent a wide range of phytoplankton absorption spectra and a size factor ( $S_{<f>}$ , dimensionless) as the linear coefficient. Modifications for the Bering Sea were made by using the phytoplankton absorption spectrum for *Phaeocystis* (see Ciotti et al. 2002 spectra “U-phae BS 97”, their Figure 7) and large diatoms (Ciotti et al. 2002 their

microphytoplankton spectral component, see their Table 3), which were the most abundant groups in 2001 (standard light microscope observations), and by normalizing to 512 nm which simplifies the interpretation of the  $\theta_3$  parameter. To keep the notation consistent with previous usage, I will use  $S_{<f>}$  to represent  $\theta_3$ , this is the same symbol as used by Ciotti et al. (2002) for their size factor (although I am using a slightly different definition).

Backscattering by particles was also modeled using two parameters,

$$b_{bpart}(\lambda) = \theta_5 - \theta_6[\lambda - 650], \quad 4.17$$

where  $\theta_5$  is the backscattering due to particles at 650 nm ( $\theta_5 = b_{bpart}(650)$ ) and  $\theta_6$  (nm<sup>-1</sup>) is the spectral decrease backscattering with wavelength. I use a linear function for the backscattering function as the data obtained with the Hydroscat 6 (see data collection section) did not warrant a decreasing power function relationship for backscattering versus wavelength. A power function is commonly used as it is the analytical solution for a Junge particle size distribution (Morel 1973). The seventh parameter,  $\theta_7$ , is the quantum yield of fluorescence,  $\phi_f$ ; while the shape used for  $f_{fQ}(\lambda)$  is for the fluorescence emission measured on *Thalassiosira pseudonana* (see Results).

#### **4.3.4 Application to Lunenburg Bay**

##### **4.3.4.1 Overview of the approach in Lunenburg Bay**

In Lunenburg Bay, standard ocean color models based on the blue-green ratio and conventional inverse models fail due to the strong influence of CDOM. Here, use a modified inverse model that uses the fluorescence signal with an assumed quantum yield to retrieve phytoplankton absorption. Although the inverse model uses all wavebands for

all constituents, the model developed below can be understood qualitatively by considering that the bulk absorption, which is mainly due to non-algal colored matter, is obtained by inverting long ultraviolet (UV, I used 380 to 400 nm) waveband, the backscattering coefficient is obtained from wavebands between ~600-650 nm, and the phytoplankton absorption is obtained by inverting the fluorescence waveband. A parameterization of the phytoplankton quantum yield as a function of irradiance level is also described to account for the variability due to the effect of quenching (mostly non-photochemical) on the retrieval of phytoplankton absorption.

#### *4.3.4.2 Selection of wavebands - Influence of CDOM on blue-green wavelengths*

Lunenburg Bay is a typical Case 2 water environment influenced strongly by colored dissolved organic matter. The relative influence of CDOM can be understood by noting that, at 490 nm, the absorption by CDOM is on average about 4 times higher than that of phytoplankton (data not shown). This makes it impossible to retrieve the phytoplankton absorption by standard algorithms of ocean color utilizing the blue and green bands. The problem is not only limited to the strong CDOM absorption in the blue region of the spectrum, but probably also by CDOM fluorescence. A simple simulation using Hydrolight with the default CDOM quantum yield and redistribution function (see Mobley 1994) for an average CDOM absorption value in Lunenburg Bay showed that CDOM fluorescence covers a broad emission band centered around 490 nm where, at its maximum, it accounts for about 20% of the upwelling radiance. Accounting for this effect is very difficult in view of the highly variable redistribution functions (Hawes 1992; Mobley 1994; Vodacek et al. 1994; Coble 1996; Seritti et al. 1998) and to a lesser

extent variability in the quantum yield of CDOM fluorescence (Blough and Del Vecchio 2002) measured in the environment. An attempt is made by Pozdnyakov and Grassl (2003) to generalize the CDOM fluorescence effect on reflectance but this is made by ignoring the change in the spectral redistribution function with excitation wavelength.

#### *4.3.4.3 Selection of wavebands - Influence of CDOM in red wavelengths*

In contrast to the blue-green region of the spectrum, at the red end of the spectrum where phytoplankton fluorescence occurs, the absorption by water dominates, and CDOM fluorescence and absorption are negligible. This allows the chlorophyll fluorescence spectrum and amplitude to be estimated without interference from other optical constituents (Roesler and Perry 1995). Therefore, the fluorescence band becomes very useful for the retrieval of phytoplankton biomass in terms of absorption in these waters (see equation 4.9) assuming that the quantum yield is constant or its variability can be predicted (see chapter 3 for a general model).

#### *4.3.4.4 Selection of wavebands – Limitation in the ultraviolet*

The wavebands below about 400 nm are much less affected by CDOM fluorescence as shown by my Hydrolight simulations (see also Vodacek et al. 1994; Pozdnyakov and Grassl 2003). However, the amount of backscattered light decreases rapidly with decreasing wavelength below 400 nm due to the rapid increase in absorption due to CDOM in coastal waters and the lower incident irradiance. Furthermore, owing to the non-linear nature of the functional relationship between reflectance and absorptions (see equation 4.13), small errors in the retrieval of reflectance in those wavebands can lead to large errors in the estimated absorption (in absolute values) when reflectance is

low; therefore instrumental limitation can prevent the extension to wavelengths below ~380 nm in high CDOM waters such as Lunenburg Bay.

#### 4.3.4.5 *Selection of wavebands – final choice*

Because CDOM affects fluorescence in the blue and green wavebands, and bottom reflectance can influence the upwelling spectrum in the green and yellow wavebands (the clearest wavebands in Lunenburg Bay) and these two processes are not included in the model of reflectance developed above, the inverse model does not fit the wavebands from 400 to 600 nm. These wavebands are usually important to obtain phytoplankton biomass in absorption based models. Instead, chlorophyll fluorescence is used to retrieve the phytoplankton absorption. Therefore, the optimization is only carried out over the wavelengths from 380 to 400 nm (influenced mostly by backscattering and CDOM absorption) and 600 to 700 nm (influenced mostly by water absorption, chlorophyll fluorescence and backscattering) while the model also uses the diffuse attenuation coefficient at 380 nm. The diffuse attenuation coefficient at 380 nm is obtained directly from the mooring using the above-surface sensor and the sensor at 2.75 m. The simultaneous inversion of the attenuation coefficient is not detailed here (see Brown et al. 2003 for details). The lower limit at 380 nm for the reflectance fit was set due to the consideration mentioned above regarding the rapid decrease in upwelling radiance and its implications for the retrieval of accurate absorption values. The wavelengths used in the model are outside the main absorption band in the blue for phytoplankton (Kirk 1994; Bricaud et al. 1995) such that the amplitude of phytoplankton absorption is not strongly constrained by the UV spectral regions.

#### 4.3.4.6 Spectral shapes in Lunenburg Bay

The Lunenburg Bay model has 5 fitted parameters and 3 spectral shapes. The spectral shapes for the absorption of phytoplankton and colored matter are kept constant at the mean values measured in Lunenburg Bay during the weekly sampling conducted from June 2002 thru September 2002, which showed very limited spectral variability,

$$a_{\phi}(\lambda) = \phi_{a\phi} = \theta_1 \bar{a}_{\phi}^{490}(\lambda), \quad 4.18$$

and

$$a_{CM}(\lambda) = \phi_{aCM} = \theta_2 \bar{a}_{CM}^{400}(\lambda), \quad 4.19$$

where  $\bar{a}_{\phi}^{490}(\lambda)$ ,  $\bar{a}_{CM}^{400}(\lambda)$ , are the average spectra for phytoplankton and non-algal colored matter normalized to 490 nm and 400 nm respectively. The backscattering shape is given by

$$b_{bpart}(\lambda) = \phi_{bpart} = \theta_3 \left( \frac{\lambda}{650} \right)^{-\theta_4}, \quad 4.20$$

where  $\theta_3$  is the backscattering coefficient by particles at 650 nm ( $b_{bpart}(650)$ ) and  $\theta_4$  is the spectral decrease of the power function used to describe the backscattering (closer to 1-2 for small particles and closer to 0 for large particles e.g. Morel and Maritorena 2001). In this model, the quantum yield of fluorescence is a prescribed function of irradiance and is not fitted and the shape  $f_{fQ}(\lambda)$  is the same as for the Bering Sea model. Note that although the same symbol,  $\theta$ , is used for the fitted parameters, for both the Bering Sea and Lunenburg Bay the same subscript is not used to represent the same optical parameters (see Table 4-2 for a comparison of the models).

**Table 4-2: Comparison of the two inverse models used in this study**

Bering Sea	Lunenburg
Number of Fitted parameters	
7	5
IOPs retrieved	
$a_\varphi, a_{CM}, b_{bpart}, \varphi_f$	$a_\varphi, a_{CM}, b_{bpart}$
The quantum yield of fluorescence	
Is retrieved	Is a prescribed a function of irradiance
Waveband fitted	
400 to 700 nm	380 to 400 nm and 600 to 700 nm
AOP used	
Reflectance	Reflectance and diffuse attenuation
Spectral shapes	
$a_\varphi(\lambda) = \theta_4 \left[ \theta_3 a_{\varphi^{512}^{Phaeo}}(\lambda) + (1 - \theta_3) a_{\varphi^{512}^{diatom}}(\lambda) \right]$ $= a_\varphi(512) \left[ S_{<f>} a_{\varphi^{512}^{Phaeo}}(\lambda) + (1 - S_{<f>}) a_{\varphi^{512}^{diatom}}(\lambda) \right]$	$a_\varphi(\lambda) = \theta_1 \bar{a}_\varphi^{490}(\lambda)$ $= a_\varphi(490) \bar{a}_\varphi^{490}(\lambda)$
$a_{CM}(\lambda) = \theta_1 \exp(-\theta_2(\lambda - 400))$ $= a_{CM}(400) \exp(-s_{CM}(\lambda - 400))$	$a_{CDOM}(\lambda) = \theta_2 \bar{a}_{CDOM}^{400}(\lambda)$ $= a_{CDOM}(400) \bar{a}_{CDOM}^{400}(\lambda)$
$b_{bpart}(\lambda) = \theta_5 - \theta_6 [\lambda - 650]$ $= b_{bpart}(650) - s_{bpart} [\lambda - 650]$	$b_{bpart}(\lambda) = \theta_3 (\lambda/650)^{-\theta_4}$ $= b_{bpart}(650) (\lambda/650)^{-s_{bpart}}$
Fluorescence : $= \theta_7 f_{fQ}(\lambda)$ $= \varphi_f f_{fQ}(\lambda)$	Fluorescence : $= \theta_5 f_{fQ}(\lambda)$ $= \varphi_f f_{fQ}(\lambda)$
$f_{fQ}(\lambda)$ is from <i>Thalassiosira pseudonana</i>	$f_{fQ}(\lambda)$ is from <i>Thalassiosira pseudonana</i>
Model	
$\mathbf{R}_{Lb}^{mod}(\lambda \boldsymbol{\theta}) = \frac{L_{ub}(\lambda, 0.65)}{E_d(\lambda, 0^+)} = T_{0.65}(\theta_{sun}, \tau_a, W, IOP) G(\theta_{sun}, \tau_a, W, IOP) \frac{b_b(\lambda)}{a(\lambda)}$	
$\mathbf{R}_{Lf}^{mod}(\lambda \boldsymbol{\theta}) = \frac{f_{fQ}(\lambda) \varphi_f}{4\pi E_d(\lambda, 0^+)} \int_{400}^{700} \frac{a_\varphi(\lambda_{ex}) \bar{E}(\lambda_{ex}, 0.65)}{K_{0.65-2.75}(\lambda_{ex}) + a_f(\lambda)} d\lambda_{ex}$	
Cost function	
$\sum_{k=1}^K \left[ \mathbf{R}_{Li}^{obs}(\lambda_k) - \left\{ \mathbf{R}_{Lb}^{mod}(\lambda_k \boldsymbol{\theta}_i) + \mathbf{R}_{Lf}^{mod}(\lambda_k \boldsymbol{\theta}_i) \right\} \right]^2$	

#### **4.3.5 Data collection and Hydrolight simulations**

##### **4.3.5.1 Bering Sea**

Reflectance data were obtained from a hyperspectral TSRB (Satlantic, Nova Scotia, Canada). The binary data stored as counts were calibrated to physical units by applying the factory calibration. The upwelling radiance and downwelling irradiance were corrected for the dark spectra using the measurements when the instrument shutter is closed every 6 measurements. The reflectance was calculated as the ratio of the upwelling radiance measured using the sensor at 0.65 m to the downwelling irradiance measured by the sensor above the sea surface. A temporal 5-point running (~10 s) average was applied to the data to decrease the variability on the second timescale. The attenuation coefficient for downwelling irradiance was obtained by a linear fit on the log transformed calibrated data obtained with a profiling radiometer (Satlantic, Nova Scotia, Canada). Before the fit, a dark value was identified and subtracted. The dark value was identified as the value of the irradiance when it no longer decreases exponentially with depth. Each wavelength was quality checked and fitted individually, with the depth range for the fit restricted to the mixed layer or shallower as necessary depending on the location of the selected dark value and the shape of the irradiance profile. For the red wavelengths, particular attention was given to restrict the range to the part where the logarithm of the irradiance is linear with depth; this can be less than 2-3 m for the longer wavelengths.

For the determination of chlorophyll concentration, 70 ml of water were filtered on GFF filters extracted in 90% acetone in a freezer on board the ship for 24 to 48 hours

and measured using a calibrated Turner Designs fluorometer. Acidification allowed the separation of the phaeopigments from the chlorophyll *a* concentration (Yentsch and Menzel 1963).

Throughout the cruise, water was pumped from ~3 m depth continuously through a fluorometer and conductivity-temperature sensor onboard. Thus providing a measure of *in vivo* fluorescence, salinity and temperature while, underway and at each station. The time from water intake to the fluorometer was estimated to be 1 to 2 minutes by the ship's scientific technician.

#### *4.3.5.2 Lunenburg*

Reflectance data in Lunenburg was obtained from a hyperspectral TSRB. The hyperspectral TSRB was deployed as part of the MB1 instrumented mooring and data were collected for 15 minutes every 30 minutes during daylight from June 4 to September 28, 2003. Simple quality control was applied to the data to remove outliers and correct for dark values, and the median of the 15 minutes acquisition was taken and used for the inversion. No further processing was applied to the optical data. The reflectance spectra were matched with the time of sampling of the discrete samples by taking the first median spectrum that passed the quality control test following the sampling time (when the optical sensors are cleaned). This provided 14 spectra usually within 1 hour of sampling.

The attenuation coefficient for the 380 nm waveband is used in the inversion. To retrieve it, the irradiance was measured at 2.75 m with an OCR-504 head (Satlantic, Nova Scotia, Canada) at the same time as the surface irradiance from the TSRB. The

attenuation coefficient was obtained as:

$K_d(380) = -\ln(E_d(380, 2.75)/E_d(380, 0^+)) / 2.75$ , where  $E_d(380, 2.75)$  is measured with the OCR-504 head and  $E_d(380, 0^+)$  is measured with the TSRB. The median was then computed for the 15-minute acquisition. No correction for reflection was applied as it is accounted for in the model simulation.

CDOM and particulate (detritus and phytoplankton) absorption coefficients were obtained according to the NASA satellite validation protocols (Pegau et al. 2003).

The scattering coefficient was measured using an ac-9 (Wetlabs, Oregon, USA) and processed according to the manufacturer protocol (using a spectrally resolved scattering correction, their method #3). Temperature and salinity corrections were made using data from a near-simultaneous CTD cast.

The backscattering coefficient was obtained with a Hydrosat-6 (Hobilabs, Arizona, U.S.A) deployed on the same package as the ac-9 and was processed according to Boss and Pegau (2001).

#### 4.3.5.3 *Hydrolight simulations*

To obtain a complete model of reflectance for fluorescence, I need to obtain a functional description of  $\hat{E}(\lambda, 0.65)$  and  $K_{0.65-2.75}(\lambda_{ex})$  in terms of known quantities and quantities obtainable from the inverse model. Because there are not analytical solution or previously described models for these parameters, I quantify them using a series of radiative transfer simulations made for Lunenburg Bay to find functions that best described them. In these radiative transfer simulations, the IOPs are the prescribed inputs

and the AOPs,  $\bar{E}(\lambda, 0.65)$  and  $K_{0.65-2.75}(\lambda_{ex})$  are the outputs. The objective is to parameterize the solution of the radiative transfer equation in terms of simple functions of IOPs and known variables. The radiative transfer calculations done in Hydrolight are described below.

The Hydrolight simulations were run for absorption and scattering coefficients that are representative of Lunenburg Bay, Nova Scotia, for which absorption is mostly dominated by CDOM, but results are valid for any location where the backscattering to absorption ratio are in the same range as those computed here (Figure 4.1).

The Hydrolight simulations were run for thirty-five combinations of two constituents: non-colored particulate matter and colored matter and 4 sun zenith angles (20, 40, 50, 70 degrees). The colored matter was assumed non-scattering and its absorption coefficient was varied in steps equal to 1 standard deviation (s.d.) of the measured range of the total absorption coefficient (minus water) measured in Lunenburg Bay on filtered particulate and dissolved water samples during the summer of 2002 at each wavelength (mean-3s.d., mean-2s.d., mean-1s.d., mean, mean+1s.d., mean+2s.d., mean+3s.d. see Figure 4.1). The absorption by non-colored particulate matter was zero at all wavelengths, while its scattering coefficient was varied in 5 steps, where each step is equal to 1 standard deviation of the measured range of the particulate scattering coefficient measured with the ac-9 in Lunenburg Bay during the summer of 2002 at each wavelength (mean-2s.d., mean-1s.d., mean, mean+1s.d., mean+2s.d., see Figure 4.1). The Fournier-Forand scattering phase function with a backscattering ratio equal to 0.011 was used for particulate matter. This backscattering ratio is the mean measured in surface

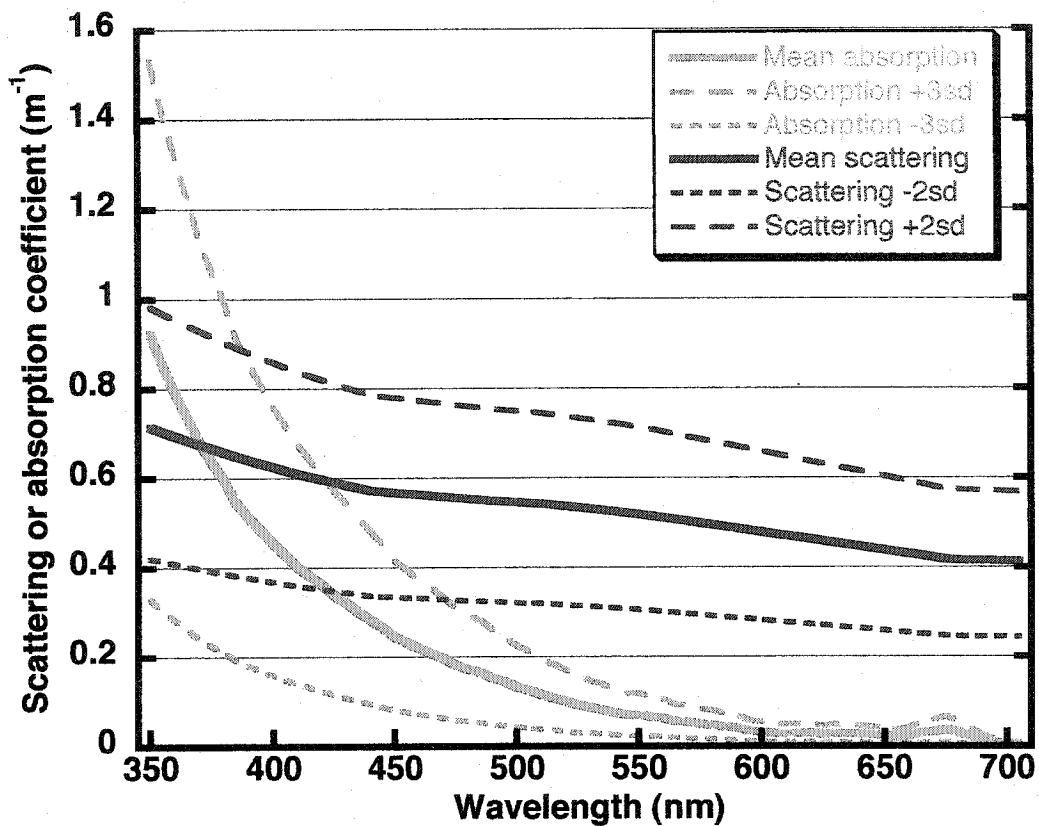


Figure 4.1: Hydrolight simulation inputs. Presented are the mean values for absorption and scattering and the range used at all wavelengths. The scattering values were obtained from the ac-9 casts during the summer 2002 while the absorption value were obtained as the sum of the absorption from discrete CDOM and particulate absorption samples during the same period. To obtain the backscattering coefficient, the scattering values were multiplied by 0.011 (within Hydrolight).

waters of Lunenburg Bay during the summer of 2002 (Hydroscat backscattering / ac-9 scattering at 510 nm). Absorption by water was from Pope and Fry (1997) and scattering was from Smith and Baker (1981). The simulated water column was infinitely deep. All runs were done with a clear sky model (Gregg and Carder 1990). The wind speed, which affects the sea-surface slope distribution function, and thus the atmosphere-ocean and ocean-atmosphere radiance transmission, was set to 2 m/s. Raman scattering was parameterized as in Morel et al. (2002), no fluorescence sources were included.

## **4.4 Results**

### **4.4.1 Fluorescence spectral components**

The fluorescence spectral component used during the inversion was measured with a spectroradiometer on thin, nutrient replete, high light grown cultures ( $\sim 1000 \mu\text{mol m}^{-2} \text{s}^{-1}$ ) of *Thalassiosira pseudonana* (Figure 4.2) by illuminating them with a broadband blue light. For comparison, fluorescence emission spectra measured or used by others are also shown in Figure 4.2.

### **4.4.2 Parameterization using the Hydrolight dataset**

In this section, I relate two AOPs ( $E^{\circ}(\lambda, 0.65)$  and  $K_{0.65-2.75}(\lambda)$  see equation 4.11) to IOPs retrievable by the inverse model and other known quantities such as the solar zenith angle. Using a radiative transfer model (Hydrolight) to provide the dataset used to derive the relationships for the inverse model is necessary since having a consistent dataset comprising all IOPs and measured AOP for the range and combination of IOPs expected to occur in the region studied is extremely difficult. The correction of upwelling radiances for bi-directional effects for satellite remote sensing conditions has also been

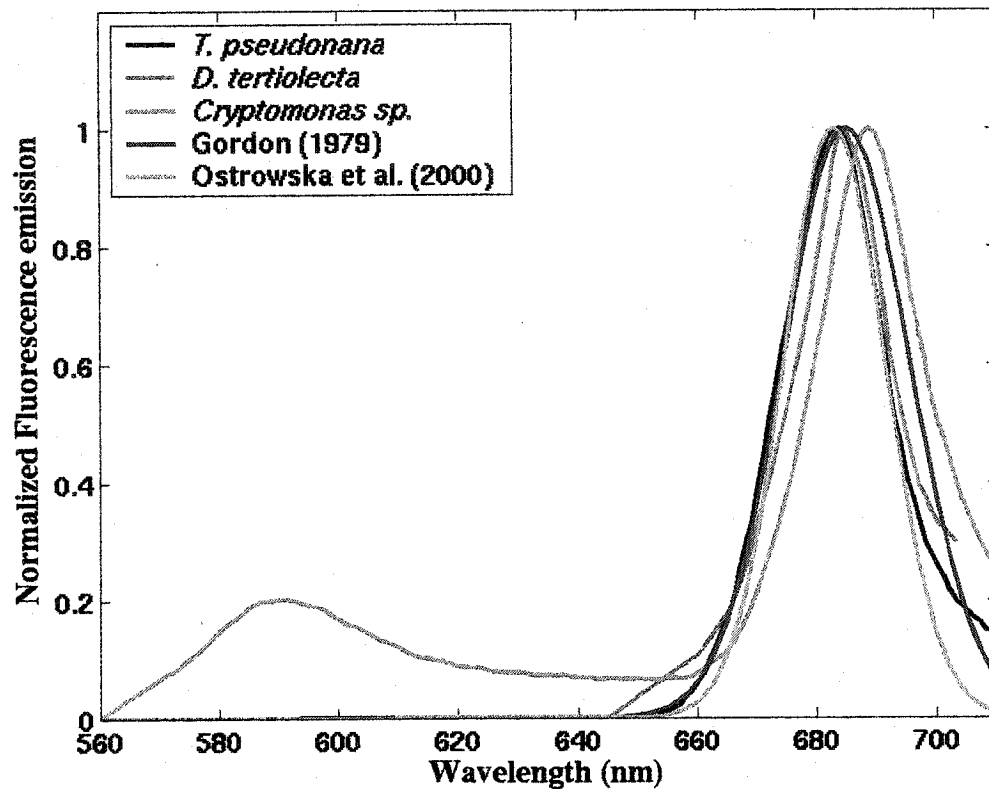


Figure 4.2: Five emission spectra for phytoplankton fluorescence normalized to their maximum values. The spectra are for *Thalassiosira pseudonana* (this study); *Dunaliella tertiolecta* (Collins et al. 1985, their “sun” spectra digitized and extrapolated in the short wavelength); *Cryptomonas* sp. (Sciandra et al. 2000 extrapolated linearly at the short wavelengths); and two theoretical shapes from Gordon (1979) and Ostrowska et al. (2000a).

accomplished using similar types of simulations (Morel and Gentili 1996; Morel et al. 2002).

The empirical relationship for the diffuse attenuation for scalar irradiance ( $K_{0.65-2.75}$  Figure 4.3, top panels) has a mean percent error of 0.4% and is valid for solar zenith angles between 20° and 70° and wavelengths from 355 to 700 nm,

$$K_{0.65-2.75}(\lambda) = \frac{a(\lambda) + k_4(\lambda)b_b(\lambda)}{k_1(\lambda) + k_2(\lambda)\cos(\theta'_{sun}) + k_3(\lambda)\cos^2(\theta'_{sun})}, \quad 4.21$$

where the parameters  $k_i(\lambda)$  are fitted using a non-linear regression routine (see Table 4-3 and Figure 4.3).

The empirical relationship for  $\overset{\circ}{E}(\lambda, 0.65)$  (Figure 4.3, bottom panels) has a mean percent error of 3.2% from the Hydrolight simulations and is described as,

$$\overset{\circ}{E}(\lambda, 0.65) = [1 + e_1 a(\lambda)] [e_2 \cos(\theta'_{sun}) + e_3 \cos^2(\theta'_{sun})] [1 + e_4 b_b(\lambda)] E_d(\lambda, 0^+), \quad 4.22$$

where  $e_i$  are fitted parameters (Figure 4.3 and Table 4-4)

#### 4.4.3 Inversion in the Bering Sea

The station 35 (55.248°N, 168.149°W) analyzed here, was visited on June 2, 2001. The surface chlorophyll concentration was 11.75 mg m<sup>-3</sup> in the mixed layer, which extended to a depth of about 30 m. The surface water temperature was 5.2°C. The timeseries shown started at 0909h local time.

The timeseries of absorption by phytoplankton and CDOM as retrieved by the model show limited variability (Figure 4.4A) during the ~10 minute deployment; given the 95% confidence interval on the parameters, the model could not resolve any variability during the time series. The CDOM absorption slope similarly showed very

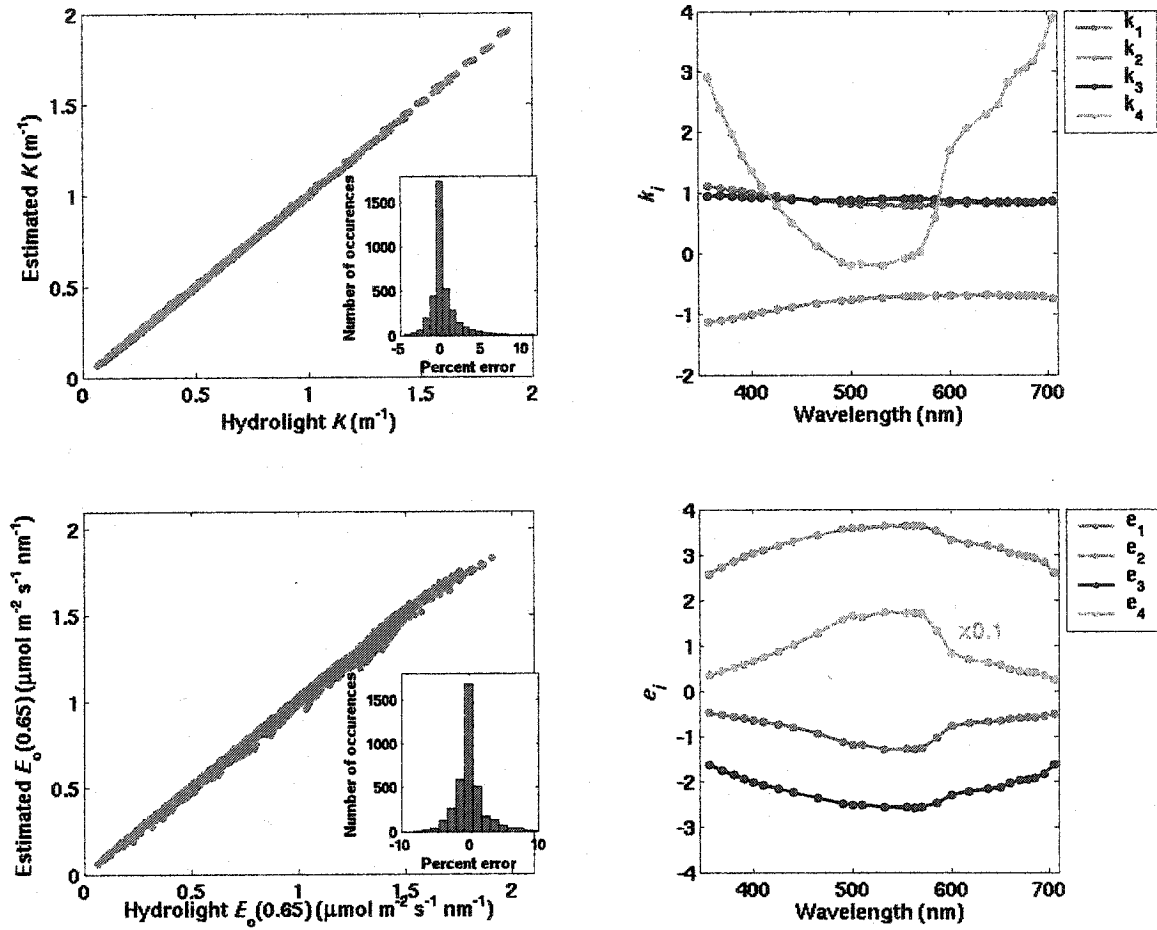


Figure 4.3: Comparison of the empirical parameterization (estimated) and the Hydrolight simulated dataset for  $K_{0.65-2.75}$  (top panels; using equation 4.21) and  $\hat{E}(\lambda, 0.65)$  (bottom panels; using equation 4.22). Left panel shows a direct comparison of the parameterized results against those of Hydrolight while the right panels show the spectral changes in the fitted coefficients. The insets on the left panels provide the percent error between the empirical relationship and Hydrolight results. The relationships are valid for zenith angles between  $20^\circ$  and  $70^\circ$ .

**Table 4-3: Fitted parameters,  $k_i$  from the Hydrolight simulations for Lunenburg Bay Nova Scotia for  $K_{0.65-2.75}$  (see equation 4.21).**

Wavelength (nm)	$k_1$ (dimensionless)	$k_2$ (dimensionless)	$k_3$ (dimensionless)	$k_4$ (dimensionless)
$K_{0.65-2.75}(\lambda) = \frac{a(\lambda) + k_4(\lambda)b_b(\lambda)}{k_1(\lambda) + k_2(\lambda)\cos(\theta'_{sun}) + k_3(\lambda)\cos^2(\theta'_{sun})}$				
355	1.1111	-1.1235	0.9531	2.9167
367.5	1.0818	-1.0978	0.9535	2.3933
380	1.0519	-1.0641	0.9475	1.9767
390	1.0243	-1.0293	0.9381	1.6167
400	0.9997	-0.9965	0.9287	1.3533
410	0.9769	-0.9651	0.9192	1.1033
425	0.9445	-0.9194	0.9052	0.7867
440	0.9146	-0.8778	0.8934	0.5033
465	0.8687	-0.818	0.8809	0.1267
490	0.8307	-0.7728	0.8785	-0.1467
500	0.8178	-0.7588	0.8814	-0.2033
510	0.8119	-0.7523	0.8872	-0.1733
532.5	0.7915	-0.7267	0.895	-0.2033
555	0.7815	-0.7054	0.8982	-0.0900
562.5	0.7804	-0.7024	0.9016	-0.0400
570	0.7806	-0.7002	0.9033	0.0167
585	0.7927	-0.689	0.8884	0.5867
600	0.8178	-0.6963	0.8685	1.6967
617.5	0.8206	-0.6924	0.8599	2.0600
637.5	0.8196	-0.6856	0.8529	2.2967
650	0.8197	-0.6826	0.8492	2.4533
660	0.8278	-0.6924	0.8487	2.8233
670	0.8305	-0.695	0.8477	2.9833
677.5	0.8312	-0.6953	0.847	3.0733
685	0.8321	-0.6962	0.8471	3.1733
695	0.839	-0.7068	0.8501	3.4367
705	0.8582	-0.7384	0.8611	3.8867

**Table 4-4: Fitted parameters,  $e_i$  from the Hydrolight simulations for Lunenburg Bay Nova Scotia for  $\bar{E}(\lambda, 65)$ .**

Wavelength (nm)	$e_1$ (m)	$e_2$ (unitless)	$e_3$ (unitless)	$e_4$ (m)
$\bar{E}(\lambda, 0.65) = [1 + e_1 \cdot a(\lambda)] [e_2 \cos(\theta'_{sun}) + e_3 \cos^2(\theta'_{sun})] [1 + e_4 \cdot b_b(\lambda)] E_d(\lambda, 0^+)$				
355	-0.4795	2.5702	-1.6263	3.5558
367.5	-0.525	2.7266	-1.7522	4.3167
380	-0.5674	2.8517	-1.8566	5.0803
390	-0.6085	2.9544	-1.9448	5.8843
400	-0.6444	3.0354	-2.0159	6.6302
410	-0.6816	3.107	-2.08	7.4546
425	-0.7388	3.1998	-2.1647	8.7484
440	-0.8038	3.287	-2.2451	10.1661
465	-0.9478	3.4263	-2.3737	12.7937
490	-1.1307	3.5477	-2.4861	15.7094
500	-1.2005	3.5804	-2.518	16.5573
510	-1.196	3.5791	-2.52	16.1823
532.5	-1.2995	3.6269	-2.5675	17.3411
555	-1.2915	3.6284	-2.5739	17.1808
562.5	-1.2953	3.6323	-2.5785	17.1438
570	-1.2743	3.6255	-2.5738	16.8996
585	-1.0354	3.5231	-2.4836	13.2533
600	-0.7761	3.3234	-2.2972	8.1741
617.5	-0.718	3.2459	-2.2245	6.8919
637.5	-0.6833	3.1885	-2.1711	6.137
650	-0.6637	3.1489	-2.1339	5.6857
660	-0.6227	3.046	-2.0366	4.7319
670	-0.6029	2.9874	-1.9823	4.313
677.5	-0.593	2.9561	-1.9533	4.1047
685	-0.5847	2.9274	-1.9266	3.916
695	-0.5592	2.8293	-1.836	3.3744
705	-0.5101	2.6033	-1.6317	2.4499

**Figure 4.4: Time series of the fitted parameters with the inverse model and measured incident irradiance. A) Absorption by CDOM at 400 nm ( $\theta_1$ ) and phytoplankton at 512 nm ( $\theta_4$ ). B) Quantum yield of fluorescence ( $\theta_7$ ) and slope of the CM absorption spectrum ( $\theta_2$ ), the blue point represents the measured of the CDOM at that station. C) Measured planar incident photosynthetically available radiation above the sea surface. D) Retrieved backscattering coefficient at 650 nm ( $\theta_5$ ) and slope of the backscattering spectrum ( $\theta_6$ ). E) Phytoplankton absorption fraction ( $\theta_3$ ,  $S_{<f>}$ ). The 95% confidence intervals (see appendix II) are in gray for the black lines and in pink for the red line; confidence intervals for  $b_b(650)$  are undistinguishable from the line.**

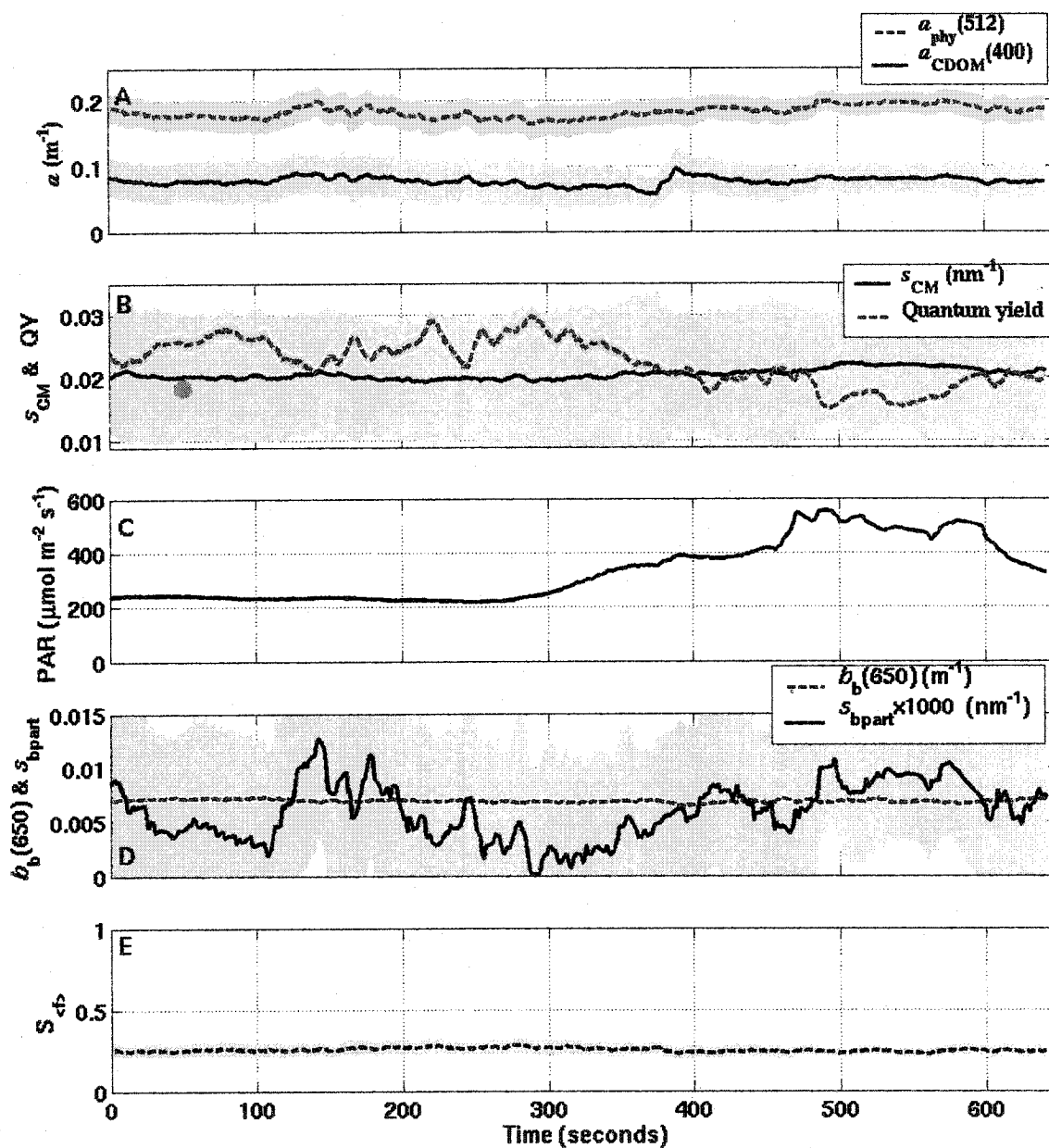
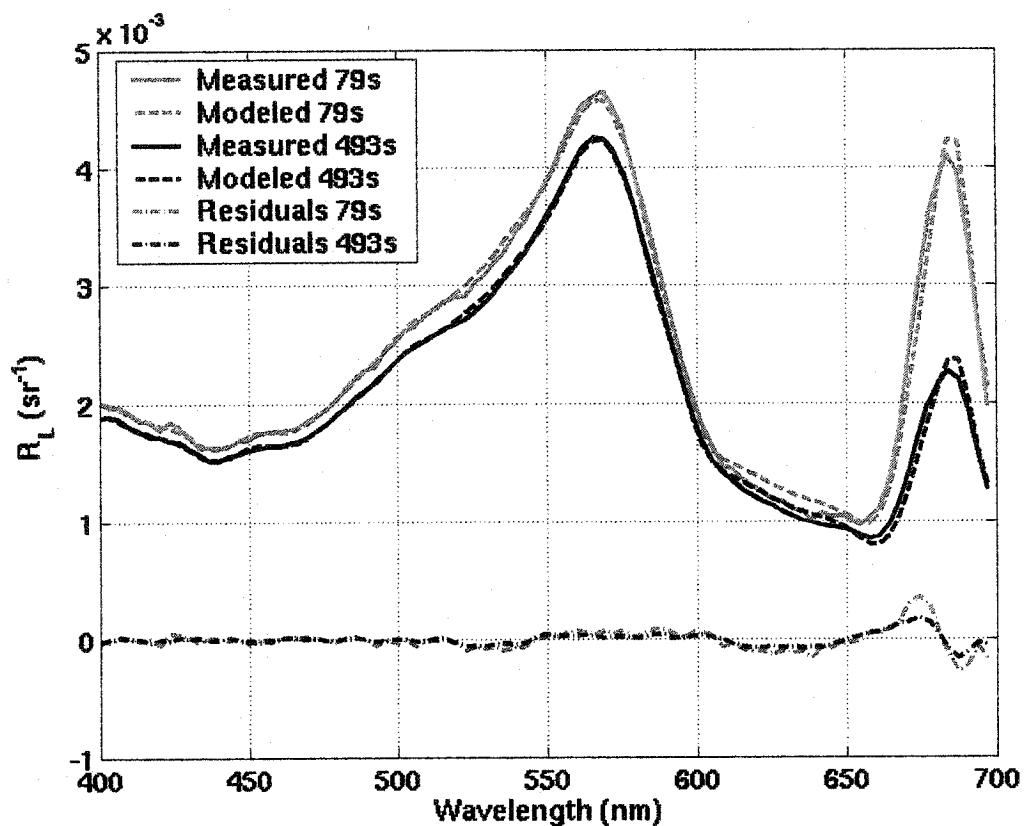


Figure 4.4: See caption on previous page.

little change as retrieved by the model while the quantum yield of fluorescence varied by about a factor of two (Figure 4.4B). The sources of variability in the fluorescence yield appear to be of two kinds, one which is unrelated to incident irradiance on time scales of the minute (Figure 4.4B), and another strongly influenced by — and inversely related to — the incident irradiance (Figure 4.4C). The retrieved backscattering coefficient (Figure 4.4C) did not change much during the 10-minute deployment. However, the backscattering slope showed a lot of variability suggesting that is a poorly constrained parameter (see Appendix II). The phytoplankton fraction is particularly stable (Figure 4.4E) at  $\sim 0.3$ . The small confidence intervals on clearly suggest that there is sufficient information in the spectrum to retrieve it (see Appendix II). The measured spectra are well fitted by the modeled reflectance spectra, with some non-random residuals in the fluorescence band (Figure 4.5). During deployment, a slight decrease in the reflectance between 400-650 nm was observed which likely originated from a change in the radiance distribution (compare the 79 s spectrum with the 493 s spectrum in Figure 4.5). This is reflected in a small change in the retrieved  $b_b(650)$ . (See below and Figure 4.4). The shape of the residuals in the fluorescence band (Figure 4.5) suggests a problem with the fluorescence shape chosen ( $f_{fd}(\lambda)$ ), the reabsorption of light outside the cells or the assumption of a constant quantum yield with depth (discussed in more detail below).

A comparison of the retrieved diffuse attenuation coefficient, total absorption and backscattering coefficient are shown in Figure 4.6. While the diffuse attenuation coefficient is overestimated slightly in the blue wavelength, the total absorption



**Figure 4.5: Modeled and measured reflectance spectra at two times in the timeseries (79 and 493 seconds) collected at station 35 in the Bering Sea on June 27, 2001. The spectra chosen represent the times at which the fluorescence yield were the highest and the lowest. Residuals are also shown for each spectrum.**

**Figure 4.6: Measured and modeled optical properties at station 35 in the Bering Sea in June 2001. Top panel: Diffuse attenuation coefficient from two drops of the profiling radiometer and modeled value of  $K_{0.65-2.75}$ . Middle panel: Measured and retrieved absorption coefficient by all colored matter (phytoplankton, detritus and CDOM). Bottom panel: total backscattering coefficient. On all panels, the dashed lines represent one standard deviation of the optical measurement retrieved using the inverse model during the 10 minutes of deployment.**

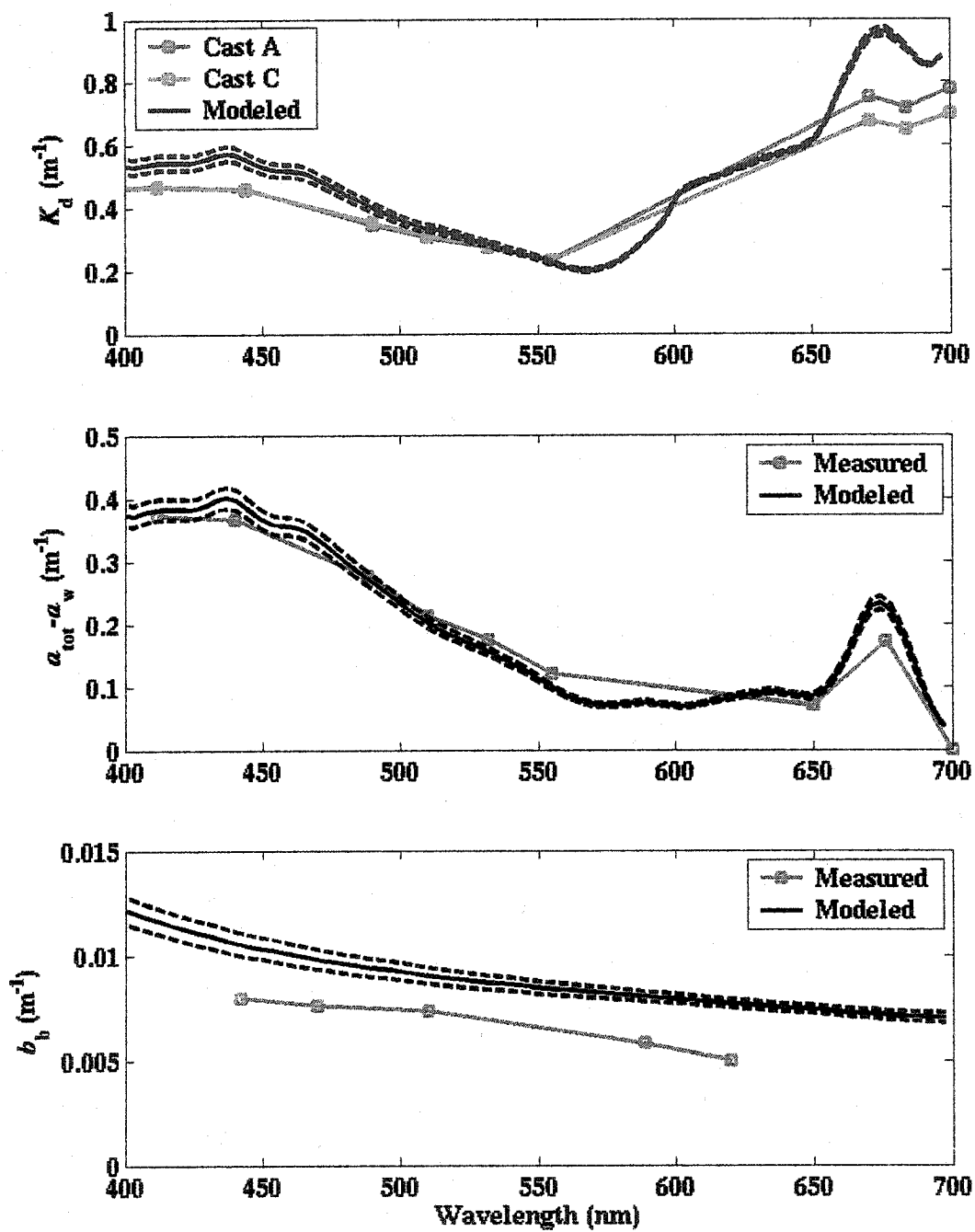


Figure 4.6 : See caption of previous page.

coefficient is retrieved very well. Because the attenuation coefficient is mostly affected by absorption and the geometrical distribution of the light field, this suggests an inaccurate model for the attenuation coefficient. However, as will be discussed in more details below, the diffuse attenuation coefficient seems to have been measured in a slightly different water mass; the flow-through fluorescence measurement was lower during the profiling radiometer deployment than during the TSRB and ac-9 deployment. The backscattering coefficient retrieved from the model is about 40% higher than the measured value.

#### **4.4.4 Inversion in Lunenburg Bay**

##### **4.4.4.1 Irradiance dependence of the quantum yield**

The reflectance measurements for the four-month deployment of mooring MB1 during the summer of 2003 were first inverted by keeping the quantum yield constant. When the quantum yield is held constant at a realistic value (here I chose 0.01) given the conditions described above for the fit, the variability in the retrieved absorption by phytoplankton is the result of the real variability in absorption, variation in the quantum yield (due to changes in light intensity, physiology or species composition) and systematic and random errors in the model and fit. As such, because absorption is not expected to vary much with irradiance, the portion of the variability explained by irradiance must originate from changes in the quantum yield of fluorescence.

For each month (see Figure 4.7) the data was fit to a second order polynomial function of the scalar irradiance weighted by the phytoplankton absorption spectrum (photosynthetically utilizable radiation, PUR) at 0.65 m ( $E_{PUR}^{0.490}(0.65)$ ) as the independent

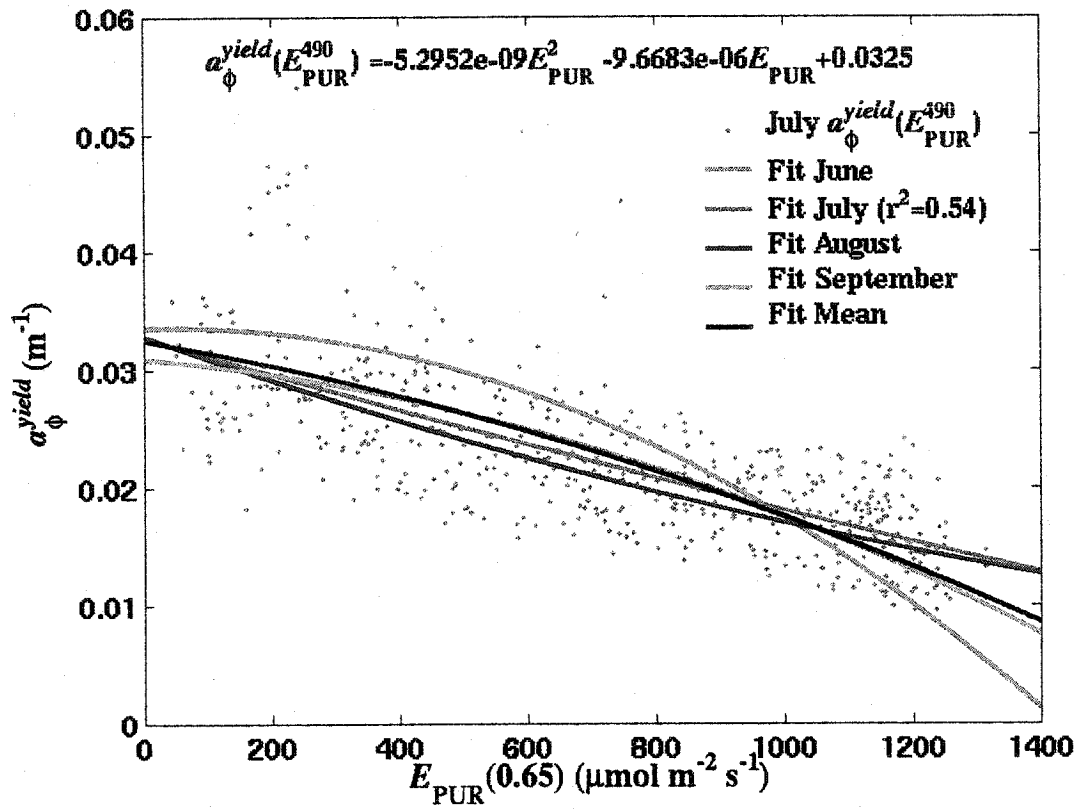


Figure 4.7: Fits and representative data of the retrieved absorption coefficient of phytoplankton if the quantum yield of fluorescence is maintained constant in the model. The blue points are the data points for the month of July. The four colored lines represents the fits to monthly datasets for the month of June, July (to blue points), August, and September, while the black line represents the mean relationship. The equation at the top of the graph is for the black line and is used in the inverse model after scaling by 0.4 m (see text).

variable,

$$\bar{E}_{PUR}^{0.490}(0.65) = \int_{400}^{700} \bar{a}_{\phi}^{490}(\lambda) \bar{E}(\lambda, 0.65) d\lambda, \quad 4.23$$

where  $\bar{a}_{\phi}^{490}(\lambda)$  is the phytoplankton absorption coefficient normalized to the value at 490 nm. I used PUR for this analysis as it was the best proxy I could obtain of the exciting radiation for phytoplankton fluorescence (the ideal weighting would be the fluorescence excitation spectrum). This definition of PUR differs from others by the manner in which I normalized the phytoplankton absorption coefficient. For example, Morel (1978) used the maximum of phytoplankton absorption while Markager and Vincent (2001) and Lehmann et al. (2004) used the mean value of the phytoplankton absorption. In practice, the normalization is only a scaling factor, and the preferred value will depend on the study and the interpretation of the data. In my case, it was practical to use 490 nm because the backscattering reflectance portion of the model was developed with the phytoplankton shape normalized to 490nm. The relationship between these different PUR ( $\mu\text{mol m}^{-2} \text{s}^{-1}$ ) irradiances using the mean Lunenburg Bay phytoplankton absorption spectrum is

$$\bar{E}_{PUR}^{0.490} = 0.669 \bar{E}_{PUR}^{0.669} = 1.65 \bar{E}_{PUR}^{0.669} \text{ where } \bar{E}_{PUR}^{0.669} \text{ is the PUR weighted irradiance when the}$$

absorption spectrum is normalized to the mean value of the spectrum and  $\bar{E}_{PUR}^{0.669}$  is the weighted irradiance when the absorption spectrum is normalized to its maximum.

As noted before, the retrieved phytoplankton coefficient when keeping the quantum yield constant reflects variability in both the phytoplankton absorption and quantum yield. Therefore, the mean relationship obtained for all four months (Figure 4.7)

for the retrieved absorption as a function of PUR using a constant quantum yield, denoted  $a_{\phi}^{yield}(E_{PUR}^{490})$  ( $\text{m}^{-1}$ ), can be used to describe the irradiance dependence of the quantum yield of fluorescence (see equation in Figure 4.7). However, this will provide only the relative irradiance dependence, and the absolute value of the quantum yield, which will scale this relationship, can only be obtained through validation with in situ data (see below).

Note that the attribution of all the irradiance dependence of  $a_{\phi}^{yield}(E_{PUR}^{490})$  to changes in the quantum yield is not necessarily correct; part of the variability could originate from diel changes in the absorption of phytoplankton (e.g. Stramski and Reynolds 1993; Ohi et al. 2002). As such, attributing all the variability to the quantum yield could bias the retrieval of  $a_{\phi}$ . For example, imagine a hypothetical situation where the quantum yield in situ remained constant and all the decrease observed in fluorescence radiance would be due to a decrease of phytoplankton absorption as light increases. My erroneous attribution of the decrease in  $L_{uf}$  at midday to changes in the quantum yield would lead to the prediction of constant phytoplankton absorption. However, the decrease of the quantum yield of fluorescence at high irradiances is well documented as originating from photoprotective mechanisms that cause non-photochemical quenching of fluorescence under high light (Kiefer 1973b; Genty et al. 1989; Demers et al. 1991; Krause and Weis 1991; Falkowski and Kolber 1995; Müller et al. 2001), while diel changes in absorption do not lead to the lowest values at the time of highest irradiance (e.g. Stramski and Reynolds 1993; Ohi et al. 2002).

#### 4.4.4.2 Weighted irradiance and quantum yield of fluorescence

In many sun-induced fluorescence studies, the unweighted PAR irradiance (or irradiance at one waveband above the surface) is used as a proxy for the exciting irradiance. To verify the importance of using the weighted absorption at 0.65 m I did the same fit as in Figure 4.7, but used the incident PAR irradiance above the surface ( $E_{PAR}(0^+)$ ) and at 0.65 m  $\overset{\circ}{E}_{PAR}(0.65)$ . For each month, the norm of the residuals was calculated ( $|\boldsymbol{\theta}(x)|$ , using this notation  $\boldsymbol{\theta}$  is the vector of differences from the fit and  $x$  is the independent variable of the fit) and followed

$$|\boldsymbol{\theta}(\overset{\circ}{E}_{PUR}^{0.490}(0.65))| < |\boldsymbol{\theta}(\overset{\circ}{E}_{PAR}(0.65))| < |\boldsymbol{\theta}(E_{PAR}(0^+))|. \text{ This implies that more of the}$$

variability in the change in the quantum yield with irradiance is explained by  $\overset{\circ}{E}_{PUR}^{0.490}(0.65)$  than by other simple measures of excitation irradiance. However, it should be noted that the scalar irradiance absorbed by phytoplankton was used in the inversion model (see equation 4.11), and as such, it is not surprising to find that PUR irradiance has the lowest norm of residuals. However, unless the model for  $\overset{\circ}{E}_{PUR}^{0.490}(0.65)$  is biased, this finding provides a strong argument for using a weighted irradiance at the depth of the radiance sensor in fluorescence studies (see also Figure 4.8 and results below) instead of other measures.

A first test of the model applied to Lunenburg Bay was made by comparing the retrieved attenuation coefficient from the inversion with the attenuation coefficient measured by the irradiance sensor at the surface and at 2.75 m (Figure 4.8, top panel). A

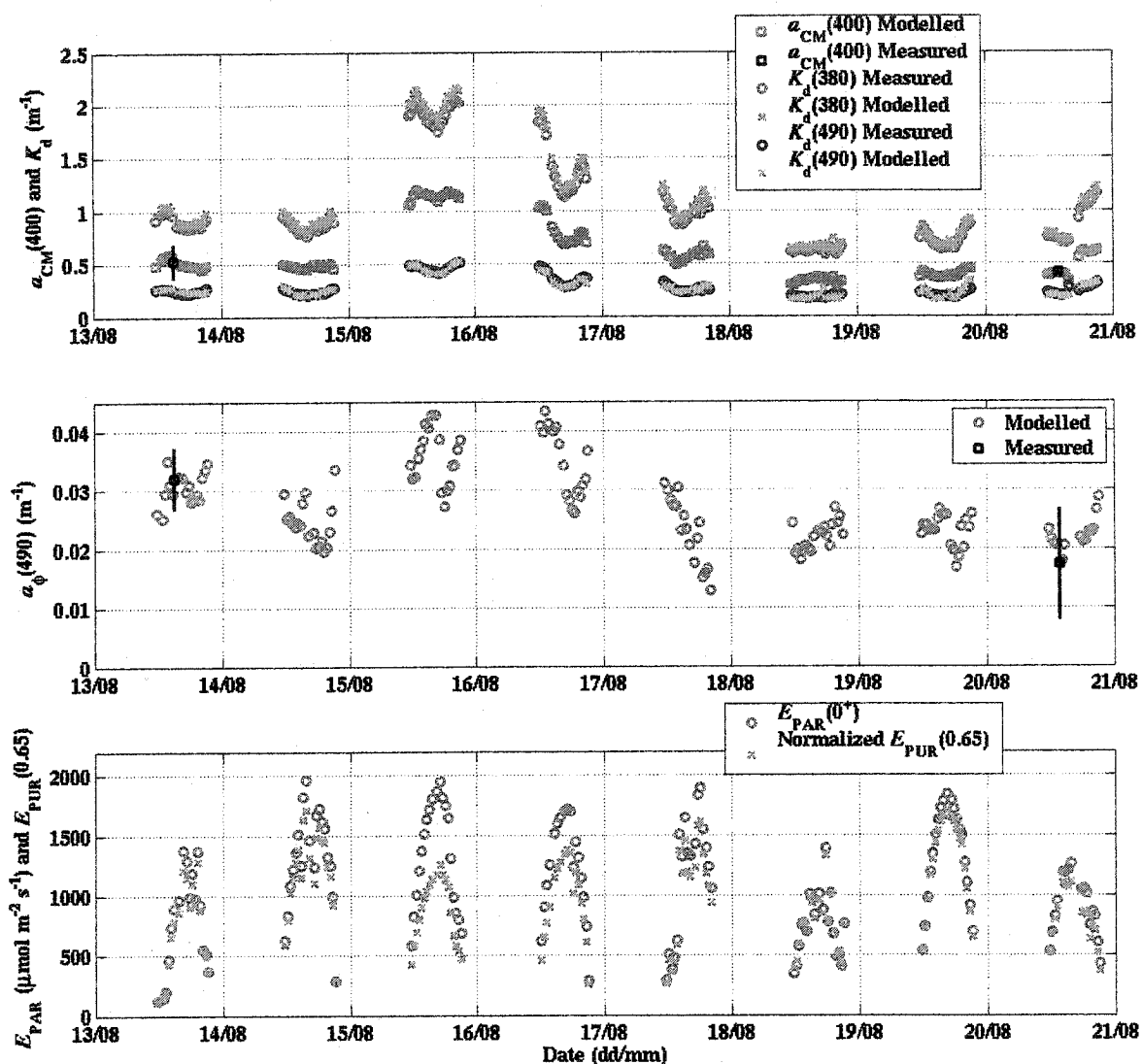


Figure 4.8: Time series comparison of measured and retrieved optical measurements with the inverse model. Top panel: Measured and retrieved absorption by non-algal colored matter (at 400 nm) and diffuse attenuation coefficient at 380 and 490 nm. Black symbols are the measured absorption by colored matter (see Figure 4.10 for error bar definition) with a spectrophotometer. Middle panel: measured and retrieved absorption coefficient by phytoplankton. Phytoplankton absorption was measured using the filter pad method (see Figure 4.10 for error bar definition). Bottom panel: measured incident planar irradiance in the PAR domain and modeled scalar PUR at 0.65 m. The PUR irradiance has been normalized to the first point of the PAR irradiance to allow assessment of the effect of variable colored matter absorption on the ratio of PAR above the surface to PUR at 0.65 m.

comparison with the attenuation at 380 nm is a measure of goodness of fit. The attenuation coefficient at 490 nm is not used during the regression and can be used as a measure of the quality of the retrieval. Because the attenuation at 490 nm is, like the attenuation at 380 nm, mostly influenced by CDOM, it is mostly a test that the shape of absorption by colored matter is appropriate and the model for the attenuation coefficient is accurate. On the same panel, the absorption by colored matter ( $a_{CM}(400)$ ) retrieved by the model and from two samples from the weekly sampling are shown. This period of the timeseries coincident with a heavy rain event in the region, which lead to increased runoff from land and a steep increase in the CDOM absorption, this absorption subsided within three days to return to values similar to those observed before the event. As retrieved by the model, the rain event led to a modest increase in the phytoplankton concentration (Figure 4.8, middle panel) at this mooring. The inversion provides relatively accurate retrievals of phytoplankton absorption at the two points measured. A comparison between  $E_{PAR}(0^+)$  and  $E_{PUR}^{490}(0.65)$  for this period shows that their ratio varies by a factor of almost 2, which would lead, if it was not accounted for, to similar errors in the retrieval of phytoplankton absorption retrieved from fluorescence (Figure 4.8, bottom panel). Note that  $E_{PUR}^{490}(0.65)$  is normalized to the  $E_{PAR}(0^+)$  value for the first point of the timeseries in Figure 4.8 to allow a better comparison of the ratios. In this example, I show only a few days that showed the greatest variability in the attenuation coefficient measured, during the summer of 2003, allowing more clarity on the graph.

To verify that the model worked for the whole season, I selected all the

reflectance spectra times when discrete samples were collected (Figure 4.9). These spectra show limited variability, while two spectra are clearly different; one from August 13 which shows a lower reflectance in the UV-blue region consistent with larger than usual CDOM absorption and one from September 17 which shows lower reflectance in the 600-650 nm region, consistent with a lower than average backscattering coefficient. After inversion of the selected spectra presented in Figure 4.9, I obtained the absorption coefficient associated with these spectra, which can be compared with the in situ samples taken at MB1 during the summer of 2003 (Figure 4.10). This comparison shows that phytoplankton absorption is retrieved well, despite the limited variability observed (Figure 4.10). One outlier is clearly observed in the phytoplankton absorption. I used a robust fit technique (which weights points further from the best fit line less than with standard methods using the square of the distance) which decreases the influence of this point on the resulting relationship. The outlier corresponds to the sampling day on September 17, 2003. In addition to having a distinct reflectance spectrum, the HPLC pigments obtained that day on discrete samples show a large peak, probably corresponding to a phaeophytin (not fluorescing), which has not been seen in any other samples that year (Claire Normandeau, personal communication). Clearly, the optical and environmental conditions on that day were different from the rest of the season.

The final quantum yield as a function of irradiance was found by scaling the relationships for  $\alpha_{\phi}^{yield}(E_{PUR}^{490})$  to follow the 1:1 line in Figure 4.10 as closely as possible. This led to a scaling factor of 0.4, such that the final relationship for the quantum yield is

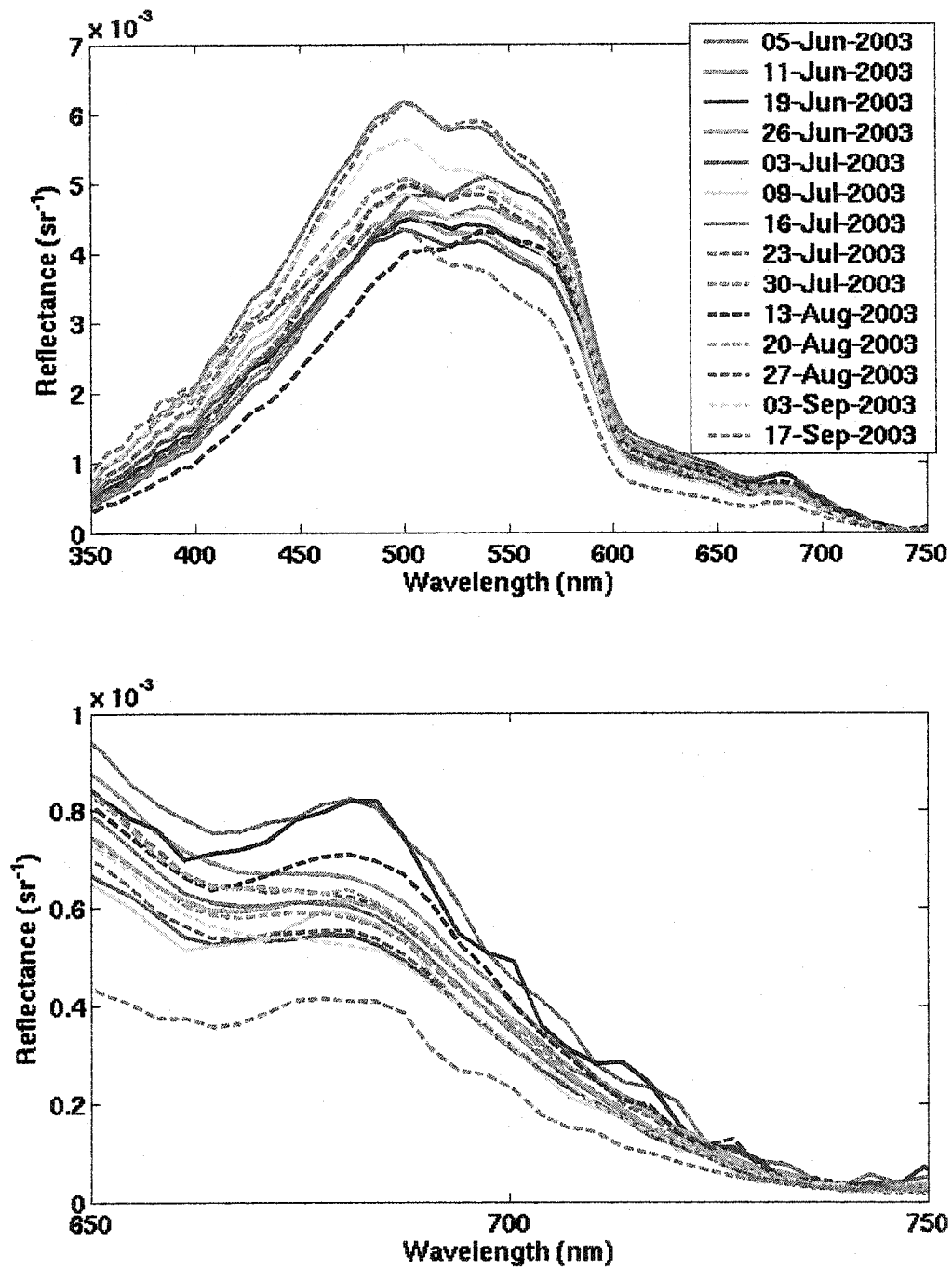


**Figure 4.9:** Selected reflectance spectra for the inversion. The spectra were selected to follow immediately the time of the discrete samples. Top panel: full spectrum. Bottom panel: Fluorescence region only.

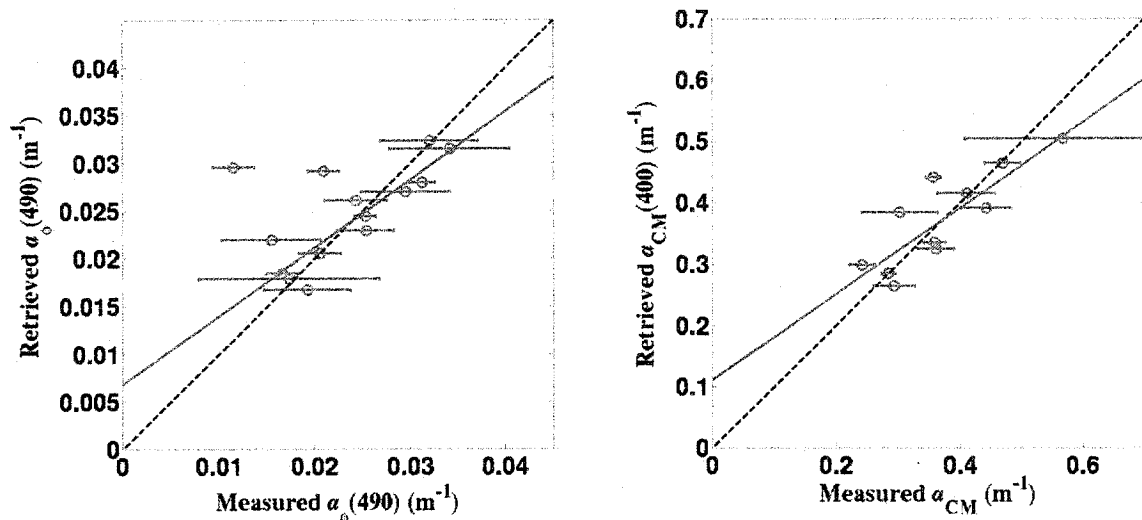


**Figure 4.10: Comparison of measured and retrieved absorption coefficients at LMB1 buoy during the summer of 2003. Left panel: absorption by phytoplankton at 490 nm. Measured points are the mean of four samples from two sets of duplicate measurements of absorption by phytoplankton collected at 1 and 7 meters. The error bars represent one standard deviation of the same measurements. Right panel: absorption by non-algal colored matter. Points represent the mean of two measurements of CDOM plus detritus absorption (1 and 7 meters) from the extracted samples of the phytoplankton filter. On both panels, the dashed black line is the 1:1 line and the blue line is a linear fit to the data (using a robust fitting technique).**

given by:  $\varphi_f = \varphi_f(E_{PUR}^{490}) = 0.4 a_{\varphi}^{yield}(E_{PUR}^{490})$ .

Absorption by non-algal colored matter at 400 nm (mostly from  $K_d(380)$  and reflectance from 380-400 nm) is similarly well retrieved, the large error bars on some of the measurements stem from the large variability with depth in the absorption. Because the absorption coefficient retrieved using the inversion model is a complicated weighted average with depth of the colored matter absorption, it is hard to provide rigorous estimates of the real error bars. As such, the error bars presented should be interpreted as a measure of the variability observed at that station near the time of the reflectance measurement plus analytical errors. Usually, analytical errors are small compared to the natural variability between different depths (0 and 7 m) where the discrete water samples are taken.

#### **4.5 Discussion**

The model used in this chapter to describe the upwelling fluorescence radiance is very similar to models developed by others (e.g. Ostrowska et al. 1997; Maritorena et al. 2000; Morrison 2003). Adapting it to the TSRB and recasting it for direct incorporation in the inverse model of reflectance was mostly a matter of accounting for the geometry of the TSRB. Therefore, the results for the retrieval of the quantum yield will be as accurate as those obtained by others as long as the geometry of the sensors was accounted for correctly and that the optical properties of the water and absorption by phytoplankton are retrieved correctly by the inverse model. For the retrieval of phytoplankton absorption, the main limitation is the variability in the quantum yield in surface waters.

#### 4.5.1 *Origin of non-random residuals*

The residuals in the Bering Sea are clearly not randomly distributed in the fluorescence band. The shape of these residuals led me to suspect at first an overestimate of the absorption effect by the red band of the phytoplankton. This effect can be due to the reabsorption inside the cells (Collins et al. 1985), or outside the cells (Babin et al. 1996b; Maritorena et al. 2000). A quick look at the measured and retrieved  $K_d$ , would suggest that the overestimate of  $K_d$  in this band is the source of the problem (this should also lead to an overestimate in  $a_f$ ). However, even if care was taken to calculate  $K_d$  as close as possible to the surface, it is possible that an effect of fluorescence or Raman could be decreasing the amplitude of the measured  $K_d$  in the red band. Furthermore, the fluorescence measurements from the flow through system on board the ship show that the measurements of  $K_d$  were made when the phytoplankton fluorescence was ~10 to 20% lower than during the reflectance and absorption measurements. This is consistent with small simultaneous changes in salinity and temperature. No effect of light on the flow through fluorescence was observed at this station. This is probably due to the ~1-2 minute delay between the intake and the fluorescence measurements which would allow much of the energy-dependent non-photochemical quenching to relax (see Chapters 2 and 3).

##### 4.5.1.1 *In water reabsorption*

To test the possibility that reabsorption in the water is overestimated, I removed altogether the phytoplankton absorption from the  $a_f$  parameter and redid the fit, the residuals maintained a very similar shape. I concluded that the reabsorption in the water

was not the sole source of the error.

#### 4.5.1.2 Intracellular reabsorption

To verify that the shape of the residuals was not due to the effect of intracellular reabsorption I used five fluorescence emission spectra (see Figure 4.2):

- 1) *Cryptomonas* sp. This spectrum was obtained from Marcel Babin (from Sciandra et al. 2000). It has strong emission due to phycobilins.
- 2) *Thalassiosira pseudonana* Used in the base model. Described earlier (See Results).
- 3) *Dunaliella tertiolecta* Different reabsorption coefficients were applied to the spectrum using the shape provided in Collins et al. (1985).
- 4) Gordon (1979) used a spectrum for fluorescence based on a Gaussian shape centered at 685 nm and with a standard deviation of 10.6 nm.
- 5) Ostrowska et al. (2000a) used a spectrum based on a Gaussian shape centered at 683 nm and with a standard deviation of 8.55 nm.

The smallest residuals were obtained for the spectrum for *T. pseudonana* used in the standard inversion while all others showed stronger non-random residuals. The *Cryptomonas* sp. spectrum did not provide appropriate fits. This clearly shows that the spectrum chosen for the fit is important, as residuals in the fluorescence band will influence the fit for the rest of the spectrum. In many studies of sun-induced fluorescence, the spectrum provided by Gordon is used (Topliss and Platt 1986; Abbott and Letelier 1999; Maritorena et al. 2000). Another important point about these spectra is that chlorophyll fluorescence is not restricted to a narrow Gaussian band but rather extends

with significant fluorescence up to about 750 nm (not shown on graph). This will have implications for the absolute value of the retrieved quantum yield, as the value used for the normalization of the spectrum should take into account the whole emission band. This can lead to errors of the order of approximately 10-20%.

#### 4.5.1.3 Depth variations in the quantum yield

Another effect that can change the shape of the fluorescence signal observed at the sensor is the non-uniformity of the phytoplankton absorption or quantum yield below the sensor. The first is unlikely on scales of a few meters near the surface, however the second is well documented and a decrease near the surface in the yield is expected due to non-photochemical quenching. Increase with depth of the quantum yield by a factor of 2-3 can be expected in the first 5 meters (Morrison 2003). In fact at the station studied in the Bering Sea, the fluorescence measured using a profiling fluorometer increased from ~5 (relative units) at the surface to ~12 at 5 meters without significant trends in absorption at 676 nm as measured with an ac-9 (WET labs) over that depth interval, suggesting that all changes were due to changes in the quantum yield. Assuming that the quantum yield can be modeled, in a first approximation, as a linear function of depth:

$$\varphi_f(z) = \varphi_{f0} + m_f z \quad 4.24$$

Using  $\varsigma(z, \lambda_{ex} \rightarrow \lambda) = f_{fQ}(\lambda) \varphi_f(z)$  and replacing this yield for  $\varphi_f(z)$  by the right hand side of equation 4.24 in equation 4.7 we find that the model for upwelling radiance at depth  $z$  becomes

$$L_{uf}(\lambda, z) = \frac{1}{4\pi} Q_a^*(\lambda) f(\lambda) \left[ \int_{400}^{700} \varphi_{f0} \frac{a_\varphi(\lambda_{ex}) \mathring{E}(\lambda_{ex}, z)}{K(\lambda_{ex}) + a_f(\lambda)} + m_f \frac{a_\varphi(\lambda_{ex}) \mathring{E}(\lambda_{ex}, z)}{[K(\lambda_{ex}) + a_f(\lambda)]^2} d\lambda_{ex} \right] \quad 4.25$$

Using this model, the new term changes the shape of the fluorescence spectrum at the surface by decreasing emission more where absorption in the water is high. This is because a greater fraction of the fluoresced light originates deeper. Including this formulation in the inversion model and increasing the  $m_f$  parameter from 0 to 0.05 increased the residuals. I thus conclude that non-uniformity of the quantum yield cannot be the reason for the non-random residuals of the fit. Negative values of  $m_f$  would imply a decreasing quantum yield with depth near the surface, which is inconsistent with observations.

#### 4.5.1.4 *Fluorescence by other pigments*

Another possibility to explain the non-random residuals is the presence of another fluorescing pigment in the same wavelength region but with a slightly different emission spectrum. Such fluorescing pigments are certainly present in these waters since the fluorometric determination of chlorophyll *a* also provided an estimate of the phaeophytin *a* concentration, which amounted to 3.55 mg chl eq. m<sup>-3</sup> in the mixed layer. This would mean that ~ 10-15% of the fluorescence emission in the Turner Designs fluorometer originated from pigments other than chlorophyll *a* (e.g. SooHoo and Kiefer 1982b; SooHoo and Kiefer 1982a). Consistent with this finding, at that station, fluorescence at 670 nm (excited with 405 nm) by pigments other than chlorophyll *a* (i.e. chlorophyllide *a*, phaeophorbide *a*, phaeophytin *a*) amounted to about 1/3 of the chlorophyll *a* fluorescence in the HPLC eluant. Although, this does not provide any spectral resolution of the peak, it could significantly affect the shape of the fluorescence emission (equivalent to  $f_{f0}(\lambda)$  but for all pigments instead of for chlorophyll *a* only) and could

lower the residual in the fluorescence band, especially if the emission was at a waveband shorter than the emission by chlorophyll *a* (see Figure 4.5).

#### *4.5.1.5 Inversion model and spectral smoothing*

At least two other possibilities remain to explain the non-random residuals in the fluorescence band. One possible source of this discrepancy is an inappropriate choice for the backscattering spectrum for the inversion. This can occur due to the influence of the blue-green part of the spectrum strongly influencing the shape of the backscattering spectrum and not representing the red end correctly. If the blue-green region is removed from the fitting procedure, it means that the prescribed spectral components can take any value in the blue-green region as long as they fit the orange-red region correctly. In the orange red region of the spectrum, phytoplankton and CDOM have little influence on the reflectance and most of the variability originates from changes in the backscattering coefficient, and fluorescence. Indeed fitting only wavelengths greater than 600 nm provided much lower residuals in the fluorescence band (while however returning values for absorption that are unrealistically low).

Another possibility to explain the residual is that the TSRB bandwidth does not correspond to the bandwidth of the measurement of the IOPs such that the TSRB is smoothing over the sharp features in the reflectance spectra while those features are present in the modeled spectra. Smoothing the spectral components with a 10 nm (3 point running average) did indeed provide a better fit in the red region while having little effect in the other spectral regions.

Because the objective of this chapter is not to describe or work on inverse models

of reflectance, but rather to describe a fluorescence model to be used with them, I will only suggest that a way of testing that the inverse model is accurately retrieving the reflectance due to the backscattered radiance in the fluorescence band is to ascertain that the radiance reflectance in the 600 to 650 waveband is retrieved accurately. In this band, backscattering by particles is the dominant source of variability such that it provides a good test to the validity of the underlying reflectance model in the fluorescence band. Any discrepancy in the 600-650 nm region will lead to a poorer estimate of the backscattered reflectance radiance in the fluorescence band.

In the case of the Bering Sea however, the temporal changes in the quantum yield should not be influenced by any discrepancies in the backscattering model since the shapes of the model parameters and their amplitudes stayed constant during the timeseries while the retrieved quantum yield varied. The highly variable spectral slope of the particle backscattering spectral shape should not lead to errors in the quantum yield as errors between these two parameters are not correlated (see appendix II). It is possible however, that the absolute value of the quantum yield may be biased, compared to one that would be retrieved if the reflectance due to backscattering were perfectly retrieved.

#### ***4.5.2 Bering Sea timeseries***

We can speculate that the variability in the quantum yield on the order of the minute that is observed in the time series may be due to coherent mixing processes, such as Langmuir cells (Thorpe 2004). In this case, the upwelling water on one side of the cell would have a higher yield as high levels of non-photochemical quenching would have been achieved in while on the other side of the Langmuir cell, the algal cells would be

quenched and have a lower yield. The TSRB could have been crossing many of these cells as the ship was drifting during the measurement (the ship's position was not dynamically maintained). It is not clear, however, if the Langmuir circulation timescales are fast enough to lead to such asymmetric levels of quenching. The rapid decline in the fluorescence yield upon increase in the incident irradiance (see Figure 4.11) clearly reflects non-photochemical quenching.

#### 4.5.3 Lunenburg Bay inversion

The Lunenburg inversion uses a dependence of the quantum yield of fluorescence on incident irradiance to retrieve phytoplankton absorption from sun-induced fluorescence. This is the first time such dependence has been applied to the retrieval of phytoplankton biomass from natural fluorescence measurements. Although this approach has been advocated by Cullen and Lewis (1995) for active fluorescence, it has rarely been applied. Without using this dependence, a decrease in phytoplankton absorption is retrieved by the model at high irradiance. The mean curve computed for the summer of 2003 suggests that over the range of irradiances measured, the quantum yield of fluorescence varies by a factor of  $\sim 3$ , *this is a considerable source of variability as it means that within one day, the observed changes in the phytoplankton absorption could be as large as those observed over the whole season during the weekly sampling (see Figure 4.10)*. Similarly, because the incident PAR irradiance at the surface is not necessarily a good predictor of the PUR irradiance at 0.65 meters (Figure 4.8, bottom), an accurate description of the latter is essential otherwise errors on the order of 40% are unavoidable in highly attenuating waters in the phytoplankton absorption. The same

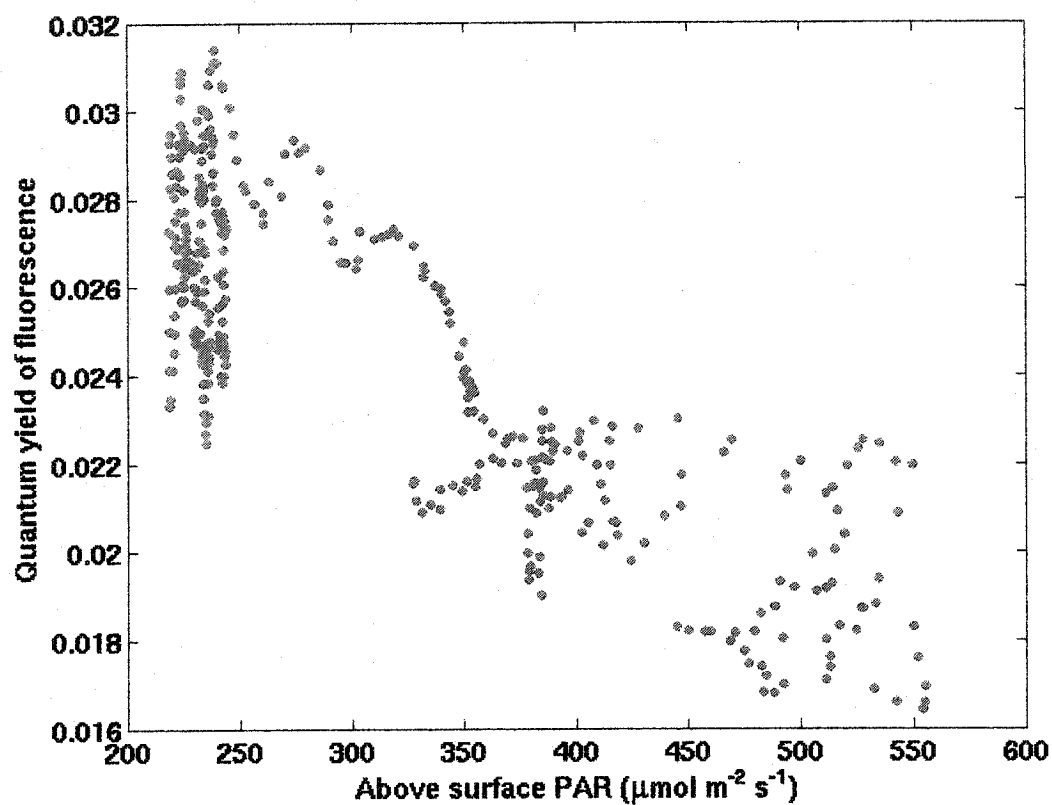


**Figure 4.11: Retrieved quantum yield versus irradiance for the Bering Sea timeseries (Figure 4.4). The decrease in quantum yield with irradiance is due to an increase in non-photochemical quenching.**

applies to regions where phytoplankton absorption is strong such as in the Bering Sea, since phytoplankton absorption, by definition, has a strong influence on changes of PUR with depth.

#### **4.5.4 *Comparison with published work***

Most determinations of the quantum yield of fluorescence in oceanic waters have involved the deployment of a profiling device and the collection of discrete samples to measure the quantum yield of fluorescence at discrete depths (Topliss and Platt 1986; Ostrowska et al. 1997; Maritorena et al. 2000), this is a tedious analysis, which provides only a few data points. Others have used simple models to approximate the absorbed irradiance by using the remote sensing chlorophyll concentration multiplied by the incident irradiance above the surface (Letelier et al. 1997). A more complete parameterization which attempts to account for variability in the optical properties of the water has also been used (e.g. Schallenberg et al. 2002). This has allowed the determination of continuous time series of a proxy of the quantum yield. In the case of the MODIS sensor, an inverse model is used to invert the reflectance in the blue and green region to obtain the absorption by phytoplankton and the attenuation coefficient whereas an independent measure of the baseline corrected fluorescence signal is used to obtain an estimate of the quantum yield (Abbott and Letelier 1999; Carder et al. 2003) (See also Chapter 5).

One of the greatest difficulties in most natural fluorescence studies is the separation of the fluorescence signal from the backscattered background signal (See Chapter 5). Roesler and Perry (1995) showed that the use of an inverse model of

reflectance provides a good tool for this purpose in as much as the backscattered spectrum is well represented. The use of an inverse model with depth profiles of irradiance has also been carried out by Morrison (2003), who emphasized the difficulty in separating the fluorescence signal from not only the backscattered light but also from the Raman signal (see also Maritorena et al. 2000). My model has this limitation with respect to Raman scattering, though it is of limited consequence at the surface in coastal waters or waters with high attenuation coefficients (Morel and Gentili 2004). Hu and Voss (1998) use a different method to separate the inelastic radiance by using highly resolved spectra (resolution  $\sim 0.008$  nm) to measure the filling of Fraunhofer lines (and in the case of fluorescence an atmospheric oxygen absorption line). This technique requires very specialized spectrophotometers, which are rarely used in ocean optics studies.

The model presented here goes beyond most other models by providing a framework that is optimized for one instrument and permits the determination of both the quantum yield of fluorescence if the phytoplankton absorption is known and the phytoplankton absorption coefficient if the quantum yield of fluorescence is estimated. The use of a measured fluorescence emission spectrum for the spectral components in an inverse model is also the first application of its kind. The inclusion of fluorescence in the inverse model instead of as an additional step after the retrieval of the IOPs with the inverse model is also novel, and allows for an extended spectral range for the inversion.

The utilization of fluorescence to retrieve the biomass of phytoplankton has focused mostly on chlorophyll concentration (Neville and Gower 1977; Gower and Borstad 1990; Fell et al. 2000). In this approach, I concentrate on the retrieval of

phytoplankton absorption. This should not be a limitation as, for many applications, the phytoplankton absorption is preferable to a measure of chlorophyll concentration (Perry 1994) and provides a more direct link between primary productivity and ocean color.

#### **4.6 Conclusions**

I presented a model of fluorescence that can be readily adapted to a commercially available and widely used instrument in the ocean optics community. The model relies heavily on the accurate retrieval of the inherent and derived optical properties and in particular the accurate representation of the backscattering spectrum and amplitude. The use of such a model opens the door to more long term, moored or drifter based studies of the absolute quantum yield of fluorescence. It could be used for example for long-term studies of physiological changes in the phytoplankton community as influenced by environmental effects. Such studies are very hard to conduct with the limited number of samples that can be acquired during traditional sampling programs such as those involving weekly or monthly sampling, or those based on ship cruises. This approach further provides the opportunity to study changes in the quantum yield on the timescale of minutes to years.

# *Chapter 5 New algorithms for MODIS sun-induced chlorophyll fluorescence and a comparison with present data products*

## **5.1 Preface to chapter 5**

This chapter is in press in *Limnology and Oceanography: Methods*. The bibliographic reference is: *Huot, Y., C. A. Brown, and J. J. Cullen. 2004. New algorithms for MODIS sun-induced chlorophyll fluorescence and a comparison with present data products. Limnology and Oceanography: Methods*. I was responsible for most of the work in this paper, including the developing the model and taking the lead role in writing the manuscript.

## **5.2 Introduction**

The launch of the MODIS instrument (Esaias et al. 1998), with a waveband dedicated to the measurement of sun-induced chlorophyll fluorescence, has taken remote sensing of marine phytoplankton in a new direction. In theory, it is now possible to obtain a global quasi-synoptic assessment of near-surface fluorescence emission and its quantum yield. While the remote measurement of in vivo fluorescence emitted by phytoplankton is in principle straightforward (but see Letelier and Abbott 1996), obtaining an estimate of the quantum yield of fluorescence (the ratio of fluoresced to absorbed photons by phytoplankton) requires a complex algorithm (Abbott and Letelier 1999). Yet, this physiological measurement could foster a major leap in our understanding of the ocean by providing global coverage of a parameter linked to algal physiology (Kiefer and

Reynolds 1992) and species composition (Loftus and Seliger 1975; Heaney 1978). In this study, we review the sources of variability of sun-induced fluorescence as they affect the MODIS data products and examine how they relate to the retrieval of the quantum yield of fluorescence and chlorophyll concentration. We propose new algorithms based on semi-empirical relationships from the bio-optical literature and compare our results to MODIS data products.

### **5.3 Nature of the MODIS fluorescence measurement**

*Quantum yield of chlorophyll fluorescence* — In this study, we define the quantum yield of chlorophyll *a* fluorescence in vivo ( $\phi$ , dimensionless; see Table 5-1 for symbols and definitions) as the ratio of photons fluoresced by chlorophyll *a* over the whole fluorescence band to the photons absorbed by all cellular pigments. Others have referred to this as the *apparent quantum yield of chlorophyll a fluorescence*, limiting the term quantum yield of chlorophyll *a* fluorescence to the ratio of photons fluoresced by chlorophyll *a* (or by chlorophyll *a* associated with photosystem II (PSII)) to those absorbed only by photosynthetic pigments associated with PSII (e.g. Gilmore and Govindjee 1999). This distinction is important for the physiological interpretation of remote sensing data and for the comparison with laboratory measurements (see Appendix IV).

There are three important proximate physiological processes that influence the quantum yield of chlorophyll fluorescence as defined here: 1) photochemical quenching (PQ); 2) non-photochemical quenching (NPQ) (Krause and Weis 1991); and 3) the

**Table 5-1: List of symbols and units.**

Symbol	Description	Units
$a_{gilvin}$	Absorption coefficient for colored dissolved matter	$m^{-1}$
$a_f$	Attenuation of upwelling fluorescence radiance	$m^{-1}$
$a_\varphi, a_w$	Absorption coefficients for phytoplankton and water	$m^{-1}$
$a_{sol}^*$	Chlorophyll specific absorption in solution	$m^2 \text{ mg chl}^{-1}$
$a_\varphi^*$	Chlorophyll specific absorption coefficient for phytoplankton	$m^2 \text{ mg chl}^{-1}$
$\bar{a}_\varphi^*$	Irradiance weighted chlorophyll specific absorption coefficient	$m^2 \text{ mg chl}^{-1}$
$A_{abs}(z)$	Absorbed radiation per unit volume	$\text{mol } m^{-3} s^{-1}$
ARP	Instantaneous absorbed radiation by phytoplankton	$\text{mol } m^{-2} s^{-1}$
$C_f$	Proportionality factor, converting fluorescence measurements made at 678 nm to the whole fluorescence band	nm
$chl$	Chlorophyll <i>a</i> concentration	$\text{mg chl } m^{-3}$
$chl_{fluo}$	Our estimate of chlorophyll concentration using fluorescence	$\text{mg chl } m^{-3}$
$chl_{MODIS}$	MODIS estimate of chlorophyll concentration	$\text{mg chl } m^{-3}$
$CFE$	Chlorophyll fluorescence efficiency: MODIS estimate of $\varphi$	unitless
$dL_{em}$	Volume fluorescence emission	$\text{mol } m^{-3} s^{-1} sr^{-1}$
$E_{PAR}$	Irradiance in the photosynthetically available radiation waveband (400-700 nm)	$\text{mol } m^{-2} s^{-1}$
$\bar{E}(\lambda, z)$	Scalar irradiance	$\text{mol } m^{-2} s^{-1} nm^{-1}$
$FLH$	Fluorescence line height	$W m^{-2} \mu m^{-1} sr^{-1}$ or $\text{mol } m^{-2} s^{-1} nm^{-1} sr^{-1}$
$ipar$	Instantaneous scalar PAR irradiance just below the sea surface. A standard MODIS algorithm product.	$\text{mol } m^{-2} s^{-1}$
$K, K_d, K_{PAR}$	Attenuation coefficients for scalar, planar and PAR planar irradiance	$m^{-1}$
$K_{abs}^{\tau_f}, \tilde{K}_{abs}^{\tau_f}$	Fitted attenuation coefficients for absorbed radiation over the depth $z_{\tau_f}$ and results of numerical calculation	$m^{-1}$
$L_f$	Upwelling radiance due to fluorescence at the surface	$\text{mol } m^{-2} s^{-1} nm^{-1} sr^{-1}$

$Q_a^*$	Portion of emitted fluorescence not reabsorbed within the cell	unitless
$\beta_\varphi, \beta_{\varphi Q}, \beta_{\varphi a Q}$	Factors applied to the <i>FLH</i> to obtain $\varphi_{est}, \varphi_Q, \varphi_{aQ}$ , respectively	$\text{mol}^{-1} \text{ m}^{-1} \text{ s nm}$ $\text{sr mg chl}$
$z$	Depth	m
$z_{678}$	Depth from which fluorescence emission is attenuated by 63.2% at the surface. Used in MODIS algorithm	m
$z_{90}$	Depth at which 90% of the fluorescence radiance at the surface originates	m
$z_{\varphi}$	Depth at which 63.2% of the fluorescence radiance at the surface originates	m
$\varphi$	Real quantum yield of fluorescence in situ	unitless
$\varphi_{chl}$	Assumed quantum yield to retrieve chlorophyll concentration from fluorescence: $chl_{\text{fluor}}$	unitless
$\varphi_{est}$	Our estimate of the quantum yield of fluorescence	unitless
$\varphi_Q$	Coefficient retrieved using <i>FLH</i> and $\beta_{\varphi Q}$ ; equivalent to a retrieval of the estimated quantum yield if reabsorption within the cell is not accounted for	unitless
$\varphi_{aQ}$	Coefficient retrieved using <i>FLH</i> and $\beta_{\varphi a Q}$ ; variability in this term includes all physiological and species-specific optical influences on fluorescence emission.	unitless
$\lambda$	Wavelength	nm
$\theta'$	Zenith angle of observation in water	radians

fraction of light absorbed by photosynthetic pigments functionally associated with PSII relative to the total light absorbed by the cell. Photochemical quenching is the diminution of  $\phi$  due to energy flow to photochemical processes (photosynthesis) in competition with fluorescence emission (e.g. Kiefer and Reynolds 1992). With increasing light intensity, photosynthetic systems become saturated and the influence of PQ diminishes causing  $\phi$  to increase. Non-photochemical quenching is a decline of  $\phi$  due to competition with non-photochemical processes (dissipation of energy as heat in the pigment bed or reaction centers). The influence of NPQ is most important at light intensities that are super-saturating for the photosynthetic systems. Non-photochemical quenching is a consequence of downregulation, other photoprotective mechanisms, or damage to photosynthetic reaction centers (Long et al. 1994; Pospisil 1997; Müller et al. 2001). Polar-orbiting satellites record ocean color data close to midday under cloud-free conditions; surface irradiance is close to the daily maximum. Also, water absorbs strongly in the red fluorescence waveband, so the depth from which water-leaving fluorescence can be detected is limited to the upper 5 m or so (Babin et al. 1996b), where irradiance is also close to maximal. Non-photochemical quenching is thus important under these midday, clear-sky, near-surface conditions (Maritorena et al. 2000; Morrison 2003) and should be considered directly in the physiological interpretation of fluorescence measured from satellites (Dandonneau and Neveux 1997; Morrison 2003).

Independent of quenching, the fraction of light absorbed by photosynthetic pigments in PSII relative to that absorbed by photoprotective pigments and pigments

associated with PSI is directly proportional to the quantum yield (as defined in this study). This is because most chlorophyll fluorescence originates from chlorophyll *a* associated with PSII *in vivo*. This point is emphasized in Appendix IV.

Another factor influencing the observed fluorescence is the reabsorption of fluoresced light within the cell. The fraction reabsorbed varies spectrally and depends on the absorption efficiency of the cell and, therefore, on its size and internal pigment content (Morel and Bricaud 1981; Collins et al. 1985; Morel and Bricaud 1986). This effect has to be addressed to obtain an absolute and accurate measure of  $\phi$  (Babin et al. 1996b).

Furthermore, there are many indirect physiological influences on the quantum yield, which affect the magnitude of PQ, NPQ, and the absorption cross-section of PSII as a function of irradiance. These factors include the interaction of incident irradiance (e.g. Kiefer 1973a; Kiefer and Reynolds 1992; Kolber and Falkowski 1993; Ibelings et al. 1994) with the species composition (Heaney 1978; Campbell et al. 1998), state of light acclimation (Ögren 1994), and nutritional status (e.g. Kiefer 1973a; Cleveland and Perry 1987) of the algal communities.

Since  $\phi$  is dependent on algal physiological status (Falkowski and Kolber 1995), and physiological responses to environmental variability are adaptive features that can be related to taxonomy (Ibelings et al. 1994; Cullen and MacIntyre 1998), remote sensing of  $\phi$  could help describe spatial and temporal variability in physiological or trophic status of phytoplankton (depending on the dominant source of variability). While this is true in

theory, we still lack the quantitative — perhaps even the qualitative — framework to interpret variability in algal fluorescence under remote sensing conditions (Cullen and Lewis 1995). More importantly, before physiological interpretations are possible, we need to assess whether remote sensing images display real variability in  $\phi$  or simply environmentally driven biases in the algorithms. For this reason, we focus our study on the measurement, rather than the interpretation, of the quantum yield of sun-induced chlorophyll fluorescence.

*Wavelength of measurement* — MODIS measures the upwelling radiance at 676.7 nm (bandwidth 673 to 683 nm, henceforth referred to as the 678 nm waveband), whereas the maximum emission of fluorescence is around 683 to 685 nm. This offset was chosen to avoid an atmospheric oxygen absorption band at 687 nm (Letelier and Abbott 1996; Abbott and Letelier 1999; Gower et al. 2004). In addition to reducing the sensitivity, the offset places the measurement closer to the absorption peak at 676 nm for chlorophyll *a* in vivo, and consequently, measured fluorescence can be decreased by up to 40% by intracellular reabsorption. If the quantum yield is to be obtained accurately, careful corrections are required to account for the absorption of the emitted radiation both inside the cell (Collins et al. 1985; Babin et al. 1996b) and within the water column.

## **5.4 Theoretical background**

Theoretical descriptions of the oceanic fluorescence field have been published (e.g. Gordon 1979; Preisendorfer and Mobley 1988; Babin et al. 1996b; Abbott and Letelier 1999; Maritorena et al. 2000). For completeness, we describe the relationships

necessary to estimate the emission of fluorescence near the surface of the ocean from measurements of upwelling radiance.

Neglecting depth variations in  $\varphi$  (assumed to be small in the thin layer from which fluorescence is detected), the infinitesimally small amount of upwelling radiance due to fluorescence at the surface of the ocean ( $dL_f$ ,  $\text{mol m}^{-2} \text{s}^{-1} \text{sr}^{-1} \text{nm}^{-1}$ ) over a narrow waveband ( $\Delta\lambda$ , nm) centered at the emission wavelength  $\lambda_{em}$  originating from a thin layer of water at depth  $z$  (m) is:

$$dL_f(\lambda_{em}, z) = \frac{1}{4\pi} \cdot \frac{\varphi}{C_f} \cdot Q_a^*(\lambda_{em}) \cdot A_{abs}(z) \cdot e^{-a_f(\lambda_{em}) \cdot z} \cdot dz \quad 5.1$$

where the factor  $1/4\pi(\text{sr}^{-1})$  converts an isotropic fluorescence field to radiance;  $C_f(\text{nm})$  is the ratio of the emission in the whole fluorescence band to that observed over  $\Delta\lambda$  (assumed independent of reabsorption fraction, but see Collins et al. 1985);  $Q_a^*$  is a parameter accounting for the fraction of emitted radiation at  $\lambda_{em}$  not reabsorbed within the cell (see Babin et al. 1996b); and  $A_{abs}(z)$  is the flux absorbed by phytoplankton at depth  $z$  ( $\text{mol m}^{-3} \text{s}^{-1}$ ). In most case 1 waters, for the MODIS band, the attenuation coefficient for upwelling fluoresced radiance at 678 nm,  $a_f(678)$  ( $\text{m}^{-1}$ ), can be approximated as  $a_w(678) + a_\varphi(678)$  with  $a_w$  and  $a_\varphi$  being the absorption coefficients for water and phytoplankton, respectively (Maritorena et al. 2000). In the remainder of this paper the dependence on  $\lambda_{em} = 678$  nm is implicit. This description is valid for nadir viewing; for non-nadir viewing conditions  $a_f$  is replaced by  $a_f / \cos(\theta')$ , where  $\theta'$  is the zenith angle of observation in water (as defined in Morel and Gentili 1996).

Neglecting variations with depth of the optical properties of phytoplankton and water, the absorbed flux is described by:

$$A_{abs}(z) = \int_{400}^{700} a_{\varphi}(\lambda) \cdot \overset{\circ}{E}(\lambda, 0) \cdot e^{-K(\lambda) \cdot z} \cdot d\lambda \quad 5.2$$

where  $\overset{\circ}{E}(\lambda, 0)$  ( $\text{mol m}^{-2} \text{s}^{-1} \text{nm}^{-1}$ ) is the scalar irradiance just below the surface and  $K(\lambda)$  ( $\text{m}^{-1}$ ) is the attenuation coefficient.

Integration over depth provides the total amount of fluorescence radiance at the surface:

$$\begin{aligned} L_f &= \frac{1}{4\pi} \cdot \frac{\varphi}{C_f} \cdot Q_a^* \cdot \int_{400}^{700} \int_0^{\infty} a_{\varphi}(\lambda) \cdot \overset{\circ}{E}(\lambda, 0) \cdot e^{-(K(\lambda) + a_f) \cdot z} \cdot dz \cdot d\lambda \\ &= \frac{1}{4\pi} \cdot \frac{\varphi}{C_f} \cdot Q_a^* \cdot chl \cdot \int_{400}^{700} \frac{a_{\varphi}^*(\lambda) \cdot \overset{\circ}{E}(\lambda, 0)}{K(\lambda) + a_f} \cdot d\lambda \end{aligned} \quad 5.3$$

Here we used  $a_{\varphi} = chl \cdot a_{\varphi}^*$ , where  $a_{\varphi}^*$  is the chlorophyll specific absorption coefficient for phytoplankton ( $\text{m}^2 \text{mg chl}^{-1}$ ).

It is convenient for the formalism presented here to assume a wavelength independent quantum yield. This is rarely the case due to different efficiencies of exciton transfer for different pigment pools and different pigment distributions between PSII and PSI (e.g. Johnsen and Sakshaug 1996; Lutz et al. 1998; 2001), such that  $\varphi$  represents a mean quantum yield weighted by the absorbed irradiance:

$$\varphi = \frac{\int_{PAR} \varphi(\lambda) \cdot a_{\varphi}(\lambda) \cdot \overset{\circ}{E}(\lambda) \cdot d\lambda}{\int_{PAR} a_{\varphi}(\lambda) \cdot \overset{\circ}{E}(\lambda) \cdot d\lambda}.$$

Solving equation 5.3 for  $chl$  and  $\varphi$  gives:

$$\begin{aligned}
chl &= \frac{L_f \cdot 4\pi \cdot C_f}{\varphi \cdot Q_a^*} \cdot \left[ \int_{400}^{700} \frac{a_{\varphi}^*(\lambda) \cdot \overset{\circ}{E}(\lambda, 0)}{K(\lambda) + a_f} \cdot d\lambda \right]^{-1} \\
\varphi &= \frac{L_f \cdot 4\pi \cdot C_f}{chl \cdot Q_a^*} \cdot \left[ \int_{400}^{700} \frac{a_{\varphi}^*(\lambda) \cdot \overset{\circ}{E}(\lambda, 0)}{K(\lambda) + a_f} \cdot d\lambda \right]^{-1}
\end{aligned}
\tag{5.4}$$

*MODIS algorithms: FLH, ARP, and CFE* — Chlorophyll fluorescence efficiency

(*CFE*, unitless) is obtained by dividing an estimate of the amount of fluoresced light at the surface (*FLH*, see below) by the amount of light absorbed by phytoplankton in the upper water column (*ARP*, see below); hence, it is intended to provide an estimate of the quantum yield of fluorescence. This section provides a short description of the methods developed by the MODIS science team to obtain the *CFE*; a complete description is given in MODIS ATBD 19 (Carder et al. 1999a), 20 (Carder et al. 2003) and 22 (Abbott and Letelier 1999).

The fluorescence line height (*FLH*, provided in  $\text{W m}^{-2} \mu\text{m}^{-1} \text{sr}^{-1}$  and converted to  $\text{mol m}^{-2} \text{s}^{-1} \text{nm}^{-1} \text{sr}^{-1}$  for our calculations) is the MODIS measurement of  $L_f$  (see equation 5.3). The *FLH* is measured by subtracting from radiance at 678 nm the radiance due to backscattered and Raman scattered photons at 678 nm, which is estimated using a linear baseline between 667 nm and 748 nm. The MODIS FLH algorithm uses the top of atmosphere upwelling radiance, which is corrected for Rayleigh scattering, but not aerosol scattering, thus assuming that upwelling radiance is a linear function of wavelength for aerosol scattering.

By applying the Beer-Bouguer-Lambert law to photons emitted at depth, we can define a depth,  $z_{678}$ , at which the upwelling fluoresced radiance is attenuated by 63.2% at

the surface:

$$z_{678} \approx \frac{\cos(\theta')}{a_w(678) + a_\varphi(678)}. \quad 5.5$$

The amount of visible radiation absorbed by phytoplankton (*ARP*) over that depth is:

$$ARP = \int_{400}^{700} \int_0^{z_{678}} a_\varphi(\lambda) \cdot \overset{\circ}{E}(\lambda, 0) \cdot e^{-K(\lambda) \cdot z} \cdot dz \cdot d\lambda = \int_{400}^{700} a_\varphi(\lambda) \cdot \overset{\circ}{E}(\lambda, 0) \cdot \left[ \frac{1 - e^{-K(\lambda) \cdot z_{678}}}{K(\lambda)} \right] \cdot d\lambda \quad 5.6$$

where  $a_\varphi(\lambda)$  and  $K(\lambda)$  are retrieved by a semi-analytical model that also retrieves chlorophyll concentration and gilvin absorption (Carder et al. 1999a; Carder et al. 2003) using MODIS measurements of water-leaving radiance in all bands from 412 to 551 nm. Since it uses the band at 412 nm, this algorithm, despite its accuracy in many locations (Carder 2003), may be more affected by a poor atmospheric correction than empirical algorithms using only longer wavelengths: the 412 nm waveband shows the largest errors in retrievals (Gordon 2002b) even under ideal conditions. Note that the MODIS ATBD 20 (version 7) describes  $z_{678}$  as  $z_{685} \approx \cos(\theta') / [a_w(685) + a_\varphi(675)]$ . The waveband for water is from an older specification of the MODIS sensor and the algorithm will be changed to 678 nm (i.e., equation 5.5) to reflect the present specifications (Ken Carder pers. comm.).

The *CFE* is obtained as  $CFE = FLH / ARP$ . To compare with equation 5.4 for  $\varphi$  this can be written as (using 5.6):

$$CFE = FLH \cdot 4\pi \cdot C_f \cdot \left[ \int_{400}^{700} a_\varphi(\lambda) \cdot \overset{\circ}{E}(\lambda, 0) \cdot \left[ \frac{1 - e^{-K(\lambda) \cdot z_{678}}}{K(\lambda)} \right] \cdot d\lambda \right]^{-1} \quad 5.7$$

where  $C_f = 43.38$  nm for the MODIS bands and was calculated as

$$C_f = \int_{-\infty}^{\infty} f(\lambda) \cdot d\lambda / (f(677) - \text{baseline}(677)) \text{ where } f(\lambda) \text{ is the fluorescence emission}$$

spectrum (assuming a Gaussian distribution with a width at half-maximum of 25 nm centered and normalized to 683nm),  $f(677)$  is the same Gaussian evaluated at 677 nm and  $\text{baseline}(677)$  is the value of a linear baseline from 665 to 747 nm at 677 nm (Ricardo Letelier pers. communication). In practice, a small constant is added to  $FLH$  before dividing by  $ARP$  to account for negative values of  $FLH$  encountered at low chlorophyll concentrations under remote sensing conditions (see below, and Abbott and Letelier 1999). The use of 677 nm is consistent with the MODIS band for fluorescence emission being centered at 676.7 nm.

## 5.5 Procedures

*Analysis of MODIS data* — MODIS level 3 datasets from reprocessing version 4.0 were obtained from the Goddard Distributed Active Archive Centers (DAAC) for 15 January 2001 (inspection of data from the 4.1 reprocessing shows very little change for the regions and days studied). The dataset comprises: three estimates of chlorophyll concentration (case 1 pigment algorithm, case 2 algorithm and SeaWiFS analog);  $CFE$ ;  $ARP$ ;  $FLH$ ; sea surface temperature; the attenuation coefficient at 490 nm ( $K_d(490)$ ,  $m^{-1}$ ); an instantaneous estimate of the photosynthetically available radiation (PAR) irradiance at the time of the satellite overpass (based on the model of Gregg and Carder 1990, referred to as  $ipar$ ) (see ATBD 20); and quality flags. We used the SeaWiFS analog chlorophyll algorithm (SeaWiFS algorithm using MODIS bands, switching between

reflectance ratios 443/551 and 488/551) to compare our algorithm for chlorophyll from fluorescence with those of MODIS. Two other chlorophyll algorithms are used during a sensitivity analysis of our algorithms. The case 2 algorithm is a semi-analytical inversion algorithm and also retrieves the absorption by gilvin (Carder et al. 1999b) while the case 1 water algorithm is an empirical relationship based on HPLC chlorophyll concentration and a blue to green waveband ratio (Clark 1999). The algorithm for the attenuation coefficient at 490 nm is described in Clark (1999) and Mueller (2000); it uses a power function of the ratio of the water leaving radiance at 488 and 551 nm. Larger uncertainties in this algorithm are expected with an increasing attenuation coefficient: from 18% at  $K_d(490) < 0.2 \text{ m}^{-1}$  to 50% at  $K_d(490) > 0.3 \text{ m}^{-1}$  (Clark 2001). In our algorithms, we used the standard *FLH* product such that a small value,  $FLH_0$ , has been added to *FLH* to avoid negative radiances encountered due to the top of the atmosphere (minus Rayleigh scattered radiance) measurement of *FLH*.

Two subscenes were selected for examination: one from the Arabian Sea and one off the west coast of Central America including the Costa Rica Dome. Only pixels that achieved the highest quality level (quality flag = 0) set by the ATBD were included in the analysis.

Note that the ipar product, despite being validated, had some spatial inconsistencies, especially near the sunglint region. The regions chosen for this analysis are relatively far from the main region of sunglint and should not be greatly affected. In any case, this should not influence the comparison of the MODIS *CFE* and our quantum yield as they will both be affected equally. However, the *CFE* or our estimate of the yield

may show trends vs. ipar or increased variability that are not natural. The ipar algorithm is being corrected by the MODIS science team.

## 5.6 The algorithms

*Overview* — We will now describe two new fluorescence algorithms for retrieving chlorophyll concentration and the quantum yield. The *FLH* contains information on both the quantum yield of fluorescence and chlorophyll concentration (see equation 5.4); however, to obtain information about one requires assumptions about — or measurement of — the other.

In case 1 waters (Morel and Prieur 1977), variability in the optical characteristics of the water column are influenced mostly by the abundance of phytoplankton and associated materials. This characteristic has allowed the development of ocean color algorithms based on phytoplankton biomass (expressed in terms of chlorophyll concentration). In this study, we use the diffuse attenuation coefficient at 490 nm ( $K_d(490)$ ,  $\text{m}^{-1}$ ) instead of chlorophyll to characterize trends of optical properties. This approach is similar to the one proposed by Babin et al. (1996b); however, we depart from their chlorophyll-based approach, thereby deriving an estimate of *chl* from fluorescence emission that does not require another estimate of *chl* as input. It should be stressed that both the standard chlorophyll algorithms and  $K_d(490)$  are obtained using ratios of the blue to green upwelling radiance; in case 1 waters, phytoplankton absorption and covarying matter are the dominant sources of variability affecting the blue to green ratio. Hence,  $K_d(490)$ , phytoplankton absorption, and chlorophyll concentration are strongly

correlated to each other (Morel and Maritorena 2001) in these waters. **Our chlorophyll algorithm should be considered an approach using information from both the blue to green ratio and fluorescence region to estimate chlorophyll.** Furthermore, we consider  $K_d(490)$  to be a more direct descriptor of the optical properties of the water column than chlorophyll, as it is directly dependent on the inherent optical properties (Kirk 1994) which themselves, in addition to the angular dependence of the light field, define the water leaving radiance measured by MODIS (e.g. Morel et al. 2002).

The empirical relationships required between  $K_d(490)$  and the optical properties of phytoplankton and the water column are those that will specify a simplified version of equation 5.4 and allow the retrieval of  $\phi$  and  $chl$ . Assuming that  $FLH$  retrieves  $L_f$  perfectly we can write:

$$FLH = \frac{chl \cdot Q_a^* \cdot \phi \cdot \bar{a}_\phi^* \cdot \bar{E}_{PAR}(0)}{4\pi \cdot C_f} \cdot \left[ K_{abs}^{\tau_f} + \frac{a_f}{\cos(\theta')} \right]^{-1} \quad 5.8$$

The parameter  $K_{abs}^{\tau_f}$  is the attenuation coefficient for downwelling absorbed irradiance, evaluated to depth,  $z_{90}$ , where 90% of the fluorescence radiance at the surface originates, and  $\bar{a}_\phi^* = \int_{PAR} a_\phi^*(\lambda) \cdot \bar{E}(\lambda, 0) \cdot d\lambda / \int_{PAR} \bar{E}(\lambda, 0) \cdot d\lambda$  is the irradiance-weighted chlorophyll specific absorption coefficient (e.g. Morel 1978). In this work, the value of  $K_{abs}^{\tau_f}$  satisfies the following equation in a least square sense from  $z = 0$  to  $z_{90}$ :

$$\ln \left[ A_{abs}(z) / A_{abs}(0^-) \right] = -K_{abs}^{\tau_f} \cdot z \Big|_{z=0}^{z_{90}}.$$

The relationships to be specified are  $Q_a^*$ ,  $\bar{a}_\phi^*$ ,  $a_f$ , and  $K_{abs}^{\tau_f}$  as a function of  $K_d(490)$

(Figure 5.1), and are described in the next sections.

Equation 5.8 represents almost all of the spectral effects in equation 5.3 in a much simpler form. This is accomplished in two ways. Firstly,  $\bar{a}_\phi^*$  is parameterized as a function of  $K_d(490)$  at the surface, thereby accounting for the variability in the phytoplankton absorption spectrum as a function of trophic status (Bricaud et al. 1995; Ciotti et al. 1999; Ciotti et al. 2002). We approximate  $\bar{a}_\phi^*$  as  $a_\phi^*(512)$ , which can be done since phytoplankton absorption at 512 nm is nearly equal to  $\bar{a}_\phi^*$  over the photosynthetically available radiation range (PAR, 400-700 nm) for a wide range of phytoplankton absorption spectra (Bricaud et al. 1995; Ciotti et al. 2002) and a typical solar irradiance spectrum at the surface (data not shown). Secondly, the depth dependence of the spectral light field influencing phytoplankton fluorescence is well accounted for by the attenuation coefficient for the absorbed irradiance (described below).

*Deriving  $Q_a^*$ ,  $\bar{a}_\phi^*$ , and  $a_f$  as functions of  $K_d(490)$  —* To derive relationships for  $Q_a^*$ ,  $\bar{a}_\phi^*$  and  $a_f$  we used the models of: 1) Bricaud et al. (1995) relating  $a_\phi^*(\lambda)$  to *chl*; and 2) Morel and Maritorena (2001) relating *chl* and  $K_d(\lambda)$ . We solved for  $a_\phi(678)$  ( $\text{m}^{-1}$ ),  $a_\phi^*(678)$  ( $\text{m}^2 \text{ mg chl}^{-1}$ ), and  $\bar{a}_\phi^*$  ( $\text{m}^2 \text{ mg chl}^{-1}$ ) as functions of  $K_d(490)$ :

$$a_\phi(678) = 0.4762 \cdot (K_d(490) - 0.016)^{1.22} \quad 5.9$$

$$a_\phi^*(678) = 0.0106 \cdot (K_d(490) - 0.016)^{-0.229} \quad 5.10$$

$$\bar{a}_\phi^* = a_\phi^*(512) = 0.00663 \cdot (K_d(490) - 0.016)^{-0.3611} \quad 5.11$$

The parameter  $Q_a^*$  was obtained from the ratio  $a_\phi^*(678)/a_{sol}^*(678)$

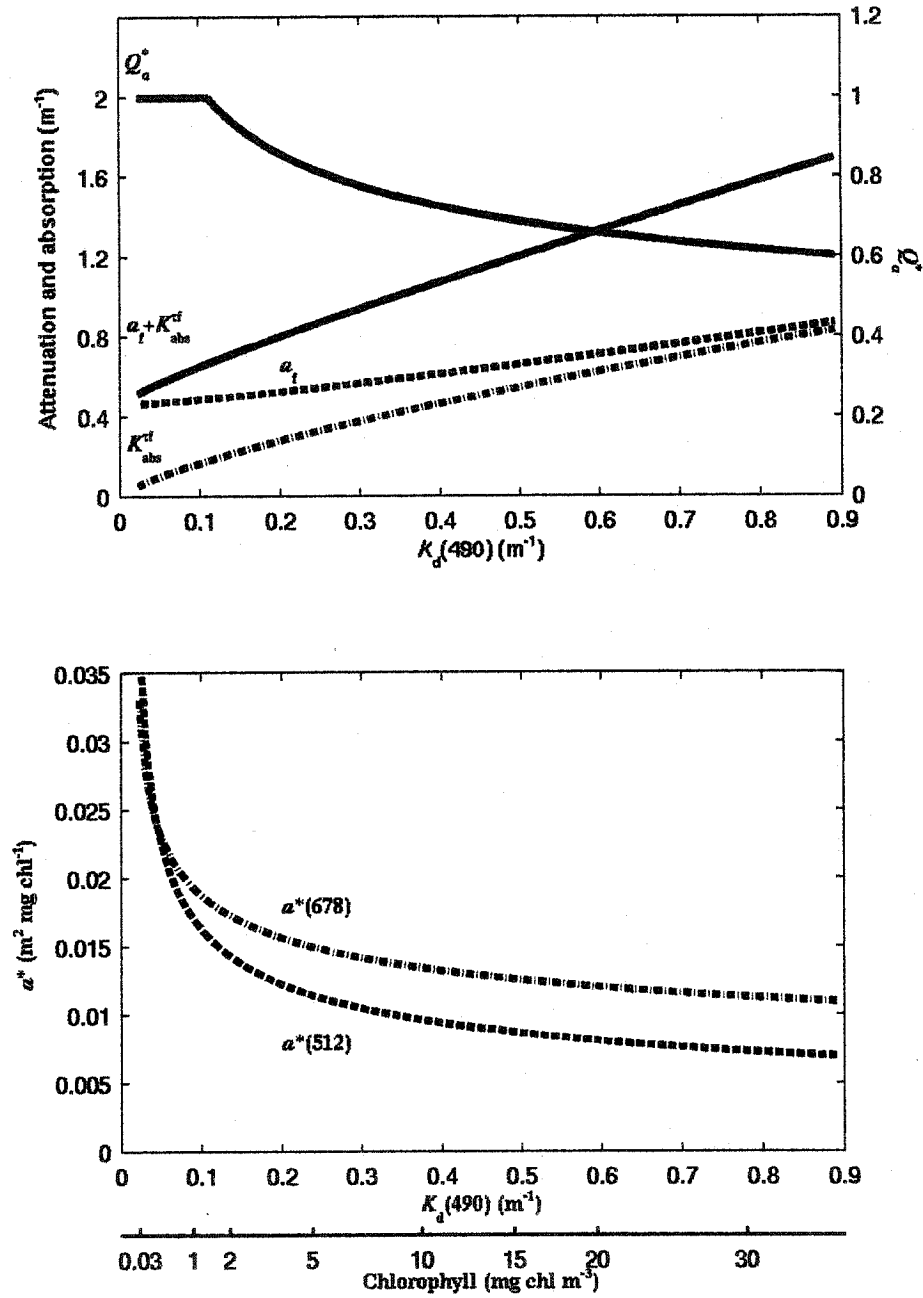


Figure 5.1: Relationships between the optical properties of phytoplankton and water. Top:  $Q_a^*$ ,  $a_f$ , and  $K_{abs}^{\tau_f}$ . Bottom:  $a^*(512)$  and  $a^*(678)$ . These parameters are applied to the upwelling fluorescence radiance to retrieve chlorophyll and  $\phi$  in our algorithms; see text and Table 1 for description of symbols. The bottom axis shows the chlorophyll concentration for a given  $K_d(490)$  from the relationship of Morel and Maritorena (2001).

(Morel and Bricaud 1981) where  $a_{sol}^*(678)=0.0182 \text{ m}^2 \text{ mg chl}^{-1}$  is the chlorophyll specific absorption coefficient for chlorophyll in solution (Bidigare et al. 1990). Using this relationship, we find that when  $K_d(490) < 0.11 \text{ m}^{-1}$ ,  $Q_a^* > 1$ , which is physically unrealistic. Thus,  $Q_a^*$  has been set to 1.0 for  $K_d(490) < 0.11 \text{ m}^{-1}$  (see Figure 5.1). We used  $a_f = a_w(678) + a_\phi(678)$  where  $a_w(678)$  is  $0.461 \text{ m}^{-1}$  from Pope and Fry (1997).

Babin et al. (1996b, their equation 3) described a relationship for  $\bar{a}_\phi^*$ , which, when recast in terms of  $K_d(490)$ , is  $\bar{a}_\phi^* = 0.00605 \cdot (K_d(490) - 0.016)^{-0.3727}$ . This is less than 10% different from our parameterization of  $\bar{a}_\phi^*$  over chlorophyll concentrations ranging from 0.03 to  $30 \text{ mg m}^{-3}$ .

*Obtaining  $K_{abs}^{\tau_f}$*  — The form of equation 5.8 implies that the depth of integration is to infinity (as in equation 5.3). However, because  $K_{abs}^{\tau_f}$  is a broadband attenuation coefficient which must decrease with depth (cf. Kirk 1994), and fluorescence is rapidly attenuated in water,  $K_{abs}^{\tau_f}$  has to be calculated near the surface. So, we used  $K_{abs}^{\tau_f}$  derived for the region from which 90% of the water-leaving fluorescence originates.

The attenuation coefficient for absorbed irradiance,  $K_{abs}^{\tau_f}$ , was obtained by an iterative procedure. First, the absorbed radiation by phytoplankton at each wavelength was computed every 0.02 m from the surface to an initial estimate of the depth above which 90% of surface fluorescence originates ( $z_{90}$ ,  $\text{m}^{-1}$ ) and summed over wavelength. This was done successively for chlorophyll concentrations from 0 to  $30 \text{ mg chl m}^{-3}$  using the spectral attenuation coefficients computed from Morel and Maritorena (2001), the

spectral chlorophyll specific absorption coefficients of Bricaud et al. (1995), and a subsurface downwelling irradiance spectrum computed using Gregg and Carder's (1990) model for noon at 45°N at the summer solstice. An attenuation coefficient,  $\tilde{K}_{abs}^{\tau_f}$ , was computed by fitting a linear function to the natural log of the absorbed radiation versus depth. The depth above which 90% of fluorescence originates was then computed as  $2.3 / [\tilde{K}_{abs}^{\tau_f} + a_f]$ . This was used in place of the initial estimate of  $z_{90}$  and the procedure was repeated; the computation converged after 4 iterations, which provided the iterative solution to the attenuation coefficient  $\tilde{K}_{abs}^{\tau_f}$ . Despite being a broadband attenuation coefficient, numerical values of absorbed irradiance and those computed using  $\tilde{K}_{abs}^{\tau_f}$  at all depths between 0 and  $z_{90}$  are within 1% for all simulations.

Finally, a fit of  $\tilde{K}_{abs}^{\tau_f}$  as a function of  $K_d(490)$  was obtained (see Figure 5.1 and Figure 5.2):

$$K_{abs}^{\tau_f} = -0.00831 + 0.908 \cdot K_d(490)^{0.718} \quad 5.12$$

Errors in this parameterization as a function of  $K_d(490)$  relative to the iterative solution are shown in the lower panel of Figure 5.2. Note that the small error at low values of  $K_d(490)$  in our parameterization is inconsequential to the retrieval of  $chl$  or  $\phi$  (equation 5.4) since  $K_{abs}^{\tau_f}$  is about 10 times lower than  $a_f$  in these waters. A comparison is also made with Morel's (1988) parameterization of  $K_{PAR}$ , which shows the error incurred if the attenuation coefficient for PAR integrated over the euphotic zone is used instead of that for the absorbed radiation calculated near the surface; an attenuation coefficient for PAR

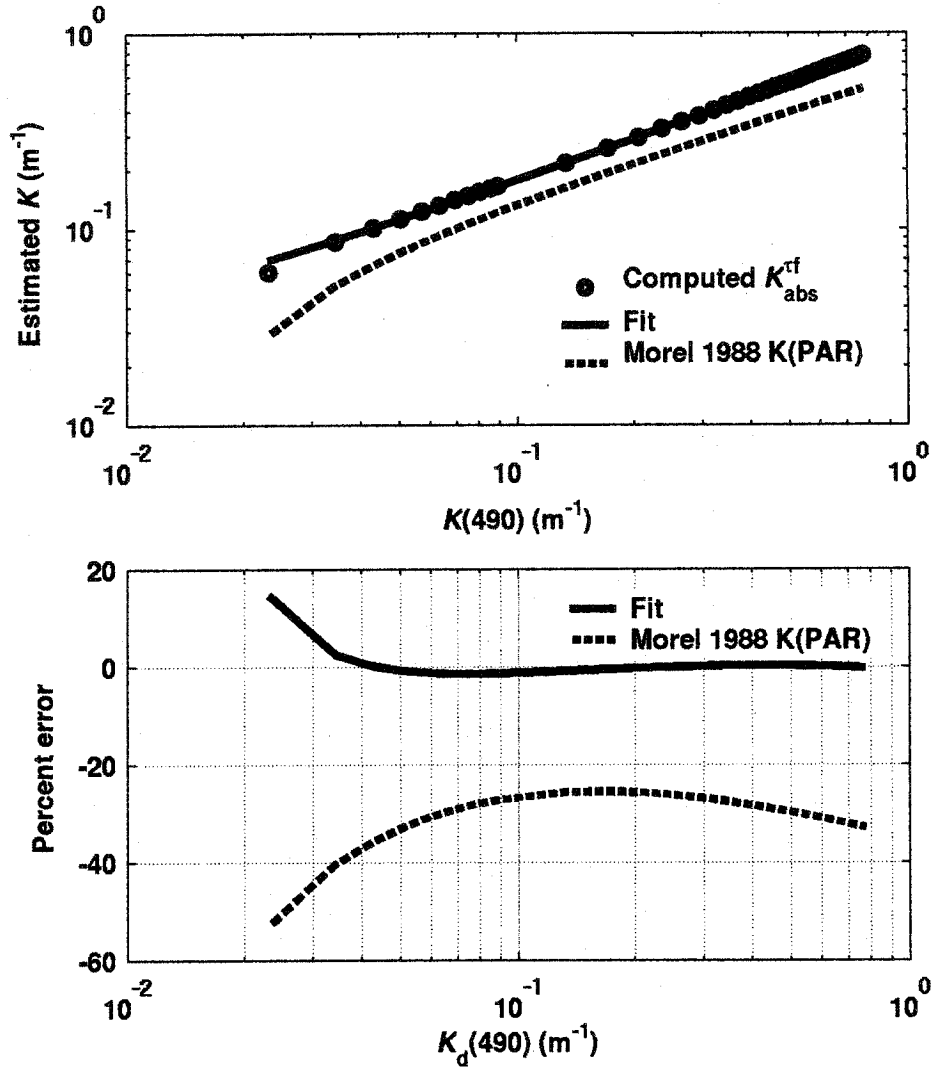


Figure 5.2: Attenuation coefficient of fluorescence excitation irradiance. Top panel shows the computed  $K_{abs}^{rf}$  using an iterative procedure and the fit to those computations given in equation 5.12, as well as a comparison with the attenuation for PAR irradiance ( $K(\text{PAR})$ , Morel 1988) for the euphotic zone, expressed as a function of  $K_d(490)$  using relationships in Morel and Maritorena (2001). Bottom panel shows the percent error between our parameterization of  $K_{abs}^{rf}$  and our iterative computation of  $\tilde{K}_{abs}^{rf}$  as well as the percent difference between the parameterization of the fluorescence exciting radiation using  $K(\text{PAR})$  and our numerical computations. Errors at low values of  $K_d(490)$  are inconsequential for the computation of fluorescence emission at the surface because  $K_{abs}^{rf} \ll a_f$  (see equation 8).

is sometimes used as an approximation for the excitation radiation (e.g. Babin et al. 1996b). For the computation of the quantum yield, this error becomes significant only when  $K_d(490)$  is of the same order as  $a_f$  (for pure water  $a_f$  is  $\sim 0.5 \text{ m}^{-1}$  in the fluorescence band). When using  $K_{PAR}$  an underestimate of  $\sim 15\%$  will occur in the quantum yield of fluorescence at  $K_d(490) = 0.5 \text{ m}^{-1}$  because a  $\sim 30\%$  error in  $K_{abs}^{\tau_f}$  with  $K_d(490) = a_f$  leads to  $\sim 15\%$  error in the quantum yield of fluorescence (Figure 5.2).

*Quantum yield of fluorescence and chlorophyll concentration* – To retrieve the quantum yield of fluorescence and the chlorophyll concentration, the surface fluorescence emission has to be corrected for the bio-optical sources of variability that we have parameterized. Here we apply a factor  $\beta_\phi$  that combines terms in the equation for *FLH* (see equation 5.8 and Figure 5.3):

$$\beta_\phi = \frac{4\pi \cdot C_f \cdot [K_{abs}^{\tau_f} + (a_f / \cos\theta')]}{\bar{a}_\phi^* \cdot Q_a^*}. \quad 5.13$$

Assuming that the statistical model is retrieving the *in situ* optical properties perfectly,  $\beta_\phi$  allows for the retrieval of the two products. First, by replacing the terms on the right-hand-side of equation 5.13 with  $\beta_\phi$  in equation 5.8 and dividing both sides by  $\phi_{chl}$ , a constant quantum yield used for estimating chlorophyll concentration, we obtain:

$$FLH \cdot \beta_\phi / (\phi_{chl} \cdot \bar{E}_{PAR}^o) = chl \cdot \phi / \phi_{chl}. \quad 5.14$$

Assuming a constant ratio of  $\phi / \phi_{chl} = 1$ , our proxy for chlorophyll concentration estimated from fluorescence is:

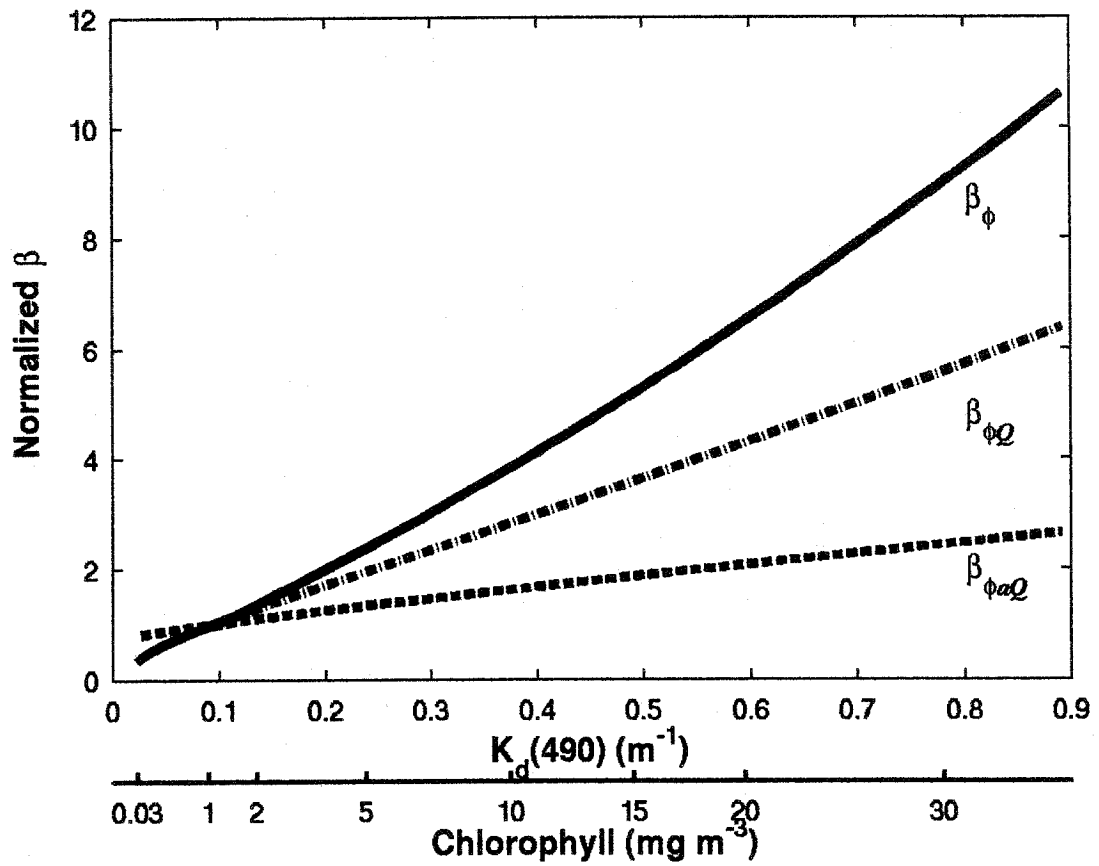


Figure 5.3: Correction factors normalized to the value at  $1\ mg\ chl\ m^{-3}$  applied to *FLH* to retrieve chlorophyll concentration and the quantum yield of fluorescence. These factors were obtained by inserting relationships derived in equations 5.9 to 5.12 into equations 5.13 and 5.17, respectively (see also Figure 5.1).

$$chl_{\text{fluo}} = FLH \cdot \beta_{\phi} / (\phi_{chl} \cdot \overset{\circ}{E}_{PAR}). \quad 5.15$$

For all estimates, we used  $\phi_{chl}=0.012$ . This is the mean quantum yield retrieved by the quantum yield algorithm described below. The MODIS product ipar was used for  $\overset{\circ}{E}_{PAR}$ . Secondly, using  $\beta_{\phi}$  and equation 5.8 as above and the MODIS retrieved chlorophyll ( $chl_{\text{MODIS}}$ ; SeaWiFS analog algorithm) we calculate

$$\phi_{est} = FLH \cdot \beta_{\phi} / (\overset{\circ}{E}_{PAR} \cdot chl_{\text{MODIS}}). \quad 5.16$$

This is our estimate of the quantum yield.

This approach is based on statistical relationships with  $K_d(490)$ , which was estimated from the blue to green ratio in remotely sensed ocean color. Areas that do not follow the central trends of phytoplankton optical properties with estimates of  $K_d(490)$  will show up as variations in the quantum yield (e.g. the presence of high  $\bar{a}_{\phi}^*$  at high  $K_d(490)$  will show up as a spuriously low quantum yield). Note that changes in  $\beta_{\phi}$  with chlorophyll concentration between 0.03 and 1 mg chl m<sup>-3</sup> are mostly due to the decrease in  $\bar{a}_{\phi}^* \cdot Q_a^*$  (see Figure 5.1). Furthermore, the parameterizations for  $\bar{a}_{\phi}^*$  and  $Q_a^*$  are only valid for chlorophyll concentrations greater than 0.03 mg chl m<sup>-3</sup> and this is also the lower limit of the algorithms developed here.

Our decision to depart from the MODIS *ARP* algorithm, which is based on the retrieval of phytoplankton absorption, and to use an empirical method based on  $K_d(490)$  and empirical chlorophyll estimates was made for several reasons: firstly, to provide an estimate of the quantum yield independent of the MODIS *CFE* algorithm (the algorithms

are different but the inputs, apart from the 412 nm channel, are the same); secondly, to make use of the robustness of the empirical chlorophyll algorithms (O'Reilly et al. 1998); and lastly, to avoid the possible interference of a poor estimate of the 412 nm radiance which can affect *ARP*.

*Deriving less specific quantum yields* — To examine bio-optical sources of variation in the relationship between emitted fluorescence and *FLH*, two parameters were created:

$$\begin{aligned}\beta_{\varphi Q} &= 4\pi \cdot C_f \cdot \left[ K_{abs}^{\tau_f} + (a_f / \cos \theta') \right] \cdot \left[ \tilde{a}_\varphi^* \cdot \tilde{Q}_a^* \right]^{-1} \\ \beta_{\varphi a Q} &= 4\pi \cdot C_f \cdot \left[ K_{abs}^{\tau_f} + (a_f / \cos \theta') \right] \cdot \left[ \tilde{a}_\varphi^* \cdot \tilde{Q}_a^* \right]^{-1}\end{aligned}\quad 5.17$$

where the tilde signifies that the parameter is held constant at the parameterized value for a chlorophyll concentration of 1 mg m<sup>-3</sup> ( $K_a(490) = 0.089 \text{ m}^{-1}$ ). Further insight can be obtained by following the same approach as above to obtain  $\varphi_{est}$  (equation 5.16), but using  $\beta_{\varphi Q}$  and  $\beta_{\varphi a Q}$ . Using  $\beta_{\varphi Q}$  we retrieve  $\varphi_Q$ , which can be interpreted as the quantum yield times a relative fraction of light not reabsorbed within the cell:

$$\varphi_Q = \varphi \cdot Q_a^* / \tilde{Q}_a^* \quad 5.18$$

Using the parameter  $\beta_{\varphi a Q}$  broadens this mixed physiological index by providing an estimate of the quantum yield divided by a relative index of pigment packaging,  $\varphi_{aQ}$ :

$$\varphi_{aQ} = \varphi \cdot \tilde{a}_\varphi^* \cdot Q_a^* \cdot \left[ \tilde{a}_\varphi^* \cdot \tilde{Q}_a^* \right]^{-1} \quad 5.19$$

It is an index of pigment packaging because both  $\tilde{a}_\varphi^*$  and  $Q_a^*$  decrease as the cell size and pigment packaging increase (Morel and Bricaud 1981). This number is informative as it includes, in one parameter, all the species- and physiologically-dependent optical

influences on fluorescence.

The subscripts for  $\varphi_Q$  and  $\varphi_{aQ}$  indicate the sources of variability present in these parameters in addition to the quantum yield: i.e.  $a$  stands for  $\bar{a}_\varphi^*$  and  $Q$  stands for  $Q_a^*$ . The  $\varphi_Q$  parameter should be the most similar to  $CFE$  because, as with the MODIS product, it does not account for the effect of  $Q_a^*$  (see Table 5-2) in the algorithm, hence, any natural variability in this factor will be included in the retrieved product ( $CFE$  or  $\varphi_Q$ ). Note that  $\varphi_Q$  and  $\varphi_{aQ}$  use fewer statistical bio-optical relationships for their retrieval than  $\varphi_{est}$ , so they should be the most accurately derived; however, they are more difficult to interpret than  $\varphi_{est}$ .

## 5.7 Assessment

*Relationship between FLH and chlorophyll* — Equation 5.15 can be rewritten as :

$$FLH = chl_{\text{fluo}} \cdot \varphi_{chl} \cdot \bar{E}_{PAR} / \beta_\varphi \quad 5.20$$

This provides a predictive relationship for the fluorescence line height under the conditions of observation encountered by MODIS (high irradiance near the surface at midday measured using a baseline method at 678 nm). This relationship is shown in Figure 5.4 and is similar to relationships derived by Babin et al. (1996b) and Gower et al. (2004 see their Figure 2).

*Baseline Correction* — The  $FLH$  distinguishes photons emitted by chlorophyll fluorescence from the Raman and inelastically scattered photons using a “baseline method”. Because our algorithm is based on the  $FLH$  we wanted to know if it was an accurate estimate of the fluorescence emitted at the surface of the ocean. We used

**Table 5-2: A comparison of the quantum yield parameters.**

Parameter	Accounts for variability in	Does not account for	Depth of calculation	Estimated variables
CFE	$chl, K(\lambda), a^*$	- $Q_a^*$ - Attenuation of incident light when calculating depth of integration	- Depth from which 63.2% of the emitted fluorescence is attenuated at the surface	$\phi \cdot Q_a^*$
$\phi_{est}$	$chl, K(\lambda), a^*, Q_a^*$		-Infinity	$\phi$
$\phi_Q$	$chl, K(\lambda), a^*$	- $Q_a^*$	-Infinity	$\frac{\phi \cdot Q_a^*}{\tilde{Q}_a^*}$
$\phi_{aQ}$	$chl, K(\lambda)$	- $a^*, Q_a^*$	-Infinity	$\frac{\phi \cdot \bar{a}_\phi^* \cdot Q_a^*}{[\tilde{a}_\phi^* \cdot \tilde{Q}_a^*]}$

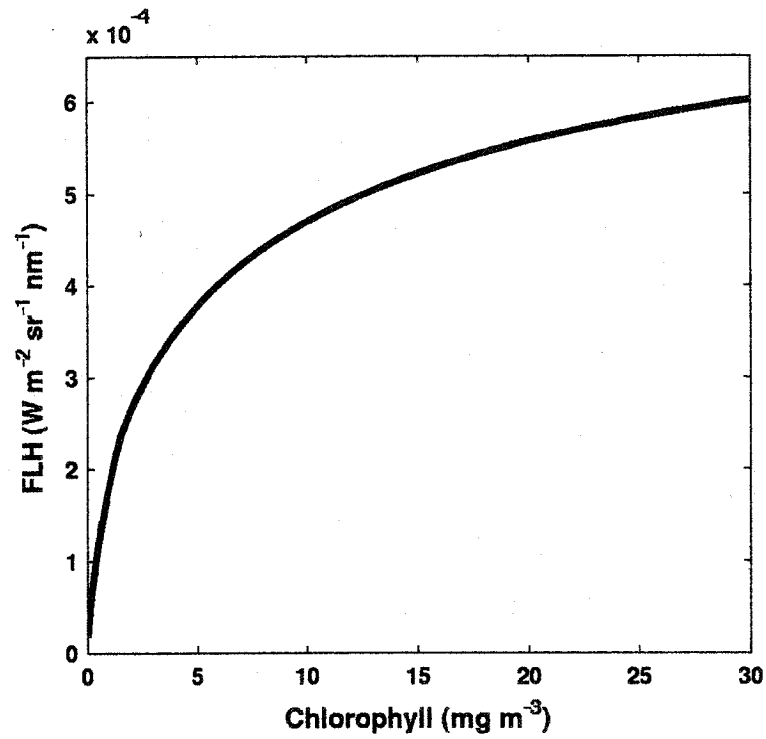


**Figure 5.4:** Relationship between the *FLH* and the chlorophyll concentration with our parameterization (see equation 5.20) using  $\phi_{chl}=0.012$ , and  $\dot{E}_{PAR}^o = 1750 \mu\text{mol m}^{-2} \text{s}^{-1}$ .

Hydrolight simulations (see Appendix III) to examine the MODIS baseline as well as, with lesser emphasis, the baseline used by the Medium Resolution Imaging Spectrometer (MERIS, the European Space Agency's ocean color sensor). The two baselines underestimated the amount of fluoresced radiance (Figure 5.5). Clearly, in the case of the MODIS baseline, the underestimate is strongly a function of the chlorophyll concentration, especially at lower quantum yields. We conclude (see Appendix III for more discussion) that:

At the sea surface, the baseline corrected fluorescence is a biased measure of the fluorescence emission. The fraction of the total fluorescence emission measured by a baseline corrected spectrum varies with chlorophyll concentration.

Given the potential underestimation of fluorescence radiance by *FLH* in low chlorophyll waters, it is expected that a quantum yield algorithm based on *FLH* will return underestimated values in low chlorophyll regions.

The addition of a small amount of fluorescence radiance ( $FLH_0$ ) offsets much of the bias observed with chlorophyll concentration.

Algorithms that do not rely on a baseline estimate for fluorescence emission have been proposed and implemented (Roesler and Perry 1995; Culver and Perry 1997; Coleman et al. 2000; Morrison 2003). Such algorithms may provide a useful method for correcting the fluorescence emission for the backscattered radiance from a remote sensing perspective and could eventually be incorporated into the semi-analytical algorithm presently used to retrieve chlorophyll concentration from MODIS data (Carder et al. 1999a; Carder et al. 1999b).

Figure 5.5: Modeled relationships between the estimates obtained using the baseline method and emitted fluorescence at 678 nm. The left panel: Ratio of the baseline-measured radiance (equivalent to the *FLH* measurement) to the emitted radiance (emitted) using Hydrolight simulations of case 1 waters. The emitted radiance was calculated by subtracting the Hydrolight simulation of upwelling radiance just above the surface without fluorescence from the one with fluorescence. Ratios are presented for four baselines using the 667-748 nm baseline (identified as MODIS) using quantum yields of 0.005, 0.01, 0.03 and 0.05 and one baseline (MERIS QY=0.01) using 667-709 nm, which is similar to MERIS (which uses 665-709 nm) with a quantum yield of 0.01. The inset shows the MODIS simulations with a small baseline value,  $FLH_0$  of  $1.26 \times 10^{-5} \text{ W m}^{-2} \text{ nm}^{-1} \text{ sr}^{-1}$  added. Right panel: Representative spectra of upwelling radiance for four chlorophyll concentrations. The colored continuous lines with circles are the simulations with fluorescence (quantum yield=0.01), the lines with crosses are the simulations without fluorescence, and the black line represents the MODIS baseline without the MODIS  $FLH_0$  value added. The logarithmic scaling represents the linear baseline as a curve. Symbols (circles or crosses) represent the wavebands simulated in Hydrolight. For a chlorophyll concentration of  $15 \text{ mg m}^{-3}$ , a comparison with three other quantum yields is given (see legend). The differences between the top colored line and black line for each chlorophyll concentration are equivalent to measured *FLH* while the differences between the line with fluorescence and without fluorescence at 678 represent the emitted fluorescence.

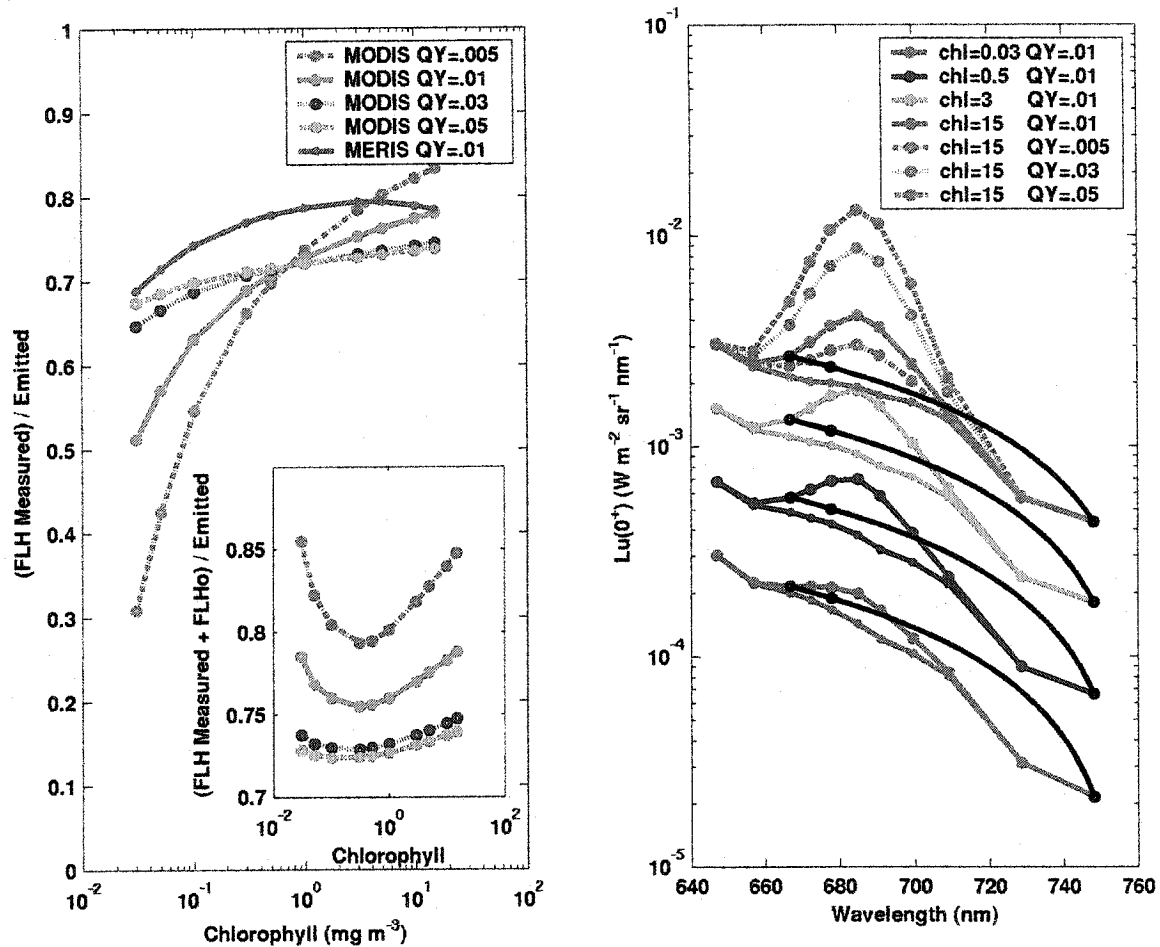


Figure 5.5: See caption on previous page.

*Comparing the finite-depth MODIS algorithm to a complete depth model —*

Other than  $Q_a^*$ , which is related to the package effect and is difficult to quantify, the MODIS equation for *CFE* (equation 2.22) differs from equation 5.4 when solved for  $\phi$ , by the maximum depth of integration representing the source of fluorescence leaving the surface. The MODIS equation integrates to the depth *from which the emitted fluorescence is attenuated by 63.2% when it reaches the surface* ( $z_{678}$ , m; equation 5.5), whereas equation 5.4 integrates to infinity. Since the *ARP* algorithm is intended to account only for absorbed radiation responsible for 63.2% of the surface fluorescence, using *FLH* and *ARP* directly to derive the quantum yield of fluorescence would lead to an overestimate of the quantum yield by approximately 1/0.632 such that a correction has to be applied (Carder et al. 2003).

Rather than integrating to the depth from which the fluorescence emission has been attenuated to 63.2% upon reaching the surface, a more useful depth for interpreting the fluorescence measurement is the depth *above which an arbitrary fraction (it could be 63.2%) of the surface-leaving fluorescence originates*  $z_{\tau_f}$  (m) (see Figure 5.6). It can be obtained by integrating to the depth  $z_{\tau_f}$  which yields 63.2% of surface leaving fluorescence, integrated to infinity (Babin et al. 1996b):

$$\int_{400}^{700} \int_0^{z_{\tau_f}} a_{\phi}(\lambda) \cdot \overset{\circ}{E}(\lambda, 0) \cdot e^{-(K(\lambda)+a_f) \cdot z} dz \cdot d\lambda = 0.632 \cdot \int_{400}^{700} \int_0^{\infty} a_{\phi}(\lambda) \cdot \overset{\circ}{E}(\lambda, 0) \cdot e^{-(K(\lambda)+a_f) \cdot z} dz \cdot d\lambda \quad 5.21$$

This cannot be solved analytically for  $z_{\tau_f}$  for all wavelengths, but for one excitation wavelength, the solution is  $z_{\tau_f}(\lambda) = 1 / (K(\lambda) + a_f)$ . Therefore, the depth above which

**Figure 5.6: Simplified model (reduced spectral dependence) of fluorescence emission in water to illustrate the different approaches to calculate the depth where 63.2% of the fluorescence originates. Top left: The incident irradiance in the PAR domain decreases exponentially with depth. Top right: With this simplified model (see equation top left), it leads to a decreasing exponential for the volume emission of fluorescence  $dL_{em}(z)$  (continuous line). The dashed lines illustrate the decrease in the fluorescence originating from three depths to the surface as it travels up in the water column. The equation above the graph represents the fluorescence just below the surface due to the emission at depth  $z$ . Bottom panel: The continuous line represents the cumulative emission (as a fraction of the total) at the surface originating from increasingly greater depth intervals. When this cumulative emission reaches 0.632 it corresponds to  $z_{rf}$ : the depth above which 63.2% of the fluorescence originates. The dashed line represents the volume emission of fluorescence originating from depth  $z$  remaining at the surface. At a value of 0.378, this corresponds to the depth from which the emitted fluorescence is attenuated by 63.2% at the surface:  $z_{678}$ . The depth  $z_{678}$  is deeper than  $z_{rf}$ , which leads to an overestimate of the absorbed irradiance for fluorescence emission. To emphasize the difference, the model presented is consistent with a chlorophyll concentration of  $20 \text{ mg m}^{-3}$ .**

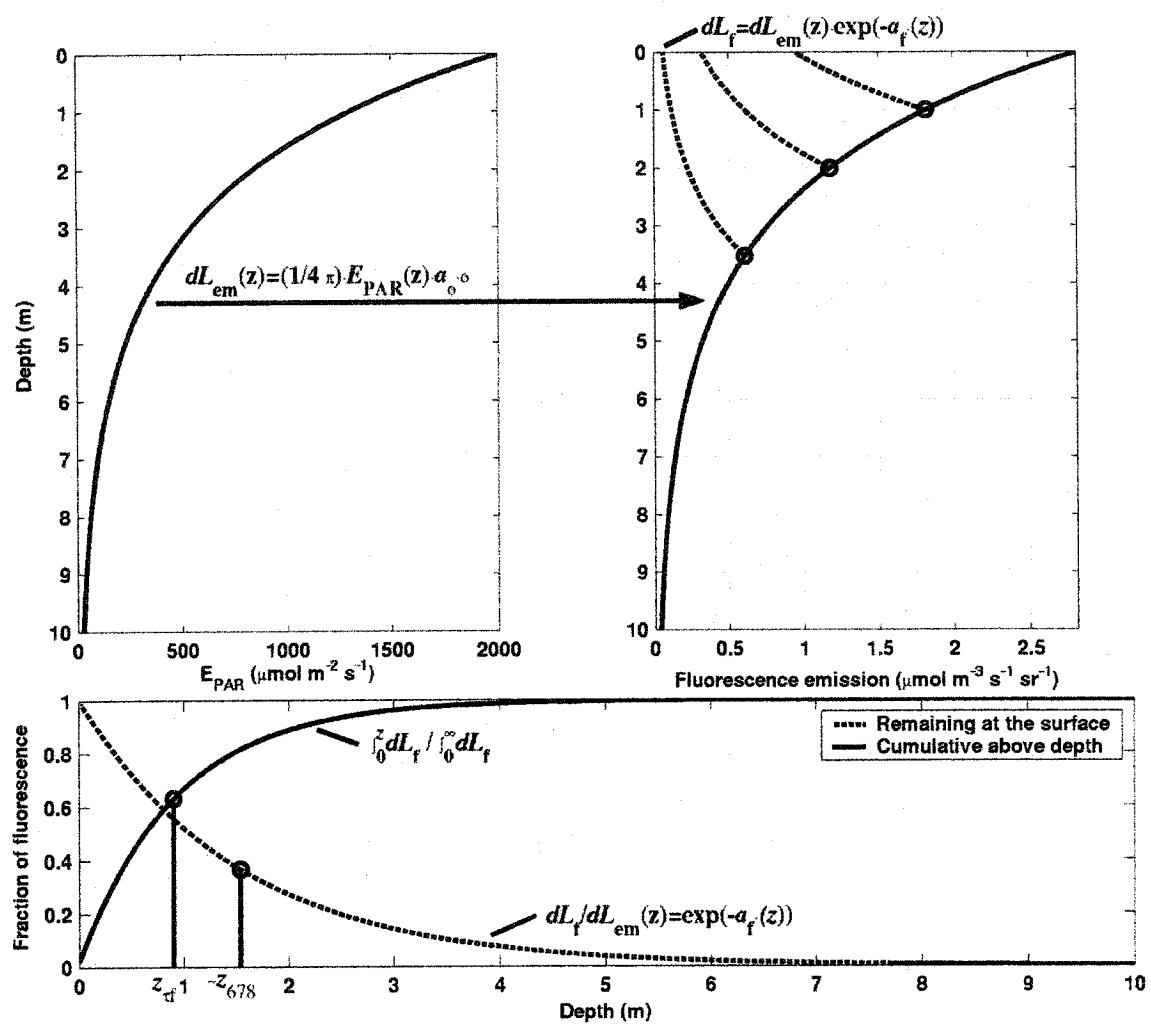


Figure 5.6: See caption on previous page.

63.2% of surface fluorescence originates depends not only on the attenuation of emitted radiation  $a_f$ , but also on the attenuation of the incident irradiance,  $K(\lambda)$ . This has been omitted in the MODIS estimation of  $z_{678}$  (equation 5.5) and should lead to an overestimate of  $ARP$  and an underestimate of the  $CFE$  when the approximation  $a_f \gg K$  does not hold, for example, when the concentration of chlorophyll is high (see Figure 5.7). Variable attenuation of absorbed radiation does have a strong influence on spatial patterns in some regions (see for example Figure 5.8 and Figure 5.12) and should be accounted for. This is particularly important when interpreting spatial changes in the quantum yield across gradients of chlorophyll.

Although integrating to  $z_g$  instead of  $z_{678}$  provides an unbiased measure of surface absorption, we do not see any advantage gained by limiting the calculation of the absorbed radiation to a restricted depth range since:

- 1) The satellite measures fluorescence coming from all depths.
- 2) It is impossible to separate fluorescence from top layers of the water column from that originating deeper.
- 3) The quantum yield and the chlorophyll concentration vary with depth, hence a given depth will not provide a given fraction of the fluoresced radiance.

**We therefore suggest integrating over the whole water column when calculating absorbed radiation for the interpretation of remotely sensed fluorescence.** While integration to infinity does not overcome the problems associated with the third point (which is probably small due to the natural weighting to surface

**Figure 5.7: Ratio of calculated absorbed irradiance weighted for its efficiency of emission at the surface:  $(= \int_{400}^{700} \int_0^Z a_{\phi}(\lambda) \cdot \overset{\circ}{E}(\lambda, 0) \cdot e^{-(K(\lambda)+a_f) \cdot z} \cdot dz \cdot d\lambda)$  for different depths**

**$Z$  and a range of chlorophyll concentrations. Our algorithm uses  $Z = \infty$ . The present algorithm (*ARP*), which does not account completely for changes in the attenuation of downwelling irradiance, uses  $Z = z_{678}$  (equation 5.5). An alternate formulation which accounts completely for the attenuation of downwelling irradiance uses  $Z = z_{\text{rf}}$  (equation 2.14). The ratio of the absorbed weighted irradiance for  $Z = z_{\text{rf}}$  and  $Z = \infty$  is equal to 0.632 for all chlorophyll concentrations showing no biases with changes in the attenuation coefficient (line  $z_{\text{rf}} / \infty$ ). In high chlorophyll waters, the attenuation of incident light by phytoplankton limits the penetration of light and restricts most of the emission of fluorescence to a layer nearer to the surface than is calculated by the MODIS algorithm, leading to a bias in absorbed radiation calculated using  $Z = z_{678}$  compared to  $Z = \infty$  (line  $z_{678} / \infty$ ). Consequently, the MODIS estimate of *ARP* is high, and estimates of fluorescence efficiency are low. This underestimate varies between ~3 to ~26% as shown by the ratio for  $Z = z_{678}$  and  $Z = z_{\text{rf}}$  (line  $z_{678} / z_{\text{rf}}$ ). The numerical calculations are based on equation 5.3 and the models of Morel and Maritorena (2001) and Bricaud et al. (1995) for nadir observation.**

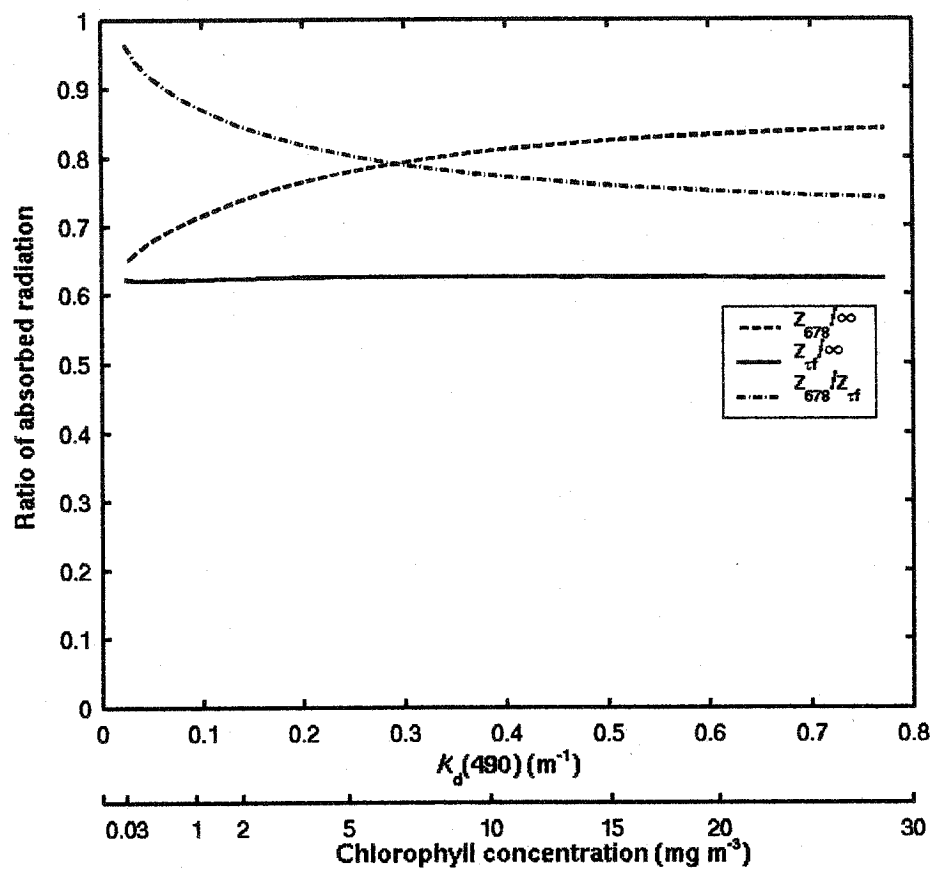


Figure 5.7: See caption on previous page.

depths for the natural fluorescence emission), it removes the false impression that a narrow depth of integration provides results that are less affected by depth variations in optical and physiological parameters.

*Comparison of the algorithms: Chlorophyll* — The MODIS estimates are shown in Figure 5.8 for the subsense off the west coast of Central America. The jet of high chlorophyll concentration observed off the coast of Costa Rica is a persistent phytoplankton bloom extending from the Costa Rica coast into the Costa Rica Dome due to wind driven upwelling (Fiedler 2002; McClain et al. 2002). Note the close correspondence between chlorophyll,  $K_d(490)$  and *FLH*: the first two parameters are derived from similar band ratios while the third is independent of ratios. The jet off the coast of Costa Rica also shows higher *CFE*.

The coefficient of determination for the untransformed values between the chlorophyll retrieved using the fluorescence algorithm developed here and the MODIS retrieved chlorophyll using the SeaWiFS analog algorithm (top panel Figure 5.9) is  $r^2=0.95$  ( $n=39424$ ), but the slope does not correspond to a constant quantum yield. The diagonal lines in the top panel are isolines of our retrieved quantum yield. The line labeled 0.012, the assumed  $\phi_{chl}$  for retrieving chlorophyll, is equivalent to a 1:1 line for  $chl_{fluor}$  vs.  $chl_{MODIS}$ . It is clear that the variability in the MODIS chlorophyll concentration explained by the fluorescence chlorophyll algorithm is lower at lower chlorophyll concentrations. Comparison between *FLH* and the MODIS estimate of chlorophyll shows a clear curvature due to changes in optical properties with increasing

**Figure 5.8: MODIS level 3 dataset for Jan 15, 2001 for the subscene off the west coast of Central America. The chlorophyll concentration is from the MODIS SeaWiFS analog algorithm,  $K_d(490)$  is derived empirically from band ratios, ipar is MODIS model output for clear sky conditions of the instantaneous PAR radiation at the time of the image,  $ARP$  is the absorbed radiation by phytoplankton,  $FLH$  is the fluorescence line height (a measure of the amount of fluoresced radiance at the surface of the ocean), and  $CFE$  is the MODIS estimate of the quantum yield of fluorescence.**

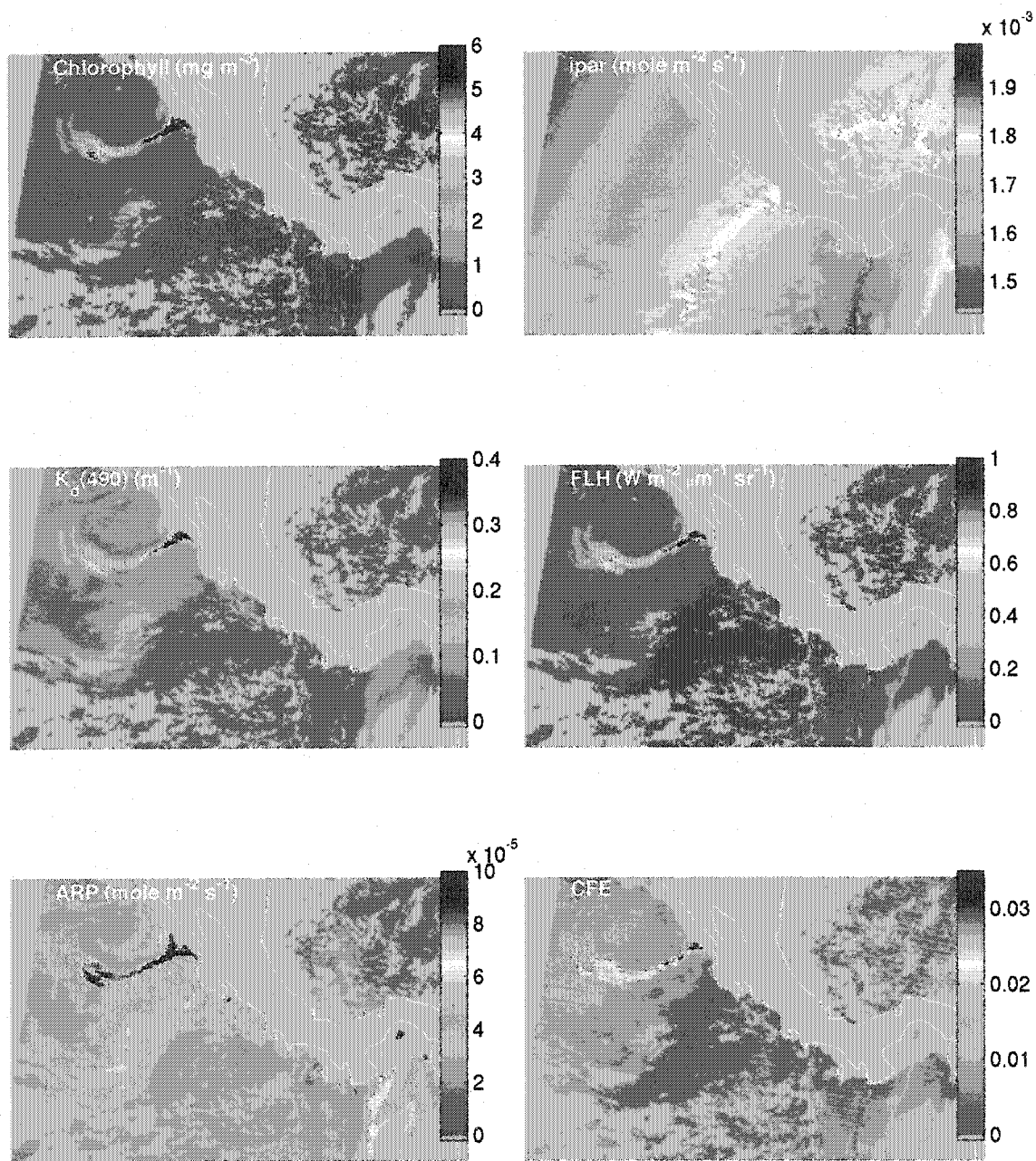


**Figure 5.8:** See caption on previous page.

Figure 5.9: Top panel: Comparison of our fluorescence estimate of the chlorophyll concentration,  $chl_{fluo} = FLH \cdot \beta_{\phi} / (\phi_{chl} \cdot E_{PAR})$  (see equations 5.8 and 5.14) with MODIS chlorophyll product (chlor\_a2, SeaWiFS analog chlorophyll algorithm). The lines are isolines of retrieved quantum yields as indicated, the line 0.012 is equivalent to a 1:1 correspondence of  $chl_{fluo}$  and  $chl_{MODIS}$ . The middle panel is the comparison between  $FLH$  and chlorophyll concentration from MODIS. The dashed black line is the relationship derived by Gower et al. (2004),  $FLH = 0.15 \cdot chl / (1 + 0.2 \cdot chl)$  multiplied by 1.65 to fit the data. Note that the  $FLH$  was not converted to quantum units for this comparison. Bottom: retrieved quantum yield of fluorescence,  $\phi_{est}$ , as a function of  $K_d(490)$ . The colored bars indicate a range of quantum yields measured at the surface of the ocean in situ: “Metal” = Maritorena et al. (2000), “Oetal” = Ostrowska et al. (1997) data for  $E_{PAR} > 1 \times 10^{20}$  quanta  $m^{-2} s^{-1}$ , and “Mo” = Morrison (2003).

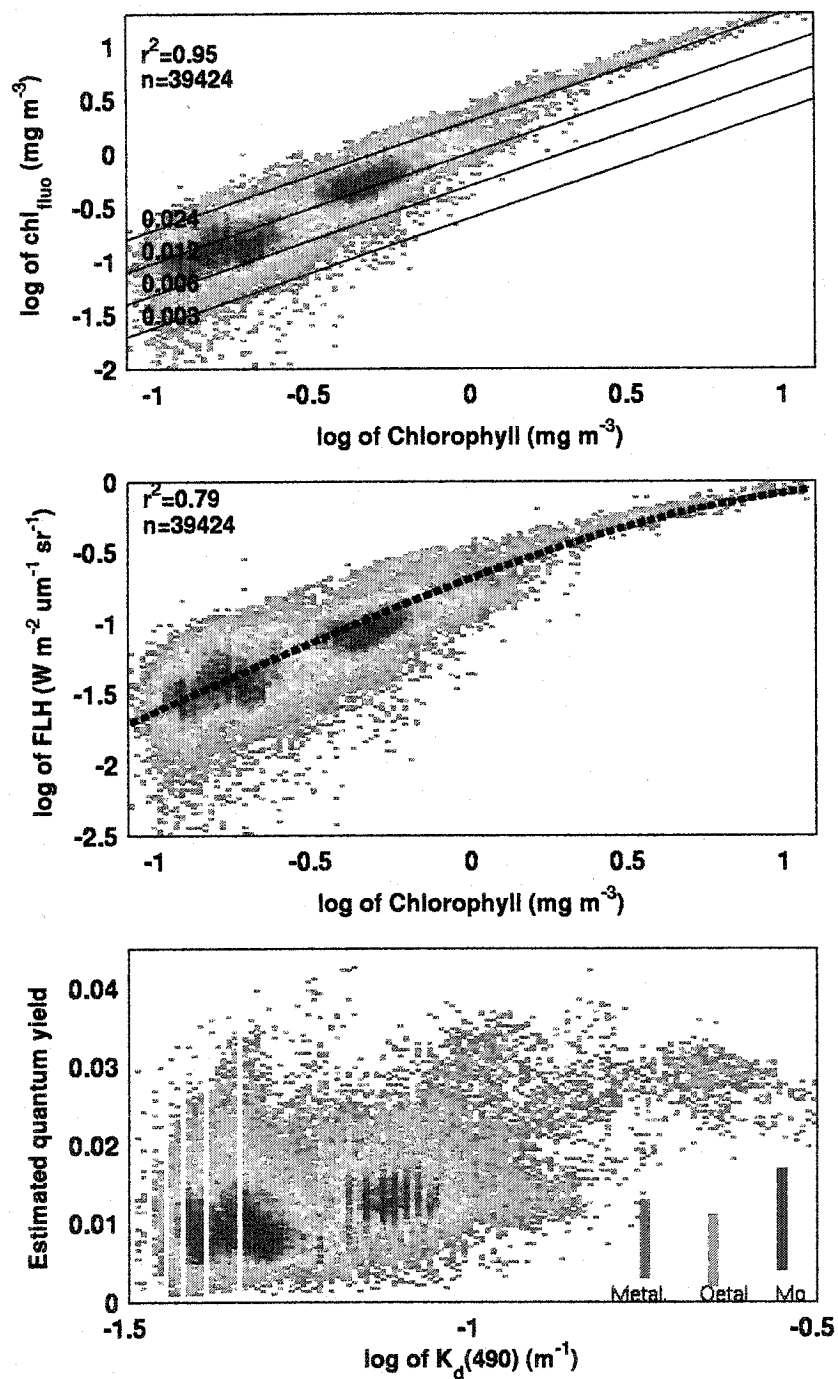
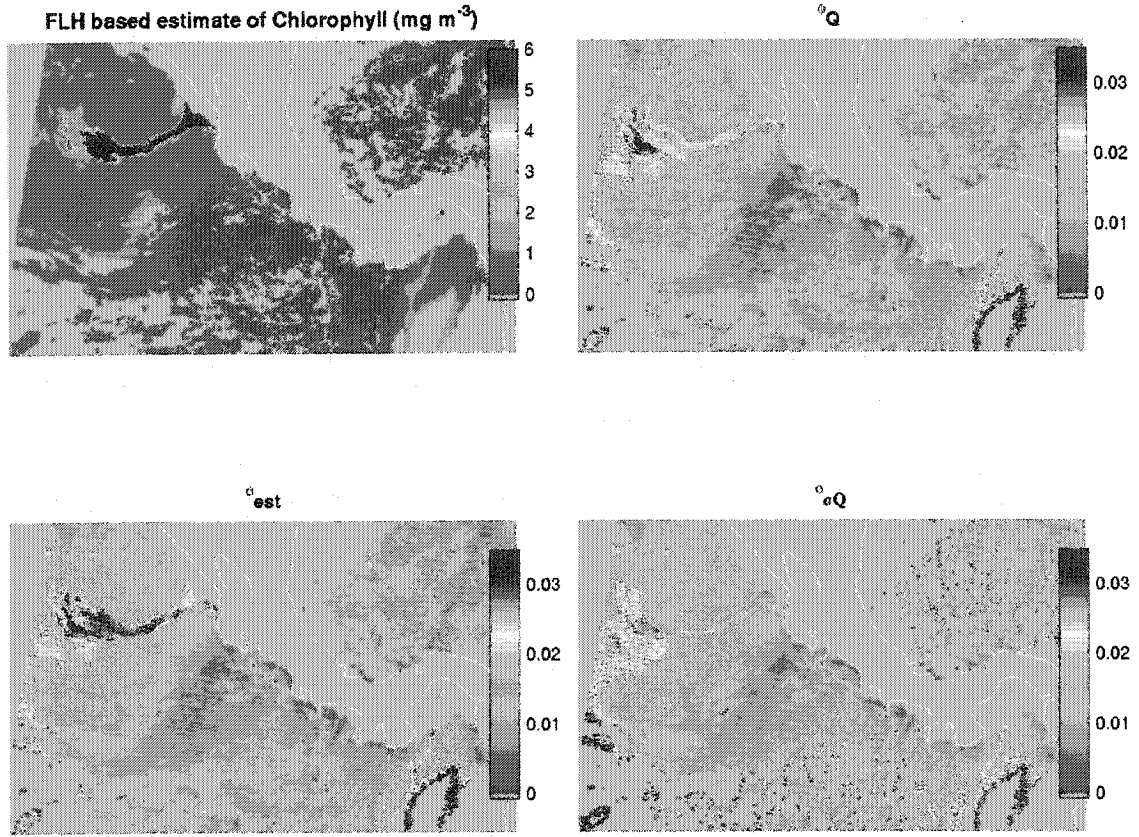


Figure 5.9: See caption on previous page.

chlorophyll concentration and a lower  $r^2$  ( $=0.79$ ,  $n=39424$  middle Figure 5.9). We also show a comparison with the model of Gower et al. (2004), which is based on average values of measured fluorescence emission scaled to irradiance for the sun at zenith (middle Figure 5.9, dashed black line). Their model follows the central trends of the MODIS data in this region. Part of the variability in the top and middle panels is due to variability in the quantum yield of fluorescence, the chlorophyll specific absorption coefficient, the error in the determination of chlorophyll from band ratios, and the striping due to detector-to-detector calibration observed in MODIS images (Gower et al. 2004; Salomonson 2004). It should also be kept in mind that the depths sampled by the ocean color and fluorescence techniques are different and become more similar as chlorophyll concentration increases. Despite these errors, for this region the chlorophyll concentration retrieved using fluorescence is, in most cases, within a factor of 2 of the MODIS estimates of chlorophyll from ocean color; 86% of the points fall within a retrieved yield of 0.006 and 0.024 while 1:1 is 0.012 (top Figure 5.9). In addition, the variability in the retrieval of chlorophyll from fluorescence seems to be reduced at higher chlorophyll concentrations (see Figure 5.9).

*Comparison of the algorithms: Sources of variability* — A map of  $chl_{\text{fluo}}$ , calculated assuming a constant  $\phi_{\text{chl}}$  of 0.012, is presented in the upper left panel of Figure 5.10; it can be compared with the chlorophyll map in Figure 5.8. Our estimate of  $\phi_{\text{est}}$ , using  $chl_{\text{MODIS}}$  (equation 5.16) is shown in the bottom left panel of Figure 5.10. Comparison with MODIS *CFE* (Figure 5.8) shows essentially the same features, and the interpretation



**Figure 5.10: Map of derived products.** Upper left panel is a fluorescence-based estimate of chlorophyll assuming a fluorescence quantum yield ( $\phi_{chl}$ ) of 0.012:  $chl_{fluo} = FLH \cdot \beta_{\phi} / (\phi_{chl} \cdot E_{PAR})$ . The bottom left shows the estimate of the quantum yield using chlorophyll concentration estimated from blue to green radiance ratios ( $chl_{MODIS}$ ):  $\phi_{est} = FLH \cdot \beta_{\phi} / (E_{PAR} \cdot chl_{MODIS})$ . Right panels are the same as bottom left except using corrections  $\beta_{\phi_Q}$  (upper) and  $\beta_{\phi_{aQ}}$  (lower) instead of  $\beta_{\phi}$ .

of spatial patterns in either map would be the same. The parameters  $\varphi_Q$  and  $\varphi_{aQ}$  retrieved using  $\beta_{\varphi_Q}$  and  $\beta_{\varphi_{aQ}}$ , respectively, are shown in the upper and lower right panels of Figure 5.10. Note the almost complete disappearance of the plume in  $\varphi_{aQ}$ , while  $\varphi_Q$  has an intermediate pattern between  $\varphi_{aQ}$  and  $\varphi_{est}$ , showing that the packaging of pigments modeled as a function of  $K_d(490)$  has a strong influence on the retrieval of the quantum yield; the effect of  $\bar{a}_\varphi^*$  being the most important.

*Comparison of the algorithms: quantum yield* — The magnitude of the retrieval of  $\varphi_{est}$  compares well (Figure 5.9 bottom) with the yields measured in situ in surface waters of the world (Ostrowska et al. 1997; Maritorena et al. 2000; Morrison 2003). A comparison of  $\varphi_{est}$  and  $CFE$  is shown in the upper left panel of Figure 5.11. To explore bias in the two yields relative to each other, the ratio of  $\varphi_{est}/CFE$  is plotted as a function of : 1)  $K_d(490)$  (upper right); 2) absorption by gilvin, which includes chromophoric dissolved organic matter and non-living particulate matter, at 400 nm (lower left); and 3)  $ARP$  (lower right). Absorption by gilvin is a standard MODIS product obtained from the same semi-analytical inversion algorithm that returns an estimate of chlorophyll concentration (the case 2 waters algorithm). Very little bias was observed in this region except for a lower ratio at high values of  $K_d(490)$  and absorption by gilvin. **The comparisons for this region (Figure 5.11) show that the CFE and our algorithm for the quantum yield provide similar results but CFE is lower by a factor of 0.58. The cause of this systematic difference is unknown, but could originate in part from our use of**

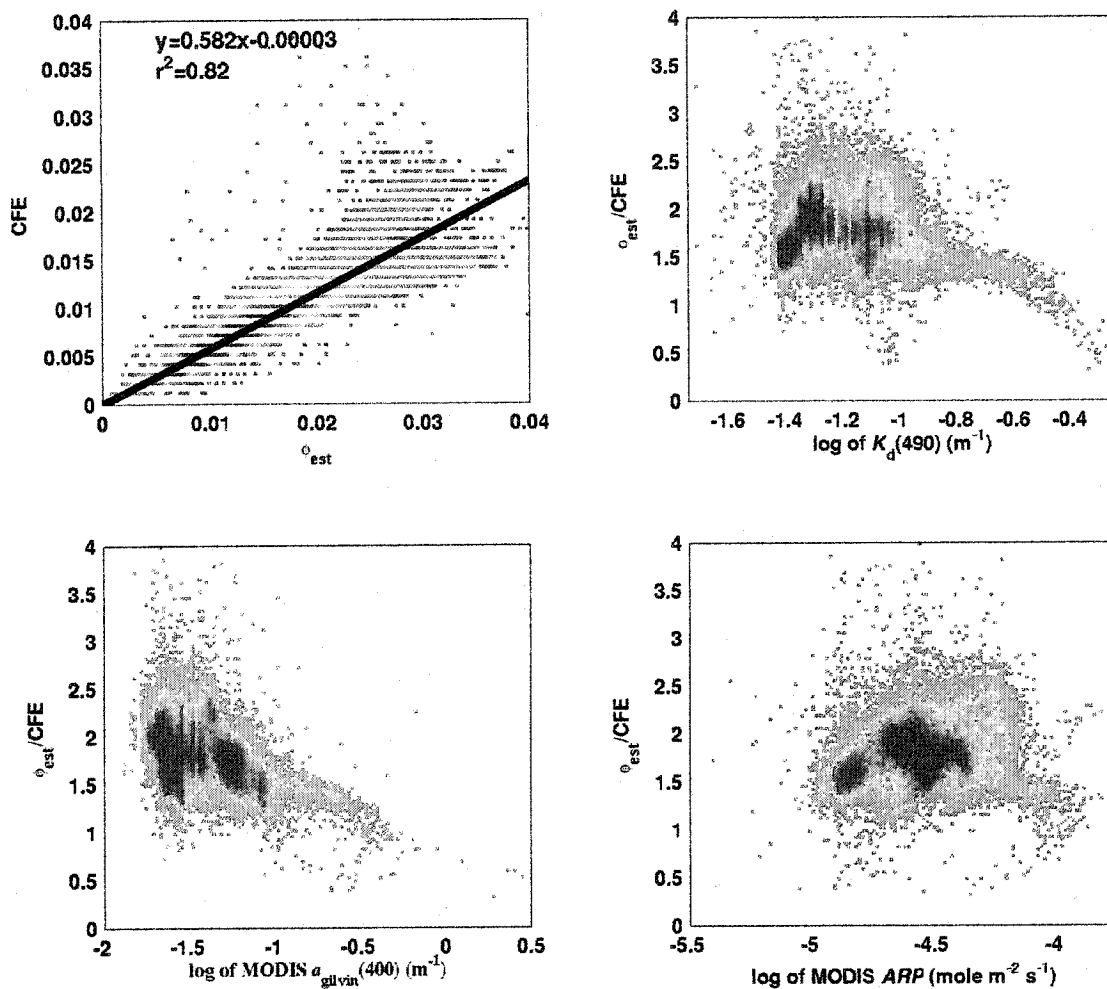
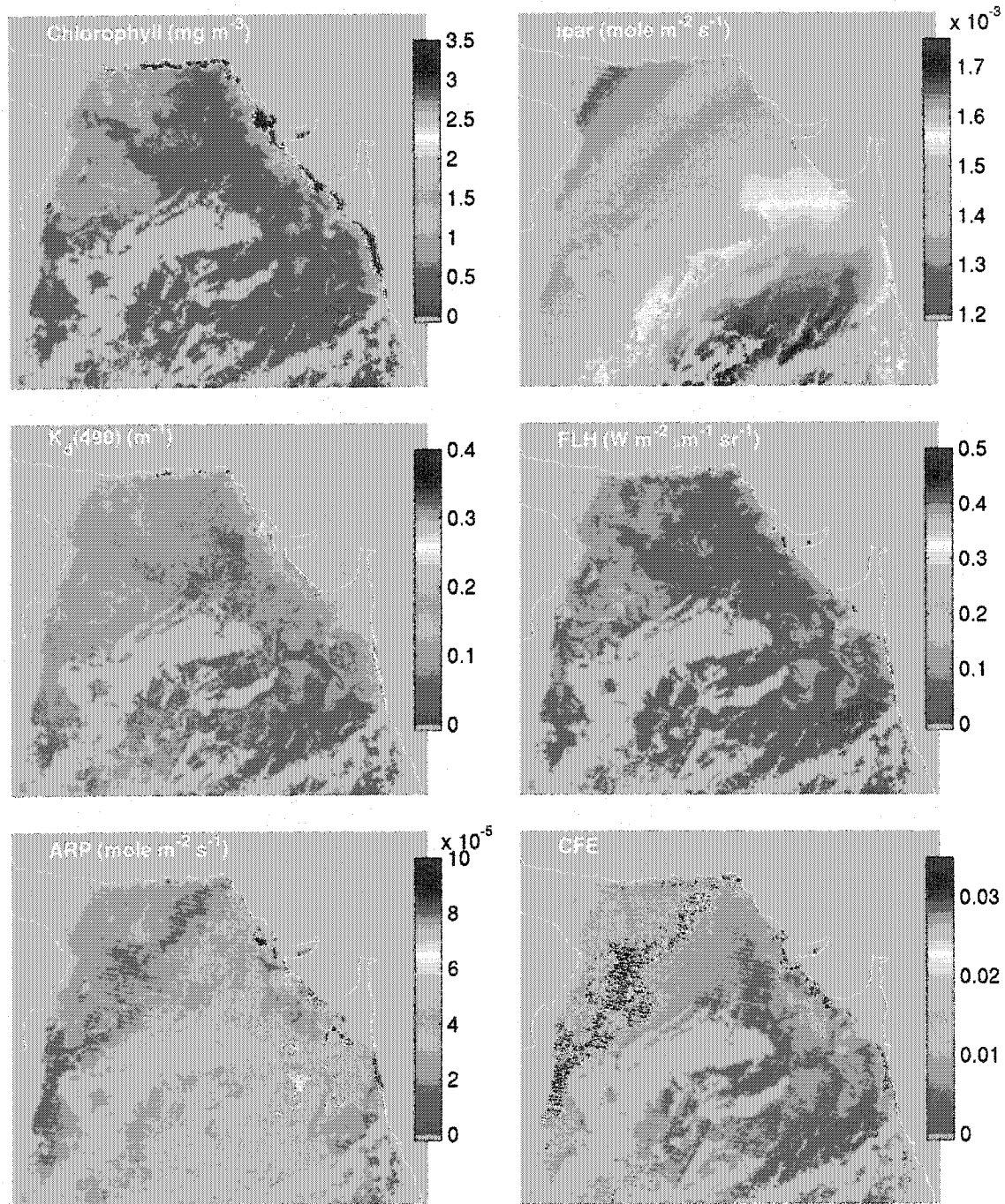


Figure 5.11: Comparison of quantum yields. Upper panel compares the quantum yield estimated from our method ( $\phi_{est}$ ) and the MODIS estimate ( $CFE$ ), the line is the best fit to the data. The remaining panels show the ratio of  $\phi_{est}$  to  $CFE$  as a function of  $K_d(490)$  (upper right), absorption by gilvin at 400 nm (lower left), and  $ARP$  (lower right).

$Q_a^*$ . It is, however, in the opposite direction from the bias that would be incurred if the correction for the overestimate of  $CFE$  by  $1/0.632$  due to the shallow depth measurement had not been applied (see above).

*Comparison of the algorithms: Arabian Sea*—The MODIS measurements for the Arabian Sea (Figure 5.12) show patterns consistent with hydrographic forcing with the possible exception of the  $ARP$  and  $CFE$  maps which show a strong feature (high  $CFE$  and low  $ARP$ ) going across the image in a northeast – southwest direction which is not present in the other maps. The relationship between the MODIS estimates of chlorophyll and fluorescence-based estimates is more variable in this region (Figure 5.13 top and middle). There is a clear offset showing lower  $chl_{flu}$  at values of MODIS chlorophyll  $\sim 1$  to  $3 \text{ mg m}^{-3}$  which corresponds mostly with coastal waters. The central trends are, however, the same as for the previous region. The Gower et al. (2004) algorithm (using the same scaling as in Figure 5.9) underestimates the chlorophyll concentration. Note that Gower and colleagues suggest that the chlorophyll-specific surface fluorescence emission should vary depending on the solar zenith angle. However, they did not describe the mathematical relationship. So we kept the same scaling as in Figure 5.9 as this provides a good reference for comparison. Because the median of our retrieved  $\phi_{est}$  was the same as for the previous region ( $\sim 0.012$ ), the difference is probably due to overall lower  $ipar$  values in this region and not a change in the quantum yield. The decreased variability explained in MODIS estimates of chlorophyll by  $chl_{flu}$  (Figure 5.9 vs. Figure 5.13) may in part be due to larger error in the MODIS chlorophyll algorithm since this region seems more optically complex, as highlighted by the apparent artifact in  $CFE$  and  $ARP$



**Figure 5.12: MODIS level 3 dataset for Jan 15, 2001 for the subscene of the Arabian Sea. See Figure 5.8 for details.**

**Figure 5.13: Comparison of algorithms. Top panel: Comparison of our fluorescence estimate of the chlorophyll concentration,  $chl_{\text{fluor}} = FLH \cdot \beta_{\phi} / (\phi_{chl} \cdot E_{PAR})$  (see equations 5.8 and 5.14) with the MODIS chlorophyll product (chlor\_a2, SeaWiFS analog chlorophyll algorithm). The middle panel is the comparison between  $FLH$  and chlorophyll concentration from MODIS. The dashed black line is the relationship derived by Gower et al. (2004),  $FLH = 0.15 \cdot chl / (1 + 0.2 \cdot chl)$  multiplied by 1.65 to fit the data in Figure 5.9. The bottom panel shows our retrieved quantum yield of fluorescence,  $\phi_{est}$ , as a function of  $K_d(490)$ . See Figure 5.9 for more details.**

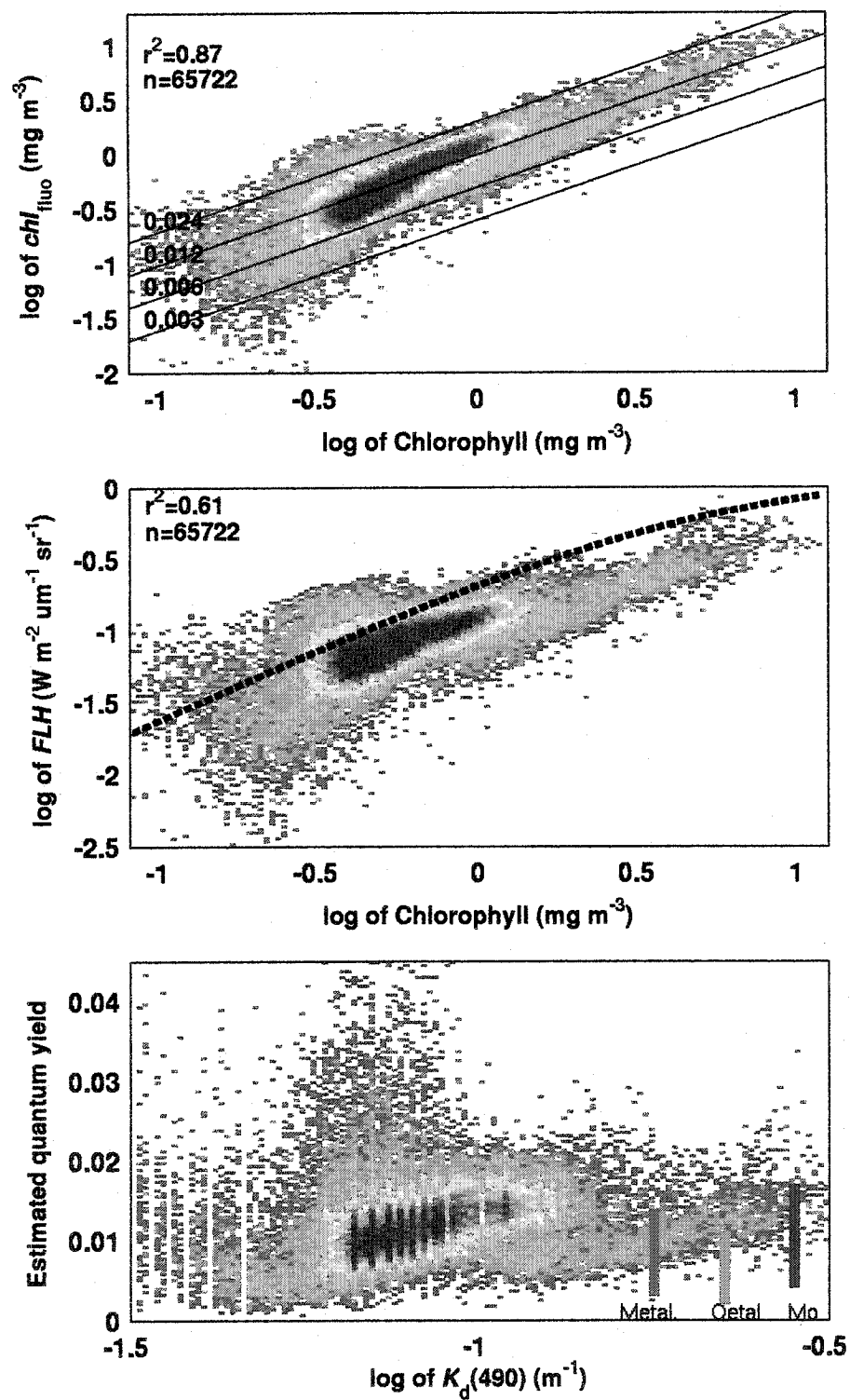


Figure 5.13: See caption on previous page.

algorithm, which lead to a stripe going across the image.

The patterns of retrieved quantum yield versus  $K_d(490)$  (Figure 5.13 bottom) are different from those observed in Figure 5.9 especially at high  $K_d(490)$ . Whereas in Figure 5.9 the high values of  $K_d(490)$  were associated with the upwelling plume, in Figure 5.13 the high values are located near the coast and are probably influenced by river runoff.

A comparison of the maps of  $\varphi_{est}$  (Figure 5.14) and  $CFE$  (Figure 5.12) shows striking differences: the stripe showing high values of  $CFE$  is not observed in  $\varphi_{est}$ , which is much more uniform. As expected, the relationship between  $CFE$  and  $\varphi_{est}$  is weaker in this region (Figure 5.15 top left); a small fraction of the points follows the trend line reproduced from Figure 5.11, but otherwise the scatter is large. In contrast to Figure 5.11 from off the coast of Central America, Figure 5.15 shows strong dependence of the ratio of  $\varphi_{est}/CFE$  vs.  $K_d(490)$ ,  $a_{gilvin}$  and  $ARP$ , which clearly shows that one of the yields is biased with respect to these retrieved optical properties. Figure 5.16 highlights the resemblance between the map of MODIS retrieved  $a_{gilvin}$  and the ratio of  $CFE/\varphi_{est}$  consistent with a strong influence of the upwelling radiance at 412 nm on the relationship.

The same inverse model (Carder et al. 1999a; Carder et al. 1999b) is used to retrieve  $a_\phi$  for the computation of  $ARP$  and to estimate  $a_{gilvin}$ . Our experience with such models, particularly implementations similar to that of Roesler and Perry(1995), has

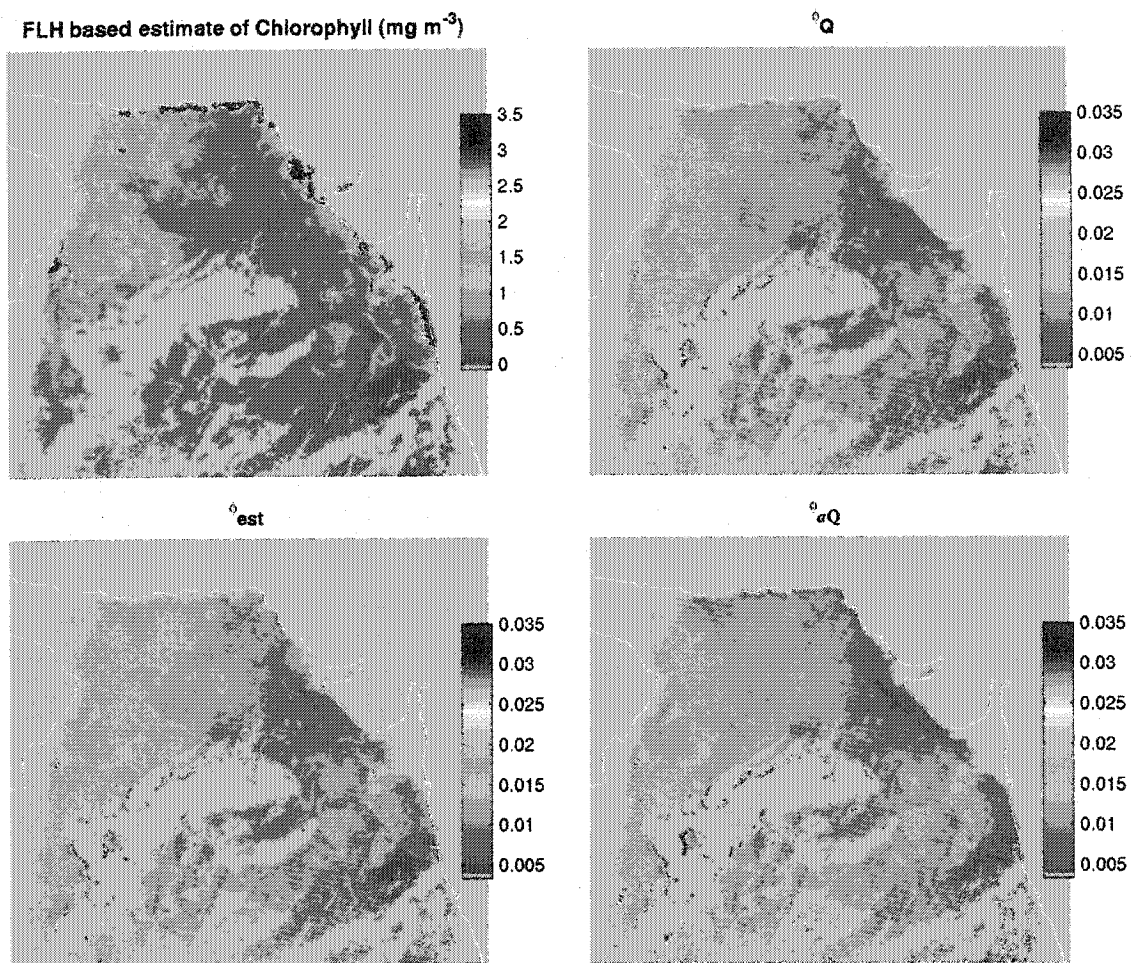


**Figure 5.14: Map of derived products for the Arabian Sea. See Figure 5.10 for more details.**

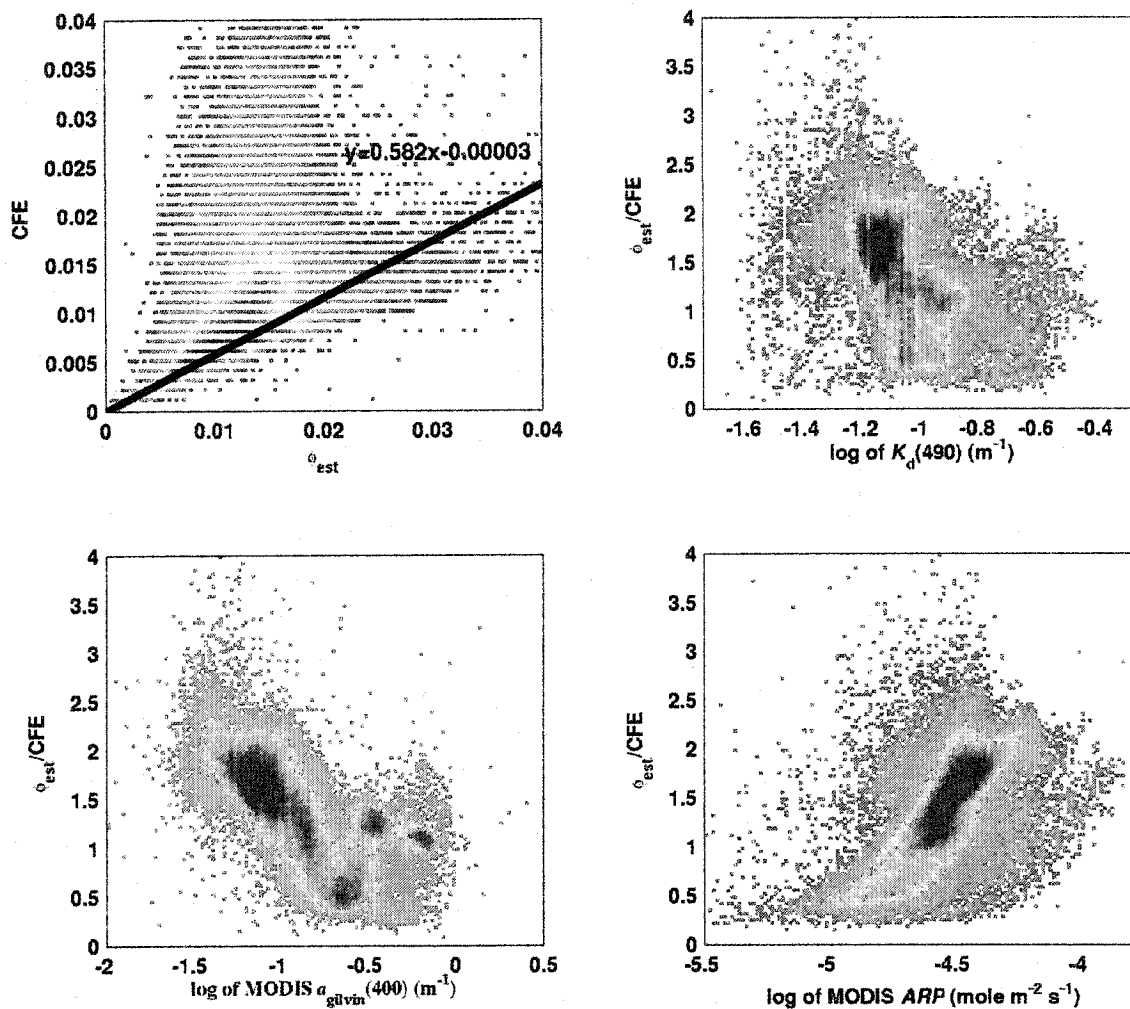


**Figure 5.15: Comparison of quantum yields for the Arabian Sea. See Figure 5.11 for more details. Line in the upper left panel is the best fit from the upper left panel in Figure 5.11.**

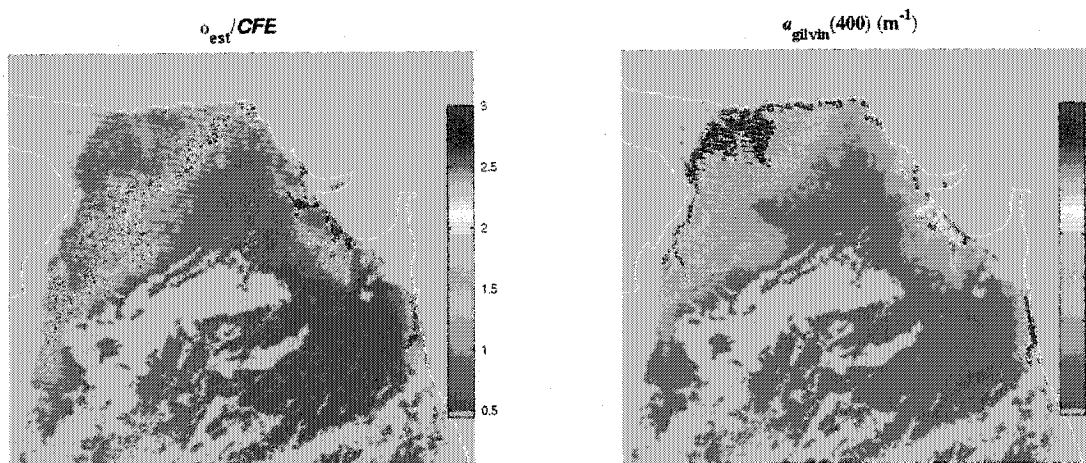


**Figure 5.16: Quantum yield and gilvin estimates. The left panel is the ratio of the quantum yields while the right panel is the gilvin absorption at 400 nm as estimated by MODIS for the two study regions. Note the correspondence of the region with high  $\phi_{est}/CFE$  with the transition region to higher  $a_{gilvin}$ .**

shown that generally an overestimate of  $a_{\text{gilvin}}$  leads to an underestimate of  $a_{\phi}$  and vice-versa. An inverse pattern to the retrieved  $a_{\text{gilvin}}$  is observed in the normalized water leaving radiance at 412 nm (lower 412 radiance where higher  $a_{\text{gilvin}}$  is present), and to a lesser extent at 443, but is not observed at 488 nm (data not shown). Along the high *CFE* line in Figure 5.12, the *ARP* algorithm probably underestimated the phytoplankton absorption while at the same time overestimated the absorption by gilvin, leading to an overestimate of *CFE*. Whether the origin of this effect is in the atmospheric correction or the *ARP* model we have not investigated.

## 5.8 Discussion

*Quantum yield of fluorescence* — Off the coast of Central America, the *CFE* was on average 58% lower than  $\phi_{\text{est}}$  and our estimate accounts for 76% of the variance found in the *CFE* (Figure 5.11) but the maps of  $\phi_{\text{est}}$  (Figure 5.10) and *CFE* (Figure 5.8) show similar patterns. In this region, the quantum yields compare well and a map of either would lead to the same interpretation. It is outside the scope of this paper to attribute the different quantum yields inside and outside the Costa Rica Dome area to physiological or physical processes, and we will merely speculate that likely candidates include different nutrient regimes, light acclimation states (for example due to different mixing layer depths and attenuation coefficients, e.g. Field et al. 1998), or dominance by small cells (Li et al. 1983, leading to an underestimate of absorption and overestimate of the quantum yield) in the upwelling region. The strong difference between patterns in  $\phi_{aQ}$ , whose variability includes effects of all physiological variables ( $\phi \cdot \bar{a}_{\phi}^* \cdot Q_a^*$ ), and  $\phi_{\text{est}}$ ,

which attempts to retrieve only  $\phi$ , clearly emphasizes the importance of the term  $\bar{a}_\phi^* \cdot Q_a^*$  when retrieving the quantum yield of fluorescence. In fact, the much smaller amplitude of  $\phi_{aQ}$  compared to  $\phi_{est}$  points to a strong effect of  $\bar{a}_\phi^* \cdot Q_a^*$  on the patterns observed in this region, whether it is an artifact due to our parameterization, or real.

## 5.9 Comments and recommendations

*Chlorophyll and absorption as proxies for phytoplankton abundance* — Because intra-cellular fluorescence emission is the product of the absorption of light by all phytoplankton pigments and the quantum yield as defined here (absorption by photoprotective pigments leads to a reduced quantum yield, e.g., Kiefer and Reynolds 1992; Gilmore and Govindjee 1999), phytoplankton absorption rather than chlorophyll is the better measure of biomass for fluorescence work. We use chlorophyll in our quantum yield model due to the lack of empirical models relating the blue to green ratio directly to absorption; presently, the only algorithms to retrieve phytoplankton absorption from satellite ocean color are based on inverse models (Carder et al. 1999b; Maritorena et al. 2002). As such, a future improvement of our quantum yield algorithm would be the use of an empirical algorithm retrieving  $\bar{a}_\phi$  and  $a_\phi(678)$  directly from the blue to green ratio. This would eliminate the need for an independent chlorophyll estimate and the relationships between  $\bar{a}_\phi^*$  and  $a_\phi(678)$  vs.  $K_d(490)$  to retrieve  $\phi_{est}$ . Our chlorophyll algorithm could also be recast to retrieve phytoplankton absorption with higher accuracy; it would, however, be harder to validate and a less desirable product in the context of our focus on the retrieval of chlorophyll concentration.

Using chlorophyll, instead of phytoplankton absorption, however, makes our algorithm very sensitive to its accurate retrieval. The estimate of  $\phi_{\text{est}}$  for the same regions using the two other MODIS chlorophyll algorithms (Figure 5.17, see Procedures section) shows clear differences in the maps when compared with Figure 5.10 and Figure 5.14. The patterns observed are strongly influenced by the chlorophyll algorithm and the physiological interpretation of these patterns would certainly be different. When using our quantum yield algorithm, we recommend using the best chlorophyll algorithm for the region and time studied. As an example, note the reappearance of the stripe in the Arabian Sea region when using the semi-analytical (case 2) algorithm underlying the *ARP* model (Figure 5.17).

The use of chlorophyll and a parameterization based on  $K_d(490)$  has a further limitation for the retrieval of the quantum yield: if the remote sensing algorithms used to retrieve  $K_d(490)$  and chlorophyll do not follow the statistical relationships used (Bricaud et al. 1995; Morel and Maritorena 2001) it could lead to a bias in the retrieval of the yield. Presently, this could lead to errors of ~30% (sensitivity analysis not shown). This should not be a major limitation, and as algorithms evolve they will likely converge.

*Validation of algorithms* — Our algorithm and the MODIS *CFE* algorithm remain to be validated by measuring the quantum yield in situ under remote sensing conditions. The conditions under which the MODIS data are collected are very consistent. It is always at the surface, under high irradiances, within 1 to 1.5 hour of the satellite's equatorial crossing time, and subject to large spatial averaging due to its resolution. This

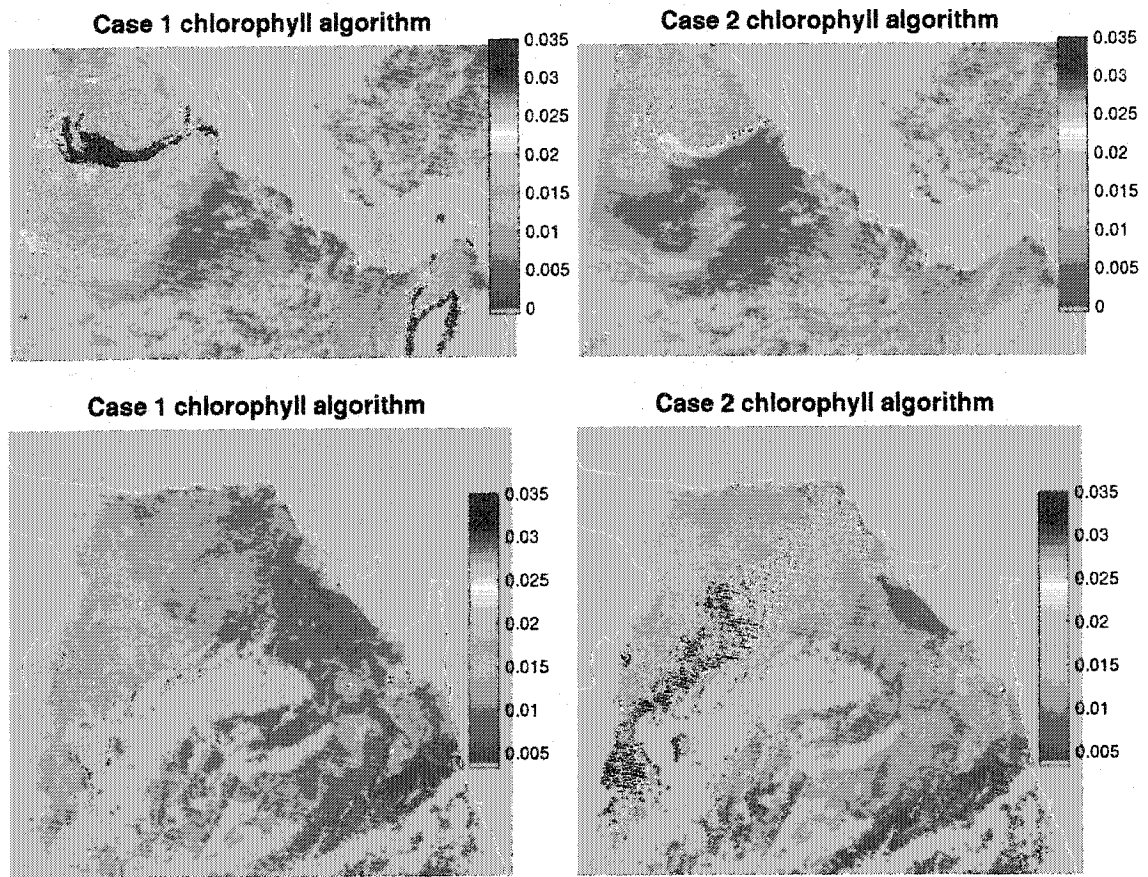


**Figure 5.17: Effect of different chlorophyll algorithms on the estimate of  $\phi_{est}$ .** Left column shows the results using the case 1 pigment algorithm (MOD 19), which provides an estimate of chlorophyll *a* and phaeopigments in case 1 waters. This algorithm is based on an empirical function of the ratio of blue to green water leaving radiance. The right column shows the application of the case 2 chlorophyll algorithm (MOD 21). The top row is for the subscene off the west coast of Central America and the bottom row is the Arabian Sea subscene.

is a narrow set of conditions compared to those encountered when taking measurements at sea. As such, field validation of fluorescence algorithms will require great care; the time of sampling and the incident irradiance will have to match those encountered by the MODIS sensor, otherwise, the time and irradiance dependence of  $\phi$  will affect the results (e.g. Morrison 2003).

*Summary* — We developed new methods to estimate the chlorophyll concentration and the quantum yield of fluorescence, incorporating the effects of pigment packaging on fluorescence emission and replacing the *ARP* algorithm used in MODIS *CFE* estimates with a different estimate of absorbed radiation, integrated to infinite depth. The new method seems robust, showing good agreement with MODIS chlorophyll and *CFE* estimates, and is apparently less sensitive to two artifacts:

It will not be affected by a poor estimate of upwelling radiance at 412 nm as it does not rely on the semi-analytical absorption algorithm, which requires the 412 nm radiance to retrieve the absorption coefficients.

The new method estimates absorbed radiation integrated to infinity, avoiding a bias in the MODIS *CFE* due to an incomplete account of the attenuation of incident irradiance. The quantum yield estimate is, however, highly dependent on the retrieval of accurate chlorophyll concentration.

## **5.10 Conclusion**

MODIS fluorescence products are relatively new and, like early chlorophyll images from the Coastal Zone Color Scanner (CZCS), they bear tremendous promise. At

present, they are still experimental, and issues such as accurate estimates of  $i_{par}$  and  $ARP$ , correction of the FLH measurement for the baseline, and proper depth integration need to be resolved. Only when these issues are settled can we assess whether the quantum yield of fluorescence under remote sensing conditions provides a measure of phytoplankton physiology on global scales.

## *Chapter 6 Conclusion & Future Prospects*

The chlorophyll molecule can emit a photon when it absorbs light or an exciton is transferred to it. The process, chlorophyll fluorescence, has no known physiological or ecological *raison d'être*. In solution, the quantum yield of this process is constant, thereby providing a simple and very sensitive method to measure the concentration of chlorophyll. The quantum yield of fluorescence *in vivo* is strongly affected by the efficiency of other pathways for deexcitation such as: 1) the transfer of energy between chlorophyll molecules and other pigments; and 2) the variable capacity for the utilization of the absorbed energy in photosynthesis or heat dissipation. The regulation by the cell of these processes and the consequences of this regulation on the partitioning of energy utilization and its impact on the fluorescence yield allows the use of active fluorescence in the study of higher plant and phytoplankton physiology. It follows from these simple concepts that sun-induced fluorescence provides information about both the biomass and the physiological state of the cell. Isolating these two sources of variability in the ocean and providing a quantitative description of the fluorescence process has been one of the main themes of this thesis. Another central focus, which was not originally planned, but developed out of necessity during the thesis, has been the development of tools and measuring techniques to avoid biases that can occur while measuring sun-induced fluorescence using standard methods.

I approached the study of sun-induced fluorescence from three different perspectives. For field studies based on floating spectroradiometers, I developed and used

an inversion model of reflectance in the fluorescence band. To analyze fluorescence data of the global ocean from the MODIS satellite sensors, I developed and applied new algorithms to retrieve the quantum yield of fluorescence and phytoplankton biomass. Lastly, I conducted a theoretical study, by developing a mechanistic model of phytoplankton fluorescence at the level of the chloroplast.

Chapter 3 focused on providing a mechanistic description of the fluorescence signal as would be observed at the reaction center level. It clearly showed the limitations inherent to the natural fluorescence signal at high light intensities for providing an estimate of the quantum yield of photosynthesis; the relationship between the quantum yield of photochemistry and the quantum yield of fluorescence can differ greatly depending on the capacity for photoprotection of a cell and its level of acclimation to the ambient irradiance. The model also provided a good mechanistic basis for studying the effects of nutrient stress on phytoplankton and the possible hysteresis effects on diel timescales due to the increased presence of inhibited reaction centers. A novel aspect of this model for oceanographic fluorescence research is the use of a three-state model where the reaction centers can be either open, closed or damaged/inhibited.

While the studies of cultures allow to easily obtain the information contained in the fluorescence signal, in the field, other factors prevent us from obtaining a signal solely influenced by the quantum yield of sun-induced fluorescence. These sources of variability are external to the cell and originate from the optical characteristics of the water and, in the case of satellites, the atmosphere. This is because all the changes in the characteristics of the water (spectral absorption and volume scattering function),

influence the observed fluorescence emission, and have to be accounted for when correcting the measured fluorescence signal. An approach to account for this variability using an inverse model was used and refined in Chapter 4 to isolate the fluorescence emission in Lunenburg Bay and in the Bering Sea. While this approach has been used before, the more complete development of the reflectance model applied here has allowed inversion of the fluorescence band in addition to the region of the spectrum below 650 nm that is traditionally inverted. However, because the model did not account for CDOM fluorescence, (which is believed to be important in Lunenburg Bay based on theoretical calculations), wavebands from 400 to 600 nm were not used in the inversion. Instead, ultraviolet wavebands were used to retrieve CDOM absorption; this was not a limitation in the Bering Sea where CDOM concentrations were much lower. Using this approach, good retrievals of the phytoplankton absorption in Lunenburg Bay, a CDOM-rich embayment, were obtained. However, in order to obtain phytoplankton absorption, changes with irradiance of the quantum yield of fluorescence had to be quantified as diel variations in the yield (factor of 3) were as large as the variations observed during the whole summer in phytoplankton absorption. An inverse modeling approach similar to this, could pave the way for better estimates of the fluorescence quantum yield from space. However, as suggested by the analysis in the Bering Sea, the region between 600 and 650 nm, which is mostly affected by variability in the backscattering coefficient, is usually not measured in a remote sensing context and this could make the application of such a method more difficult. Another aspect of the analysis in the Bering Sea suggested the presence of other fluorescing pigments, mostly chlorophyll degradation pigments,

which could affect the estimates of the quantum yield of fluorescence, quantifying the contribution of these pigments could be important to future understanding of the variability observed in the fluorescence emission.

Chapter 5 has focused on the development of an algorithm to retrieve the quantum yield of fluorescence and the chlorophyll concentration from satellite observations. This algorithm uses blue and green wavebands in addition to the fluorescence bands to estimate the characteristics of the water column that influence the penetration of excitation irradiance. The conclusions of that chapter were simple: previously developed algorithms will lead to biases in the retrieval of the quantum yield of fluorescence from space and these biases are likely to be especially important across gradients of biomass in the ocean. Some of these limitations were addressed in Chapter 5 but much more work is required before satellite retrievals of the fluorescence yield are reliable on global scales. One of the first steps towards this goal is currently being undertaken by the NASA ocean color team who are reprocessing the Aqua satellite data to obtain reliable estimates of the radiances (at the top of the atmosphere and at the sea surface). Another problem with the MODIS satellite imagery was described in Appendix III and concerned the limitations of the baseline approach using the wavebands chosen for MODIS. The MERIS sensor does not seem to be affected by this type of bias and a comparison of results for the two sensors will probably provide a good way to correct for biases.

## **6.1 *Future prospects and directions***

Perhaps it is because radiance and irradiance have become simple measurements to obtain in the ocean that, for the past 30 years sun-induced fluorescence has been

studied in the ocean in an exploratory, often ad hoc, fashion. Though exceptions exist, most studies to date involve deployments of a spectroradiometer, most of the time with very little ancillary data. This provides a large amount of information on the water leaving radiance but very few options for interpreting it; this is particularly evident with the deployment of moored spectroradiometers and ocean color drifters. Therefore, interpretation of the data has been based more on conjecture than on solid datasets or models: in fact, the literature contains more speculation on the possible sources of variability rather than interpretation based on solid ancillary information. Furthermore, the methods used to separate the fluorescence signal from background radiation, to account for the water optical properties and absorbed radiation are extremely simple and could be the cause of some of the observed changes in the reported proxy for the quantum yield, usually interpreted in terms of light or nutrient stress. While these studies have contributed much to our curiosity about fluorescence processes in the ocean, they have provided little hard science to aid the interpretation of the data we can now obtain from space or in real time from moored sensors. In my opinion, we have done little more than verify the presence in the environment of sources of variability in the fluorescence yield that were measured in the lab; I believe it is now time to move into a rigorous, quantitative, study of biological sources of variability in sun-induced fluorescence.

Possibly the most important task ahead is to identify which of all the sources of variability observed influences most strongly the quantum yield of fluorescence at the surface of the ocean: Is it the nutrient status, the irradiance, or the species composition? This answer can only partly be answered in the lab or with models. The diversity of

species and mode of variability cannot all be assessed, therefore, such studies will require extensive fieldwork. The fieldwork will have to use techniques such as the ones developed in this thesis and some recent studies (Ostrowska et al. 1997; Maritorena et al. 2000; Morrison 2003) to obtain rigorous estimates of the quantum yield. A series of ancillary data will have to be collected, most importantly: phytoplankton absorption, chlorophyll, nutrients, and species identification. In addition, experiments at sea involving active fluorometry and nutrient limitation assays will have to be conducted. In essence, an understanding of the physiological state and composition of the phytoplanktonic community at each deployment site has to be the central focus of future advances; the measured natural fluorescence signal has to become complementary.

Satellite imagery also provides tremendous potential for advances, but it will have to be properly groundtruthed with the set of measurements suggested above; opportunities such as the Atlantic Meridional Transect cruises series (<http://www.pml.ac.uk/amt/index.htm>) that cross several different trophic regimes should be sought. The utilization of models of circulation and mixing with models such as the one developed in chapter 3 should also provide insights into the processes observed from space. Timeseries data obtained from moorings, which would ideally include floating spectroradiometers, absorption, nutrient, active fluorometers, conductivity and temperature sensors hold tremendous promises. Data from moorings will be particularly insightful if they are located where the optical characteristics of the water are simple such that inversion of the reflectance data can be trusted and where physical models can provide information about the physical forcing.

In the near future, I expect to continue working with the model developed in Chapter 3, and use it in a mixing model of the ocean to simulate changes in photosynthesis and fluorescence that are expected as a function of mixing parameters, nutrient, and incident irradiance. Further work on the model will be done through the addition of results from new laboratory experiments. Furthermore, I want to continue using satellite imagery to obtain qualitative information about the most important source of variability in the observed fluorescence from satellite measurements. On this note, I would like to finish this thesis by presenting, a simple figure that I obtained and presented at the last meeting of the American Society of Limnology and Oceanography (Honolulu, January 2004, see Figure 6.1). The figure represents the correlation coefficient between the weekly average of the concentration of remote sensing chlorophyll and the fluorescence emission measured by the MODIS sensor over two years. Its interpretation is simple: in regions where the coefficient of correlation is low, variations in chlorophyll do not explain most of the variability in the fluorescence emission at the surface of the ocean, and in the regions where the correlation coefficient is high, chlorophyll explains most of the variability. The regions showing the lowest correlation coefficient, such as the Southern Ocean, North Eastern Pacific, tropical and subtropical Atlantic and the eastern side of continent in the southern hemisphere are perhaps the most interesting. This analysis suggest that, in these regions, changes in  $a_\phi^*$ ,  $\phi_f$ , and  $Q_a^*$  are more important than those in chlorophyll concentration, hence leading to more of the variability observed and lower correlation coefficients (see equation 2.2). The most compelling feature of this figure is the presence of clear oceanographic patterns that

**Figure 6.1: Correlation coefficient between fluorescence and chlorophyll (see legend). The color of each pixel represents the value of the correlation coefficient between the ratio of the fluorescence line height over the incident irradiance at the time of the measurement (FLH/ipar) and chlorophyll concentration from blue-to-green ratio ocean color algorithms (FLH/ipar vs. chlorophyll) between July 19, 2000 and July 27 2002 (see chapter 5 for more information on these MODIS products). A high correlation coefficient means that the ratio FLH/ipar and chlorophyll covaried strongly during the two years and hence biomass explains most of the variability at that location, conversely low correlation coefficients mean that biomass does not explain the variability observed by the MODIS sensor.**



**Figure 6.1**

cannot be linked to one common cause based on our knowledge of oceanographic systems. Clearly, information is present but we do not know what it means. When looking at this figure, my feeling is similar to those expressed by Cullen and Renger (1979), who concluded their study showing some of the first results of active fluorometry with DCMU in the ocean by: "We may not know what we are measuring, but the patterns observed are too strong to ignore". Many processes unknown at the time, have been discovered to explain the patterns observed by Cullen and Renger. However, new patterns that elude our understanding are arising (e.g. Figure 6.1), like those of the past they are also, I believe, "too strong to ignore". New discoveries, and insights about the oceans will surely emerge as the causes underlying these new patterns are unraveled.

## *Appendix I : Absorption coefficient as a measure of the attenuation of fluorescence radiance*

To test the validity of the approximation that the attenuation of upwelling fluorescence radiance can be approximated by the absorption coefficient, a series of Hydrolight simulations with a variable scattering coefficient was used for turbid Case 2 waters. The approximation was found to be valid within 5% up to values of the particle scattering coefficient ( $b_p(678)$ ) of  $0.31 \text{ m}^{-1}$  (see Figure I.1). At higher  $b_p(678)$ , the approximation increasingly underestimates the attenuation of upwelling radiance.

### *Hydrolight simulations*

Different concentrations of yellow silt (0, 0.005, 0.01, 0.05, 0.1, 0.5, 1, 2, and 3 g  $\text{m}^{-3}$ ) were added to a water body with a constant background of absorbing matter. The yellow silt was modeled using Haltrin's (2000) phase function for small particles and the weight specific absorption and scattering coefficient of yellow silt as provided with the Hydrolight code (data from Ahn 1990). The highest silt concentration provides a scattering coefficient for particles of  $4.82 \text{ m}^{-1}$  at 443 nm, which is consistent with the upper range of the scattering coefficient observed by Babin *et al.* (2003). The absorption by chromophoric dissolved organic matter was modeled as  $a_{\text{CDOM}} = 0.05 \exp(-0.014(\lambda - 400))$ ; CDOM was assumed non-scattering. The attenuation of upwelling fluoresced radiation was simulated in Hydrolight by using a thin layer of chlorophyll at 3m instead

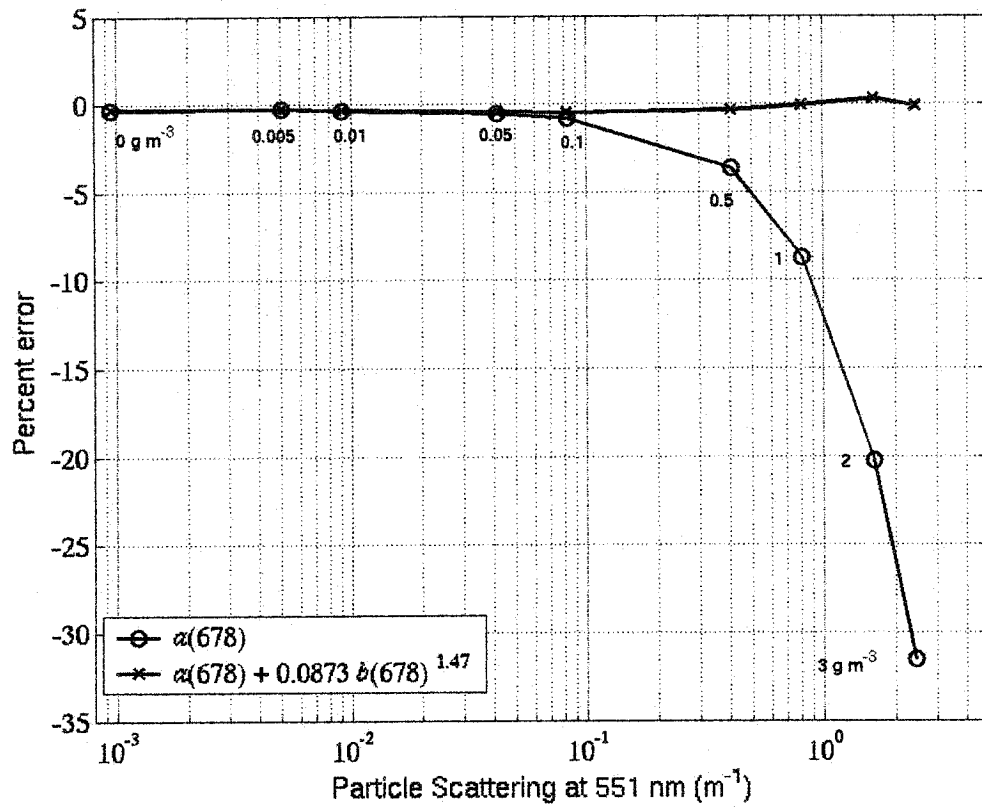


**Figure I.1: Percent error when using  $a(678)$  to approximate the attenuation of upwelling fluorescence radiance at 678 nm (see text for details). The error is lower under the conditions modeled here when using  $a(678) + 0.0873 b(678)^{1.47}$ . Numbers on the graph indicate the concentration of yellow silt. Yellow silt was used because of its strong scattering characteristics and to model highly scattering case 2 waters.**

of a constant concentration with depth allowing the attenuation of the light coming from that layer only to be computed ( $a_f$  in equation 5); if a uniform concentration of chlorophyll is used, the upwelling radiance due to fluorescence would increase approaching the surface due to emission from the upper layers of water. In this simulation, the surface is hence depleted in phytoplankton and contains only yellow silt, colored dissolved matter and water in terms of optically active constituents. To obtain the attenuation coefficient, two series of simulations were run, one with fluorescence one without, such that subtraction of one from the other provided only the fluoresced light.

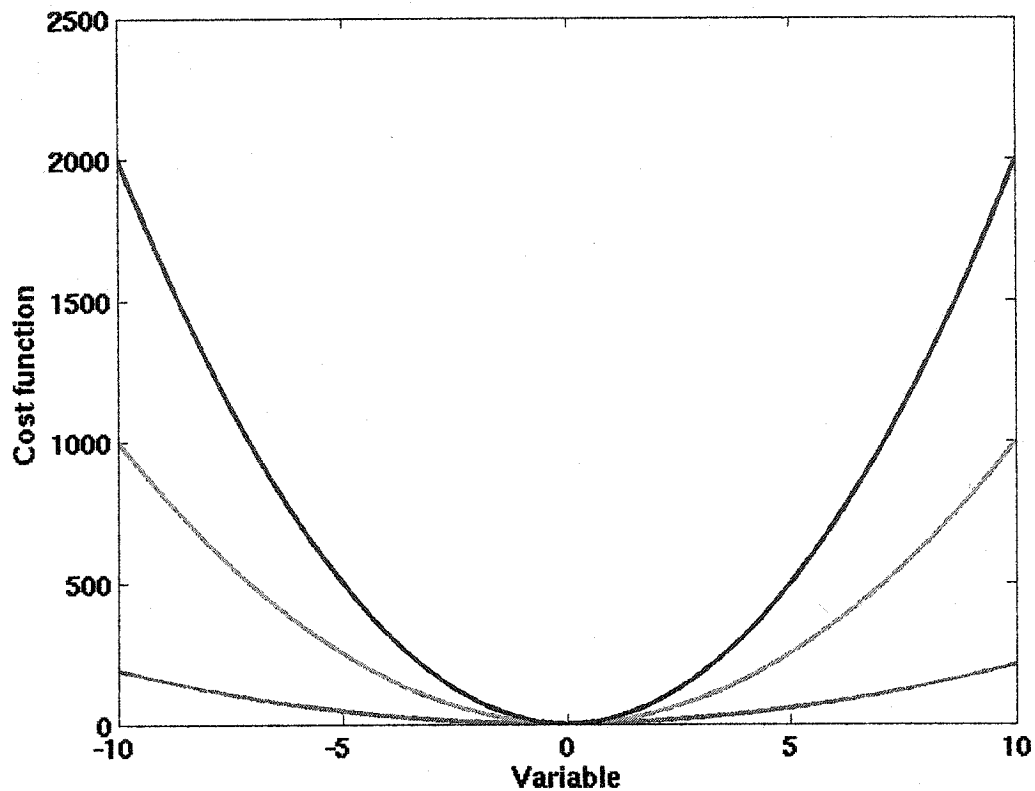
### **Results**

Figure I.1 shows the error associated with using the absorption coefficient for the attenuation of the upwelling fluoresced radiance. An error of ~12 % occurs at  $b_p(551) = 1 \text{ m}^{-1}$ . For comparison, Babin et al. (2003) found values of  $b_p(555)$  of  $1 \text{ m}^{-1}$  at a concentration of suspended particulate matter of  $\sim 2 \text{ g m}^{-3}$ ; roughly half of their data set for Case 2 waters had values higher than this. In Case 1 waters, using the relationship of Loisel and Morel (1998) for surface waters, and a wavelength dependence of  $\lambda^{-1}$  for scattering,  $b_p(551) = 1 \text{ m}^{-1}$  corresponds to chlorophyll concentration of  $\sim 2.5 \text{ mg m}^{-3}$ . Over the range of clay concentration tested, the error was lower when  $a_f$  was replaced by  $a_f(678) + 0.0873 \cdot b(678)^{1.47}$  where  $b(678)$  is the total scattering coefficient at 678 nm.

## *Appendix II: Errors and correlation of the retrieved parameters.*

The errors presented on Figure 4.4 represent 95% confidence interval on the parameters taken one at a time given the residuals observed for the fit. They follow from a property of the (scaled) Hessian of the log likelihood function of the least-square cost function; the diagonal terms of the Hessian correspond to the variance of the corresponding estimated parameter and the off diagonal terms correspond to the covariance terms (Priestley 1981). The Hessian, calculated at  $\hat{\theta}$  provides an estimate of the curvature of the cost-function, the greater the curvature, the more information is contained about a parameter (see Figure II.1). It should be noted however, that the errors estimates are strictly valid only if the regression errors ( $\epsilon_i$ ) are randomly distributed, additive, with common variance and non-correlated, the residuals of the fits for the reflectance spectra fail these three criterion, as such the errors shown should be taken approximations of the expected errors. Subsampling the spectra may provide a way to address this issue, it was not investigated here.

The error ellipses can be calculated using the Hessian. Figure II.2 shows the error ellipses for the last fitted spectrum, this provide similar information about the error on the estimated parameter (horizontal and vertical extend of the ellipse) and on the covariance of the fitted parameters. Plotted are the ellipses for the 95% confidence intervals when parameters are taken two at a time. The ellipses provide redundant information about the



**Figure II.1: Three idealized cost-functions for a one dimensional regression. The cost-function (in this chapter the sum of squared differences) is minimum at the best-fit parameter values  $\hat{\theta}$ . The curvature of the function at that point provides an indication of the amount of information contained in the data fitted. In this example, the blue line (lowest) contains less information than the red line (highest), which has a stronger curvature.**

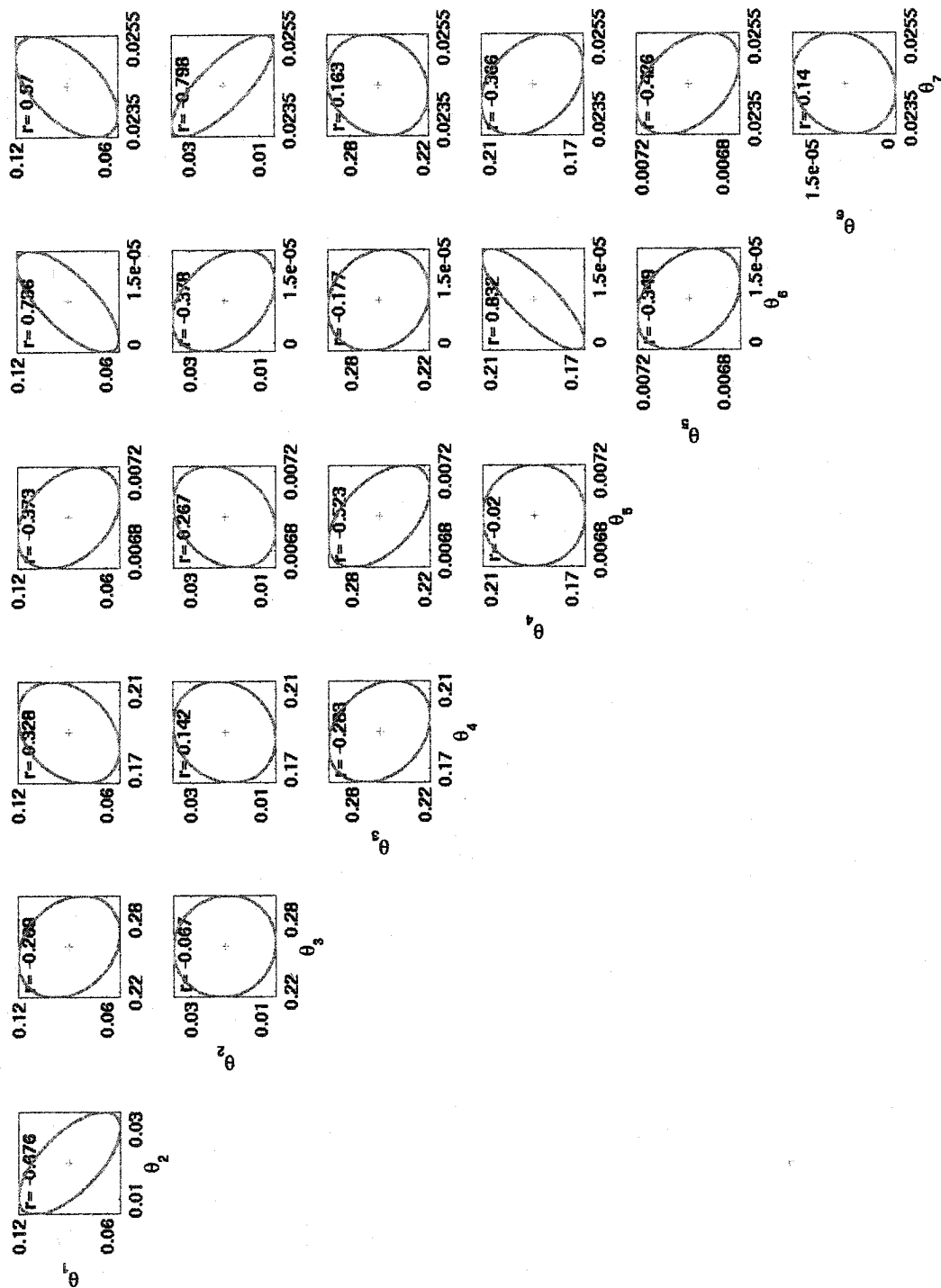


Figure II.2: Error ellipses for the fitted parameters taken two at a time on last spectra of the Bering Sea timeseries. The expected correlation coefficient between the two plotted parameters is also provided in each graph.

amplitude of the error compared to Figure 4.4, furthermore they only apply to the last point of the timeseries. However, they provide insights into the expected covariation between the estimated parameters. Figure II.2 shows that most estimates are not expected to show much correlation, except for a positive correlation between  $\theta_4 (a_\phi(512))$  and  $\theta_6 (s_{bpart})$ , and  $\theta_1 (a_{CM}(400))$  and  $\theta_6 (s_{bpart})$  a negative correlation between  $\theta_1 (a_{CM}(400))$  and  $\theta_2 (s_{CM})$ , and  $\theta_2 (s_{CM})$  and  $\theta_7 (\phi_f)$ .

The negative correlation between  $a_{CM}(400)$  and  $s_{CM}$  is expected, and mean that there is not enough information in the reflectance spectrum to separate accurately, at the same time, the slope and the magnitude of the CM spectrum. Using a fixed value for  $s_{CM}$  seems an appropriate way to remediate to this problem when  $s_{CM}$  is known.

The negative correlation between  $\phi_f$  and  $s_{CM}$  is hard to understand and merits further attention. It is hard to propose any simplification to the model, which would help with this covariation without understanding where it originates.

The positive correlation between  $a_\phi(512)$  and  $s_{bpart}$  is easily understood, when considering that increasing the slope of  $s_{bpart}$  will lead to more blue light being reflected and increasing  $a_\phi(512)$  will have an opposite effect. This shows that there is little information in the spectrum for separating the increase of one versus the decrease of the other. The positive correlation between  $a_{CM}(400)$  and  $s_{bpart}$  occurs for the same reason. Fixing the parameter  $s_{bpart}$  at one value or using a measured shape for the absorption by colored matter would solve this problem.

## *Appendix III : Baseline correction of FLH*

*Hydrolight simulations* — Five series of simulations using Hydrolight (a numerical modeling package using invariant imbedding methods to solve the radiative transfer equation, Sequoia Scientific Inc., Version 4.2), four with chlorophyll fluorescence (differing by their quantum yield) and one without, were performed to study the baseline algorithm used by MODIS in case 1 waters. In these simulations, the statistical model of Morel and Maritorena (2001) was followed as closely as possible. The underwater light field was computed for chlorophyll concentrations of 0.03, 0.05, 0.1, 0.3, 0.5, 1.0, 3.0, 5.0, 10.0, and 15.0 mg m<sup>-3</sup>. The parameterization for scattering and the backscattering fraction is according to Morel and Maritorena (2001). To obtain the appropriate backscattering fraction we used Fournier-Forand phase functions (Fournier and Forand 1994). The absorption coefficients measured by Pope and Fry (1997) were used for pure water. Absorption by dissolved matter and phytoplankton were modeled following Appendix B in Morel and Maritorena (2001), except that the background  $a_{\text{gilvin}}$  was set to 0 m<sup>-1</sup> when the chlorophyll concentration was 0 mg m<sup>-3</sup>. Scattering and absorption were specified as constant with depth and water depth was infinite. All Hydrolight series were calculated at the MODIS wavebands and additional wavebands, including 709 nm, a Medium Resolution Imaging Spectroradiometer (MERIS) band; MERIS uses 665 and 709 nm for the baseline correction and 681 nm for the fluorescence measurement (Anonymous 2002). All simulations included Raman emission parameterized following Morel et al. (2002) and Bartlett et al. (1998) (i.e. spectral

dependency  $\lambda^{-5}$  and Raman scattering coefficient of  $2.6 \times 10^{-4} \text{ m}^{-1}$  at 488 nm). In all cases, Radtran with Hydrolight's default parameters was used to calculate the incident irradiance for the equator and a sun zenith angle of  $31^\circ$ ; this is consistent with the equatorial crossing time of MODIS on the autumnal equinox. The quantum yield of fluorescence was set to 0.005, 0.01, 0.03 and 0.05.

*Results and Discussion* — The choice of the 665 nm waveband for the lower bound of the baseline, leads partly to the underestimate for the MODIS algorithm; assuming a Gaussian fluorescence emission with a width at half-maximum of 25 nm centered at 683 nm, the baseline is 0.2878 of the signal at 678 nm. This factor is accounted for in the MODIS  $C_f$  parameter and is included in the *CFE* algorithm (Ricardo Letelier, personal communication). The trends with chlorophyll and quantum yield, however, are not accounted for, and originate from the relative amplitude of the backscattered upwelling radiance emission to fluorescence emission and the increasing concavity of the backscattered emission as chlorophyll increases around 676 nm (Figure 5.5 right panel).

The simulations in this study were conducted for just above the sea surface. Additional biases that may originate in the use of the atmospheric aerosol scattered radiance plus water leaving radiance (top of atmosphere minus Rayleigh scattered photons) to obtain *FLH* have not been investigated. The observed negative radiances in the MODIS *FLH* before the addition of a constant (Abbott and Letelier 1999) did not occur in our simulation and are attributable to the shape of the atmospheric radiance (Ricardo Letelier, personal communication). **Nevertheless, even at the sea surface,**

**baseline corrected fluorescence is not a direct measure of the fluorescence emission. The fraction of the total fluorescence emission it measures varies with chlorophyll concentration.** The addition of a small baseline value,  $FLH_o$ , of  $1.26 \times 10^{-5} \text{ W m}^{-2} \text{ nm}^{-1} \text{ sr}^{-1}$  to the measured upwelling radiance eliminated much of the trend with chlorophyll concentration (Figure 5.5 inset), this however cannot be applied directly to the  $FLH$  measurement without further correction accounting for scattering in the atmosphere.

The use of the baseline method to retrieve fluorescence emission has been examined in the past mostly with the objective of obtaining chlorophyll concentration. Fisher and Kronfeld (1990), using 645 and 725 nm for the baseline and 685 nm for the measurement, found a slight overestimate of the upwelling radiance due to fluorescence at chlorophyll concentrations below  $\sim 20 \text{ mg m}^{-3}$  and an underestimate above  $20 \text{ mg m}^{-3}$ . This is different from our simulation (Figure 5.5), which shows an increasing underestimate of the fluorescence radiance below the surface with decreasing chlorophyll concentrations in case 1 waters, especially at lower quantum yields. Our results are more in line with those of Gower et al. (1999), which suggest that, in the MERIS configuration, the fluorescence radiance measurement would be underestimated by approximately 30% at  $15.4 \text{ mg chl m}^{-3}$ . Gower et al. (1999) did not verify this relationship for a range of chlorophyll concentrations but suggest it should be nearly constant. The different results are likely the result of varying modeling approaches for the incident irradiance, the inherent optical properties of the water, the parameterization of Raman scattering, the quantum yield of fluorescence or the wavebands used. Application of the results from Figure 5.5 to the data requires an iterative scheme or a precalculated look-up table (e.g.

Fell et al. 2000) as the quantum yield must be known to correct the *FLH*. This was not attempted here. Further work will be necessary to completely account for this effect in case 1 waters and possibly extend it to the top of the atmosphere (corrected for molecular scattering) measurement of *FLH* (Abbott and Letelier 1999). **At this point, however, given the potential underestimation of fluorescence radiance by *FLH* in low chlorophyll waters, it is not surprising to find CFE or our algorithm returning lower quantum yields in regions with lower chlorophyll concentration.** This artifact could account for more than half of the increasing trend observed in  $\phi_{est}$  vs. MODIS chlorophyll in Figure 5.9 and Figure 5.13.

## *Appendix IV : Interpretation of the quantum yield of sun-induced chlorophyll fluorescence quantum yield*

We have defined the quantum yield of fluorescence *in vivo*,  $\phi$ , as the ratio of photons fluoresced by chlorophyll *a* over the whole fluorescence band to the photons absorbed by all cellular pigments. This is the definition typically used for sun-induced fluorescence studies (e.g. Babin et al. 1996b; Ostrowska et al. 1997; Maritorena et al. 2000; Morrison 2003). This definition has important implications for the interpretation of the retrieved yields, especially in terms of photosynthetic capabilities.

Even if retrieved perfectly,  $\phi$  is not directly interpretable in terms of photosynthetic and non-photosynthetic rate processes. This is because a variable fraction of photons is absorbed by the fluorescing photosystem II (Johnsen et al. 1997). The quantum yield retrieved by our approach will therefore be related to  $\phi_{\text{PSII}}$ , the quantum yield of fluorescence used in models of photosynthesis and electron transport and interpretable in terms of rate constants as:

$$\phi = \phi_{\text{PSII}} \cdot \frac{\int a_{\text{PSII}}(\lambda) \cdot \overset{\circ}{E}(\lambda) \cdot d\lambda}{\int_{\text{PAR}} a_{\phi}(\lambda) \cdot \overset{\circ}{E}(\lambda) \cdot d\lambda} \quad 5.22$$

where  $a_{\text{PSII}}$  ( $\text{m}^{-1}$ ) represents the absorption by photosynthetic pigments in the PSII antenna and core, and  $a_{\phi}$  is the total absorption by phytoplankton which also includes

absorption by photoprotective pigments (Bidigare et al. 1990; Jeffrey et al. 1997) and the photosynthetic pigment associated with PSI. To relate  $\phi$  to  $\phi_{\text{PSII}}$ , the spectral optical cross-section of PSII and the spectral total optical cross-section have to be measured (e.g. Sosik and Mitchell 1995). Variability on the order of 2 to 8 have been observed in situ for the ratio of photosynthetic to non-photosynthetic pigment absorption (e.g. Bidigare et al. 1992; Babin et al. 1996a; Allali et al. 1997) and on the order of about 2 for photosystem II to total absorption (e.g. Sosik and Mitchell 1995) but the ranges could be larger (see for example Johnsen et al. 1997; Lutz et al. 1998; 2001).

In a study of vertical profiles of  $\phi$  in the Baltic Sea, Ostrowska *et al.* (1997) found that the yield was not correlated with incident PAR, correlated weakly with temperature and chlorophyll concentration, and correlated best with  $\bar{a}_\phi^*$ . The quantum yield was decreasing with increasing  $\bar{a}_\phi^*$  from  $\phi \sim 0.012$  at  $\bar{a}_\phi^* = 0.005 \text{ m}^2 \text{ mg chl}^{-1}$  to  $\phi \sim 0.005$  at  $\bar{a}_\phi^* = 0.025 \text{ m}^2 \text{ mg chl}^{-1}$ . This is consistent with an increase in the fraction of absorption by non-photosynthetic pigments decreasing the yield and is another possible explanation of the increasing  $\phi_{\text{est}}$  with increasing chlorophyll concentration (see also eq. 15 in Babin et al. 1996b) observed in the top panels of Figure 5.9 and Figure 5.13, since  $\bar{a}_\phi^*$  generally decreases with increasing chlorophyll a concentration (Bricaud et al. 1995; Ciotti et al. 2002).

The implication is that variability in the pigment composition is probably as much a determinant of  $\phi$  as are the rate constants for photochemistry and heat dissipation (e.g. Gilmore and Govindjee 1999). Any interpretation of the yields in terms of

photosynthetic or non-photochemical capacities should take these changes into account (e.g. Maritorena et al. 2000). For example, the increase with depth of the ratio of absorption by photosynthetic to non-photosynthetic pigments should be reflected in an increase in the quantum yield sun-induced chlorophyll fluorescence; however, this does not imply a decrease in non-photochemical quenching or in the photochemical quantum yield.

## Appendix V: Copyrights agreement form

November 20, 2004

Limnology and Oceanography: Methods

ASLO Business Office  
5400 Bosque Boulevard, Suite 680  
Waco, Texas 76710-4446

I am preparing my Ph.D. thesis for submission to the Faculty of Graduate Studies at Dalhousie University, Halifax, Nova Scotia, Canada. I am seeking your permission to include a manuscript version of the following paper(s) as a chapter in the thesis:

Huot, Y., C. A. Brown, J.J. Cullen, (2004). "New algorithms for MODIS sun-induced chlorophyll fluorescence and a comparison with present data products." *Limnology and Oceanography: Methods*.

Canadian graduate theses are reproduced by the Library and Archives of Canada (formerly National Library of Canada) through a non-exclusive, world-wide license to reproduce, loan, distribute, or sell theses. I am also seeking your permission for the material described above to be reproduced and distributed by the LAC(NLC). Further details about the LAC(NLC) thesis program are available on the LAC(NLC) website ([www.nlc-bnc.ca](http://www.nlc-bnc.ca)).

Full publication details and a copy of this permission letter will be included in the thesis.

Yours sincerely,




Yannick Huot

---

Permission is granted for:

- a) the inclusion of the material described above in your thesis.
- b) for the material described above to be included in the copy of your thesis that is sent to the Library and Archives of Canada (formerly National Library of Canada) for reproduction and distribution.

Name:	<u>Paul Kemp</u>	Title:	<u>Editor in Chief, L&amp;O: Methods</u>
Signature:		Date:	<u>Nov 21 2004</u>

## Bibliography

- Abbott, M. R., and R. M. Letelier. 1999. Algorithm theoretical basis document chlorophyll fluorescence (MODIS product number 20). web document. NASA.
- Abbott, M. R., J. G. Richman, R. M. Letelier, and J. S. Bartlett. 2000. The spring bloom in the Antarctic Polar Frontal Zone as observed from a mesoscale array of bio-optical sensors. *Deep-Sea Research II* 47: 3285-3314.
- Ahn, Y.-H. 1990. Propriétés optiques des particules biologiques et minérales présentes dans l'océan. Application : inversion de la réflectance, 214. Université Pierre et Marie Curie.
- Albert, A., and C. D. Mobley. 2003. An analytical model for subsurface irradiance and remote sensing reflectance in deep and shallow case-2 waters. *Optics Express* 11: 2873-2890.
- Allali, K., A. Bricaud, and H. Claustre. 1997. Spatial variations in the chlorophyll-specific absorption coefficient of phytoplankton and photosynthetically active pigments in the equatorial Pacific. *Journal of Geophysical Research* 102: 12413-12423.
- Allen, J. F. 1995. Thylakoid protein phosphorylation, state 1-state 2 transitions, and photosystem stoichiometry adjustment: redox control at multiple levels of gene expression. *Physiologia Plantarum* 93: 196-205.
- Alvain, S., C. Moulin, Y. Dandonneau, and F. M. Bréon. 2004. Remote sensing of phytoplankton groups in case 1 waters from global SEAWIFS imagery, p. CD. *In* S. G. Ackleson [ed.], *Ocean Optics XVII*. ONR.
- Anderson, J. M., Y.-I. Park, and W. S. Chow. 1998. Unifying model for the photoinactivation of photosystem II *in vivo* under steady-state photosynthesis. *Photosynthesis Research* 56: 1-13.
- Anonymous. 2002. MERIS product handbook, <http://envsat.esa.int/dataproducts/meris/CNTR.htm>
- Arar, E. J., and G. B. Collins. 1997. In vitro determination of chlorophyll a and pheophytin a in marine and freshwater algae by fluorescence. Method 445.0. U.S. Environmental Protection Agency.

- Aro, E.-M., I. Virgin, and B. Andersson. 1993. Photoinhibition of photosystem II. Inactivation, protein damage and turnover. *Biochimica et Biophysica Acta* 1143: 113-134.
- Austin, R. W., and T. J. Petzold. 1980. The determination of the diffuse attenuation coefficient of sea water using the coastal zone color scanner, p. 239-255. *In* J. F. R. Gower [ed.], *COSPAR/SCOR/IUCRM Symposium on Oceanography from space*. Plenum Press.
- Babin, M., A. Morel, H. Claustre, A. Bricaud, Z. Kolber, and P. G. Falkowski. 1996a. Nitrogen- and irradiance-dependent variations of the maximum quantum yield of carbon fixation in eutrophic, mesotrophic and oligotrophic marine systems. *Deep-Sea Research I* 43: 1241-1272.
- Babin, M., A. Morel, V. Fournier-Sicre, F. Fell, and D. Stramski. 2003. Light scattering properties of marine particles in coastal and open ocean waters as related to the particle mass concentration. *Limnology and Oceanography* 48: 843-859.
- Babin, M., A. Morel, and B. Gentili. 1996b. Remote sensing of sea surface sun-induced chlorophyll fluorescence: consequences of natural variations in the optical characteristics of phytoplankton and the quantum yield of chlorophyll *a* fluorescence. *International Journal of Remote Sensing* 17: 2417-2448.
- Barber, J., and W. Kühlbrandt. 1999. Photosystem II. *Current Opinion in Structural Biology* 9: 469-475.
- Bartlett, J. S., K. J. Voss, S. Sathyendranath, and A. Vodacek. 1998. Raman scattering by pure water and seawater. *Applied Optics* 37: 3324-3332.
- Behrenfeld, M. J., E. Boss, D. A. Siegel, and D. M. Shea. in press. Carbon-based ocean productivity and phytoplankton physiology from space. *Global Biogeochemical Cycles*.
- Behrenfeld, M. J., O. Prasil, M. Babin, and F. Bruyant. 2004. In search of a physiological basis for covariations in light-limited and light-saturated photosynthesis. *Journal of Phycology* 40: 4-25.
- Behrenfeld, M. J., O. Prasil, Z. S. Kolber, M. Babin, and P. G. Falkowski. 1998. Compensatory changes in Photosystem II electron turnover rates protect photosynthesis from photoinhibition. *Photosynthesis Research* 58: 259-268.
- Bernardt, K., and H.-W. Trissl. 1999. Theories for kinetics and yields of fluorescence and photochemistry: how, if at all, can different models of antenna organization be distinguished experimentally? *Biochimica et Biophysica Acta* 1409: 125-142.

- Bidigare, R. R., M. E. Ondrusek, J. H. Morrow, and D. A. Kiefer. 1990. In vivo absorption properties of algal pigments, p. 290-302, *Ocean Optics X*.
- Bidigare, R. R., B. B. Prézelin, and R. C. Smith. 1992. Bio-optical models and the problems of scaling, p. 175-212. *In* P. G. Falkowski and A. Woodhead [eds.], *Primary Productivity and Biogeochemical Cycling in the Sea*. Plenum Press.
- Björkman, O., and W. Bilger. 1990. Role of the xanthophyll cycle in photoprotection elucidated by measurements of light induced absorbance changes, fluorescence and photosynthesis in leaves of *Hedera Canariensis*. *Photosynthesis Research* 4: 11-18.
- Björkman, O., and B. Demmig-Adams. 1994. Regulation of photosynthetic light energy capture, conversion, and dissipation in leaves of higher plants, p. 17-47. *In* E.-D. Schultz and M. M. Caldwell [eds.], *Ecophysiology of photosynthesis*. Ecological Studies. Springer-Verlag.
- Blough, N. V., and R. Del Vecchio. 2002. Chromophoric DOM in the coastal environment, p. 509-546. *In* D. A. Hansell and C. A. Carlson [eds.], *Biogeochemistry of Marine Dissolved Organic Matter*. Academic Press.
- Boss, E., and W. S. Pegau. 2001. Relationship of light scattering at an angle in the backward direction to the backscattering coefficient. *Applied Optics* 40: 5503-5507.
- Bricaud, A., M. Babin, A. Morel, and H. Claustre. 1995. Variability in the chlorophyll-specific absorption coefficients of natural phytoplankton: Analysis and parameterization. *Journal of Geophysical Research* 100: 13321-13332.
- Bricaud, A., H. Claustre, J. Ras, and K. Oubelkheir. in press. Natural variability of phytoplankton absorption in oceanic waters: influence of the size structure of algal populations. *Journal of Geophysical Research*.
- Brown, C. A., Y. Huot, R. F. Davis, S. Kirchhoff, C. Ryan, M. R. Lewis, and J. J. Cullen. 2003. Towards assessing algal physiology from real time in situ optical measurements, [http://www.obs-vlfr.fr/~habwatch/Presentations/posters/p04\\_brown.pdf](http://www.obs-vlfr.fr/~habwatch/Presentations/posters/p04_brown.pdf)
- Bruyant, F., M. Babin, B. Genty, O. Prasil, M. J. Behrenfeld, H. Claustre, A. Bricaud, J. Holtzendorff, M. Koblížek, L. Garczarek, and F. Partensky. accepted. Diel variations in the photosynthetic parameters of *Prochlorococcus* strain PCC 9511: combined effects of light and cell cycle. *Limnology and Oceanography*.

- Bruyant, F., M. Babin, B. Genty, O. Prasil, L. Garczarek, H. Claustre, M. J. Behrenfeld, A. Bricaud, and F. Partensky. 2000. Diel variation in the quantum yield of *in vivo* chlorophyll fluorescence, p. CD, Oceans Optics XV.
- Bukata, R. P., J. H. Jerome, G. A. Borstad, L. N. Brown, and J. F. R. Gower. 2004. Mitigating the impact of trans-spectral processes on multivariate retrieval of water quality parameters from case 2 waters. *Canadian Journal of Remote Sensing* 30: 8-16.
- Butler, W. L. 1978. Energy distribution in the photochemical apparatus of photosynthesis. *Annual Reviews of Plant Physiology* 29: 345-378.
- Campbell, D., H. Vaughan, A. K. Clarke, P. Gustafsson, and G. Öquist. 1998. Chlorophyll fluorescence analysis of cyanobacterial photosynthesis and acclimation. *Microbiology and Molecular Biology Reviews* 62: 667-683.
- Carder, K. L. 2003. Terra chlorophyll\_a pigment concentration (Case 2 waters) Data quality summary, <http://modis-ocean.gsfc.nasa.gov/qa/terra/dataqualsum/>
- Carder, K. L., F. R. Chen, and S. K. Hawes. 2003. Algorithm theoretical basis document ATBD 20 Instantaneous Photosynthetically Available Radiation and Absorbed Radiation by Phytoplankton. web document. NASA.
- Carder, K. L., F. R. Chen, Z. P. Lee, and S. K. Hawes. 1999a. Algorithm theoretical basis document ATBD 19 Case 2 Chlorophyll a. web document. NASA.
- Carder, K. L., F. R. Chen, Z. P. Lee, S. K. Hawes, and D. Kamykowski. 1999b. Semianalytic Moderate-Resolution Imaging Spectrometer algorithm for chlorophyll *a* concentration and absorption with bio-optical domains based on nitrate-depletion temperatures. *Journal of Geophysical Research* 104: 5403-5421.
- Casper-Lindley, C., and O. Björkman. 1998. Fluorescence quenching in four unicellular algae with different light-harvesting and xanthophyll-cycle pigments. *Photosynthesis Research* 56: 277-289.
- Chamberlin, S., and J. Marra. 1992. Estimation of photosynthetic rate from measurements of natural fluorescence: analysis of the effects of light and temperature. *Deep-Sea Research* 39: 1695-1706.
- Chamberlin, W. S., C. R. Booth, D. A. Kiefer, J. H. Morrow, and R. C. Murphy. 1990. Evidence for a simple relationship between natural fluorescence, photosynthesis and chlorophyll in the sea. *Deep-Sea Research* 37: 951-973.
- Chisholm, S. W., P. G. Falkowski, and J. J. Cullen. 2001. Dis-crediting ocean fertilization. *Science* 294: 309-310.

- Chow, W. S. 2001. The photoinactivation of photosystem II in Leaves: A personal perspective. *Journal of Photoscience* 2001: 43-53.
- Ciotti, Á. M. 1999. Influence of phytoplankton communities on relationships between optical properties of coastal surface waters, 208 pp., *Oceanography*. Dalhousie.
- Ciotti, Á. M., J. J. Cullen, and M. R. Lewis. 1999. A semi-analytical model of the influence of phytoplankton community structure on the relationship between light attenuation and ocean color. *Journal of Geophysical Research* 104: 1559-1578.
- Ciotti, Á. M., M. R. Lewis, and J. J. Cullen. 2002. Assessment of the relationship between dominant cell size in natural phytoplankton communities and the spectral shape of the absorption coefficient. *Limnology and Oceanography* 47: 404-417.
- Clark, D. K. 1999. Algorithm theoretical basis document ATBD 18 Case 1 Waters. web document. NASA.
- . 2001. Terra - Diffuse attenuation coefficient at 490 nm (K490) Data Quality Summary, <http://modis-ocean.gsfc.nasa.gov/qa/terra/dataqualsum/>
- Clayton, R. K. 1980. *Photosynthesis physical mechanisms and chemical patterns*. Cambridge University Press. Cambridge
- Cleveland, J. S., and M. J. Perry. 1987. Quantum yield, relative specific absorption and fluorescence in nitrogen-limited *Chaetoceros gracilis*. *Marine Biology* 94: 489-497.
- Coble, P. G. 1996. Characterization of marine and terrestrial DOM in seawater using excitation-emission matrix spectroscopy. *Marine Chemistry* 51: 325-346.
- Coleman, J. E., R. A. Reynolds, M. C. Talbot, M. Twardowski, and M. J. Perry. 2000. Utilization of solar-induced chlorophyll a fluorescence as an indicator of phytoplankton biomass in coastal waters, *Ocean Optics* XV.
- Collins, D. J., D. A. Kiefer, J. B. Soohoo, and I. S. McDermid. 1985. The role of reabsorption in the spectral distribution of phytoplankton fluorescence emission. *Deep-Sea Research* 32: 983 -1003.
- Cullen, J. J. 1982. The deep chlorophyll maximum: Comparing vertical profiles of chlorophyll *a*. *Canadian Journal of Fisheries and Aquatic Sciences* 39: 791-803.
- . 1990. On models of growth and photosynthesis in phytoplankton. *Deep-Sea Research* 37: 667-683.

- Cullen, J. J., Á. M. Ciotti, R. F. Davis, and P. J. Neale. 1997. The relationship between near-surface chlorophyll and solar-stimulated fluorescence: biological effects. *Ocean Optics XIII, Proc. SPIE 2963*: 272-277.
- Cullen, J. J., and R. F. Davis. 2003. The blank can make a big difference in oceanographic measurements. *Limnology and Oceanography Bulletin* 12: 21-35.
- Cullen, J. J., and M. R. Lewis. 1988. The kinetics of algal photoadaptation in the context of vertical mixing. *Journal of Plankton Research* 10: 1039-1063.
- . 1995. Biological processes and optical measurements near the sea-surface: some issues relevant to remote sensing. *Journal of Geophysical Research* 100: 13255-13266.
- Cullen, J. J., and J. G. MacIntyre. 1998. Behavior, physiology and the niche of depth-regulating phytoplankton, p. 559-580. *In* D. M. Anderson, A. D. Cembella and G. M. Hallegraeff [eds.], *Physiological Ecology of Harmful Algal Blooms*. Springer-Verlag.
- Cullen, J. J., and P. J. Neale. 1997. Biological weighting functions for describing the effects of ultraviolet radiation on aquatic systems, p. 97-118. *In* D.-P. Häder [ed.], *The effects of ozone depletion on aquatic ecosystems*. R.G. Landes Company.
- Cullen, J. J., P. J. Neale, and M. P. Lesser. 1992a. Biological weighting function for the inhibition of phytoplankton photosynthesis by ultraviolet radiation. *Science* 258: 646-650.
- Cullen, J. J., and E. H. Renger. 1979. Continuous measurement of the DCMU-induced fluorescence response of natural phytoplankton populations. *Marine Biology* 53: 13-20.
- Cullen, J. J., Y. Xiaolong, and H. L. MacIntyre. 1992b. Nutrient limitation of marine photosynthesis, p. 69-88. *In* P. G. Falkowski [ed.], *Primary productivity and biogeochemical cycles in the sea*. Plenum Press.
- Cullen, J. J., C. S. Yentsch, T. L. Cucci, and H. L. MacIntyre. 1988. Autofluorescence and other optical properties as tools in biological oceanography. *Proceedings of SPIE, International Society of Optical Engineering* 925: 149-156.
- Culver, M. E., and M. J. Perry. 1997. Calculation of solar-induced fluorescence in surface and subsurface waters. *Journal of Geophysical Research* 102 (C5): 10563-10572.
- Dandonneau, Y., and J. Neveux. 1997. Diel variations of the *in vivo* fluorescence in the eastern equatorial Pacific: an unvarying pattern. *Deep-Sea Research II* 44: 1869-1880.

- Dau, H. 1994. Molecular mechanisms and quantitative models of variable photosystem II fluorescence. *Photochemistry and Photobiology* 60: 1-23.
- Demers, S., S. Roy, R. Gagnon, and C. Vignault. 1991. Rapid light-induced changes in cell fluorescence and in xanthophyll-cycle pigments of *Alexandrium excavatum* (Dinophyceae) and *Thalassiosira pseudonana* (Bacillariophyceae): a photo-protection mechanism. *Marine Ecology Progress Series* 76: 185-193.
- Demmig-Adams, B., and W. W. Adams III. 1992. Photoprotection and other responses of plants to high light stress. *Annual Reviews of Plant Physiology and Plant Molecular Biology* 1992: 599-626.
- . 1996. Xanthophyll cycle and light stress in nature: uniform response to excess direct sunlight among higher plant species. *Planta* 198: 460-470.
- Dubinsky, Z., P. G. Falkowski, and K. Wyman. 1986. Light Harvesting and utilization by Phytoplankton. *Plant and Cell Physiology* 27: 1335-1349.
- Eilers, P. H. C., and J. C. H. Peeters. 1988. A model for the relationship between light intensity and the rate of photosynthesis in phytoplankton. *Ecological modelling* 42: 199-215.
- . 1993. Dynamic behaviour of a model for photosynthesis and photoinhibition. *Ecological modelling* 69: 113-133.
- Emerson, R., and W. Arnold. 1932. The photochemical reaction in photosynthesis. *The Journal of General Physiology* 16: 191-205.
- Esaias, W. E., M. R. Abbott, I. Barton, O. B. Brown, J. W. Campbell, K. L. Kendall, D. K. Clark, R. H. Evans, F. E. Hoge, H. R. Gordon, W. M. Balch, R. Letelier, and P. J. Minnett. 1998. An overview of MODIS capabilities for ocean science observations. *IEEE Transactions on Geoscience and Remote Sensing* 36: 1250-1265.
- Escoubas, J.-M., M. Lomas, J. LaRoche, and P. G. Falkowski. 1995. Light intensity regulation of CAB gene-transcription is signaled by the redox state of the plastoquinone pool. *Proceedings of the National Academy of Sciences of the United States of America* 92: 10237-10241.
- Falkowski, P. G., R. Greene, and Z. Kolber. 1994. Light utilization and photoinhibition of photosynthesis in marine phytoplankton, p. 407-432. *In* N. R. Baker and J. R. Bowyer [eds.], *Photoinhibition of Photosynthesis from molecular mechanisms to the field*. Environmental Plant Biology. BIOS Scientific.

- Falkowski, P. G., and Z. Kolber. 1993. Estimation of phytoplankton photosynthesis by active fluorescence. ICES Marine Science Symposium 197: 92-103.
- . 1995. Variations in chlorophyll fluorescence yields in phytoplankton in the world oceans. Australian Journal of Plant Physiology 22: 341-355.
- Falkowski, P. G., and J. LaRoche. 1991. Acclimation to spectral irradiance in algae. Journal of Phycology 27: 8-14.
- Falkowski, P. G., and T. G. Owens. 1980. Light-Shade adaptation two strategies in marine phytoplankton. Plant and Cell Physiology 66: 592-595.
- Falkowski, P. G., and J. A. Raven. 1997. Aquatic Photosynthesis, First ed. Blackwell Science. Malden
- Falkowski, P. G., and C. D. Wirick. 1981. A simulation model of the effects of vertical mixing on primary productivity. Marine Biology 65: 69-75.
- Fell, F., E. Dilligeard, C. Olbert, M. Babin, and G. M. Ferrari. 2000. Using the sun-induced chlorophyll fluorescence for the remote retrieval of phytoplankton in case-II waters: a case study. In S. G. Ackleson [ed.], Ocean Optics XV.
- Fichot, C. G., and W. L. Miller. 2002. Towards the remote sensing of CDOM optical properties. In S. Ackleson [ed.], Ocean Optics XVI. Office of Naval Research.
- Fiedler, P. C. 2002. The annual cycle and biological effects of the Costa Rica Dome. Deep-Sea Research I 49: 321-338.
- Field, C. B., M. J. Behrenfeld, J. T. Randerson, and P. G. Falkowski. 1998. Primary production of the biosphere: Integrating terrestrial and oceanic components. Science 281: 237-240.
- Fisher, J., and U. Kronfeld. 1990. Sun-stimulated chlorophyll fluorescence 1: Influence of oceanic properties. International Journal of Remote sensing 11: 2125-2147.
- Flameling, I. A., and J. Kromkamp. 1998. Light dependence of quantum yields for PSII charge separation and oxygen evolution in eukaryotic algae. Limnology and Oceanography 43: 284-297.
- Flynn, K. J., S. Page, G. Wood, and C. R. Hipkin. 1999. Variations in the maximum transport rates for ammonium and nitrate in the prymnesiophyte *Emiliania huxleyi* and the raphidophyte *Heterosigma carterae*. Journal of Plankton Research 21: 355-371.

- Fournier, G. R., and J. L. Forand. 1994. Analytic phase function for ocean water, p. 194-201. *In* J. Jaffe [ed.], *Ocean Optics XII*. SPIE.
- Franklin, L. A., C. B. Osmond, and A. W. D. Larkum. 2003. Photoinhibition, UV-B and algal photosynthesis, p. 351-384. *In* A. W. D. Larkum, S. E. Douglas and J. A. Raven [eds.], *Photosynthesis in Algae*. Kluwer Academic Publishers.
- Franks, P. J. S., and J. Marra. 1994. A simple new formulation for phytoplankton photoresponse and an application in a wind-driven mixed-layer model. *Marine Ecology Progress Series* 111: 145-153.
- Fuchs, E., R. C. Zimmerman, and J. S. Jaffe. 2002. The effect of elevated levels of phaeophytin in natural water on variable fluorescence measured from phytoplankton. *Journal of Plankton Research* 24: 1221-1229.
- Garcia-Mendoza, E., and H. Maske. 1996. The relationship of solar-stimulated natural fluorescence and primary productivity in Mexican Pacific waters. *Limnology and Oceanography* 41: 1697-1710.
- Garver, S. A., and D. A. Siegel. 1997. Inherent optical property inversion of ocean color spectra and its biogeochemical interpretation 1. Time series from the Sargasso Sea. *Journal of Geophysical Research* 102: 18607-18625.
- Geider, R. J., E. H. Delucia, P. G. Falkowski, A. C. Finzi, J. P. Grime, J. Grace, T. M. Kana, J. La Roche, S. P. Long, B. A. Osborne, T. Platt, I. C. Prentice, J. A. Raven, W. H. Schlesinger, V. Smatecek, V. Stuart, S. Sathyendranath, R. B. Thomas, T. C. Vogelmann, P. J. I. Williams, and F. I. Woodward. 2001. Primary productivity of planet earth: biological determinants and physical constraints in terrestrial and aquatic habitats. *Global Change Biology* 7: 849-882.
- Geider, R. J., R. M. Greene, Z. Kolber, H. L. MacIntyre, and P. G. Falkowski. 1993. Fluorescence assessment of the maximum quantum efficiency of photosynthesis in the western North Atlantic. *Deep-Sea Research I* 40: 1205-1224.
- Geider, R. J., and H. L. MacIntyre. 2002. Physiology and biochemistry of photosynthesis and algal carbon acquisition, p. 44-77. *In* P. J. I. Williams, D. N. Thomas and C. S. Reynolds [eds.], *Phytoplankton productivity Carbon assimilation in marine and freshwater ecosystems*. Blackwell Science.
- Geider, R. J., H. L. MacIntyre, and T. M. Kana. 1996. A dynamic model of photoadaptation in phytoplankton. *Limnology and Oceanography* 41: 1-15.
- . 1997. Dynamic model of phytoplankton growth and acclimation: responses of the balanced growth rate and the chlorophyll a: carbon ratio to light, nutrient-limitation and temperature. *Marine Ecology Progress Series* 148: 187-200.

- . 1998. A dynamic regulatory model of phytoplankton acclimation to light, nutrient, and temperature. *Limnology and Oceanography* 43: 679-694.
- Genty, B., J.-M. Briantais, and N. R. Baker. 1989. The relationship between the quantum yield of photosynthetic electron transport and quenching of chlorophyll fluorescence. *Biochimica et Biophysica Acta* 990: 87-92.
- Gilmore, A. M., and Govindjee. 1999. How higher plants respond to excess light: Energy dissipation in photosystem II, p. 513-548. *In* G. S. Singhal, R. Renger, S. K. Sopory, K.-D. Irrgang and Govindjee [eds.], *Concepts in photobiology: photosynthesis and photomorphogenesis*. Concepts in photobiology. Narosa-Publishing.
- Gilmore, A. M., V. P. Shinkarev, T. L. Hazlett, and Govindjee. 1998. Quantitative analysis of the effects of intrathylakoid pH and xanthophyll cycle pigment on chlorophyll *a* fluorescence lifetime distributions and intensity in thylakoids. *Biochemistry* 37: 13582-13593.
- Gordon, H. R. 1974. Spectral variations in the volume scattering function at large angles in natural waters. *Journal of the Optical Society of America* 64: 773-775.
- . 1979. Diffuse reflectance of the ocean: the theory of its augmentation by chlorophyll *a* fluorescence. *Applied Optics* 21: 2489-2492.
- . 1999. Contribution of Raman scattering to water-leaving radiance: a reexamination. *Applied Optics* 38: 3166-3174.
- . 2002a. Inverse methods in hydrologic optics. *Oceanologia* 44: 9-58.
- . 2002b. Terra normalized water-leaving radiance data quality summary, <http://modis-ocean.gsfc.nasa.gov/qa/terra/dataqualsum/>
- Gordon, H. R., O. B. Brown, R. H. Evans, J. W. Brown, R. C. Smith, K. S. Baker, and D. K. Clark. 1988. A semianalytic radiance model of ocean color. *Journal of Geophysical Research* 93: 10909-10924.
- Govindjee. 1995. Sixty-three years since Kautsky: Chlorophyll *a* fluorescence. *Australian Journal of Plant Physiology* 22: 131-160.
- Gower, J. F. R., and G. A. Borstad. 1990. Mapping of phytoplankton by solar-stimulated fluorescence using an imaging spectrometer. *International Journal of Remote Sensing* 11: 313-320.

- Gower, J. F. R., L. Brown, and G. A. Borstad. 2004. Observations of chlorophyll fluorescence in west coast waters of Canada using the MODIS satellite sensor. *Canadian Journal of Remote Sensing* 30: 17-25.
- Gower, J. F. R., R. Doerffer, and G. A. Borstad. 1999. Interpretation of the 685 nm peak in water-leaving radiance spectra in terms of fluorescence, absorption and scattering, and its observation by MERIS. *International Journal of Remote sensing* 20: 1771-1786.
- Graziano, L. M., R. J. Geider, W. K. W. Li, and M. Olaizola. 1996. Nitrogen limitation of North Atlantic phytoplankton: analysis of physiological condition in nutrient enrichment experiments. *Aquatic Microbial Ecology* 11: 53-64.
- Greer, D. H., J. A. Berry, and O. Björkman. 1986. Photoinhibition of photosynthesis in intact bean leaves: role of light and temperature, and requirement for chloroplast-protein synthesis during recovery. *Planta* 168: 253-260.
- Greer, D. H., C. Ottander, and G. Öquist. 1991. Photoinhibition and recovery of photosynthesis in intact barley leaves at 5 and 20°C. *Physiologia Plantarum* 81: 203-210.
- Gregg, W. W., and K. L. Carder. 1990. A simple spectral solar irradiance model for cloudless maritime atmosphere. *Limnology and Oceanography* 35: 1657-1675.
- Haldrup, A., P. E. Jensen, C. Lunde, and H. V. Scheller. 2001. Balance of power: a view of the mechanism of photosynthetic state transitions. *Trends in Plant Science* 6: 301-305.
- Hall, D. O., and K. K. Rao. 1999. *Photosynthesis*, sixth ed. Cambridge University Press. Cambridge
- Han, B. P. 2001. Photosynthesis-irradiance response at physiological level: A mechanistic model. *Journal of Theoretical Biology* 213: 121-127.
- . 2002. A mechanistic model of algal photoinhibition induced by photodamage to Photosystem-II. *Journal of Theoretical Biology* 214: 519-527.
- Harm, W. 1980. *Biological effects of ultraviolet radiation*. Cambridge University Press. New-York
- Harris, G. P. 1978. Photosynthesis, productivity and growth: The physiological ecology of phytoplankton. *Archive Für Hydrobiologie Beihefte Ergebnisse Der Limnologie* 10: 1-171.

- Havaux, M., R. J. Strasser, and H. Greppin. 1991. A theoretical and experimental analysis of the  $q_p$  and  $q_n$  coefficients of chlorophyll fluorescence quenching and their relation to photochemical and nonphotochemical events. *Photosynthesis Research* 27: 41-55.
- Hawes, S. K. 1992. Quantum fluorescence efficiencies of marine fulvic and humic acids, 92 pp., *Marines Science*. University of South Florida.
- He, J., and W. S. Chow. 2003. The rate coefficient of repair of photosystem II after photoinactivation. *Physiologia Plantarum* 118: 297-304.
- Heaney, S. I. 1978. Some observations on the use of the *in vivo* fluorescence technique to determine chlorophyll *a* in natural populations and cultures of freshwater phytoplankton. *Freshwater Biology* 8: 115-126.
- Henriksen, P., B. Riemann, H. Kaas, H. M. Sørensen, and H. L. Sørensen. 2002. Effects of nutrient-limitation and irradiance on marine phytoplankton pigments. *Journal of Plankton Research* 24: 835-858.
- Hoge, F. E., P. E. Lyon, R. N. Swift, J. K. Yungel, M. R. Abbott, R. Letelier, and W. E. Esaias. 2003. Validation of Terra-MODIS phytoplankton chlorophyll fluorescence line height. I. Initial airborne lidar results. *Applied Optics* 42: 2767-2771.
- Horton, P., A. V. Ruban, and M. Wentworth. 2000. Allosteric regulation of the light-harvesting system of photosystem II. *Philosophical Transactions of the Royal Society of London* 355: 1361-1370.
- Houghton, J. T., Y. Ding, D. J. Griggs, M. Noguer, P. J. van der Linden, X. Dai, K. Maskell, and C. A. Johnson. (Eds.). 2001. *Climate Change 2001: The Scientific Basis*. Cambridge University Press. Cambridge
- Hu, C., and K. J. Voss. 1998. Measurement of solar-stimulated fluorescence in natural waters. *Limnology and Oceanography* 43: 1198-1206.
- Huot, Y., W. H. Jeffrey, R. F. Davis, and J. J. Cullen. 2000. Damage to DNA in bacterioplankton: a model of damage by ultraviolet radiation and its repair as influenced by vertical mixing. *Photochemistry and Photobiology* 72: 62-74.
- Ibelings, B. W., B. M. A. Kroon, and L. R. Mur. 1994. Acclimation of photosystem II in a cyanobacterium and a eukaryotic green alga to high and fluctuating photosynthetic photon flux densities, simulating light regimes induced by mixing in lakes. *New Phytologist* 128: 407-424.

- Jassby, A. D., and T. Platt. 1976. Mathematical formulation of the relationship between photosynthesis and light for phytoplankton. *Limnology and Oceanography* 21: 540-547.
- Jeffrey, S. W., R. F. C. Mantoura, and S. W. Wright. (Eds.). 1997. *Phytoplankton pigments in oceanography*. UNESCO publishing. Paris
- Johannessen, S. C., W. L. Miller, and J. J. Cullen. 2003. Calculation of UV attenuation and colored dissolved organic matter absorption spectra from measurement of ocean color. *Journal of Geophysical Research* 108: 3301, doi:3310.1029/2000JC000514.
- Johnsen, G., B. B. Prézelin, and R. V. M. Jovine. 1997. Fluorescence excitation spectra and light utilization in two red tide dinoflagellates. *Limnology and Oceanography* 42: 1166-1177.
- Johnsen, G., and E. Sakshaug. 1996. Light harvesting in bloom-forming marine phytoplankton: species specificity and photoacclimation. *Scientia Marina* 60: 47-56.
- Joliot, P., and A. Joliot. 2003. Excitation transfer between photosynthetic units: the 1964 experiment. *Photosynthesis Research* 76: 241-245.
- Joshua, S., and C. W. Mullineaux. 2004. Phycobilisome diffusion is required for light-state transition in cyanobacteria. *Plant Physiology* 135: 2112-2119.
- Kana, T. M., R. J. Geider, and C. Critchley. 1997. Regulation of photosynthetic pigments in micro-algae by multiple environmental factors: a dynamic balance hypothesis. *New Phytologist* 137: 629-638.
- Kiefer, D. A. 1973a. Chlorophyll a fluorescence in marine centric diatoms: responses of chloroplasts to light and nutrient stress. *Marine Biology* 23: 39-46.
- . 1973b. Fluorescence properties of natural phytoplankton populations. *Marine Biology* 22: 263-269.
- Kiefer, D. A., W. S. Chamberlin, and C. R. Booth. 1989. Natural fluorescence of chlorophyll *a*: relationship to photosynthesis and chlorophyll concentration in the western South Pacific gyre. *Limnology and Oceanography* 34: 868-881.
- Kiefer, D. A., and R. A. Reynolds. 1992. Advances in understanding phytoplankton fluorescence and photosynthesis, p. 155-174. *In* P. G. Falkowski [ed.], *Primary Productivity and Biogeochemical Cycles in the Sea*. Plenum Press.

- Kjørboe, T. 1993. Turbulence, phytoplankton cell size, and the structure of pelagic food webs. *Advances in Marine Biology* 29: 1-72.
- Kirk, J. T. O. 1994. *Light and Photosynthesis in Aquatic Ecosystems*, Second ed. Cambridge University Press. Cambridge, Great Britain
- Kishino, M., S. Sugihara, and N. Okami. 1984. Influence of fluorescence of chlorophyll a on underwater upward irradiance spectrum. *La Mer* 22: 224-232.
- Koblížek, M., M. Ciscato, J. Komenda, J. Kopecky, P. Siffel, and J. Masojídek. 1999. Photoadaptation in the green alga *Spongiocloris* sp. A three fluorometer study. *Photosynthetica* 37: 307-323.
- Koblížek, M., D. Kaftan, and L. Nedbal. 2001. On the relationship between the non-photochemical quenching of the chlorophyll fluorescence and the photosystem II light harvesting efficiency. A repetitive flash fluorescence induction study. *Photosynthesis Research* 68: 141-152.
- Kolber, Z., and P. G. Falkowski. 1993. Use of active fluorescence to estimate phytoplankton photosynthesis in situ. *Limnology and Oceanography* 38: 1646-1665.
- Kolber, Z., J. R. Zehr, and P. G. Falkowski. 1988. Effects of growth irradiance and nitrogen limitation on photosynthetic energy conversion in photosystem II. *Plant Physiology* 88: 923-929.
- Kolber, Z. S., O. Prásil, and P. G. Falkowski. 1998. Measurements of variable chlorophyll fluorescence using fast repetition rate techniques: defining methodology and experimental protocols. *Biochimica et Biophysica Acta* 1367: 88-106.
- Kramer, D. M., G. Johnson, O. Kiirats, and G. E. Edwards. 2004. New fluorescence parameters for the determination of Q(A) redox state and excitation energy fluxes. *Photosynthesis Research* 79: 209-218.
- Kramer, D. M., C. A. Sacksteder, and J. A. Cruz. 1999. How acidic is the lumen. *Photosynthesis Research* 60: 151-163.
- Krause, G. H., and E. Weis. 1988. The photosynthetic apparatus and chlorophyll fluorescence. An introduction, p. 3-11. *In* H. K. Lichtenthaler [ed.], *Application of Chlorophyll Fluorescence*. Kluwer Academic.
- . 1991. Chlorophyll fluorescence: The basics. *Annual Reviews of Plant Physiology* 42: 313-349.

- Krey, J. 1958. Chemical methods of estimating standing crop of phytoplankton. *Rapports et procès-verbaux des réunions - Conseil international pour l'exploration de la mer* 144: 20-27.
- Külheim, C., Å. Jon, and S. Jansson. 2002. Rapid regulation of light harvesting and plant fitness in the field. *Science* 297: 91-93.
- Lakowicz, J. R. 1983. *Principles of fluorescence spectroscopy*. Plenum Press. New-York
- Laney, S., R. M. Letelier, and M. R. Abbott. 2001. Physiological variability in the natural fluorescence of *Thalassiosira weissflogii*, NASA Ocean Color Research Team meeting.
- Laney, S. R., R. M. Letelier, and M. R. Abbott. in prep. Natural fluorescence dynamics in a marine diatom. *Limnology and Oceanography*.
- Latasa, M. 1995. Pigment composition of *Heterocapsa* sp. and *Thalassiosira weissflogii* growing in batch cultures under different irradiances. *Scientia Marina* 59: 25-37.
- Latowski, D., J. Grzyb, and K. Strzalka. 2004. The xanthophyll cycle - molecular mechanism and physiological significance. *Acta Physiologiae Plantarum* 26: 197-212.
- Lavaud, J., B. Rousseau, and A.-L. Etienne. 2004. General features of photoprotection by energy dissipation in planktonic diatoms (Bacillariophyceae). *Journal of Phycology* 40: 130-137.
- Lavergne, J., and H.-W. Trissl. 1995. Theory of fluorescence induction in photosystem II: Derivation of analytical expressions in a model including exciton-radical-pair equilibrium and restricted energy transfer between photosynthetic units. *Biophysical Journal* 68: 2474-2492.
- Laws, E., E. Sakshaug, M. Babin, Y. Dandonneau, P. G. Falkowski, R. J. Geider, L. Legendre, A. Morel, M. Sondergaard, M. Takahashi, and P. J. I. Williams. 2002. Photosynthesis and primary productivity in marine ecosystems: Practical aspects and application of techniques. 36. JGOFS.
- Lazár, D. 1999. Chlorophyll *a* fluorescence induction. *Biochimica et Biophysica Acta* 1412: 1-28.
- Lee, H.-Y., Y.-N. Hong, and W. S. Chow. 2001. Photoinactivation of photosystem II complexes and photoprotection by non-functional neighbours in *Capsicum annuum* L. leaves. *Planta* 212: 332-342.

- Lehmann, M. K., R. F. Davis, Y. Huot, and J. J. Cullen. 2004. Spectrally-weighted transparency in models of water-column photosynthesis and photoinhibition by ultraviolet radiation. *Marine Ecology Progress Series* 269: 101-110.
- Lesser, M. P., J. J. Cullen, and P. J. Neale. 1994. Carbon uptake in a marine diatom during acute exposure to ultraviolet B radiation: Relative importance of damage and repair. *Journal of Phycology* 30: 183-192.
- Letelier, R., and M. R. Abbott. 1996. An analysis of chlorophyll fluorescence algorithms for the Moderate Resolution Imaging Spectrometer (MODIS). *Remote Sensing of Environment* 58: 215-223.
- Letelier, R. M., M. R. Abbott, and D. M. Karl. 1997. Chlorophyll fluorescence response to upwelling events in the Southern Ocean. *Journal of Geophysical Research* 102: 409-412.
- Leverenz, J. W. 1994. Factors determining the nature of the light dosage response curve of leaves, p. 239-254. *In* N. R. Baker and J. R. Bowyer [eds.], *Photoinhibition of photosynthesis from molecular mechanisms to the field*. BIOS Scientific Publishers.
- Lewis, M. R., E. P. W. Horne, J. J. Cullen, N. S. Oakey, and T. Platt. 1984. Turbulent motions may control phytoplankton photosynthesis in the upper ocean. *Nature* 311: 49-50.
- Li, W. K. W., D. V. Rao, J. C. Harrison, J. C. Smith, J. J. Cullen, B. Irwin, and T. Platt. 1983. Autotrophic picoplankton in the tropical ocean. *Science* 219: 292-295.
- Lizotte, M. P., and J. C. Priscu. 1994. Natural fluorescence and quantum yields in vertically stationary phytoplankton from perennially ice-covered lakes. *Limnology and Oceanography* 39: 1399-1410.
- Loftus, M. E., and H. H. Seliger. 1975. Some limitations of the *in vivo* fluorescence technique. *Chesapeake Science* 16: 79-92.
- Logan, B. A., S. C. Grace, W. W. Adams III, and B. Demmig-Adams. 1998. Seasonal differences in xanthophyll cycle characteristics and antioxidants in *Mahonia repens* growing in different light environments. *Oecologia* 116: 9-17.
- Lohr, M., and C. Wilhelm. 1999. Algae displaying the diadinoxanthin cycle also possess the violaxanthin cycle. *Proceedings of the National Academy of Sciences of the United States of America* 96: 8784-8789.
- Loisel, H., and A. Morel. 1998. Light scattering and chlorophyll concentration in case 1 waters: a reexamination. *Limnology and Oceanography* 43: 847-858.

- Loisel, H., and D. Stramski. 2000. Estimation of the inherent optical properties of natural waters from the irradiance attenuation coefficient and reflectance in the presence of Raman scattering. *Applied Optics* 39: 3001-3011.
- Lomas, M. W., and P. M. Glibert. 1999. Temperature regulation of nitrate uptake: A novel hypothesis about nitrate uptake and reduction in cool-water diatoms. *Limnology and Oceanography* 44: 556-572.
- . 2000. Comparisons of nitrate uptake, storage, and reduction in marine diatoms and flagellates. *Journal of Phycology* 36: 903-913.
- Lomas, M. W., C. J. Rumbley, and P. M. Glibert. 2000. Ammonium release by nitrogen sufficient diatoms in response to rapid increases in irradiance. *Journal of Plankton Research* 22: 2351-2366.
- Long, S. P., S. Humphries, and P. G. Falkowski. 1994. Photoinhibition of photosynthesis in nature. *Annual Reviews of Plant Physiology and Plant Molecular Biology* 45: 633-662.
- Longhurst, A. R. 1996. *Ecological Geography of the Sea*. Academic Press. San Diego
- Lorenzen, C. J. 1966. A method for the continuous measurement of *in vivo* chlorophyll concentration. *Deep-Sea Research* 13: 223-227.
- Lutz, V. A., S. Sathyendranath, E. J. H. Head, and W. K. W. Li. 1998. Differences between *in vivo* absorption and fluorescence excitation spectra in natural samples of phytoplankton. *Journal of Phycology* 34: 214-227.
- . 2001. Changes in the *in vivo* absorption and fluorescence excitation spectra with growth irradiance in three species of phytoplankton. *Journal of Plankton Research* 23: 555-569.
- Macintyre, H. L., and R. J. Geider. 1996. Regulation of Rubisco activity and its potential effect on photosynthesis during mixing in a turbid estuary. *Marine Ecology Progress Series* 144: 247-264.
- MacIntyre, H. L., T. M. Kana, T. Anning, and R. J. Geider. 2002. Photoacclimation of photosynthesis irradiance response curves and photosynthetic pigments in microalgae and cyanobacteria. *Journal of Phycology* 38: 17-38.
- MacIntyre, H. L., T. D. Sharkey, and R. J. Geider. 1997. Activation and deactivation of ribulose-1,5-bisphosphate carboxylase/oxygenase (Rubisco) in three marine microalgae. *Photosynthesis Research* 51: 93-106.

- Maerker, M., and K.-H. Szekiolda. 1976. Chlorophyll determination of phytoplankton: A comparison of *in vivo* fluorescence with spectrophotometric absorption. *Journal du Conseil International d'Exploration de la Mer* 36: 217-219.
- Maritorena, S., A. Morel, and B. Gentili. 2000. Determination of the fluorescence quantum yield by oceanic phytoplankton in their natural habitat. *Applied Optics* 39: 6725-6737.
- Maritorena, S., D. A. Siegel, and A. R. Peterson. 2002. Optimization of a semianalytical ocean color model for global-scale applications. *Applied Optics* 41: 2705-2714.
- Markager, S., and W. F. Vincent. 2001. Light absorption by phytoplankton: development of a matching parameter for algal photosynthesis under different spectral regimes. *Journal of Plankton Research* 23: 1373-1384.
- Marra, J. 1978. Effect of short-term variation in light intensity on photosynthesis of a marine phytoplankton: a laboratory simulation study. *Marine Biology* 46: 191-202.
- . 1997. Analysis of diel variability in chlorophyll fluorescence. *Journal of Marine Research* 55: 767-784.
- Marshall, B. R., and R. C. Smith. 1990. Raman scattering and in-water ocean optical properties. *Applied Optics* 29: 71-84.
- Marshall, H. L., R. J. Geider, and K. J. Flynn. 2000. A mechanistic model of photoinhibition. *New Phytologist* 145: 347-359.
- Masojídek, J., G. Torzillo, M. Koblízek, J. Kopecký, P. Bernardini, A. Sacchi, and J. Komenda. 1999. Photoadaptation of two members of the Chlorophyta (*Scenedesmus* and *Chlorella*) in laboratory and outdoor cultures: changes in chlorophyll fluorescence quenching and the xanthophyll cycle. *Planta* 209: 126-135.
- Maxwell, D. P., S. Falk, and N. P. A. Huner. 1995. Photosystem II excitation pressure and development of resistance to photoinhibition. *Plant Physiology* 107: 687-694.
- Maxwell, D. P., S. Falk, C. G. Trick, and N. P. A. Huner. 1994. Growth at low temperature mimics high-light acclimation in *Chlorella vulgaris*. *Plant Physiology* 105: 535-543.
- Maxwell, K., and G. N. Johnson. 2000. Chlorophyll fluorescence - a practical guide. *Journal of Experimental Botany* 51: 659-668.

- McClain, C. R., J. R. Christian, S. R. Signorini, M. R. Lewis, I. Asanuma, D. Turk, and C. Dupouy-Douchement. 2002. Satellite ocean-color observations of the tropical Pacific Ocean. *Deep-Sea Research II* 49: 2533-2560.
- Mingyuan, Z., Y. Xiaolong, and J. J. Cullen. 1992. The study of fluorescence characteristics and biochemical composition of a marine diatom *Thalassiosira pseudonana* 3H in light and dark cycles. *Acta Oceanologica Sinica* 11: 593-602.
- Mitchell, B. G., and D. A. Kiefer. 1988. Chlorophyll *a* specific absorption and fluorescence excitation spectra for light-limited phytoplankton. *Deep-Sea Research* 35: 639-663.
- Mobley, C. D. 1994. *Light and Water Radiative Transfer in Natural Waters*, First ed. Academic press, Inc. San Diego
- Morel, A. 1973. Diffusion de la lumière par les eaux de mer résultats expérimentaux et approche théorique, 161 pp., Laboratoire d'Océanographie Physique. Université de Paris.
- . 1978. Available, usable, and stored radiant energy in relation to marine photosynthesis. *Deep Sea Research* 25: 673-687.
- . 1988. Optical modeling of the upper ocean in relation to its biogenous matter content (case 1 waters). *Journal of Geophysical Research* 93: 10749-10768.
- Morel, A., D. Antoine, and B. Gentili. 2002. Bidirectional reflectance of oceanic waters: accounting for Raman emission and varying particle scattering phase function. *Applied Optics* 41: 6289-6306.
- Morel, A., and A. Bricaud. 1981. Theoretical results concerning light absorption in a discrete medium, and application to specific absorption of phytoplankton. *Deep-Sea Research* 28: 1375-1393.
- . 1986. Inherent properties of algal cells including picoplankton: Theoretical and experimental results., p. 521-559. *In* T. Platt and W. K. W. Li [eds.], *Photosynthetic Picoplankton*. Canadian Bulletin of Fisheries and Aquatic Sciences.
- Morel, A., and B. Gentili. 1996. Diffuse reflectance of oceanic waters. III. Implication of bidirectionality for the remote-sensing problem. *Applied Optics* 35: 4850-4862.
- . 2004. Radiation transport within oceanic (case 1) water. *Journal of Geophysical Research* 109: C06008, doi:06010.01029/02003JC002259.

- Morel, A., and S. Maritorena. 2001. Bio-optical properties of oceanic waters: A reappraisal. *Journal of Geophysical Research* 106: 7163-7180.
- Morel, A., and L. Prieur. 1977. Analysis of variations in ocean color. *Limnology and Oceanography* 22: 709-722.
- Morrison, J. R. 2003. In situ determination of the quantum yield of phytoplankton chlorophyll a fluorescence: a simple algorithm, observations, and a model. *Limnology and Oceanography* 48: 618-631.
- Mueller, J. L. 2000. SeaWiFS algorithm for the diffuse attenuation coefficient,  $K(490)$ , using water-leaving radiances at 490 and 555 nm. Chapter 3 of SeaWiFS Postlaunch Calibration and Validation analyses., p. 24-27. NASA GSFC.
- Mueller, J. L., and C. C. Trees. 1997. Revised SeaWiFS Prelaunch Algorithm for the diffuse Attenuation Coefficient  $K(490)$ , p. 18-21. *In* S. B. Hooker and E. R. Firestone [eds.], NASA Technical Memorandum 104566. NASA.
- Müller, P., X.-P. Li, and K. K. Niyogi. 2001. Non-photochemical quenching. A response to excess light energy. *Plant Physiology* 125: 1558-1566.
- Myers, R. A., and B. Worm. 2003. Rapid worldwide depletion of predatory fish communities. *Nature* 423: 280-283.
- Neale, P. J. 1987. Algal photoinhibition and photosynthesis in the aquatic environment, p. 39-65. *In* D. J. Kyle, C. B. Osmond and C. J. Arntzen [eds.], *Photoinhibition*. Elsevier Science Publisher.
- . 2000. Spectral weighting functions for quantifying effects of UV radiation in marine ecosystems, p. 72-100. *In* S. J. de Mora, S. Demers and M. Vernet [eds.], *The Effects of UV Radiation in the Marine Environment*. Cambridge University Press.
- Neale, P. J., R. F. Davis, and J. J. Cullen. 1998. Interactive effects of ozone depletion and vertical mixing on photosynthesis of Antarctic phytoplankton. *Nature* 392: 585-589.
- Neale, P. J., and J. Marra. 1985. Short-term variation of  $P_{max}$  under natural irradiance conditions: a model and its implication. *Marine Ecology Progress Series* 26: 113-124.
- Neville, R. A., and J. F. R. Gower. 1977. Passive remote sensing of phytoplankton via chlorophyll fluorescence. *Journal of Geophysical Research* 82: 3487-3493.
- Niyogi, K. K. 1999. Photoprotection revisited: Genetic and molecular approaches. *Annual Reviews of Plant Physiology and Plant Molecular Biology* 50: 333-359.

- Noctor, G., and C. H. Foyer. 2000. Homeostasis of adenylate status during photosynthesis in a fluctuating environment. *Journal of Experimental Botany* 51: 347-356.
- O'Reilly, J. E., S. Maritorena, B. G. Mitchell, D. A. Siegel, K. L. Carder, S. A. Garver, M. Kahru, and C. R. McClain. 1998. Ocean color chlorophyll algorithm for SeaWiFS. *Journal of Geophysical Research* 103: 24937-24953.
- Ögren, E. 1994. The significance of photoinhibition for photosynthetic productivity, p. 433-447. *In* W. J. Davies [ed.], *Photoinhibition of Photosynthesis from molecular mechanisms to the field*. Environmental Plant Biology. BIOS Scientific Publisher.
- Ohi, N., Y. Ishiwata, and S. Taguchi. 2002. Diel patterns in light absorption and absorption efficiency factors of *Isochrysis galbana* (Prymnesiophyceae). *Journal of Phycology* 38: 730-737.
- Olaizola, M., R. J. Geider, W. G. Harrison, L. M. Graziano, G. M. Ferrari, and P. M. Schlittenhardt. 1996. Synoptic study of variations in the fluorescence-based maximum quantum efficiency of photosynthesis across the North Atlantic Ocean. *Limnology and Oceanography* 41: 755-765.
- Ort, D. R. 2001. When there is too much light. *Plant Physiology* 125: 29-32.
- Ort, D. R., and N. R. Baker. 2002. A photoprotective role for O<sub>2</sub> as an alternative electron sink in photosynthesis? *Current Opinion in Plant Biology* 5: 193-198.
- Osmond, C. B. 1994. What is photoinhibition? Some insights from comparisons of shade and sun plants, p. 1-24. *In* N. R. Baker and J. R. Bowyer [eds.], *Photoinhibition: Molecular Mechanisms to the Field*. Bios Scientific Publisher.
- Osmond, C. B., J. Ramus, G. Levavasseur, L. A. Franklin, and W. J. Henley. 1993. Fluorescence quenching during photosynthesis and photoinhibition of *Ulva rotundata* Blid. *Planta* 190: 97-106.
- Ostrowska, M., M. Darecki, and B. Wozniak. 1997. An attempt to use measurements of sun-induced chlorophyll fluorescence to estimate chlorophyll a concentration in the Baltic Sea. *Proceedings of SPIE, International Society of Optical Engineering* 3222: 528-537.
- Ostrowska, M., R. Majchrowski, D. N. Matorin, and B. Wozniak. 2000a. Variability of the specific fluorescence of chlorophyll in the ocean. Part 1. Theory of classical *in situ* chlorophyll fluorometry. *Oceanologia* 42: 203-219.

- Ostrowska, M., D. N. Matorin, and D. Ficek. 2000b. Variability of the specific fluorescence of chlorophyll in the ocean. Part 2. Fluorometric method of chlorophyll *a* determination. *Oceanologia* 42: 221-229.
- Oxborough, K., and N. R. Baker. 2000. An evaluation of the potential triggers of photoinactivation of photosystem II in the context of a Stern-Volmer model for downregulation and the reversible radical pair equilibrium. *Philosophical Transactions of the Royal Society of London* 355: 1489-1498.
- Oxborough, K., A. R. M. Hanlon, G. J. C. Underwood, and N. R. Baker. 2000. In vivo estimation of the photosystem II photochemical efficiency of individual microphytobenthic cells using high-resolution imaging of chlorophyll *a* fluorescence. *Limnology and Oceanography* 45: 1420-1425.
- Park, Y.-I., W. S. Chow, and J. M. Anderson. 1995. Light inactivation of functional photosystem II in leaves of peas grown in moderate light depends on photon exposure. *Planta* 196: 401-411.
- Parkhill, J.-P., G. Maillet, and J. J. Cullen. 2001. Fluorescence-based maximal quantum yield for PSII as a diagnostic of nutrient stress. *Journal of Phycology* 37: 517-529.
- Pegau, W. S., J. R. Zaneveld, B. G. Mitchell, J. L. Mueller, M. Kahru, J. Wieland, and M. Stramska. 2003. Inherent optical properties: Instrument, characterization, field measurement and data analysis protocols, p. 83. TM-2003-211621. NASA.
- Perry, M. J. 1994. Measurements of phytoplankton absorption other than per unit of chlorophyll *a*, p. 107-116. *In* R. W. Spinrad, K. L. Carder and M. J. Perry [eds.], *Ocean Optics*. Oxford monographs on geology and geophysics. Oxford University Press.
- Pfündel, E. E. 1998. Estimating the contribution of photosystem I to total leaf chlorophyll fluorescence. *Photosynthesis Research* 56: 185-195.
- Pope, R. M., and E. S. Fry. 1997. Absorption spectrum (380-700 nm) of pure water. II. Integrating cavity measurements. *Applied Optics* 36: 8710-8723.
- Pospisil, P. 1997. Mechanisms of non-photochemical chlorophyll fluorescence quenching in higher plants. *Photosynthetica* 34: 343-355.
- Pozdnyakov, D., and H. Grassl. 2003. *Colour of Inland and Coastal Waters A Methodology for its Interpretation*, First ed. Praxis Publishing Ltd. Chichester
- Preisendorfer, R. W. 1976. *Hydrologic Optics*. National Oceanic and Atmospheric Administration. Honolulu

- Preisendorfer, R. W., and C. D. Mobley. 1988. Theory of fluorescent irradiance fields in natural waters. *Journal of Geophysical Research* 93: 10831-10855.
- Prézelin, B. B. 1981. Light reactions in photosynthesis, p. 1-43. *In* T. Platt [ed.], *Canadian Bulletin of Fisheries and Aquatic Sciences*. Canadian government.
- Prézelin, B. B., G. Samuelsson, and H. A. Matlick. 1986. Photosystem II photoinhibition and altered kinetics of photosynthesis during nutrient-dependent high-light photoadaptation in *Gonyaulax polyedra*. *Marine Biology* 93: 1-12.
- Priestley, M. B. 1981. *Spectral Analysis and Timeseries*. Academic Press. London
- Raateoja, M., J. Seppälä, and H. Kuosa. 2004a. Bio-optical modelling of primary production in the SW Finnish coastal zone, Baltic Sea: fast repetition rate fluorometry in Case 2 waters. *Marine Ecology Progress Series* 267: 9-26.
- Raateoja, M., J. Seppälä, and P. Ylöstalo. 2004b. Fast repetition rate fluorometry is not applicable to studies of filamentous cyanobacteria from the Baltic Sea. *Limnology and Oceanography* 49: 1006-1012.
- Rae, R., and W. F. Vincent. 1998. Phytoplankton production in subarctic lake and river ecosystems: development of a photosynthesis-temperature-irradiance model. *Journal of Plankton Research* 20: 1293-1312.
- Reda, I., and A. Andreas. 2003. Solar position algorithm for solar radiation applications, p. 55. NREL/TP-560-34302. National Renewable Energy Laboratory.
- Richardson, K., J. Beardall, and J. A. Raven. 1983. Adaptation of unicellular algae to irradiance: an analysis of strategies. *New Phytologist* 93: 157-191.
- Roelofs, T. A., C.-H. Lee, and A. R. Holzwarth. 1992. Global target analysis of picosecond chlorophyll fluorescence kinetics from pea chloroplasts. *Biophysical Journal* 61: 1147-1163.
- Roesler, C. S. 2003. A novel ocean color inversion model: retrieval of beam attenuation and particle size distribution. *Geophysical Research Letters* 30: 1468, doi:1410.1029/2002GL016185.
- Roesler, C. S., and M. J. Perry. 1995. In situ phytoplankton absorption, fluorescence emission, and particulate backscattering spectra determined from reflectance. *Journal of Geophysical Research* 100: 13279-13294.
- Roháček, K. 2002. Chlorophyll fluorescence parameters: the definitions, photosynthetic meaning, and mutual relationships. *Photosynthetica* 40: 13-29.

- Roháček, K., and M. Barták. 1999. Technique of the modulated chlorophyll fluorescence: basic concepts, useful parameters, and some applications. *Photosynthetica* 37: 339-363.
- Ross, O. N., and J. Sharples. 2004. Recipe for 1-D lagrangian particle tracking models in space-varying diffusivity. *Limnology and Oceanography: Methods* 2: 302.
- Roy, S., and L. Legendre. 1979. DCMU-enhanced fluorescence as an index of photosynthetic activity of phytoplankton. *Marine Biology* 55: 93-101.
- . 1980. Field studies of DCMU-enhanced fluorescence as an index of in situ phytoplankton photosynthetic activity. *Canadian Journal of Fisheries and Aquatic Sciences* 37.
- Ruban, A. V., and P. Horton. 1995. Regulation of non-photochemical quenching of chlorophyll fluorescence in plants. *Australian Journal of Plant Physiology* 22: 221-230.
- Rubio, F. C., F. G. Camacho, J. M. F. Sevilla, Y. Chisti, and E. M. Grima. 2003. A mechanistic model of photosynthesis in microalgae. *Biotechnology and Bioengineering* 81: 459-473.
- Sakshaug, E., A. Bricaud, Y. Dandonneau, P. G. Falkowski, D. A. Kiefer, L. Legendre, A. Morel, J. Parslow, and M. Takahashi. 1997. Parameters of photosynthesis: definitions, theory and interpretation of results. *Journal of Plankton Research* 19: 1637-1670.
- Sakshaug, E., and O. Holm-Hansen. 1977. Chemical composition of *Skeletonema costatum* (Grev.) Cleve and *Pavlova (Monochrysis) lutheri* (Droop) Green as a function of nitrate-, phosphate-, and iron-limited growth. *Journal of Experimental Marine Biology and Ecology* 29: 1-34.
- Salomonson, V. 2004. MODIS Characterization Support Team (MCST) Web page
- Samuelsson, G., and G. Öquist. 1977. A method for studying photosynthetic capacities of unicellular algae based on in vivo chlorophyll fluorescence. *Physiologia Plantarum* 40: 315-319.
- Samuelsson, G., G. Öquist, and P. Halldal. 1978. The variable chlorophyll a fluorescence as a measure of photosynthetic capacity in algae. *Mitteilungen Internationale Vereinigung für Limnologie* 21: 207-215.
- Sathyendranath, S., and T. Platt. 1998. Ocean-color model incorporating transspectral processes. *Applied Optics* 37: 2216-2227.

- Schallenberg, C., M. R. Lewis, D. E. Kelley, and J. J. Cullen. 2002. Variability in the quantum yield of sun-induced fluorescence in the Bering Sea: effects of light and nutrients. *In* S. G. Ackleson [ed.], *Ocean optics XVI*.
- Schatz, G. H., H. Brock, and A. R. Holzwarth. 1988. Kinetic and energetic model for the primary processes in photosystem II. *Biophysical Journal* 54: 397-405.
- Schreiber, U., U. Schliwa, and W. Bilger. 1986. Continuous recording of photochemical and non-photochemical chlorophyll fluorescence quenching with a new type of modulation fluorometer. *Photosynthesis Research* 10: 51-62.
- Sciandra, A., L. Lazzara, H. Claustre, and M. Babin. 2000. Responses of growth rate, pigment composition and optical properties of *Cryptomonas* sp. to light and nitrogen stresses. *Marine Ecology Progress Series* 201: 107-120.
- Seritti, A., D. Russo, L. Nannicini, and R. Del Vecchio. 1998. DOC, absorption and fluorescence properties of estuarine and coastal waters of the Northern Tyrrhenian Sea. *Chemical Speciation and Bioavailability* 10: 95-106.
- Siegel, D. A., S. Maritorena, N. B. Nelson, D. A. Hansell, and M. Lorenzi-Kayser. 2002. Global distribution and dynamics of colored dissolved and detrital organic materials. *Journal of Geophysical Research* 107: 3228.
- Slovacek, R. E., and P. J. Hannan. 1977. In vivo fluorescence determinations of phytoplankton chlorophyll *a*. *Limnology and Oceanography* 22: 919-925.
- Smith, R. C., and K. S. Baker. 1981. Optical properties of the clearest natural waters (200-800 nm). *Applied Optics* 20: 177-184.
- SooHoo, J. B., and D. A. Kiefer. 1982a. Vertical distribution of phaeopigments — I. A simple grazing and photooxidative scheme for small particles. *Deep Sea Research* 29: 1539-1551.
- . 1982b. Vertical distribution of phaeopigments — II. Rates of production and kinetics of photooxidation. *Deep Sea Research* 29: 1553-1563.
- SooHoo, J. B., D. A. Kiefer, D. J. Collins, and I. S. McDermid. 1982. *In vivo* fluorescence excitation and absorption spectra of marine phytoplankton: I. Taxonomic characteristics and responses to photoadaptation. *Journal of Plankton Research* 8: 197-214.
- Sosik, H. M. in press. Characterizing seawater constituents from optical properties. *In* M. Babin, C. S. Roesler and J. J. Cullen [eds.], *Real time coastal observing systems for ecosystems dynamics and harmful algal blooms*.

- Sosik, H. M., and B. G. Mitchell. 1995. Light absorption by phytoplankton, photosynthetic pigments and detritus in the California Current System. *Deep-Sea Research I* 42: 1717-1748.
- Sournia, A. 1973. Comments on the diel periodicity of phytoplankton photosynthesis, with an example from the Indian ocean. *Spl. Publ. Mar. Biol. Ass. India.*: 52-59.
- . 1974. Circadian periodicities in natural population of marine phytoplankton. *Advances in Marine Biology* 12: 325-389.
- Srivastava, A., H. Greppin, and R. J. Strasser. 1995. The steady state chlorophyll fluorescence exhibits in vivo an optimum as a function of light which reflects the physiological state of the plant. *Plant and cellular physiology* 36: 839-848.
- Steeman Nielsen, E. 1962. Inactivation of the photochemical mechanism in photosynthesis as a means to protect the cells against too high light intensities. *Physiologia Plantarum* 15: 161-171.
- Steeman Nielsen, E., and E. G. Jørgensen. 1968. The adaptation of plankton algae I. General part. *Physiologia Plantarum* 21: 401-413.
- Stegmann, P. M., M. R. Lewis, C. O. Davis, and J. J. Cullen. 1992. Primary production estimates from recordings of solar-stimulated fluorescence in the Equatorial Pacific at 150°W. *Journal of Geophysical Research* 97: 627-638.
- Stramski, D., and R. A. Reynolds. 1993. Diel variations in the optical properties of a marine diatom. *Limnology and Oceanography* 38: 1347-1364.
- Strickland, J. D. H. 1968. Continuous measurements of *in vivo* chlorophyll; a precautionary note. *Deep-Sea Research* 15: 225-227.
- Strickland, J. D. H., and T. R. Parsons. 1972. A Practical handbook of seawater analysis. *Bulletin of the Fisheries and Research Board of Canada* 167: 1-310.
- Suggett, D. J., G. Kraay, P. Holligan, M. Davey, J. Aiken, and R. J. Geider. 2001. Assessment of photosynthesis in a spring cyanobacterial bloom by use of a fast repetition rate fluorometer. *Limnology and Oceanography* 46: 802-810.
- Suggett, D. J., H. L. MacIntyre, and R. J. Geider. 2004. Evaluation of biophysical and optical determination of light absorption by photosystem II in phytoplankton. *Limnology and Oceanography: Methods* 2: 316-332.
- Sukenic, A., J. Bennett, and P. G. Falkowski. 1987. Light-saturated photosynthesis - limitation by electron transport or carbon fixation. *Biochimica et Biophysica Acta* 891: 205-215.

- Thorpe, S. A. 2004. Langmuir circulation. *Annual Review of Fluids Mechanics* 36: 55-79.
- Topliss, B. J., and T. Platt. 1986. Passive fluorescence and photosynthesis in the ocean: Implications for remote sensing. *Deep-Sea Research* 33: 849-864.
- Trissl, H.-W. 1999. Theory of fluorescence induction, [www.biologie.uni-osnabrueck.de/biophysik/trissl/Teaching/fi.PDF](http://www.biologie.uni-osnabrueck.de/biophysik/trissl/Teaching/fi.PDF)
- Trissl, H.-W., and J. Lavergne. 1995. Fluorescence Induction from photosystem II: Analytical equations for the yields of photochemistry and fluorescence derived from analysis of a model including exciton-radical pair equilibrium and restricted energy transfer between photosynthetic units. *Australian Journal of Plant Physiology* 22: 183-193.
- Tyler, J. E., and R. C. Smith. 1970. *Measurements of Spectral Irradiance under Water*. Gordon and Breach science publishers. New-York
- Valvilin, D. V., E. Tyystjärvi, and E.-M. Aro. 1998. Model for the fluorescence induction curve of photoinhibited thylakoids. *Biophysical Journal* 75: 503-512.
- Vincent, W. F. 1981. Photosynthetic capacity measured by DCMU-induced chlorophyll fluorescence in an oligotrophic lake. *Freshwater Biology* 11: 61-78.
- Vodacek, A., N. V. Blough, M. D. Degrandpre, E. T. Peltzer, and R. K. Nelson. 1997. Seasonal variation of CDOM and DOC in the Middle Atlantic Bight: Terrestrial inputs and photooxidation. *Limnology and Oceanography* 42: 674-686.
- Vodacek, A., S. A. Green, and N. V. Blough. 1994. An experimental model of the solar-stimulated fluorescence of chromophoric dissolved organic matter. *Limnology and Oceanography* 39: 1-11.
- Walker, D. A. 1988. Some aspects of the relationship between chlorophyll *a* fluorescence and photosynthetic carbon assimilation. *In* H. K. Lichtenthaler [ed.], *Applications of Chlorophyll Fluorescence*. Kluwer Academic Publishers.
- White, A. J., and C. Critchley. 1999. Rapid light curves: A new fluorescence method to assess the state of the photosynthetic apparatus. *Photosynthesis Research* 59: 63-72.
- Whitmarsh, J., and Govindjee. 1999. The photosynthetic process, p. 11-51. *In* G. S. Singhal, R. Renger, S. K. Sopory, K.-D. Irrgang and Govindjee [eds.], *Concepts in photobiology: photosynthesis and photomorphogenesis*. Concepts in photobiology. Narosa-Publishing.

- Wollman, F.-A. 2001. State transitions reveal the dynamics and flexibility of the photosynthetic apparatus. *The EMBO journal* 20: 3623-3630.
- Wozniak, B., J. Dera, D. Ficek, R. Majchrowski, S. Kaczmarek, M. Ostrowska, and O. I. Koblentz-Mishke. 2000. Model of the in vivo spectral absorption of algal pigments. Part 1 Mathematical apparatus. *Oceanologia* 42: 177-190.
- Wünschmann, G., and J. J. Brand. 1992. Rapid turnover of a component required for photosynthesis explains temperature dependence and kinetics of photoinhibition in a cyanobacterium *Synechococcus* 6301. *Planta* 186: 426-433.
- Yentsch, C. S. 1960. The influence of phytoplankton pigments on the colour of sea water. *Deep-Sea Research* 7: 1-9.
- Yentsch, C. S., and D. W. Menzel. 1963. A method for the determination of phytoplankton chlorophyll and phaeophytin by fluorescence. *Deep-Sea Research* 10: 221-231.
- Yentsch, C. S., and D. A. Phinney. 1989. A bridge between ocean optics and microbial ecology. *Limnology and Oceanography* 34: 1694-1705.
- Yoshikawa, T., and K. Furuya. 2004. Long-term monitoring of primary production in coastal waters by an improved natural fluorescence method. *Marine Ecology Progress Series* 273: 17-30.
- Zonneveld, C. 1997. Modeling the effects of photoadaptation on the photosynthesis-irradiance curve. *Journal of Theoretical Biology* 186: 381-388.
- . 1998. Photoinhibition as affected by photoacclimation in phytoplankton: a model approach. *Journal of Theoretical Biology* 193: 115-123.